Thesis entitled

Real-Time Electromagnetic Electromechanical Hybrid Transient Simulation for Large Power Systems

submitted by

SU Hongtian

for the degree of Doctor of Philosophy
at The Hong Kong Polytechnic University
in September 2004

Supervisors: Dr. K.W. Chan, Prof. T.S. Chung, Prof. D.Z. Fang, and
Dr L.A. Snider
(Department of Electrical Engineering)

A thesis submitted in partial fulfillment of the requirements for the Degree of Doctor of Philosophy

Abstract of the thesis entitled

Real-Time Electromagnetic Electromechanical Hybrid Transient Simulation for Large Power Systems

submitted by

SU Hongtian

for the degree of Doctor of Philosophy

at The Hong Kong Polytechnic University in September 2004

ABSTRACT:

In this research a new hybrid real-time fully digital simulator capable of simulating both electromagnetic and electromechanical transients over a broad range of frequencies was developed. This simulator is capable of performing transient stability studies over a wide range of contingencies, including asymmetrical faults and mal-operation of power electronic systems. This type of simulator will play an increasing role in power system operations, and will contribute towards the enhancement of power system security.

The research was motivated by the profound effect of deregulation on the planning and operation of interconnected power systems leading to the virtual elimination of integrated generation and transmission least-cost planning and traditional economic-dispatch-based unit commitment. The new environment is characterized by rapid reconfigurations of the transmission systems, with consequent increasing uncertainty related to system security. Furthermore the increasing

demands on transmission resulting from limited expansion of transmission systems has led to the proliferation of novel approaches to increase transmission capability, notably the utilization of power electronic systems. This has placed increasing demands on improved dynamic security assessment, and it is here where modern real-time or accelerated-time hybrid simulators have an increasingly important role. These simulators, coupled with real-time data acquisition, will have the ability to capture system behaviour at any instant of time, and will allow operators to study an increasingly comprehensive contingency list (including mal-operation of power electronic systems) and "what if" scenarios for different system conditions and configurations, with the obvious benefit of increasing system security.

The hybrid simulator includes both Electromagnetic Transients (EMT) and Transient Stability (TS) simulators within an integrated analysis tool operating on a UNIX based multi-processor server, and is, capable of effective simulation of large-size networks, while providing accurate representation of highly nonlinear components, such as FACTS devices and HVDC links. Real-time operation was realized on a Silicon Graphics (SGI) multi-processor server simultaneously running a real-time EMT program called HYPERSIM (developed by the Hydro Quebec Research Institute) and a comprehensive transient stability program developed by the author.

In this research the difficulties related to the interface of two very different programs were overcome. EMT is normally aimed at detailed studies of relatively small networks; however, the mandatory small time step results in a computationally intensive simulator, impracticable for the simulation of very large systems. On the other hand, TS simulators are aimed at solving the electromechanical equations of very large systems where the solution is usually based on a single phase equivalent and as such contingencies such as asymmetrical faults are somewhat difficult to deal with. Furthermore their large time steps preclude modelling of power electronic systems at the device level: FACTS equipment and HVDC converters have to be

represented as relatively simple mathematical models. Consequently it is not practicable to study such contingencies as unbalanced and/or mal-operation of power electronic equipment in a TS program.

In the hybrid simulator, the EMT and TS simulators each take responsibility for one part of power system: the EMT simulator models a *detailed system* (such as a FACTS system) and the TS simulator models the rest, referred to as the *external system*. Each simulator sees the other as an equivalent, and both simulators proceed in parallel and communicate with each other at specified time intervals. The communication between the detailed and external systems is maintained through a well-defined common interfacing location. The two simulators have different integration time steps and component modelling techniques, and this mandated the development of a novel parallel interaction protocol in order to coordinate the variables transferring between the two simulators while being compatible with real-time operation. Significant problems had to be overcome, for example the EMT simulator must run continuously while the TS simulator must perform iterations. Consequently the TS simulator must perform some of its iterations with incomplete data from EMT, and to overcome this problem a prediction scheme was developed and incorporated into the TS simulator.

Based on the parallel implementation of protocol, a parallel hybrid simulation was built employing multi-thread techniques. Several case studies were run on two different multi-processor computers to verify the operation of the hybrid simulator. Performance studies were made based both on serial and parallel protocol implementation, and the results compared well. Visual comparisons were made between the hybrid simulation and benchmark cases run on conventional simulators, again with good results. A case study involving a commutation failure of a FACTS system on a 39 bus system showed the system to be unstable following this contingency: this case could not have been run on a conventional TS simulator.

DECLARATION

I declare that this thesis represents my own work, except where due acknowledgement is made, and that it has not been previously included in a thesis, dissertation or report submitted to this University or to any other institution for a degree, diploma or other qualification.

Signed _____

SU Hongtian

ACKNOWLEDGEMENTS

The work presented in this thesis was carried out under the supervision of Dr. Ka Wing Chan and Dr. Laurence A. Snider, Department of Electrical Engineering, The Hong Kong Polytechnic University. It is great pleasure and deep gratitude that the author acknowledges their invaluable guidance and criticism, and kind and continuous encouragement which enable the completion of this work.

The author gratefully acknowledges the help and encouragement given by his colleagues and all the faculties of Department of Electrical Engineering, The Hong Kong Polytechnic University, in particular, the valuable guidance given by Prof. Tak Shing Chung and Prof. Dazhong Fang. The author wishes to express his gratitude to the staff in IREQ, Quebec, Canada. The author's gratitude is also sincerely extended to Mr. Alain Vallee of Transenergie Technologies Inc, Quebec, Canada.

The financial assistance given by the Research Grants Council of the Hong Kong Special Administrative Region, PRC (RGC No: PolyU 5118/00E) is also gratefully acknowledged.

SU Hongtian

TABLE OF CONTENTS

LIST OF PUBLICATIONS

1. K.W.Chan, C.H.Cheung, H.T.Su: Time Domain Simulation Based Transient Stability Assessment and Control. PowerCon 2002, pp.1578-1582, Kunming, 13-17 Oct 2002.
2. H.T.Su, K.W.Chan, L.A.Snider: Interfacing an Electromagnetic SVC Model into the Transient Stability Simulation. PowerCon 2002, pp.1568-1572, Kunming, 13-17 Oct 2002.
3. H.T.Su, L.A.Snider, K.W.Chan, B.R.Zhou: A New Approach for Integration of Two Distinct Types of Numerical Simulator. IPST 2003, New Orleans, USA, CDROM, 28 Sep - 2 Oct 2003.
4. L.A.Snider, H.T.Su, K.W.Chan, D.Van Que: Development of a broadband real-time fully digital simulator for the study and control of large power systems. Mathematics and Computers in Simulation, Vol.63, Issues 3-5, pp.137-149, Nov 2003.
5. H.T.Su, K.W.Chan, L.A.Snider: Investigantion of the Use of Electromagnetic Transient Models for Transient Stability Simulation. APSCOM 2003, pp.787-792, Hong Kong, 11-14 Nov 2003.
6. B.R.Zhou, K.W.Chan, L.A.Snider, H.T.Su: The Applications of Hybrid Simulator in Transient Stability Assessment. APSCOM 2003, pp.398-402, Hong Kong, 11-14 Nov 2003.
7. H.T.Su, K.W.Chan, L.A.Snider, T.S.Chung: A Parallel Implementation of Electro- magnetic Electromechanical Hybrid Simulation Protocol. DRPT 2004, Hong Kong, 5-8 Apr 2004.
8. H.T.Su, K.W.Chan, L.A.Snider: A Parallel Interaction Protocol for Electromagnetic and Electromechanical Hybrid Simulation. IEE Proceedings

Generation, Transmission & Distribution, vol.152, no.3, pp.406-414, May 2005.

9. H.T.Su, K.W.Chan, L.A.Snider, J.C.Soumagne: Advancements on the Integration of Electromagnetic Transients Simulator and Transient Stability Simulator. International Conference on Power Systems Transients (IPST'05), CDROM, Montreal, 19-23 Jun 2005.

10. H.T.Su, K.W.Chan, L.A.Snider: Evaluation Study for the Integration of Electromagnetic Transients Simulator and Transient Stability Simulator. Electric Power Systems Research, vol.75, pp.67-78, Jul 2005.

11. H.T.Su, K.W.Chan, L.A.Snider: Hybrid Simulation of Large Electrical Networks with Assymmetrical Fault Modelling. International Journal of Modelling and Simulation, Paper 205-4290, submitted on 3 Mar 2004.

LIST OF ABBREVIATIONS

TS	Transient Stability
EMT	Electromagnetic Transients
HVDC	High Voltage Direct Current
FACTS	Flexible AC Transmission System
SVC	Static VAR Compensators
SGI	Silicon Graphics
CDA	Critical Damping Adjustment
PSB	Power System Blockset
HVAC	High Voltage Alternative Current
FDNE	Frequency Dependent Network Equivalent
UCB	User Code Block
TSC	Thyristor Switched Capacitor
TCR	Thyristor Controlled Reactor
FC	Fixed Capacitor

LIST OF FIGURES

LIST OF TABLES

Chapter I INTRODUCTION

Hybrid simulation is significant step towards the realization of a powerful digital power system simulator, capable of efficient simulation of large size networks, while providing accurate representation of highly nonlinear components, such as FACTS devices and HVDC links. In this research a functional hybrid simulator based on a novel interface between an Electromagnetic Transients (EMT) simulator and a comprehensive Transient Stability (TS) simulator was developed. Real-time operation was realized on a Silicon Graphics (SGI) multi-processor server simultaneously running a real-time EMT program called HYPERSIM (developed by the Hydro Quebec Research Institute) and a comprehensive transient stability program developed by the author.

Towards the realization of this hybrid simulator a novel approach for the communication protocol was developed such that for the first time true real-time EMT/TS hybrid simulation was realized. This new hybrid simulator is capable of simulating mal-functions of FACTS devices in a transient stability study, without compromising the integrity of the transient stability simulator.

The driving force behind such developments is the impact of deregulation mandating open access to utility transmission systems. The effect on planning and operation of interconnected power systems has been profound, with the virtual elimination of integrated generation and transmission least-cost planning and traditional economic-dispatch-based unit commitment. Before these changes operators could analyze conditions offline using predictable patterns of power flow and related generation dispatch. The new environment, however, is characterized by rapid reconfigurations of the transmission systems, with consequent increasing uncertainty related to system security. Furthermore the increasing demands on transmission resulting from limited expansion of transmission systems has led to the proliferation of novel approaches to increasing transmission capability, notable the

utilization of power electronic systems. This has placed increasing demands on improved dynamic security assessment, and it is here where modern real-time or accelerated-time hybrid simulators will have an increasingly important role. These simulators, coupled with real-time data acquisition, will have the ability to capture system behaviour at any instant of time, and will allow operators to study an increasingly comprehensive contingency list (including mal-operation of power electronic systems) and "what if" scenarios for different system conditions and configurations, with the obvious benefit of increasing system security.

While the traditional operation pattern has to be changed to meet the new demands from the power industrial deregulation, there are new requirements on study tools. The traditional power system software tools may be adequate for small-size networks and conventional contingency lists. They become increasingly limited in their capability to deal with large-size interconnected systems employing power electronic devices and modern control systems. The main limitation of EMT simulators is simulation speed on the large-size interconnected systems. One way to increase the simulation speed for large systems is to use dynamic equivalents for large parts of large systems, however confidence is not high and it is generally accepted the representation is not good beyond a relatively short simulation time. A possible alternative is to use modern scalable fully digital simulators, which can represent larger and larger systems by becoming larger and larger simulators. With the advances in computing technologies, EMT simulators would become more and more powerful, and important for the study on HVDC and FACTS. However, there has to be a limit, and it is unlikely that "conventional" EMT simulators will ever be practicable to fully represent a two thousand-bus system. TS simulators, on the other hand, will still have an important role in the future on large-size interconnected power systems stability and security analysis for conventional contingencies, in which detailed modelling of power electronic devices is not required, because of its fast simulation speed.

With the limitations of conventional simulators, no single program provides both detailed circuit analysis and large-scale system modelling. It is readily apparent that the future of simulation lies in the development of very large bandwidth digital simulators capable of modelling large scale power systems in real time or faster than real time. These hybrid simulators would allow practicable simulation of extensive power systems comprehensively with no need for dynamic equivalents, and would provide the capability of 'zooming in' on parts of the system, incorporating, for example, power electronic devices such as FACTS or HVDC.

The challenge of the development of hybrid simulators lies in the very different attributes of TS and EMT simulators. TS simulators are based on fundamental frequency positive sequence modeling and can only provide phasor-like solutions in the time domain. They have a speed advantage because they employ relatively simple models and much larger time steps than EMT simulators. TS simulators normally only take fundamental frequency positive sequence component into account, and they are compromised by their limited representation of non-linear components. Furthermore they usually require iteration as part of their solution process, another consequence of the relatively large time step. On the other hand, EMT simulators usually use a very small time step and can represent system components and control systems in detail; however, they are impracticable for modeling very large systems.

The relatively recent development of fully digital real-time EMT simulators has paved the way towards the new breed of hybrid broadband simulators which can generate solutions to electrical power system transients over a broad range of frequencies, from fast electromagnetic transients (durations ranging from microseconds to a few periods) to slow electromechanical transients (durations ranging from a few periods to hours), with a fast simulation speed.

The underlying idea of the hybrid simulation is to partition a network into two parts, one for the TS simulator and the other for the EMT simulator. Of course,

in order to exploit the speed advantage of the TS simulator, the part simulated by the TS simulator should include most components of the system, while the part simulated by the EMT simulator would contain the components that require detailed simulation, as well as parts of the network close to where they are connected. Thus, the slow dynamics of machines are adequately modeled by the TS simulator while the fast dynamic responses of selected devices are accurately represented by EMT simulation models.

In order to ensure that the hybrid simulation can predict the correct dynamics of the EMT simulator, the EMT simulator requires the TS simulator to be represented by a correct driving point impedance. The TS simulator is a fundamental frequency phasor-type solution, and at each interchange it can provide voltage, current and equivalent impedance under the system frequency. This is presented to the EMT simulator at the interface bus as a Norton equivalent which includes a dynamically updated current source and a frequency-dependent equivalent circuit.

There are a number of ways to represent the EMT simulator in the TS simulator. System-level models presuppose that devices work as designed, consequently, malfunctions, such as valve failures, cannot be adequately represented. Device-level models are based on variables on interface buses extracted from three-phase broad bandwidth waveforms from the EMT simulator. In order to take any kind of disturbance into consideration, the research proposes that the EMT simulator should be represented in the TS simulator in a form of dynamically updated load or impedance.

Previously, the main concern in determining the interaction location was consideration of the effects of waveform distortion on the EMT modelling. However, with the use of frequency dependent equivalent, this consideration has become less important, and instead, the quality of the variables transferred across the interface bus to the TS simulator has now become more of a concern. Thus the research proposes that the location of interchange can be assessed by the quality of extraction.

The EMT and TS simulators interchange variables periodically at specified time points following an interaction protocol. With the interchanging variables, the equivalents are updated to make sure the hybrid simulation work well. The EMT simulator is an instantaneous analysis program, producing three-phase solutions with broad bandwidth. The TS simulator uses per-unit values and simulates three-phase AC power systems by phasor analysis. The protocol is to coordinate the two simulators to eliminate any possible error caused by the differences between them.

The interaction protocol has two implementation modes, i.e. serial and parallel. In serial mode, the EMT and TS simulators execute one by one. Under the mode when one simulator is running the other is idle. In parallel mode, which is the basis of real-time simulation, the EMT and TS simulators proceed in parallel, running simultaneously. The total execution time is the EMT simulator time because the simulator is not allowed to stop. The research led to the development of a method to implement the parallel mode.

In the thesis, the following issues relating to the research are expressed in theory and demonstrated by examples:

- representation of TS simulators in EMT simulators
- representation of EMT simulators in TS simulators
- the factors which the choice of the location of interface is based on
- protocol between EMT and TS simulators
- parallel implementation of the interface protocol

The major original contributions of this work include the follows:

- The causes of frequency mismatch during transients and frequency drift in steady-state in hybrid simulation have been identified. A remedy based on adaptive adjustment of the exchange interval was proposed and tested.

- The modeling of asymmetrical disturbances occurred within the hybrid simulation has been fully studied. In short, for any kind of disturbances, only positive-sequence fundamental frequency components of voltages and currents are needed by TS simulators.
- A quantitative measure based on the extraction quality of the transferring variables has been proposed for the selection of the interaction locations.
- A parallel interaction protocol based on the extraction prediction has been proposed. It allows the implementation of hybrid simulation to be able to run in real-time.

Based on the findings from this research, a parallel hybrid simulator prototype has been built and tested on the New England 39 bus system. Test results showed that the accuracy of the parallel implementation is comparable with the serial version. The performance of the simulation was assessed from both EMT and TS point of view. It allows practicable simulation of extensive interconnection power systems subject to an extended contingency lists and provides the capability of ‘zooming in’ on parts of the system, for example, power electronic devices such as FACTS or HVDC.

Chapter II ELECTROMAGNETIC TRANSIENT SIMULATION

II.1 INTRODUCTION

Electromagnetic transients refer to the transients that involve the interaction between the energy stored in the magnetic field of inductors and electric field of capacitors in power system. The transients are usually in the range of from microseconds to a few periods (a period is 20 microseconds for a 50Hz system).

Accurate dynamic simulation for the transients is essential in power system design to minimize the disruption and possible damage of equipment due to the overvoltages and overcurrents caused by disturbances. Any study related to individual devices, such as protection relays and power electronic devices, must involve electromagnetic transients simulation before the devices are commissioned into operation, because electromagnetic transients simulation can provide the most accurate and detailed resolution to all types of transients. However, because of the small time step, the powerful capability is compromised by high demands on computational resources. Consequently, electromagnetic transients simulators are not ideal tools to study dynamics and security of large size network.

Component modeling must be tailored to the scope of study. The main criterion for the selection of modeling is the time span of the study and the solution time step. For instance, when analyzing fast transients, such as lightning phenomena, stray capacitances and inductances must be represented and the solution step size needs to be at least one tenth of the smallest time constant introduced by the stray parameters.

Regardless of the type of system equivalent and size of the integration steps, the concept proposed by Dommel [1] is now universally accepted for the simulation of complex power systems containing non-linearities, power electronic components and their controllers. A number of EMT simulators have been developed by different research groups nowadays.

This chapter introduces electromagnetic transients simulation, based on the works in those references listed. Models of some commonly used components in power system are presented and a simulation of 9-bus system is presented to demonstrate the capability of EMT simulators. Discussion is also presented on how to overcome their limitation on high demand of computational resource.

II.2 COMPONENTS MODELING

Modeling of major components in power networks will be discussed in brief in this section in order to give a general understanding of electromagnetic transients simulation. Under the following modeling techniques, individual branches are converted to companion circuits which are assembled into node equations and parallel current sources.

II.2.1 SYNCHRONOUS MACHINE MODEL [2]

For general purpose, the electrical part of synchronous machine models discussed here is designed with three-phase ac armature windings (a, b, c) on the stator, a dc field winding (f) connecting to a source of direct current and a hypothetic winding (D) on direct axis, and two hypothetic windings (g, Q) on quadrature axis, as shown in Figure 2.1.

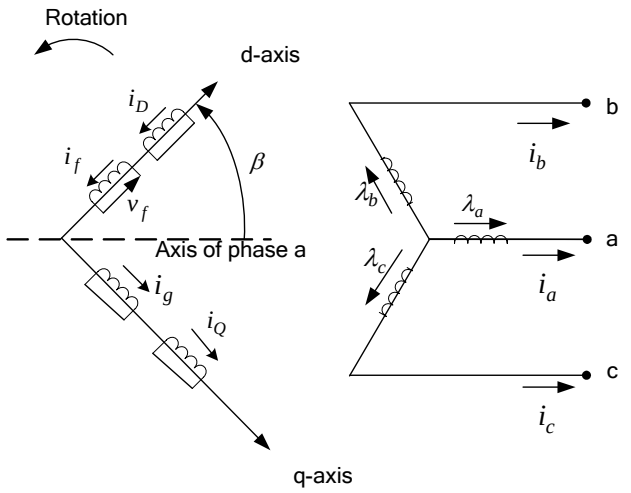

Figure 2.1: Stator and Rotor Circuits of a Synchronous Machine

Any modeling of generators must be established under a frame of modeling rules. The modeling used in the thesis follows the rules below.

The generation convention is used for all windings, that is, each winding k is described by:

$$v_k(t) = -R_k i_k(t) - \frac{d\lambda_k(t)}{dt} \tag{2.1}$$

In Park's original work [3], the direct axis is lagging 90 degrees behind the quadrature axis in the machine phasor diagram. Here the newly recommended leading position is adopted [4]. The rotor position relative to the stator is designated by the angle β by which the direct axis lead the axis of phase a.

In the process of modeling, a number of idealized and reasonable characteristics [2] are needed to make the modeling manageable.

In the modeling, transformation between coordinate frames is commonly used to deal with the fact that the 7 inductances are functions of time through their dependence on β. Park transformation decouples the equations on direct, quadrature and zero axes.

$$[\lambda_{dq0}] = [T]^{-1}[\lambda_{abc}]$$

where

$$[T]^{-1} = \begin{bmatrix} \frac{\sqrt{2}}{\sqrt{3}}\cos\beta & \frac{\sqrt{2}}{\sqrt{3}}\cos(\beta-120^\circ) & \frac{\sqrt{2}}{\sqrt{3}}\cos(\beta+120^\circ) & 0 & 0 & 0 & 0 \\ \frac{\sqrt{2}}{\sqrt{3}}\sin\beta & \frac{\sqrt{2}}{\sqrt{3}}\sin(\beta-120^\circ) & \frac{\sqrt{2}}{\sqrt{3}}\sin(\beta+120^\circ) & 0 & 0 & 0 & 0 \\ \frac{1}{\sqrt{3}} & \frac{1}{\sqrt{3}} & \frac{1}{\sqrt{3}} & 0 & 0 & 0 & 0 \\ 0 & 0 & 0 & 1 & 0 & 0 & 0 \\ 0 & 0 & 0 & 0 & 1 & 0 & 0 \\ 0 & 0 & 0 & 0 & 0 & 1 & 0 \\ 0 & 0 & 0 & 0 & 0 & 0 & 1 \end{bmatrix} \tag{2.2}$$

with $[\lambda_{dq0}] = [\lambda_d \quad \lambda_q \quad \lambda_0 \quad \lambda_f \quad \lambda_g \quad \lambda_D \quad \lambda_Q]^T$

$[\lambda_{abc}] = [\lambda_a \quad \lambda_b \quad \lambda_c \quad \lambda_f \quad \lambda_g \quad \lambda_D \quad \lambda_Q]^T$

Eq. (2.2) is an orthogonal Park transformation. It therefore follows that $[T]=[T]^{-1}_{transposed}$. The matrix $[T]$ and $[T]^{-1}$ are normalized here. This has the advantage that the power is invariant under transformation, and that the inductance matrix in d, q, 0-quantities is always symmetrical.

Finally, the electrical part of generators can be described as the following equations

$$[v_{dq0}]=-[R][i_{dq0}]-\frac{d}{dt}[\lambda_{dq0}]+\begin{bmatrix}-\omega\lambda_q\\+\omega\lambda_d\\0\\0\\0\\0\\0\end{bmatrix} \tag{2.3}$$

where

$$\lfloor v_{dq0}\rfloor=\lfloor v_d \quad v_q \quad v_0 \quad v_f \quad 0 \quad 0 \quad 0\rfloor$$

$$\lfloor i_{dq0}\rfloor=\lfloor i_d \quad i_q \quad i_0 \quad i_f \quad i_g \quad i_D \quad i_Q\rfloor$$

$$[\lambda_{dq0}]=[\lambda_d \quad \lambda_q \quad \lambda_0 \quad \lambda_f \quad \lambda_g \quad \lambda_D \quad \lambda_Q]^T$$

$[R]=$ diag $R_a, R_a, R_a, R_f, R_g, R_D, R_Q$ (subscript “a” for armature)

$-\omega\lambda_q$ and $\omega\lambda_d$ = voltage speed (voltage induced in armature because of rotating field poles).

$$\begin{bmatrix}\lambda_d\\\lambda_f\\\lambda_D\end{bmatrix}=[L_{direct}]\begin{bmatrix}i_d\\i_f\\i_D\end{bmatrix} \tag{2.4a}$$

$$\begin{bmatrix}\lambda_q\\\lambda_g\\\lambda_Q\end{bmatrix}=[L_{quadrature}]\begin{bmatrix}i_q\\i_g\\i_Q\end{bmatrix} \tag{2.4b}$$

$$\lambda_0 = L_0 i_0 \tag{2.4c}$$

where

$$[L_{direct}] = \begin{bmatrix} L_d & M_{df} & M_{dD} \\ M_{df} & L_{ff} & M_{fD} \\ M_{dD} & M_{fD} & L_{DD} \end{bmatrix}$$ direct axis inductance in dq0 frame

$$[L_{quadrature}] = \begin{bmatrix} L_q & M_{qg} & M_{qQ} \\ M_{qg} & L_{gg} & M_{gQ} \\ M_{qQ} & M_{gQ} & L_{QQ} \end{bmatrix}$$ quadrature axis inductance in dq0 frame

L_0 = zero axis inductance in dq0 frame

The simplest model for the mechanical part is the single mass representation as used in stability studies

$$\begin{aligned} J\frac{d\omega}{dt} + D\frac{d\beta}{dt} &= T_{turbine} - T_{gen} \\ \frac{d\beta}{dt} &= \omega \end{aligned} \tag{2.5}$$

where

$J =$ moment of inertia of rotating turbine-generator mass

$\beta =$ rotor position , $\omega =$ speed

$D =$ damping coefficient for viscous and windage friction

$T_{turbine} =$ torque input to turbine

$T_{gen} =$ electromagnetic torque of generator

Eq. (2.5) is valid for quantities referred to the electrical or the mechanical side with the conversion as follows.

$$\begin{aligned} J_{elec} &= \frac{J_{mech}}{(p/2)^2} \\ \beta_{elec} &= \frac{p}{2}\beta_{mech} \\ D_{elec} &= \frac{D_{mech}}{(p/2)^2} \\ T_{elec} &= \frac{T_{mech}}{p/2} \end{aligned} \tag{2.6}$$

According to [2], for the turbine torque *it is best to assume that the turbine power* $P_{turbine} = \omega * T_{turbine}$ *remains constant*.

In Eq. (2.5) the moment of inertia *J* has two other equivalent quantities. They are *E* (in kWs), the kinetic energy at synchronous speed which is identical for the mechanical and electrical side, and *h* (in second), the inertia constant which is a function of *E* and *S* (in kVA).

$$E = \frac{1}{2} J\omega^2 \tag{2.7}$$

$$h = \frac{E}{S} \tag{2.8}$$

The electromagnetic torque and the rotor position of the generator provide the link between the equations of the electrical and mechanical part.

$$\begin{aligned} \beta_{elec} &= \frac{p}{2}\beta_{mech} \\ T_{elec} &= \lambda_d i_q - \lambda_q i_d \end{aligned} \tag{2.9}$$

A single mass representation is usually adequate for hydro units, where turbine and generator are close together on a stiff shaft. It is not good enough, however, for thermal units, if subsynchronous resonance or similar problems involving torsional vibrations are being studied. In such cases, a number of lumped masses must be represented [5-9].

Generally speaking, the parameters which are needed in the systems of Eqs. (2.4a)-(2.4c) are not directly available from calculations or measurements. According to IEEE standards [10,11] the known quantities are armature resistance R_a, armature leakage reactance X_l, zero-sequence reactance X_0, transient reactances $X_d^{'}, X_q^{'}$, subtransient reactances $X_d^{''}, X_q^{''}$, transient short-circuit time constants $T_d^{'}, T_q^{'}$, and subtransient short-circuit time constants $T_d^{''}, T_q^{''}$.

The reason for short-circuit time constants being preferred as test data instead of open-circuit time constants is that the measurement of the latter is influenced by

saturation effects. In EMTP Theory Book [2], the Canay method is considered as the best data conversion procedure [12].

The above description is the traditional modeling of synchronous generators. Another, more modern approach is to measure the frequency response from the terminals. The measurement can be used to represent the machine with transfer functions between the terminals, without assuming a given number of lumped windings. One can also use curve-fitting techniques to match this measured response with that from a series and parallel combination of R-L branches [13,14]. According to the reports, the modeling in the latter case has basically the same effect as the traditional ones, except that the bars are sometimes represented by more than one winding, and the data are obtained from frequency response tests.

Completing the modeling of synchronous generators, electromagnetic transient simulation has to solve how to interface it with the rest of the network. The method generally available was firstly proposed in [15], where the authors opted for an iterative solution at each time step. The rest of the system is represented by a three-phase Thevenin equivalent circuits, as seen from the machine terminals. Brandwajn suggested another alternative. He used the iterative approach also, but dealt with the machine as an internal voltage source behind some impedance. The voltage source is recomputed for each time step, and the impedance becomes part of the nodal conductance matrix [2]. This is the actual simulation scheme used in some non-real time electromagnetic transient simulators.

II.2.2 TRANSFORMER

Transformers are represented as mutual coupled windings if the exciting current is not ignored. For a two windings transformer, illustrated in Figure 2.2, the voltages across the windings can be expressed as,

$$\begin{bmatrix} v_p \\ v_s \end{bmatrix} = \begin{bmatrix} R_p & 0 \\ 0 & R_s \end{bmatrix} \begin{bmatrix} i_p \\ i_s \end{bmatrix} + \begin{bmatrix} L_{pp} & L_{ps} \\ L_{sp} & L_{ss} \end{bmatrix} \frac{d}{dt} \begin{bmatrix} i_p \\ i_s \end{bmatrix} \tag{2.10}$$

where R_p and R_s are resistance of primary and secondary windings, respectively, L_{pp} and L_{ps} are the self-inductance of primary and secondary windings, respectively, L_{sp} and L_{ss} are the mutual inductance of primary and secondary windings, respectively. The mutual coupling is bilateral, i.e. $L_{ps} = L_{sp}$

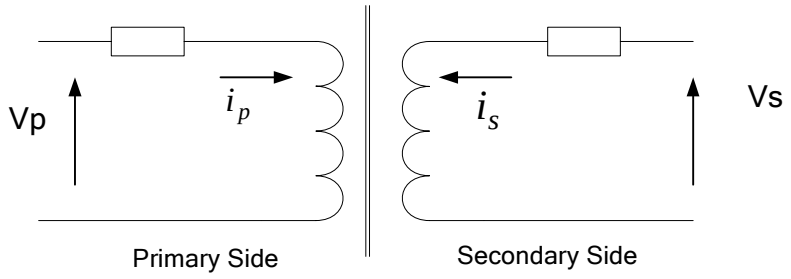

Figure 2.2: Equivalent Circuit of a Two-Winding Transformer

Normally, transformer data are not available in this format. Instead, either results from short-circuit and open-circuit tests are available or the magnetizing current and leakage reactances are given based on machine rating. Most programs can convert them internally.

In reference [2], two commonly encountered problems are listed in the case of transformer modeling, i.e. ill-conditioning because the inductance matrix of Eq. (2.10) is almost singular, and floating delta-connection windings as shown in Figure 2.3. The solutions are discussed too.

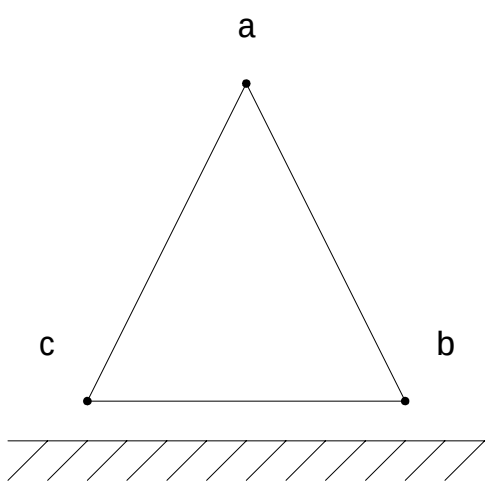

Figure 2.3: Floating Delta-Connected Windings

II.2.3 TRANSMISSION LINES

The three transmission-line models commonly used in electromagnetic transient simulation are π sections, Bergeron and frequency-dependent line; the latter two being classed as traveling wave models.

The π section model is used for short lines, where the travel time is less than the time step. This corresponds to approximately 15km for using a $50\mu s$ time step. Typically, this model is adopted in distribution rather than transmission system, and is unsuitable for long lines as the number of π sections required for an adequate representation makes the solution very inefficient.

Bergeron's method uses distributed parameters; that is, the effects represented by the parameters are distributed throughout the length of the line. In three-phase line case, the equations are first written down in the modal domain, where the coupled three-phase line appears as if it consists of three single-phase lines. Since the solution for single-phase lines is already known, this is straightforward. For solving the line equations together with the rest of the network, which is always defined in phase quantities, these modal equations must then be transformed to phase quantities through $\alpha, \beta, 0-$ transformation.

If the line is assumed transposed, the line performance on a per-phase basis can be analyzed as shown in Figure 2.4.

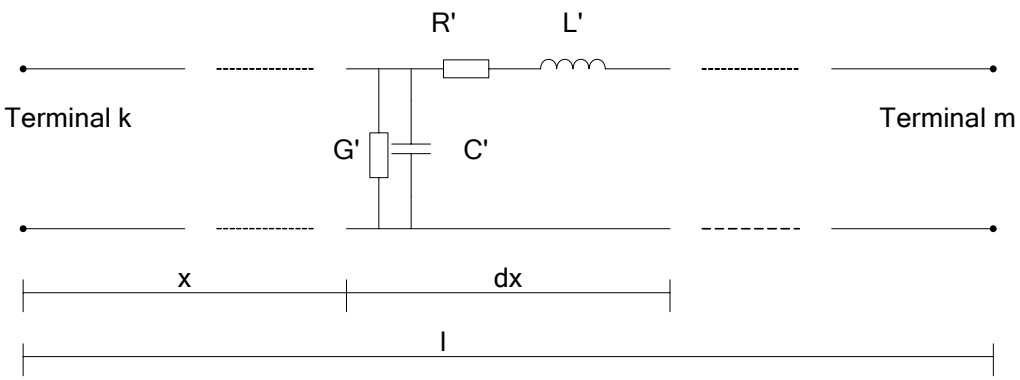

Figure 2.4: Distributed-Parameter Modeling of a Transmission Line

For the simplest lossless distributed parameter line, the solutions in wave propagation form are

$$\begin{aligned} i_{k,m}(t) &= \frac{1}{Z} v_k(t) + hist_k(t-\tau) \\ i_{m,k}(t) &= \frac{1}{Z} v_m(t) + hist_m(t-\tau) \end{aligned} \tag{2.11}$$

with equivalent current sources $hist_k$ and $hist_m$, which are known at state t from the past history at time $t-\tau$,

$$\begin{aligned} hist_k(t-\tau) &= -\frac{1}{Z} v_m(t-\tau) - i_{m,k}(t-\tau) \\ hist_m(t-\tau) &= -\frac{1}{Z} v_k(t-\tau) - i_{k,m}(t-\tau) \end{aligned} \tag{2.12}$$

where $Z = \sqrt{\frac{L'}{C'}}$ is the surge impedance, and $\tau = \frac{l}{v} = l\sqrt{L'C'}$ is the travel time.

Figure 2.5 shows the corresponding equivalent impedance network.

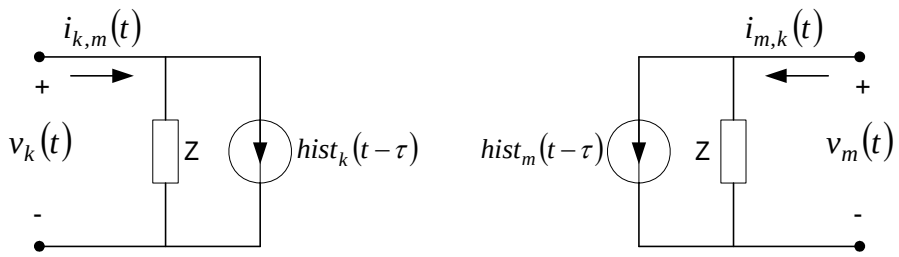

Figure 2.5: Equivalent Circuit of Transmission Line

The solution is exact as long as the travel time τ is an integer multiple of the step size Δt. If this is not the case, techniques such as linear interpolation must be used.

The distributed series resistance of the line is dealt with by treating the line as three sections of lossless lines and adding R/4 at both ends and R/2 in the middle, as shown in Figure 2.6. Full equations are detailed in the Theory Book [2].

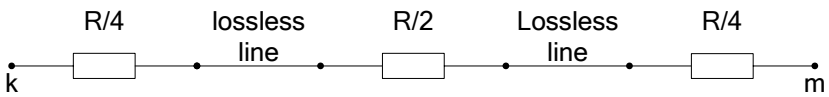

Figure 2.6: Line Representation with Lumped Resistances

In many cases traveling wave solutions are reasonable accurate to take into account the effect of constant distributed constant L', C' and constant lumped R, there are also cases where the frequency dependence, especially of the zero sequence impedance, could not be ignored. In the case, frequency-dependent modeling must be employed to represent transmission lines [16-23].

II.2.4 LINEAR LUMPED ELEMENTS

For the inductance L, we have $v_L = L\dfrac{di_L}{dt}$. Using trapezoidal rule of integration yields the branch equation,

$$i_L(t) = \frac{\Delta t}{2L} v_L(t) + \frac{\Delta t}{2L} v_L(t-\Delta t) + i_L(t-\Delta t) \tag{2.13}$$

For the capacitance C, we have $i_C = C\dfrac{dv_C}{dt}$. Using trapezoidal rule of integration yields the branch equation,

$$i_c(t) = \frac{2C}{\Delta t} v_C(t) - \frac{2C}{\Delta t} v_C(t-\Delta t) - i_c(t-\Delta t) \tag{2.14}$$

The equivalent impedance networks for L and C are shown in Figure 2.7.

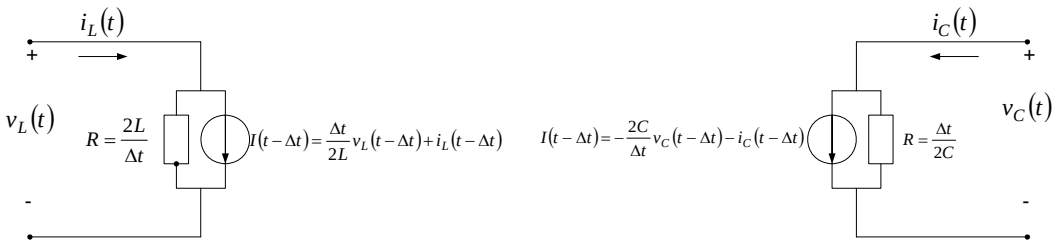

(a) Inductor (b) Capacitor

Figure 2.7: Equivalent Circuit of Inductor and Capacitor

Magnetically coupled circuits are much more prevalent in power systems. Coupled lumped elements appear primarily in the three-phase π - circuit representation of transmission lines. The equation for coupled elements has similar form to that of uncoupled elements, except replacing scalars to vectors or matrices.

$$\begin{aligned} [i_L(t)] &= \frac{\Delta t}{2}[L]^{-1}[v_L(t)] + \frac{\Delta t}{2}[L]^{-1}[v_L(t-\Delta t)] + [i_L(t-\Delta t)] \\ [i_C(t)] &= \frac{2}{\Delta t}[C]^{-1}[v_C(t)] - \frac{2}{\Delta t}[C]^{-1}[v_C(t-\Delta t)] - [i_C(t-\Delta t)] \end{aligned} \tag{2.15}$$

II.2.5 POWER ELECTRONIC DEVICES

Power electronic devices, which appear in HVDC links and FACTS devices, are featured by the behavior of unspecifiable switching discontinuities with intervals often within the millisecond range. Considerable effort is being made to accommodate the presence of the power electronics components, within the framework of the trapezoidal discretization technique. However, there are some disadvantages of this approach.

As the occurrences of the discontinuities do not coincide with the discrete time intervals used by the fixed trapezoidal techniques, a relatively small time step is required to avoid spikes whenever switching takes place and therefore renders less effective. It is difficult to change the time step dynamically during the simulation run, because that would mean re-calculation of the nodal matrix and history value vector and re-inverse of the matrix, a premium in terms of CPU time for the overall simulation.

For the above mentioned reason, references [24-26] decide to use an alternative approach in modeling the HVDC and FACTS, featured by power electronic devices, by developing a stand-alone state variable model for the HVDC and FACTS, but retaining the powerful network modeling capabilities for modeling the external network. This formulation permits the use of variable step length integration, capable of locating the exact instants of switching and hence avoiding the appearance of spurious spikes in the waveforms.

II.3 SOLUTION TECHNIQUES

II.3.1 NODAL EQUATIONS

Once all the network components are represented by an equivalent current source and a resistance in parallel, a nodal formulation is used to solve for complete system. The nodal equation is:

$$[G][v(t)] = [i(t)] + \lfloor I_{history} \rfloor \tag{2.22}$$

where $[G] =$ conductance matrix,

$[v(t)] =$ vector of nodal voltages at time t,

$[i(t)] =$ vector of injected node currents at time t, and

$\lfloor I_{history} \rfloor =$ known current vector which is made up of known equivalent current sources.

For linear time-invariant network, the elements of [G] are dependent on the time step, by keeping the time step constant, [G] is constant and triangular factorization can be performed before entering the time loop.

II.3.2 NUMERICAL OSCILLATION

The numerical oscillation which occurs in the voltages across inductances at points of discontinuities in di/dt, or in current through capacitances at points of discontinuities in dv/dt, oscillates around the correct answer.

Assume an inductance L, the through current is shown in Figure 2.8 (a). Before T, the current is $i = kt$, it falls steadily to zero at T. Thus, the voltage across the inductance is kL before T. At T, voltage will fall instantaneously to zero, since $di/dt = 0$, as shown in Figure 2.8 (b).

The trapezoidal integration equation for the inductor is Eq. (2.18). From $(t + \Delta t)$ onwards

$$i_L(t) = i_L(t - \Delta t) = 0$$

so

$$v_L(t) = -v_L(t - \Delta t)$$

The inductor voltage consequently oscillates between $\pm kL$ instead of falling to zero (Figure 2.8(c)). However, the average inductor voltage is correct at zero, the chatter does not grow larger.

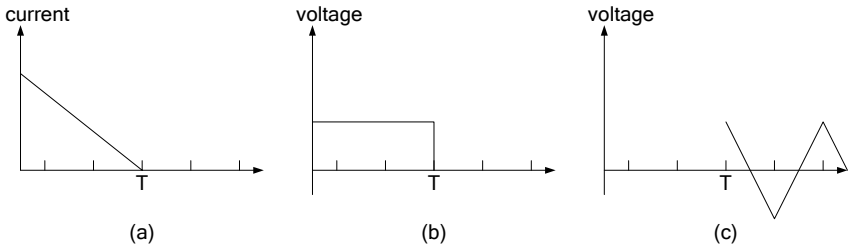

Figure 2.8: Numerical Oscillation at Discontinuity

The numerical oscillation had been noticed in [27-29]. The critical damping adjustment scheme (CDA) was developed in [28,29] to deal with the problem. It uses the trapezoidal rule for the normal part of the simulation and temporarily changes to the backward Euler rule to go over discontinuities.

II.3.3 ROOT-MATCHING TECHNIQUES

The oscillation problem is associated with the numerical error of the trapezoidal rule, i.e. it is inherent in the numerical integrator substitution method. In [30,31], an always numerical stable and more efficient technique, root-matching method, was proposed to solve the numerical oscillation.

The root-matching objective in simulation is to form a system of difference equations whose dynamics are similar to the dynamics of the continuous system to be simulated. Since the dynamics of the continuous system are completely characterized by its roots and final value, it seems appropriate to make the roots and final value of the simulating difference equation match those of the system being simulated. This objective can be met for transfer functions by a 9-step algorithm [32].

Root-matching is only formulated for the branches containing at least two or more elements (i.e. RL, RC, RLC, LC…). The performance comparison between Dommel's method and root-matching can be found in [31].

According to the 9 steps, the Norton equivalent of RL branch derived by root-matching methods is

$$i(t) - e^{-\frac{R}{L}T} i(t-\Delta t) = \frac{1-e^{-\frac{R}{L}T}}{R} v(t) \tag{2.23}$$

The equivalent of RC branch is somewhat complicated

$$i(t) - e^{-\frac{T}{RC}} i(t-\Delta t) = \frac{C\left(1-e^{-\frac{T}{RC}}\right)}{T} v(t) - \frac{C\left(1-e^{-\frac{T}{RC}}\right)}{T} v(t-\Delta t) \tag{2.24}$$

II.3.4 PARALLEL COMPUTATION

The presence of transmission lines in the system being simulated introduces decoupling into the conductance matrix. This is because the transmission line model injects current at one terminal as a function of the voltage and current at the other previous time steps. In the present time step, there is no dependence on electrical conditions at distant terminal of the line, leading to a block diagonal conductance matrix.

Figure 2.9(a) illustrates coupled systems that are to be separated into subsystems. Each subsystem in Figure 2.9(b) is represented in the other by a linear equivalent. The Norton equivalent is constructed using information from the previous time step.

Each decoupled block in the matrix corresponds to a subsystem, and can be solved at each time step independently of all other subsystems. The characteristics can be utilized to convert a large dimension matrix to a number of small dimension matrices. By mapping the matrices onto multiple computation processes, lots of computation cost can be saved. This is the basic idea of parallel computation for electromagnetic transient simulation.

The decoupled feature of transmission lines model sheds the light on real-time electromagnetic transient simulation. By distributing multiple processes to multiple processors, all computation tasks are completed within required time interval. Then processes begin to communicate each other and prepare for the next round computation. Except the nature decoupled feature, some changes have to be made on some components modeling to be suitable for real-time computation [33-35].

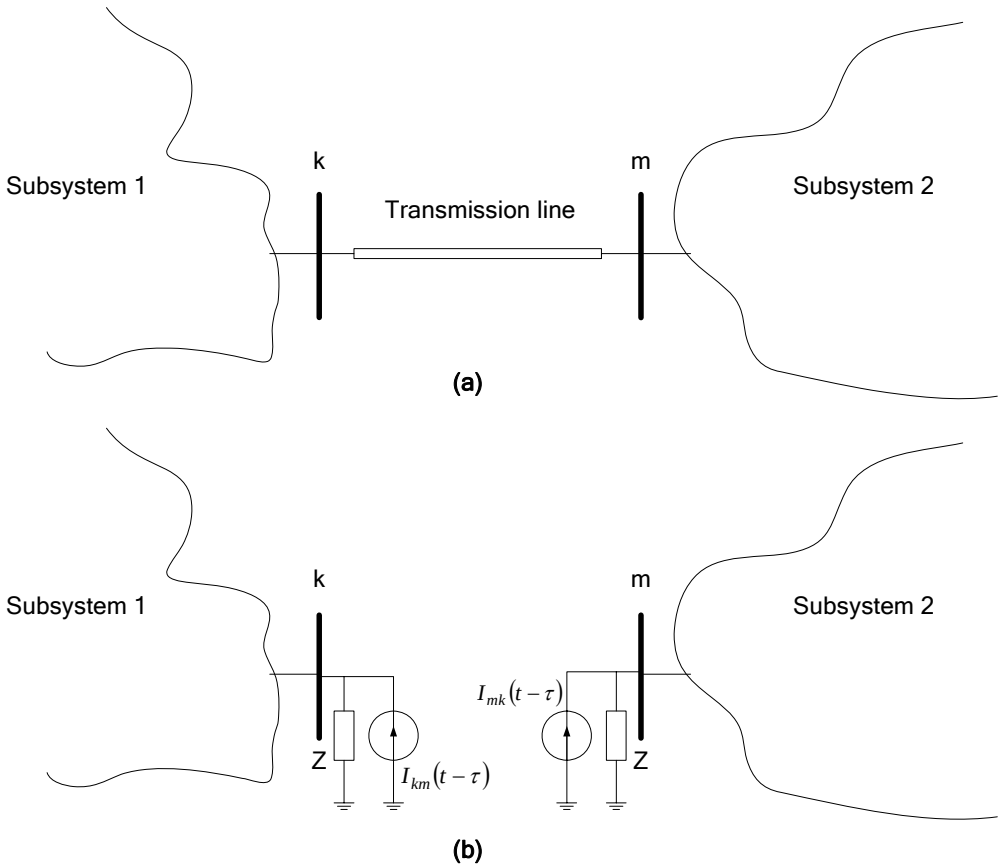

Figure 2.9: Subsystems in Parallel Computation

II.4 ELECTROMAGNETIC TRANSIENTS SIMULATORS

In nowadays, there already exist several electromagnetic transients simulators developed by different groups. Most of them are based on Dommel's method.

II.4.1 DCG/EMTP

The ElectroMagnetic Transient Program was originally developed by Professor Hermann W. Dommel, and is now believed to be a standard.

II.4.2 ATP

ATP was started from a copy of BPA's public-domain EMTP. The use of ATP is limited in those non-profitable areas.

II.4.3 PSCAD/EMTDC [36,37]

EMTDC (electromagnetic transient and d.c.) is an implementation of the EMTP-type method, initially designed for the solution of ac-dc power system. PSCAD acts as a powerful and flexible graphical user interface to the EMTDC transients and POWER FLOW simulation engines.

II.4.4 RTDS [38]

The Real Time Digital Simulator (RTDS) is essentially a parallel processor implementation of the EMTDC program (although quite different in detail). Through careful coding, the EMTDC algorithm and component models have been distributed over many processors running in parallel, so that the simulation can proceed in real time for time steps typically in the 50-75 microseconds range.

II.4.5 HYPERSIM [39]

Hypersim is an all-digital real-time simulator developed by the power system simulation laboratory, IREQ, in Canada. It can be used to model a medium-sized transmission system and interface it with control system hardware, such as protection relays or more complex systems such as AC/DC converter controls and other FACTS controllers.

II.4.6 ARENE

ARENE is a Real-Time Digital Electromagnetic Transient Power System Simulator, developed by EDF (Electricite de France).

II.4.7 POWER SYSTEM BLOCKSET

Except the simulators based on Dommel's method, state variable analysis [40] is an alternative approach to electromagnetic transient simulation. State variable analysis was the dominant technique for transient simulation prior to the appearance of Dommel's numericl integration substitution. Due to their suitability to model non-linearities, state variables are still used for the modeling of some components. In particular they are suited to the modeling of frequent switching, as they require no overhead to change the step length. Their main disadvantages are solution speed and code complexity; also the modeling of components with distributed parameters becomes more difficult in the state variable analysis. Power System Blockset (PSB) under Matlab was developed using the state variable analysis approach.

II.5 EXAMPLE

In this section, an electromagnetic transients simulation was performed on a 9-bus system (as shown in Appendix A1). The system as a whole was simulated in DCG/EMTP. There are no exciters and prime movers in the three machines' modelings. Of the three transformers, the secondary windings (high voltage) are in Wye-grounded connection, and the primary windings (low voltage) are in delta connection. Transmission lines are represented by distributed-parameter models. Three loads are modeled as constant impedances.

A three-phase solid fault was applied at bus 9, from 0.1 to 0.14 second. Waveforms of voltage on bus 5 were plotted in Figure 2.10, along with current waveforms flowing through line 5-9 showed in Figure 2.11. Output currents from generator 1 were also given in Figure 2.12.

From the curves, it is obvious that under disturbances, both bus voltages and line currents are distorted by many harmonics. Additionally, dc offset components are presented in the currents.

From the figures, it is clear that electromagnetic transient simulators do give very detailed broadband outputs of any component, which is the most significant advantage over other kinds of digital simulators.

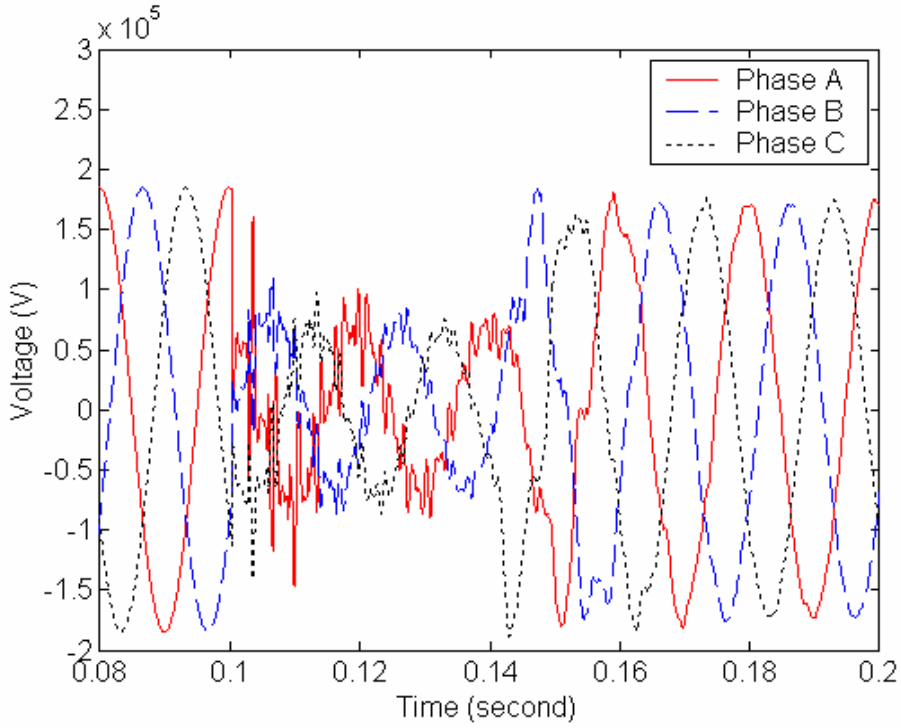

Figure 2.10: Bus 5 Voltage Waveforms

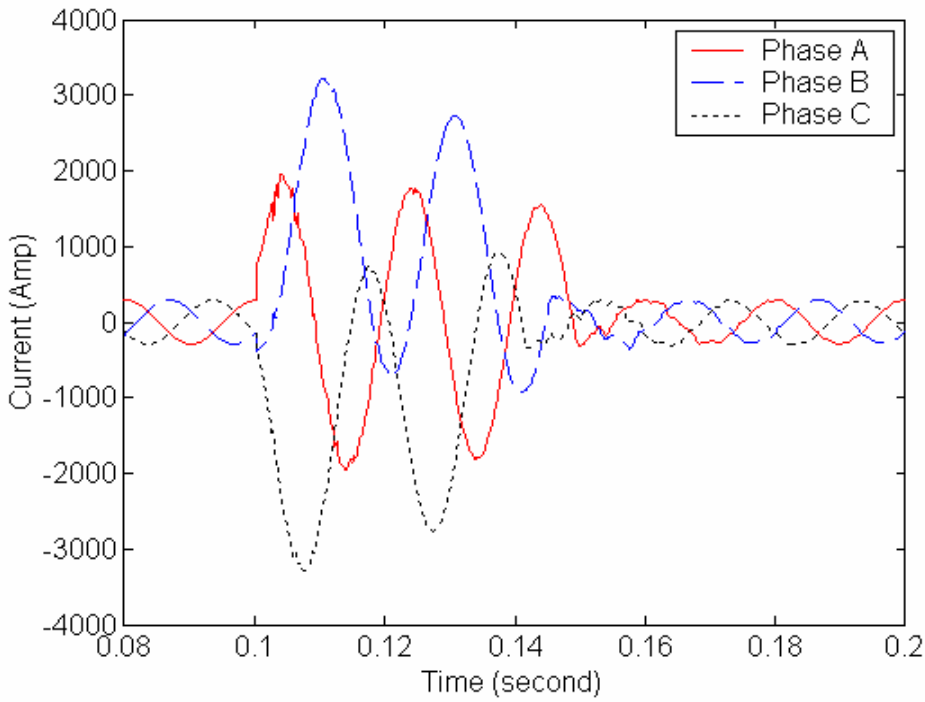

Figure 2.11: Line 5-9 Current Waveforms

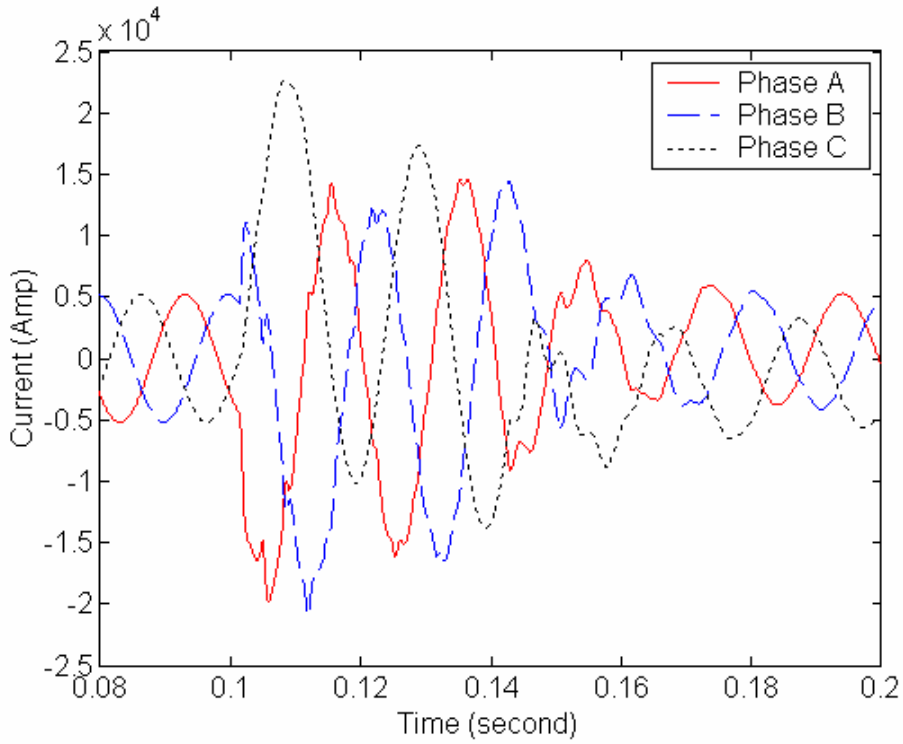

Figure 2.12: Generator 1 Output Current Waveforms

On the other hand, because of the detailed device level modeling and small time step, electromagnetic transient simulators require much more computational resources. For example, for the above simulation on the 9-bus system, on a PC with Intel P4 1.7 GHz CPU the 4-second electromagnetic transients simulation with time step of 50μs takes around 11 actual seconds. The common way to speed up the simulation is to use more hardware resource, such as multi-processor parallel computer. For example, the full 735kV Hydro-Quebec network, using standard components such as AC sources, transmission lines, circuit breakers and saturable transformers, has been simulated in real-time on a 32 processors Origin 2000 with a 60 microseconds time step [41].

Speeding-up the electromagnetic transients simulators is a very attractive research topic. Given the modern scalable digital computers, the simulators become more and more powerful. However, there has to be a limit, and it is unlikely "conventional" electromagnetic transient simulators will ever practically represent fully a two thousand-bus system. An interesting idea is to integrate the

electromagnetic transient simulators with other kind of digital simulators to simulate large-size power systems together. Transient stability simulators, which will be introduced in chapter 3, are one of the best choices.

II.6 CONCLUSION

The most commonly concerned aspects of EMT simulation have been introduced in the chapter. Its powerful capability of detailed analysis is based on device-level modeling and small integrated time step. This advantage can be fully exploited in the proposed hybrid simulation to simulate those non-linear, switching components, such as power electronics devices. However, for the consideration of the overall performance, the part of network simulated by EMT simulators in the hybrid simulation should be minimal in order to minimize the total computational resources.

Chapter III TRANSIENT STABILITY SIMULATION

III.1 INTRODUCTION

The stability problem is connected with the behavior of the synchronous machines after they have been perturbed. If the perturbation does not involve any net change in power, the machines should return to their original state. If an unbalance between the supply and demand is created by a change in load, in generation, or in network conditions, a new operating state is necessary. In any case all interconnected synchronous machines should remain in synchronism if the system is stable; i.e. they should all remain operating in parallel and at the same speed.

The transient following a system perturbation is oscillatory in nature, but if the system is stable, these oscillations will be damped toward a new quiescent operating condition. These oscillations, however, are reflected as fluctuation in power flow over the transmission lines. If a certain line connecting two groups of machines undergoes excessive power fluctuation, it may be tripped out by its protective equipment thereby disconnecting the two groups of machines.

Distinction should be made between large impacts and smaller and more normal random impacts. Faults on the high-voltage transmission network or the loss of a major generating unit are examples of large impacts. If one of these large impacts occurs, the synchronous machines may lose synchronism. This problem is referred to as the transient stability problem. Transient stability problem depends strongly upon the magnitude and location of the disturbance and the initial state or operating condition of the system.

In the dynamics of the transition from one operating point to another, to adjust for load changes, the stability of machines will be determined by many factors. The problem of studying the stability of synchronous machines under the condition of small load changes has been called steady-state stability or a more recent and

certainly more appropriate name - dynamic stability. In contrast to transient stability, dynamic stability tends to be a property of the state of the system. Transient stability and dynamic stability are both questions that must be answered to the satisfaction of the engineer for successful planning and operation of the system in spite of the fact that an artificial separation between the two problems has been made in the past. This was simply a convenience to accommodate the different approximations and assumptions made in the mathematical treatments of the two problems.

III.2 COMPONENTS MODELING

In transient stability simulation, power system components modeling are relative simpler than those in electromagnetic transient simulation, since a larger integration time step is used. Components parameters are in phasor value under system frequency, even during transients. As a matter of fact, all components except rotating machines and controllers use the same model as in power flow analysis.

III.2.1 SYNCHRONOUS MACHINES [42-44]

For convenience, the electrical equations after Park transformation for synchronous machines developed in Chapter 2 are rewritten as Eq. (3.1).

$$\left[v_{dq0}\right] = -\left[R\right]\left[i_{dq0}\right] - \frac{d}{dt}\left[\lambda_{dq0}\right] + \begin{bmatrix} -\omega\lambda_q \\ +\omega\lambda_d \\ 0 \\ 0 \\ 0 \\ 0 \\ 0 \end{bmatrix} \tag{3.1}$$

However, this synchronous machines model still cannot be used directly for system stability studies. A variety of degrees of simplification [42] are required for the representation of synchronous machines in stability studies. The simplified Eq. 3.1 is in the algebraic form with the electrical speed ω set to 1.

In practice, a more common set of equations is used in transient stability studies. Notations such as subtransient and/or transient reactances, voltages behind subtransient and/or transient reactances and time constants are adopted in the formulation of the equations. Also, there are several versions in the form due to different simplifications to the synchronous machine model.

With the armotisseurs included (one on direct axis and two on quadrature axis), electrical equations are

$$\begin{cases} v_d = -ri_d + e_d^{''} + x_q^{''} i_q \\ v_q = -ri_q + e_q^{''} - x_d^{''} i_d \\ pe_q^{''} = \dfrac{1}{T_{d0}^{''}}\left[-e_q^{''} - \left(x_d^{'} - x_d^{''}\right)i_d + e_q^{'}\right] \\ pe_d^{''} = \dfrac{1}{T_{q0}^{''}}\left[-e_d^{''} + \left(x_q^{'} - x_q^{''}\right)i_q + e_d^{'}\right] \\ pe_q^{'} = \dfrac{1}{T_{d0}^{'}}\left[-e_q^{'} - \left(x_d - x_d^{'}\right)i_d + e_f\right] \\ pe_d^{'} = \dfrac{1}{T_{q0}^{'}}\left[-e_d^{'} + \left(x_q - x_q^{'}\right)i_q\right] \end{cases} \tag{3.2}$$

where

$e_d^{''}$ = voltage behind subtransient circuit on d-axis

$e_q^{''}$ = voltage behind subtransient circuit on q-axis

$e_d^{'}$ = voltage behind transient circuit on d-axis

$e_q^{'}$ = voltage behind transient circuit on q-axis

e_f = voltage proportional to field voltage v_f

$x_d^{''}$ = subtransient reactance on d-axis

$x_q^{''}$ = subtransient reactance on q-axis

$x_d^{'}$ = transient reactance on d-axis

$x_q^{'}$ = transient reactance on q-axis

T''_{do} = open-circuit subtransient time constant on d-axis

T''_{qo} = open-circuit subtransient time constant on q-axis

T'_{do} = open-circuit transient time constant on d-axis

T'_{qo} = open-circuit transient time constant on q-axis.

With only one amortisseur winding (on q-axis), electrical equations are

$$\begin{cases} v_d = -ri_d + e'_d + x'_q i_q \\ v_q = -ri_q + e'_q - x'_d i_d \\ pe'_q = \dfrac{1}{T'_{d0}}\left[-e'_q - \left(x_d - x'_d\right)i_d + v_f\right] \\ pe'_d = \dfrac{1}{T'_{q0}}\left[-e'_d + \left(x_q - x'_q\right)i_q\right] \end{cases} \tag{3.3}$$

where symbols have the same meanings as defined above.

The flux-decay model assumes the flux of the only amortisseur to be constant, and this result in only one differential equation remaining. The electrical equations become

$$\begin{cases} v_d = -ri_d + e'_d + x'_q i_q \\ v_q = -ri_q + e'_q - x'_d i_d \\ pe'_q = \dfrac{1}{T'_{d0}}\left[-e'_q - \left(x_d - x'_d\right)i_d + v_f\right] \end{cases} \tag{3.4}$$

This is the simplest of all the synchronous machine models. By assuming e'_q constant throughout the study period, this model eliminates the only differential equation associated with the electrical characteristics of the machine. A further approximation, which simplifies the machine model significantly, is to ignore transient saliency by assuming $x'_d = x'_q$.

$$\begin{cases} v_d = -ri_d + e'_d + x'_q i_q \\ v_q = -ri_q + e'_q - x'_d i_d \end{cases} \tag{3.5}$$

Equations of motion in per unit in transient stability studies are

$$J\frac{d\Delta\omega}{dt}+D\frac{d\delta}{dt}=T_{turbine}-T_{gen}$$
$$\frac{d\delta}{dt}=\omega_0\Delta\omega \tag{3.6}$$

where $\omega_0 = 2\pi f_0$ electrical rad/s , $\Delta\omega =$ pu rotor speed deviation

Since we have assumed $\omega_0 = 1.0$ pu in the stator voltage equations, in per unit the air-gap torque is equal to the air-gap power.

$$T_{gen}=P_{gen}=P_{terminal}+R_aI_{terminal}^2=e_di_d+e_qi_q+R_aI_{terminal}^2 \tag{3.7}$$

The above equations are in the individual machine d-q reference frame which rotates with the machine's rotor. For the solution of the interconnecting transmission network equations, a synchronously rotating common x-y reference is used. The relationships shown in Figure 3.1 are used to transform variables from one reference frame to the other.

The variables under two reference frames can be transformed by using the following equation.

$$\left(v_d+jv_q\right)e^{j(\delta-\pi/2)}=v_x+jv_y \tag{3.8}$$

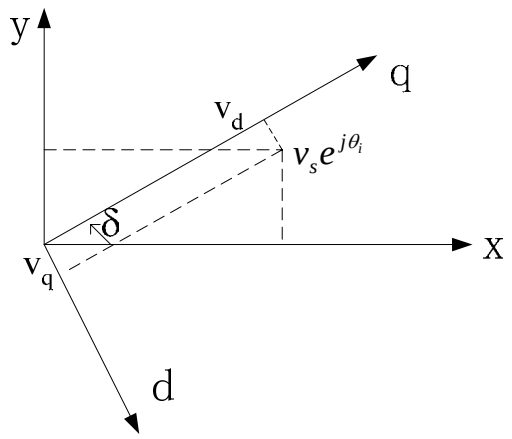

Figure 3.1: Relationship between xy and dq Reference Frames

III.2.2 PASSIVE ELEMENTS

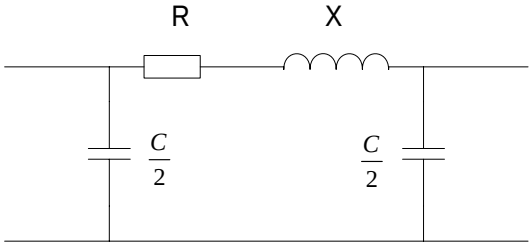

Figure 3.2: Pi-Representation of Transmission Lines

A π circuit with lumped parameters, as shown in Figure 3.2, can be used to represent the transmission lines.

R and X represent the total series resistance and reactance, C stands for the total capacitance. The resultant circuit model is called the normal π equivalent circuit.

Overhead lines may be classified according to length, based on the approximations justified in their modeling:

1. Short lines: lines shorter than about 80km. They have negligible shunt capacitance, and may be represented by their series impedance.
2. Medium-length lines: lines with lengths in the range of 80km to 200km. They may be represented by the nominal π equivalent circuit.
3. Long lines: lines longer than about 200km. For such lines the distributed effects of the parameters are significant. They may be represented by cascaded sections of short lengths, with each section represented by a nominal π equivalent.

In stability programs, two-winding transformers are represented by an impedance in series with a ideal transformer. In general, the impedance is located on the side with standard turns ratio (node 1). Thus, the mathematical model used by stability programs can be derived by follows,

$$
\begin{aligned}
i_1 &= \frac{v_1 - v_2/k}{z} = \frac{v_1}{z} - \frac{v_2}{kz} \\
i_2 &= -\frac{i_1}{k} = \frac{v_2}{k^2 z} - \frac{v_1}{kz}
\end{aligned}
\tag{3.9}
$$

III.2.3 HVDC LINKS AND FACTS DEVICES

The development and use of HVDC and FACTS systems for power transmission systems has led to the application of power electronic devices to improve the stability of power networks [45-53]. Many studies have been carried out and reported in the literature on the use of power electronics in a variety of voltage and angle stability applications, proposing diverse control schemes and location techniques for enhancing voltage and angle oscillation control [42,52,53].

Each HVDC and FACTS system tends to have unique characteristics tailored to meet the special needs of its application. However the models of HVDC links and FACTS devices, developed for transient stability, are all based on the assumption that voltages and currents are sinusoidal, balanced, and operate near fundamental frequency, which are typical assumptions in transient stability and power flow studies.

This imposes a fundamental limitation on the modeling of the system. In particular the effects of commutation failures, which are common for power electronic devices, cannot be accurately studied. Notwithstanding the above limitations, models of various degrees of detail have been effectively used to represent the HVDC links and FACTS devices, featured by the power electronic device, in stability studies.

III.3 SOLUTION METHOD

III.3.1 SOLVING DIFFERENTIAL-ALGEBRAIC EQUATIONS

Analysis of transient stability of power system involves the computation of their nonlinear dynamic response to large disturbances. The power stability

calculation is a differential-algebraic initial value problem as formulated in Eq. 3.10. Large infrequent discontinuities in the form of faults and branch switching are introduced into the algebraic transmission network equations, usually at predetermined times. Smaller random discontinuities occur due to limiting in the differential equations of the automatic control apparatus which gives the problem the characteristic of stiffness.

$$\begin{aligned} \dot{x} &= f\left(x, y\right) \\ 0 &= g\left(x, y\right) \end{aligned} \tag{3.10}$$

where $x = \text{state variables vector of the system}$, and

$y = \text{network variables vector of the system}$

The differential equations comprise the synchronous machines' stator differential equations and swing equations, and the equations of the associated control system. The algebraic equations consist of the stator algebraic equations and the network equations. The purpose of the stator algebraic equations is to express the generator currents under dq reference frame in terms of the stator variables and the network variables which are in network reference frame.

The network equations can be expressed in power-balance or current-balance form [44]. The latter form is more popular since the network-admittance matrix has to be re-factored only if there is a network change.

A wide range of approaches has been reported in reference [54] for solving these differential-algebraic equations, depending on the numerical networks and modeling details used. The many possible schemes for the solution of Eq. (3.10) are characterized in [42].

The partitioned solution with explicit integration is the traditional approach used widely in stability programs. Its advantages are programming flexibility and simplicity, reliability, and robustness. Its principle disadvantage is susceptibility to

numerical instability. For a stiff system, a small time step is required throughout the solution period, as dictated by the smallest time constant.

The simultaneous solution with implicit integration is numerically much more stable than the partitioned solution with explicit integration. Furthermore the derived nonlinear algebraic equations are very sparse, and this property can be used to improve computational efficiency.

III.3.2 SIMULATION OF UNSYMMETRICAL DISTURBANCES

Symmetrical Components

"Balanced operation of the power system allows for analysis of system performance by solving for the variables in only one of the phases in a manner similar to single-phase circuits. The solution of unbalanced three-phase circuit does not permit this simplification. The method of symmetrical components is preferred to deal with unbalanced condition since it offers considerable simplicity in the analysis of power system stability problems involving unbalanced faults." [42]

In a three-phase system, a set of three unbalanced phasors, say voltage, can be resolved into three balanced systems of phasors known as positive-, negative-, and zero-sequence through the following transformation, and visa versa.

$$\begin{bmatrix} V_{a0} \\ V_{a1} \\ V_{a2} \end{bmatrix} = \frac{1}{3}\begin{bmatrix} 1 & 1 & 1 \\ 1 & \alpha & \alpha^2 \\ 1 & \alpha^2 & \alpha \end{bmatrix}\begin{bmatrix} V_a \\ V_b \\ V_c \end{bmatrix} \tag{3.11}$$

$$\begin{bmatrix} V_a \\ V_b \\ V_c \end{bmatrix} = \begin{bmatrix} 1 & 1 & 1 \\ 1 & \alpha^2 & \alpha \\ 1 & \alpha & \alpha^2 \end{bmatrix}\begin{bmatrix} V_{a0} \\ V_{a1} \\ V_{a2} \end{bmatrix} \tag{3.12}$$

where operator α denotes 120 degrees phase shift.

In a symmetrical system there is no interaction between quantities of different sequences, currents of any one sequence may be considered to flow in an independent network associated with that sequence only. The single-phase equivalent

circuit composed of the impedances to currents of any one sequence is called the sequence network for that particular sequence. To analyze the system performance where there is an unbalanced fault, the sequence networks are interconnected at the fault location to represent the interaction between quantities of different sequence due to unbalanced created by the fault.

Sequence Impedances

The impedance of a circuit when positive-sequence currents alone are flowing is called the impedance to positive-sequence currents or positive-sequence impedance. Similarly, impedance to negative sequence currents is called negative-sequence impedance, and the impedance to zero-sequence currents the zero-sequence impedance.

The detailed representation of synchronous machines in the positive-sequence network appropriated for stability studies is discussed in section 3.2.

The detailed analysis of negative-sequence reactance can be found in reference [54-58]. Some of the major findings are summarized here.

$$X_2 = \frac{X_d'' + X_q''}{2} \tag{3.13}$$

$$R_2 = R_a + \frac{R_r}{2} \tag{3.14}$$

where R_r is the rotor total copper loss.

The swing equation Eq. (3.6) is appropriately modified to include the negative-sequence braking torque associated with R_r.

$$T_{b2} = \frac{R_r}{2} I_{a2}^2 = (R_2 - R_a) I_{a2}^2 \tag{3.15}$$

The zero-sequence resistance R_0 is slightly higher than the positive-sequence resistance R_1. The zero-sequence impedance is meaningful only when the machine is star-connected; otherwise there won't be any zero-sequence current flow.

In a symmetrical three phase static circuit, the positive- and negative-sequence impedances are identical because the impedance of such a circuit is independent of the phase order of the applied voltages.

For transformers, the equation of transformer developed in section 3.2 is applicable to the positive-sequence as well as the negative-sequence network. The impedance offered by a transformer to the flow of zero-sequence currents depends on the winding connections, which has been detailed described in [42].

Simulation of Different Types of Short-Circuited Faults

Now the simulation of a power system that is essentially symmetrical but is rendered unbalanced by an asymmetrical fault at a particular location in the system, as illustrated in Figure 3.3, is considered. Such faults can be analyzed by appropriately interconnecting positive-, negative-, and zero-sequence networks at the fault point as shown in Figure 3.4.

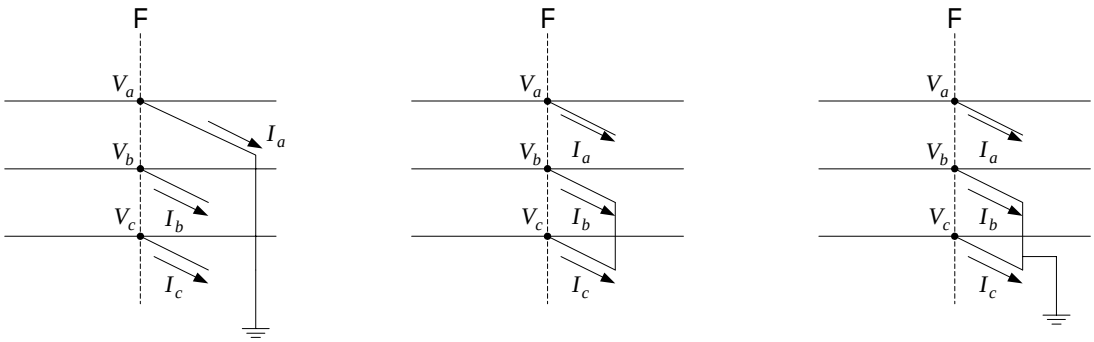

Figure 3.3: Asymmetrical Faults

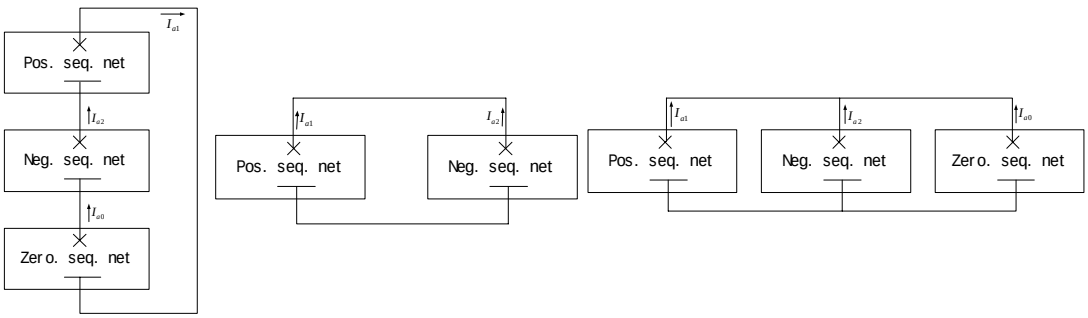

(a) Single-Phase-Ground (b) Double-Phase (c) Double-Phase-Ground

Figure 3.4: Equivalent Circuit of Asymmetrical Faults

III.3.3 PARALLEL ALGORITHM FOR TRANSIENT STABILITY

Parallel algorithms for transient stability have been a hot topic for decades [59-64]. The area of real-time transient stability simulation has attracted particular attention because there is a strong industrial need for fast on-line analysis to determine the dynamic security of power system. The advancement in parallel computer architecture has provided new powerful tools which are advantageous at solving large scale complex power system problems. Any breakthrough in the area will be of tremendous benefit to the power system operation and engineering efficiency.

The difficulty in the area lies in the fact that the elements in the network admittance matrix, state matrix and Jacobian matrix from Eq. (3.10) are correlated tightly. In transient stability modeling there is no time delay as in electromagnetic transient modeling. Thus the matrix cannot be partitioned into small dimensional diagonal block sub-matrices naturally. Some alternative approaches must be found.

Partitioning a network or a group of generators into subgroups among processors is the common way to achieve parallelism. Taking into account different buses connectivity and complexity of the differential equations, a good partition method can distribute even computation loads among processors. Among considerations of implementation, convergence and the number of iterations are the two most important factors. Many theoretically promising algorithms do not produce significant gains because of the inefficiency of implementation techniques.

HKPolyU has developed a real-time parallel-processor based transient stability program [65-67], which originated at the University of Bath, UK. This program can solve very large systems in real-time.

III.4 EXAMPLE

In this section, a transient stability simulation was performed on the same 9-bus system as used in the Chapter 2 example section. The system was simulated by

the BPA transient stability program. There are no exciters and prime movers in the generators' modeling. The high voltage windings are Wye-grounded, while the generator side windings are connected in delta. That means no zero-sequence current can flow through generators. Three loads are modeled as constant impedances.

A variety of faults were applied at bus 7, from 0.2 to 0.24 second. Swing curves of generators 2 and 3 with respect to generator 1 are plotted for each fault type. Figures 3.5(a) and 3.5(b) are swing curves for symmetrical fault, while Figures 3.6(a) and 3.6(b) are swing curves in case of single-phase-to-ground fault.

Because of the simplicity of the models and the relatively large time step, the transient stability simulation runs much faster then electromagnetic transient simulation. For the above 9-bus system, the actual computer time is noticeably smaller than one second. The following example can provide a better insight on the speed of transient stability simulation. On a UK power system consisting of 922 buses, 1533 lines, 122 generators and 10 SVCs, using the transient stability simulator with time step of 10 milliseconds developed in HKPolyU to simulate system dynamics caused by a three-phase fault for 30 seconds, the solution time on SGI-Origin 2100 (350 MHz) is only 3.9 seconds on a single processor.

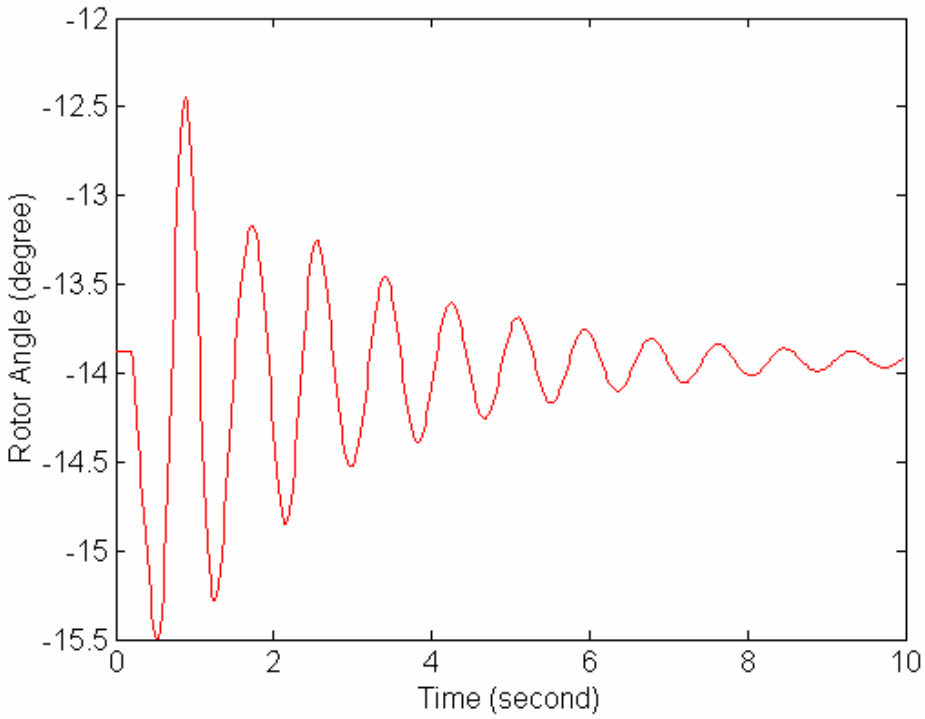

(a) Generator 2 vs. Generator 1

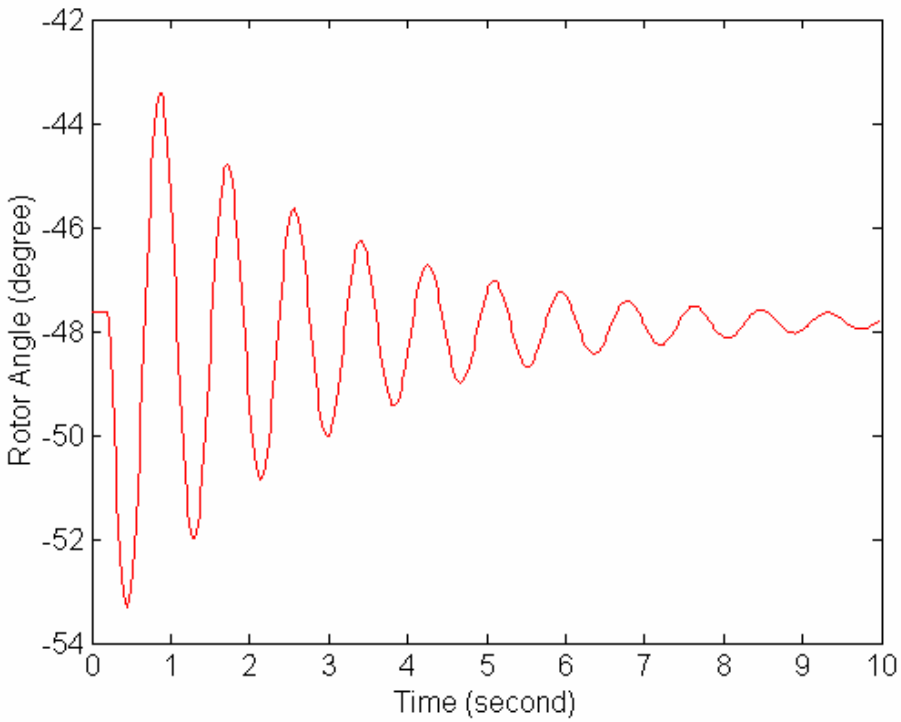

(b) Generator 3 vs. Generator 1

Figure 3.5: Swing Curves for Three-Phase Solid Fault

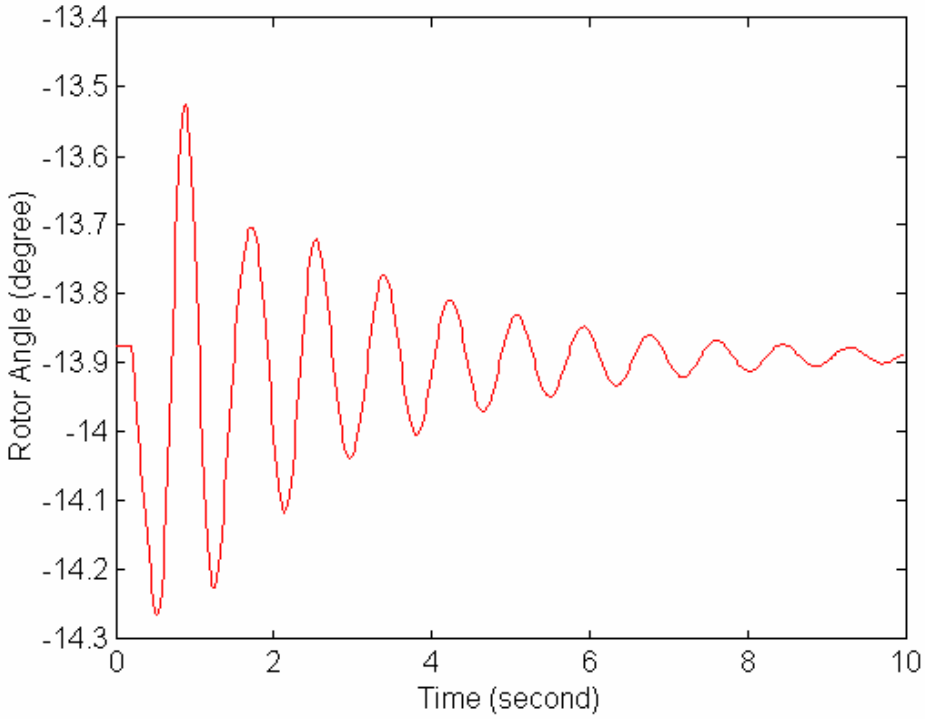

(a) Generator 2 vs. Generator 1

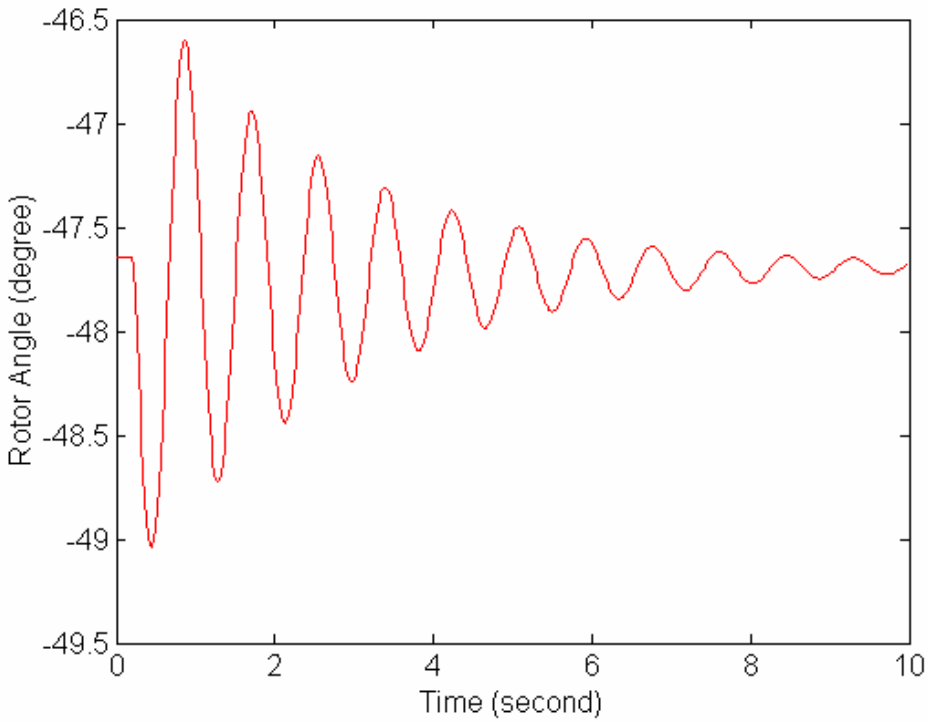

(b) Generator 3 vs. Generator 1

Figure 3.6: Swing Curves for Single-Phase-to-Ground Fault

III.5 CONCLUSION

In this chapter the basis of transient stability simulation was introduced. Transient stability simulation places emphasis on generators' synchronism, and consequently does not deal with high frequency transients. Network elements are modeled at system level and the integration time step is in the order of millisecond. Based on a balanced network assumption, the transient stability simulators solve a single-phase equivalent of the three-phase network with fast execution speed. Nevertheless, they also have their limitations, such as simulating HVDC links and FACTS devices only as quasi steady state models.

The limitations of transient stability simulators would be the advantages of electromagnetic transient simulators, and vise versa. If these two kinds of simulators could be seamlessly integrated together, their respective limitations would be covered and the overall characters which could be observed would be the speed of transient stability simulators and accurate modeling of electromagnetic transient simulators.

Chapter IV HYBRID SIMULATION – OVERVIEW

IV.1 INTRODUCTION [81-88]

From the descriptions in chapters 2 and 3, it is obvious that those conventional EMT and TS simulators cannot have their application on modern power systems because of the speed limitation of EMT and TS's limitation on modelling accuracy. It is readily apparent that the future of simulation lies in the development of very large bandwidth digital simulators capable of modeling large scale power systems in real time or faster than real time.

The hybrid simulation package takes advantage of the computationally inexpensive dynamic representation of the main network in a stability program, with the accurate dynamic modeling of the control systems and switching devices of HVDC and FACTS systems. This chapter presents the concepts related to hybrid simulation. General ideas of hybrid simulation are presented, the issues relating how to build the interface are listed, and the methods to develop frequency dependent equivalents are introduced.

IV.2 CONCEPT OF HYBRID SIMULATION

The idea of hybrid simulation was first proposed by Heffernan et al [89-91] to solve HVAC-HVDC systems. They modeled a HVDC link in detail within a stability based AC system framework, thus exploiting the advantages of both EMT simulators and TS simulators. They achieved this by simultaneously performing the TS simulator and the EMT simulator with periodic coordination of the results.

Reeve et al. [92-93] proposed that the location of interface should be extended into the AC network further for taking into consideration the effect of harmonics generated by power electronics on the AC network. Anderson et al. [94] presented another approach to take the harmonics into account. In the EMT program, the

network part simulated by the TS program is represented by frequency-dependent equivalent, instead of a simple fundamental frequency equivalent circuit used by Heffernan and Reeve.

The paper presented by Sultan et al. [95] basically adopted the approaches described above, i.e. extending the interface location into AC network to some extent, and at the same time representing the network simulated by the TS program with frequency-dependent equivalent. Also, Kasztenny et al. [96] have discussed a general method for linking different modelling techniques such as waveform-type, phasor-type, and algebraic-type simulation techniques into one complete model.

The basic approach for the development of the hybrid simulator in this research is to incorporate both the detailed device level simulation and system wide functional modeling within an integrated analysis tool. The whole system is partitioned to two parts along a data exchange interface. The two parts are named as the detailed system (solved with a small time step) and the external system (solved with a relatively large time step). The detailed system may contain a single component, such as an HVDC link or a FACTS device or other network elements, or contain a combination of them. The detailed and external systems are simulated by the EMT and TS simulators, respectively.

The interaction and communication between the detailed and external networks is maintained through a well-defined common data exchange interface, such as a network bus or transmission line. While reference [97] chose the line as common medium, most other approaches use network bus as the interface location as shown in Figure 4.1.

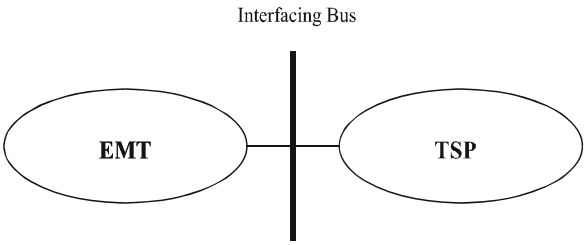

Figure 4.1: EMT-TS Integration

Each simulator sees the other as a dynamic network equivalent, as shown in Figure 4.2.

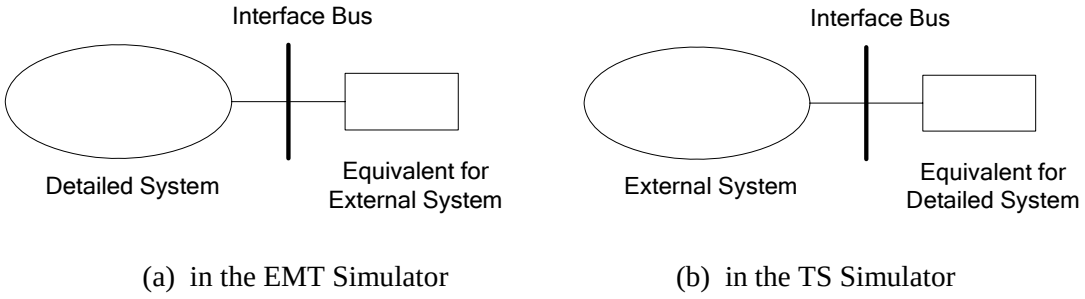

(a) in the EMT Simulator (b) in the TS Simulator

Figure 4.2: Equivalents Representation in Hybrid Simulation

Both the EMT and TS simulations proceed in parallel and at specified time points they communicate with each other as shown in Figure 4.3. With the interchange of variables the equivalents are updated periodically.

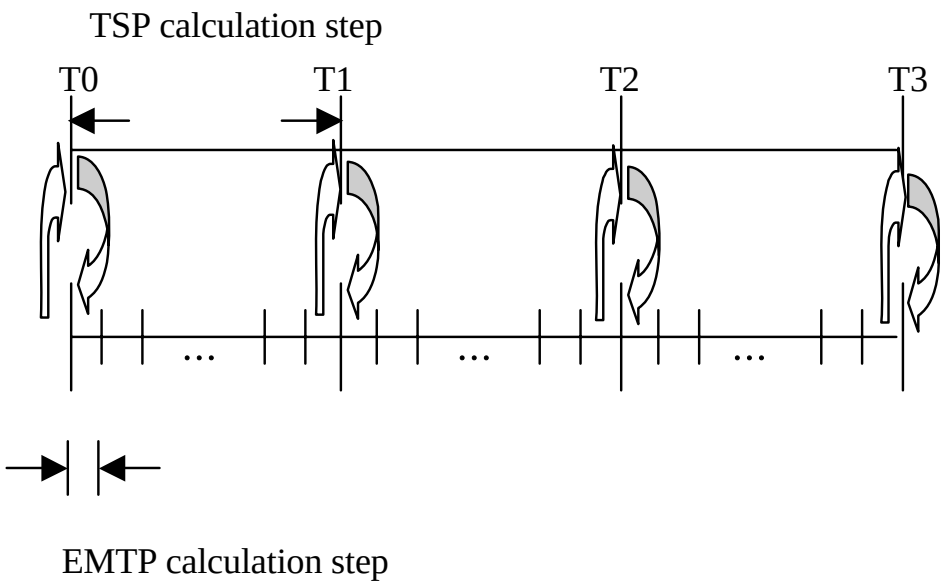

Figure 4.3: Interface Protocol of Hybrid Simulation

The EMT simulator is time-domain analysis program, producing three-phase solutions with broad bandwidth. A broad range of time steps can be used, but for the purposes of this research the time step is typically 50 microseconds. The TS simulator simulates three-phase AC power systems by phasor analysis and uses 20 milliseconds as a typical integration time step.

EMT and TS are distinctly different simulators and in order to develop the hybrid simulator the following factors must be considered:

1. modeling of frequency dependent equivalent of the external system to be presented to the detailed system,
2. modeling of an equivalent for the detailed system to be presented to the external system,
3. selection of interaction locations, and
4. protocol for interaction between TSP and the detailed system

IV.3 BUILDING FREQUENCY DEPENDENT EQUIVALENT

Development of network equivalents is a very old topic. By replacing a network with another set of circuits, huge computation resource can be saved while retaining the required computational accuracy. Usually, the purpose of building an equivalent of the network is to look at its effect on the circuit of concern.

Different types of simulators have different requirements for network equivalents. For transient stability simulators, an impedance at system frequency may be good enough to represent part of a network [68-69]. For electromagnetic transient simulators, an equivalent must reflect the dynamics of original network over a wide frequency range.

A number of approaches have been developed to build frequency dependent equivalents. They can be roughly divided into two groups. In group one, the parameters of the equivalent are derived directly by analyzing the network topology and network elements' internal connection (such as different windings connection of transformers). In group two, an excitation is applied at one of the network terminal ports and the response is recorded at all other ports. The parameters of the equivalent can be derived by analyzing these measurements.

IV.3.1 GROUP ONE

In reference [70], the authors proposed an approach which has been implemented in EMTP, known as Frequency Dependent Network Equivalent (FDNE). The first step in the creation of a network equivalent is to build the nodal admittance matrix of the portion of the system to be represented over a given frequency range. Rather than using the EMTP itself to produce frequency scans of the entire network, the FDNE calculates the admittance matrix of each system component independently according to its mathematical description.

The nodal admittance matrices of the network have to be calculated at every frequency, and decomposed into positive and zero sequence networks. The sequence admittance matrices are then reduced between a given number of terminals, or ports, producing a family of frequency-dependent reduced-order admittance matrices. In this process, the network is divided into layers.

The network admittance matrix is kept to a relatively small size during this process and the final reduction produces an NxN matrix for a network with N references ports. The matrix is symmetrical with N(N+1)/2 distinct elements. The admittance matrix is calculated over a range of frequencies. Each element of the matrix produces a frequency response curve, to be matched by a multi-branch linear network.

Once the equivalent positive and zero sequence admittance matrices are calculated as functions of frequency, their elements are fitted using modules of the type shown in Figure 4.4. Each module consists of a number of parallel RLC branches. An RLC module consists of one RC branch (R_∞, C_∞), one RL branch (R_0, L_0), and a number of RLC branches ($R_k, L_k, C_k, k = 1,2,\cdots M$) connected in parallel. The method described in [71] is used to generate a module that matches the frequency characteristic at series resonance frequencies only.

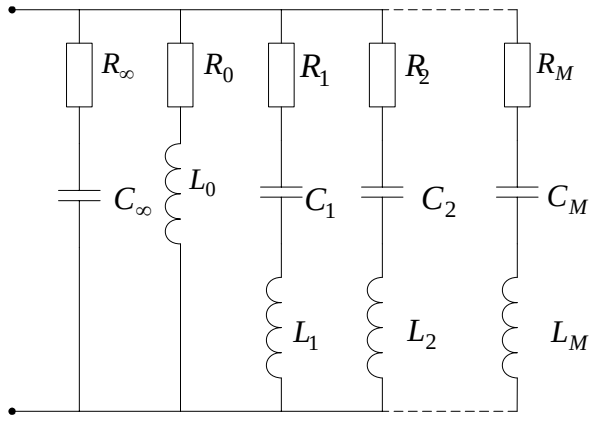

Figure 4.4: Structure of an FDNE Module

Another method was developed to derive three-phase AC system harmonic equivalents for HVDC behavior studies [72]. The method derives the system harmonic impedances analytically in the frequency domain. The final equivalent circuits consist of a number of single-tuned parallel branches as shown in Figure 4.5.

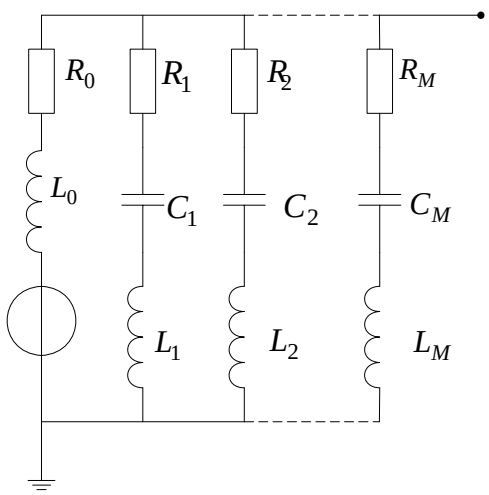

Figure 4.5: Single-Phase Network Equivalent Matching M Resonant Frequencies

Mehdi Vakilian and Abbas Ketabi [73] proposed that the analysis could also be done in the *z* domain. The approach has a very close relation to Dommel's method which involves substituting a numerical integration formula, such as the trapezoidal rule, into the differential equations and rearranging them into an appropriate form. Once all the network components are represented by an equivalent current source and a resistance in parallel, a nodal formulation is used to solve the complete system.

$$[G][v(t)] = [i(t)] + [I_{history}] \tag{4.1}$$

where

[G] = conductance matrix

v(t) = vector of nodal voltage

i(t) = vector of external current source

$I_{history}$ = vector of equivalent current sources representing past history terms

Every element of the vector of history terms is the combination of equivalent current sources of the components which are connected to that node. Thus $I_{history}$ can be expressed as follows:

$$[I_{history}] = [A][I_{component}(t - n\Delta t)] \tag{4.2}$$

where

[A] = coefficient matrix which elements are 0, -1 and 1

$I_{component}(t - n\Delta t)$ = vector of component equivalent current source

And $I_{component}(t - n\Delta t)$ is the combination of the components of past voltage and current, so we have,

$$[I_{component}(t - n\Delta t)] = [B][v(t - n\Delta t)] + [C][i(t - n\Delta t)] \tag{4.3}$$

where

[B] = coefficient matrix of past voltage vector

[C] = coefficient matrix of past current vector

Substituting Eq. 4.2 and 4.3 into Eq. 4.1 yields

$$[G][v(t)] = [i(t)] + [A][B][v(t - n\Delta t)] + [A][C][i(t - n\Delta t)] \tag{4.4}$$

or in *z*-transformation form

$$[G][v] = [i] + [D(z)][v] + [E(z)][i] \tag{4.5}$$

Thus a polynomial matrix of function *z* can be obtained. Reducing the matrix makes its dimension equal to the number of boundary buses. Each element of the

admittance matrix is decomposed into a sum of a set of fractions which have polynomials of power one or two of *z* in the denominator. Each fraction of type one can be simulated with a series RL or RC branch and each fraction of type two can be simulated with a RLC branch.

IV.3.2 GROUP TWO

Generally, when applying an excitation to a network, the output responses include all information defining the characteristics of the network. All the methods in this group are based on this idea.

In references [74-75], a time domain equivalence method is introduced. The method generates a discrete-time equivalent by using the response of an external system to a specific excitation signal. No explicit network of RLC is synthesized to replace the external system. Instead, a discrete-time Norton equivalent for the external system is directly obtained and connected to the boundary nodes.

The external system can, in general, be described by a driving-point admittance function *H(s)* relating the terminal voltage and the injected current at the boundary bus, as given below:

$$H(s) = \frac{I(s)}{V(s)} = K\,\frac{N(s)}{D(s)} \tag{4.6}$$

where $N(s) = n_0 + n_1 s + \cdots + n_p s^p$,

$D(s) = d_0 + d_1 s + \cdots + d_p s^p$, and

K=scalar gain.

Replacing the Laplace operator s by $\frac{d}{dt}$, Eq. (4.6) can be rewritten in time domain as:

$$\left(d_0 + d_1\frac{d}{dt} + \cdots + d_p\frac{d^p}{dt^p}\right)i(t) = \left(n_0 + n_1\frac{d}{dt} + \cdots + n_p\frac{d^p}{dt^p}\right)v(t) \tag{4.7}$$

The above p^{th} order linear differential equation can be converted recursively into a linear difference equation by using a numerical integration method, by following the procedure given in chapter 13 of the EMTP Theory Book [2].

$$i(t)+a_1 i(t-\Delta t)+\cdots+a_p i(t-p\Delta t)=g_0 v(t)+g_1 v(t-\Delta t)+\cdots+g_p v(t-p\Delta t) \tag{4.8}$$

A difference equation in the form given in Eq. (4.8) can be used to represent the external system over a broad frequency range. No attempt is made to express the coefficients a_i and g_i in terms of d_i and n_i, and its order *p* can be specified by the user.

The choice of the model order *p* is referred to as model identification. Once the order *p* is specified, then the parameters a_i and g_i of the model have to be estimated and this constitutes the parameter estimation step.

The model identification is carried out in an iterative manner. For an initial choice of the model order *p*, the model's parameters are estimated and the rms error e_{rms} of the fitted model is computed. The rms model-fit error e_{rms} is defined as:

$$e_{rms}=\frac{1}{(N-p)}\sqrt{\sum_{k=p+1}^{N}\left(i(k\Delta t)-\hat{i}(k\Delta t)\right)^2} \tag{4.9}$$

where

N is the total number of time-steps in the EMTP simulation of the external system response,

$i(k\Delta t)$ is the boundary current injection at time step $k\Delta t$, and $\hat{i}(k\Delta t)$ is the estimated boundary current injection at time step $k\Delta t$, using Eq. (4.8).

If e_{rms} is greater than a certain threshold, ε, the model order *p* is increased and the above procedure is repeated.

Eq. (4.8) is rearranged below by collecting all the delay terms together and denoting them by *h* (history term):

$$i(t)=g_0 v(t)+\sum_{k=1}^{p}\left[g_k v(t-k\Delta t)-a_k i(t-k\Delta t)\right]=g_0 v(t)+h \tag{4.10}$$

This is the equation of a discrete-time Norton equivalent circuit given in Figure 4.6. The circuit represents the frequency-dependent admittance of the external system, as seen from the boundary node, in the time domain.

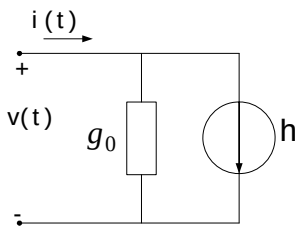

Figure 4.6: Discrete-Time Norton Equivalent Circuit

Thus, a single-phase equivalent for the external system can be put together by connecting the circuit of Figure 4.6 in series with an approximate Thevenin voltage source. The phasor value of the Thevenin source's voltage can be specified by finding the open-circuit steady-state solution for the boundary bus voltage using EMTP itself with all the external system sources remaining active.

The same approach can be extended to generate multi-port equivalents as well [75].

IV.3.3 APPLICATION OF PRONY METHOD [76-79]

In building equivalents of a network, Prony method belongs to Group Two, that is, the method obtains parameters based on the network measurements. The mathematical description of the method is in Appendix A5. Here the feasibility of its application for deriving network equivalents is discussed.

The Prony method requires the measurements consisting of a sum of exponentials. In power system modeling, if every network component is represented by a combination of R, L, and C, the system can be expressed in a transfer function form in the s-plane, as viewed from any port as shown in equation 4.11:

$$Y(s) = \frac{I(s)}{V(s)} = \frac{N(s)}{D(s)} \tag{4.11}$$

As the numerator and denominator are polynomials of *s*, *Y(s)* can be decomposed into a set of fractions of types one and two and constants without loss of generality. Thus *Y(s)* can be written as:

$$Y(s) = \frac{N(s)}{D(s)} = const + \sum_{k=1}^{n} \frac{R_k}{s - \lambda_k} \tag{4.12}$$

where *n* represents the order.

If a unit impulse voltage source at the port, the current response can be expressed in s-plane as:

$$I(s) = const + \sum_{k=1}^{n} \frac{R_k}{s - \lambda_k} \tag{4.13}$$

or in time domain,

$$I(s) = const * \delta(t) + \sum_{k=1}^{n} R_k e^{\lambda_k t} \tag{4.14}$$

Thus, the requirements of the Prony method are met, and the network can be replaced with a set of simple circuits of order one and/or two as illustrated in Figure 4.7. Each fraction of order one represents a RL or RC circuit, and every fraction of order two represents an RLC circuit. Therefore, the transfer function Eq. (4.11) can be replaced by a system of RLC circuits in parallel.

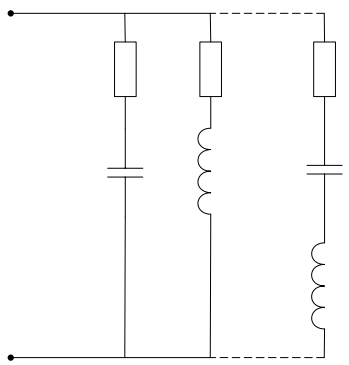

Figure 4.7: Equivalent Circuit of Prony Method

In practical applications, the equivalent represents not only the topology of the power network, but elements internal connections (such as delta-connection of transformer windings) and couplings as well. This is important for analysis of

asymmetrical disturbances in the system to be studied. Therefore, the equivalent for asymmetrical transients is much more complicated than that for symmetrical transients.

The following procedure outlines the steps required to develop an equivalent. The procedure only considers symmetrical networks.

1. Turn off all active sources in the network, i.e. short-circuit voltage sources and open-circuit current sources.
2. Apply a unit impulse voltage source at one phase of one terminal port while the other phases are grounded.
3. Determine the currents in all grounded phases (the measurements contain all modes of the network).
4. Use the Prony method for modal analysis.
5. Synthesize a network based on the parameters outputted from the Prony method in the form as shown in Figure 4.7.

The MATLAB built-in Prony function *[b,a] = prony(h,n,m)* generates a ratio of polynomials in s-domain. Feeding a vector of measurements h and specifying the orders of polynomials n and m, Prony returns the polynomials coefficients in row vectors b and a, of length n + 1, respectively.

$$H(s) = \frac{B(s)}{A(s)} = \frac{b_0 + b_1 s + \cdots + b_n s^{-n}}{a_0 + a_1 s + \cdots + a_n s^{-n}} \tag{4.15}$$

The ratio of polynomials cannot be used directly for our purpose, and need to be converted to a sum of fractions of orders one and two. The MATLAB built-in function *[r,p,k] = residue(b,a)* finds the residues, poles, and direct terms of a partial fraction expansion of the ratio of two polynomials *B(s)* and *A(s)*.Vectors b and a specify the coefficients of the polynomials. The returned column vector *r* contains residues, column vector *p* contains pole locations, and row vector *k* contains direct

terms. The function results in a constant and a sum of fractions of order one if there are no multiple roots.

$$\frac{B(s)}{A(s)} = const + \frac{r_1}{s-p_1} + \frac{r_2}{s-p_2} + \cdots + \frac{r_n}{s-p_n} \tag{4.16}$$

The elements of vectors r and p are not necessarily real values. If complex numbers appear, they must appear in conjugate pairs [80].

In fact, the fractions in Eq. (4.16), which are the ratio of current and voltage in the s-domain, can be directly used by electromagnetic transient simulators. Applying the trapezoidal rule to the s-domain fraction of order one $\frac{I(s)}{V(s)} = \frac{r}{s-p}$, a discrete-time form of expression can be derived easily.

$$\frac{i(t) - i(t-\Delta t)}{\Delta t} = \frac{r*v(t) - r*v(t-\Delta t) + p*i(t) - p*i(t-\Delta t)}{2} \tag{4.17}$$

Because complex coefficients always appear in conjugate pairs, the final results from Eq. (4.17) are always in real value; even if the intermediate variables are complex.

For Prony analysis the order of vector b (or a) must be chosen. The larger the value of the order, the more accurate the equivalent will be. However, larger orders result in larger number of terms in Eq. (4.16) and this results decreased computational efficiency of the equivalent. This is the work of experience. The choice of order is a compromise between accuracy and the computational cost, and is based on experience.

After Prony analysis, a practical network becomes a set of mathematical expressions. The performance of the Prony method can be illustrated by the following example.

The diagram shown in Figure 4.8 is a part of 3-machine-9-bus system. Three machines are replaced by their respective internal impedance x_d''.

The windings of the high voltage side of three transformers are in star-grounded connection, and in delta connection for the low voltage side. Transmission lines are represented by π section models for both positive- and zero-sequences. Three loads are treated as constant impedances. Thus in this example there is the coupling and delta connections of the transformer windings. The developed equivalent must faithfully reflect these connections.

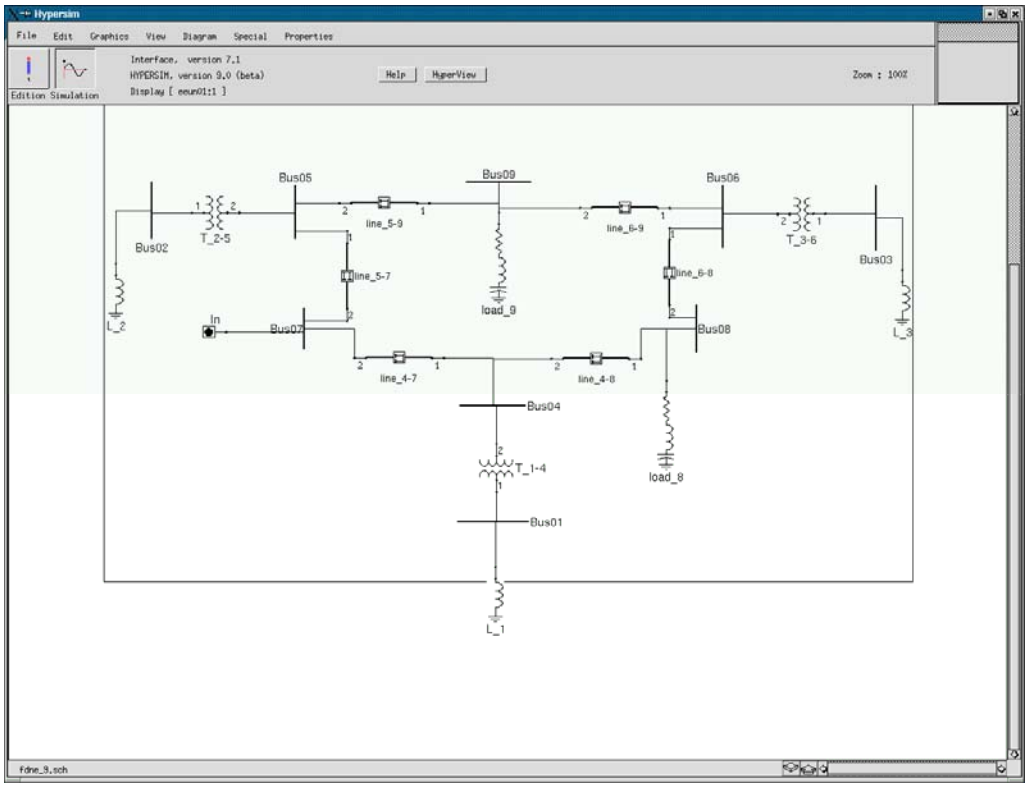

Figure 4.8: 3-Machine-9-Bus Network

Of the following sets of numbers, the first column corresponds to the real part of residue *r*, the second column the imaginary part of the residue, the third column the real part of the root *p*, the forth column the imaginary part of the root *p*.

The orders of denominator and numerator of the equivalents between phases and are 10 and 9 respectively, and those of the equivalents between phases are 18 and 17 respectively.

Parameters of the equivalents between phases and ground:

Real(r)	Imag(r)	Real(p)	Imag(p)
2.7679109943	0.0000000000	-34.9984935240	0.0000000000
0.2668272289	0.0000000000	-115.6252865541	0.0000000000
0.1754249456	0.0025346437	-8.3249666378	3151.5874842842
0.1754249456	-0.0025346437	-8.3249666378	-3151.5874842842
0.0087852633	-0.0014474030	-11.0929966727	2320.4086741290
0.0087852633	0.0014474030	-11.0929966727	-2320.4086741290
0.0394388672	0.0006284357	-17.7205476518	2697.4105686706
0.0394388672	-0.0006284357	-17.7205476518	-2697.4105686706
0.0368748990	0.0013667925	-187.6482737670	1393.6608773652
0.0368748990	-0.0013667925	-187.6482737670	-1393.6608773652

Parameters of the equivalent between phases:

Real(r)	Imag(r)	Real(p)	Imag(p)
0.0063305106	0.0000000000	-2298.5639173227	0.0000000000
0.8938747234	0.0000000000	-16.3208386670	0.0000000000
-0.0615440831	-0.0081276174	-8.9746344856	3149.4671405447
-0.0615440830	0.0081276174	-8.9746344856	-3149.4671405447
0.3414499721	-0.0033205671	-21.6649520076	4610.6174328300
0.3414499721	0.0033205671	-21.6649520076	-4610.6174328300
-0.0113810558	-0.0057953268	-26.4011072891	2669.7662018260
-0.0113810558	0.0057953268	-26.4011072891	-2669.7662018260
0.1572893560	0.0169400531	-26.5780075697	3086.8618285373
0.1572893561	-0.0169400533	-26.5780075697	-3086.8618285373
0.0015974310	0.0024324132	-27.9012925819	4544.9107484564
0.0015974310	-0.0024324132	-27.9012925819	-4544.9107484564
0.2751258103	-0.0007183736	-61.4805084281	1698.2626396424
0.2751258103	0.0007183736	-61.4805084281	-1698.2626396424
-0.0079240924	0.0010508936	-215.2560066187	2118.3880042437
-0.0079240924	-0.0010508936	-215.2560066187	-2118.3880042437
0.0358664551	-0.0241089518	-539.9101558327	589.1589265188
0.0358664551	0.0241089517	-539.9101558327	-589.1589265188

Thus, there are 2 RL circuits and 4 equivalent RLC circuits between single phase and ground, and 2 RL circuits and 8 equivalent RLC circuits between three phases.

The responses of the equivalent subject to a unit impulse voltage source are visually compared with those of the original network. Figure 4.9 gives the current responses of the original network. Figure 4.10 shows the current responses of the equivalent.

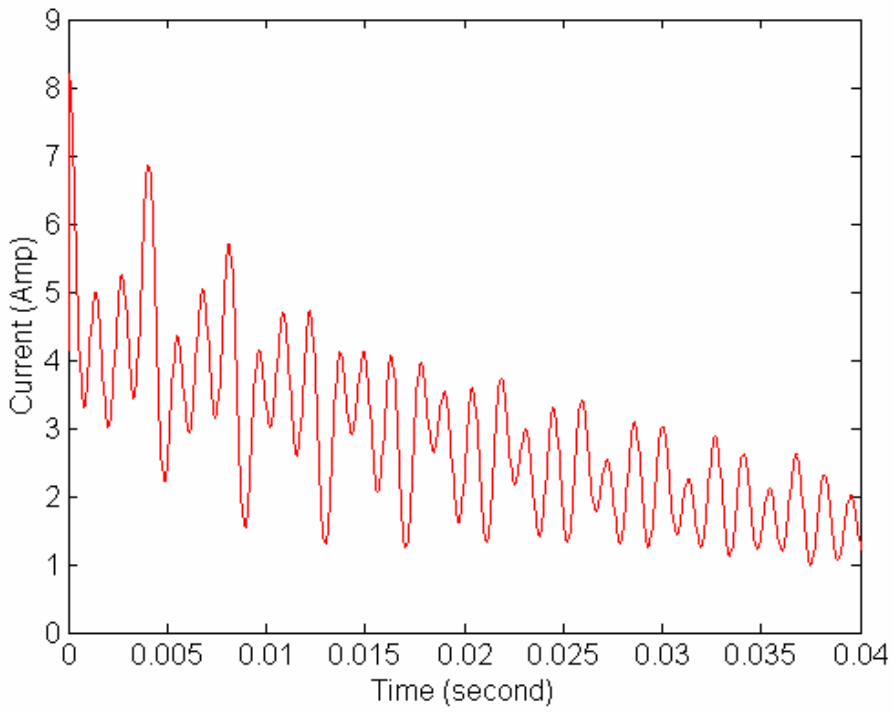

Figure 4.9: Response of the Original Network to Unit Impulse Voltage Source

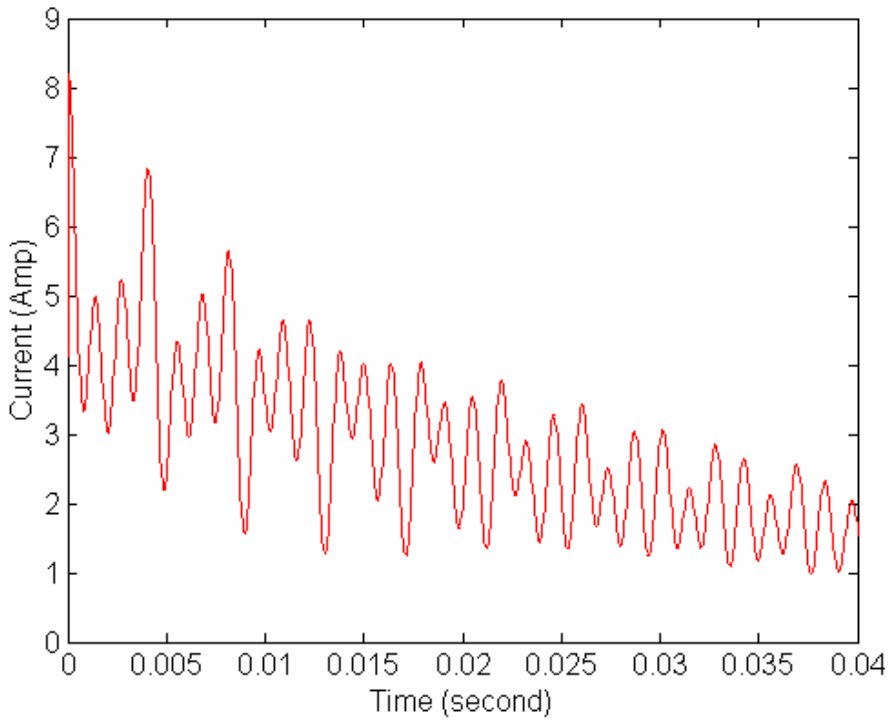

Figure 4.10: Response of Equivalent to Unit Impulse Voltage Source

Curves of Figure 4.9 and 4.10 match very well. The example illustrates that the equivalent derived can faithfully represent the dynamics of the original system.

After the Prony analysis, the equivalent is a set of mathematical equations in the form of Eq. 4.16. For the purposes of this application, they are converted into equivalent RLC networks using network synthesis techniques.

IV.4 NETWORK SYNTHESIS

Network synthesis is the process of designing and constructing a network to provide a prescribed response to a specified excitation. This is the converse of the network analysis problem where a response is to be calculated when a prescribed excitation is applied to a given network. In contrast with the latter, the synthesis problem may not have a unique solution.

In this section, the discussion is limited only to some basic issues. For a detailed description, please refer to reference [40].

The Prony method has given us the locations of poles and zeros, or residues. Thus the remaining task is to realize a network. There are various classes of networks, which can be characterized by the number of external terminals, by the structure (ladder, grounded, etc).

IV.4.1 RL CIRCUIT

The circuit can be expressed in the s domain as follows:

$$\frac{I(s)}{V(s)} = \frac{1/L}{s + R/L} \tag{4.18}$$

Thus, if both root p and residue r are real, and the sign of the residue is positive, an RL circuit can be synthesized:

$$\begin{aligned} R &= -\frac{p}{r} \\ L &= \frac{1}{r} \end{aligned} \tag{4.19}$$

IV.4.2 RC CIRCUIT

The circuit can be expressed in s domain as follows:

$$\frac{I(s)}{V(s)} = \frac{s/R}{s + 1/RC} = \frac{1}{R} - \frac{1/R^2C}{s + 1/RC} \tag{4.20}$$

Thus, if both the root *p* and the residue *r* are real, and the sign of the residue is negative, an RC circuit can be synthesized. To do so, an additional resistance (-*R*) must be added in parallel with the RC circuit.

$$R = \frac{p}{r}$$
$$C = -\frac{r}{p^2} \tag{4.21}$$

IV.4.3 RLC CIRCUIT

If both the root and the residue are complex, they must appear in conjugate pairs. The corresponding synthesis comprises two RLC circuits. Let's express the *r* and *p* as follow: $p_{1,2} = \alpha \pm j\omega, r_{1,2} = \beta \pm j\sigma$. Combining two conjugate terms yields

$$\frac{\delta s - \varepsilon}{s^2 - \phi s + \varphi} \tag{4.22}$$

where $\delta = 2\alpha$, $\varepsilon = 2(\alpha\beta + \omega\sigma)$, $\phi = 2\beta$, $\varphi = \beta^2 + \sigma^2$

Different synthesis approaches result in different structures of the circuit. The two common forms of the resulting circuit are Forster form and ladder form.

The Forster form is a combination of elementary one-port networks as shown in Figure 4.12. If Eq. (4.22) is to be an impedance, it can be represented as a series combination of networks. If Eq. (4.22) is to be an admittance, it can be represented as a parallel combination of networks. According to the unique correspondence between the fundamental function and the one-port network in series or in parallel, each function has a unique network representation in series connection or in parallel connection.

Impedance	function	R	Ls	$\frac{1}{Cs}$	$\frac{1+RCs}{Cs}$	$\frac{R}{1+RCs}$	$R+Ls$	$\frac{LRs}{Ls+R}$	$Ls+\frac{1}{Cs}$	$\frac{Ls}{1+LCs^2}$
	network								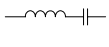	
Admittance	function	$\frac{1}{R}$	$\frac{1}{Ls}$	Cs	$\frac{Cs}{1+RCs}$	$\frac{1}{R}+Cs$	$\frac{1}{R+Ls}$	$\frac{1}{R}+\frac{1}{Ls}$	$\frac{Cs}{LCs^2+1}$	$\frac{1}{Ls}+Cs$
	network								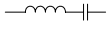	

Figure 4.12: Representation of Partial-Fraction Summands

The process can be illustrated by the following example.

$$Y(s)=\frac{\delta s-\varepsilon}{s^2-\phi s+\varphi}=\frac{\delta}{\dfrac{s^2-\phi s+\varphi}{s-\dfrac{\varepsilon}{\delta}}}=\frac{\delta}{\dfrac{s^2-\dfrac{\varepsilon}{\delta}s+\left(\dfrac{\varepsilon}{\delta}-\phi\right)s+\varphi}{s-\dfrac{\varepsilon}{\delta}}}=\frac{\delta}{s+\dfrac{\gamma s+\varphi}{s-\dfrac{\varepsilon}{\delta}}}$$

where $\gamma=\dfrac{\varepsilon}{\delta}-\phi$

$$Y(s)=\frac{\delta}{s+\dfrac{\gamma s+\varphi}{s-\dfrac{\varepsilon}{\delta}}}=\frac{\delta}{s+\dfrac{\gamma s-\gamma\dfrac{\varepsilon}{\delta}+\varphi+\gamma\dfrac{\varepsilon}{\delta}}{s-\dfrac{\varepsilon}{\delta}}}=\frac{\delta}{s+\gamma+\dfrac{\eta}{s-\dfrac{\varepsilon}{\delta}}}$$

where $\eta=\varphi+\gamma\dfrac{\varepsilon}{\delta}$

$$Z(s)=\frac{1}{Y(s)}=\frac{s+\gamma+\dfrac{\eta}{s-\dfrac{\varepsilon}{\delta}}}{\delta}=\frac{s+\gamma+\dfrac{\delta\eta}{\delta s-\varepsilon}}{\delta}$$

So the equivalent can be represented by a series combination an inductor ($Z(s)=\dfrac{s}{\delta}$), a resistor ($Z(s)=\dfrac{\gamma}{\delta}$), and a RC circuit in parallel ($Z(s)=\dfrac{\eta}{\delta s-\varepsilon}$).

The ladder-network method has several implementations, and only one of them is discussed here as an example. A ladder network having arbitrary branches is shown in Figure 4.13.

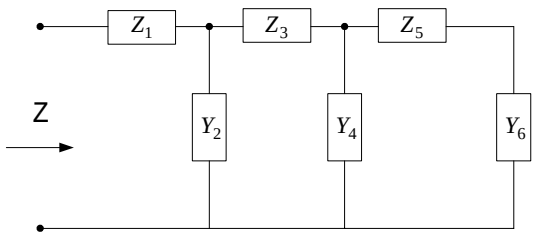

Figure 4.13: Ladder Network with Arbitrary Branch Impedances

Its impedance can be written in the following continued-fraction form:

$$Z = Z_1 + \cfrac{1}{Y_2 + \cfrac{1}{Z_3 + \cfrac{1}{Y_4 + \cfrac{1}{Z_5 + \cfrac{1}{Y_6}}}}} \tag{4.23}$$

The realization can be illustrated according to the ladder-network method by treating Eq. (4.22) as follows:

$$Z(s) = \frac{s^2 - \phi s + \varphi}{\delta s - \varepsilon} = \frac{s}{\delta} + \frac{1}{\frac{\delta s - \varepsilon}{\gamma s + \varphi}} = \frac{s}{\delta} + \frac{1}{\frac{\delta}{\gamma} - \frac{\frac{\delta\eta}{\gamma} + \varepsilon}{\gamma s + \varphi}} = \frac{s}{\delta} + \frac{1}{\frac{\delta}{\gamma} + \frac{1}{\frac{\gamma}{\rho} s + \frac{\varphi}{\rho}}}$$

where $\gamma = \frac{\varepsilon}{\delta} - \phi$, $\eta = \varphi\delta$, $\rho = -\frac{\eta\delta}{\gamma} - \varepsilon$.

Therefore, refer to Figure 4.13, we have $Z_1 = \frac{s}{\delta}, Y_2 = \frac{\delta}{\gamma}, Z_3 = \frac{\gamma}{\rho} s, Y_4 = \frac{\eta}{\rho}$. The resulting network is a resistance-inductance ladder-network, as shown in Figure 4.14.

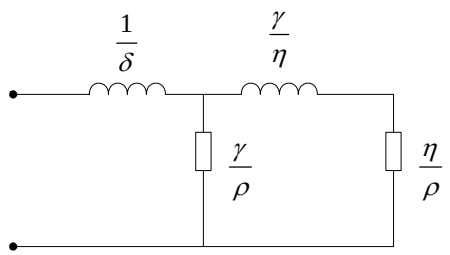

Figure 4.14: Resistance-Inductance Ladder Network Corresponding to Complex Roots Partial Fractions

The equivalent network of the 9-bus network is a set of RL and RLC circuits in parallel. From their mathematical expressions and the above analysis, it is not difficult to obtain their parameters.

Parameters (R in ohms, L in H and C in F) of the circuits between phases and ground (RLC circuit in the form of Forster form) are:

RL1: R=12.6444, L=0.3613

RL2: R=433.3339, L=3.7477

RLC1: L =2.8502, R =153.5157, RC =-7.6095e+005, C =3.5316e-008

RLC2: L =56.9135, R =-2.1126e+004, RC = 8.0012e+005, C =3.1771e-009

RLC3: L =12.6778, R =769.5738, RC =-3.6526e+006, C =1.0838e-008

RLC4: L =13.5594, R =3.2448e+003, RC =1.9393e+005, C =3.7918e-008

Parameters (R in ohms, L in H and C in F) of the circuits between phases (RLC circuit in the form of Forster form) are:

RL1: L =157.9651, R =3.6309e+005

RL2: L =1.1187, R =18.2585

RLC1: L =-8.1243, R =-3.4520e+003, RC =2.0148e+005, C =-1.2196e-008

RLC2: L =1.4643, R =-33.9330, RC =4.6813e+005, C =3.2122e-008

RLC3: L =-43.9327, R =-6.0885e+004, RC =2.9581e+005, C =-2.5359e-009

RLC4: L =3.1789, R =1.1413e+003, RC =-1.0018e+005, C =3.2635e-008

RLC5: L =313.0026, R =2.1749e+006, RC =-3.1129e+006, C =4.6606e-011

RLC6: L =1.8174, R =103.6730, RC =7.9519e+004, C =1.9079e-007

RLC7: L =-63.0987, R =4.1446e+003, RC =-5.8070e+005, C =-3.4705e-009

RLC8: L =13.9406, R =2.0058e+003, RC =7.5062e+003, C =1.4234e-007

IV.5 CONCLUSIONS

In this chapter, the reason and benefits of using hybrid simulation were discussed.

The hybrid simulator requires network equivalents which adequately represent the components of the hybrid, i.e. the detailed system and the external system, at the interface bus. The derivation of an equivalent can be complex for the external

system, and in this chapter a number of methods to build a frequency dependent equivalent were introduced. These techniques have extensive application in power system electromagnetic transients simulation, since they can represent the original network well, and are computationally much more efficient.

The equivalents can be derived either from analysis of network connections, or from network response to network stimuli. For the purposes of this project, Prony analysis, which obtains the equivalent based on network response to an impulse source, was found to be the most suitable means to derive an appropriate equivalent. An example was used to demonstrate the effectiveness of the method, and network synthesis was used to realize a representative RLC network.

Chapter V HYBRID SIMULATION – MODELING AND COMMUNICATION

V.1 INTRODUCTION

The concept of hybrid simulation was introduced in chapter 4. In this chapter a detailed discussion of the main issues related to hybrid simulation will be presented. Sections 2 to 5 are dedicated to the main issues. In section 2, the effects of different modeling techniques of the external system are compared using a 9-bus system. In section 3, emphasis is placed on the choice of variables needed by the transient stability simulator subjected to a variety of disturbances, and on how to obtain these variables. In section 4, issues relating the choice of interface location are evaluated, from conventional approach to a new selection viewpoint. In section 5, interfacing protocol is presented. Some practical problems in implementing the protocol are also discussed.

V.2 MODELING OF EXTERNAL SYSTEMS

While the detailed system is simulated by the EMT simulator, the external system must be presented to the EMT simulator at the interface as an dynamic equivalent. To this a dynamic Norton equivalent, including a current source and a RLC circuit, is used.

In the reference [89-93], the circuit used in the Norton equivalent is a simple RL circuit, derived from the impedance of the external system under the fundamental frequency. However, as discussed in reference [94] the simple equivalent circuit is fundamental frequency based such that the harmonic impedances are not represented, and this is inadequate for the purposes of producing the correct waveform. In reference [94,95] frequency dependent equivalent circuits were presented in place of the simple equivalent, as shown in Figure 5.1. The frequency dependent equivalent circuit adequately represents the harmonic impedances and has a frequency response

closely matched to the original external network.

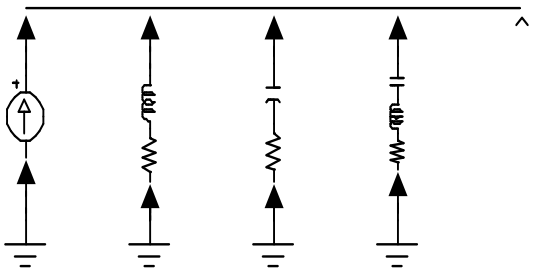

Figure 5.1: Frequency-Dependent Equivalent

In order to validate the frequency dependent equivalent, a test on the 9-bus system, as shown in Appendix A, with an SVC connected to bus 7, which is also chosen as the interface location, was performed. The structure and parameters of the 9-bus system are also detailed in Appendix A. The external system is the 9-bus network, while the detailed system comprises the SVC and the associated transformer. The interface bus voltage and SVC injection current with the SVC connected to the network were evaluated. The test was carried out on HYPERSIM with a TS simulator interfaced through a User Code Block (UCB).

Figure 5.2 shows the waveforms when the SVC is directly connected to the actual 9-bus network. Figure 5.3 and 5.4 show the waveforms when the 9-bus network is replaced by a simple equivalent and a frequency dependent equivalent respectively.

It is clear that when the 9-bus network is represented by a frequency dependent equivalent, the waveforms in Figure 5.3 are quite close to those in Figure 5.2, while some differences exist between the waveforms shown in Figures 5.2 and 5.4. Consequently a frequency dependant equivalent is a necessity.

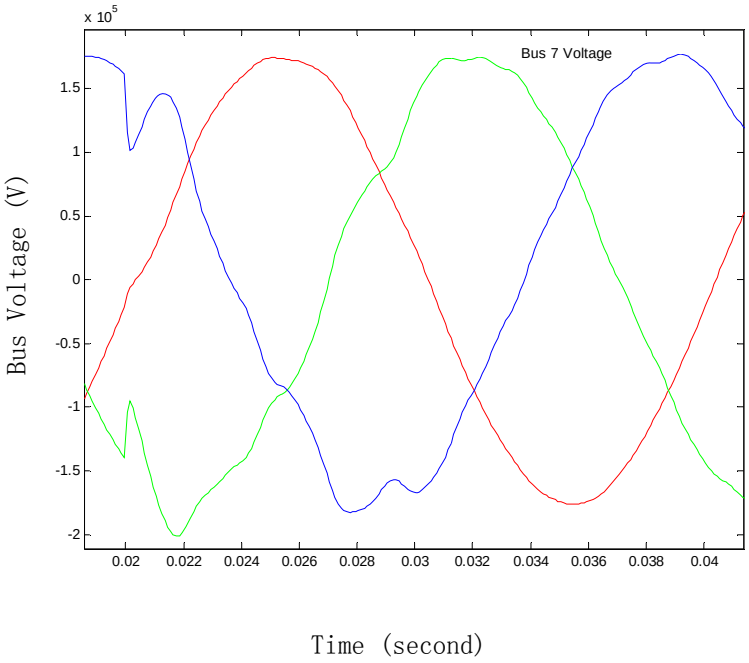

(a) Bus 7 Voltage

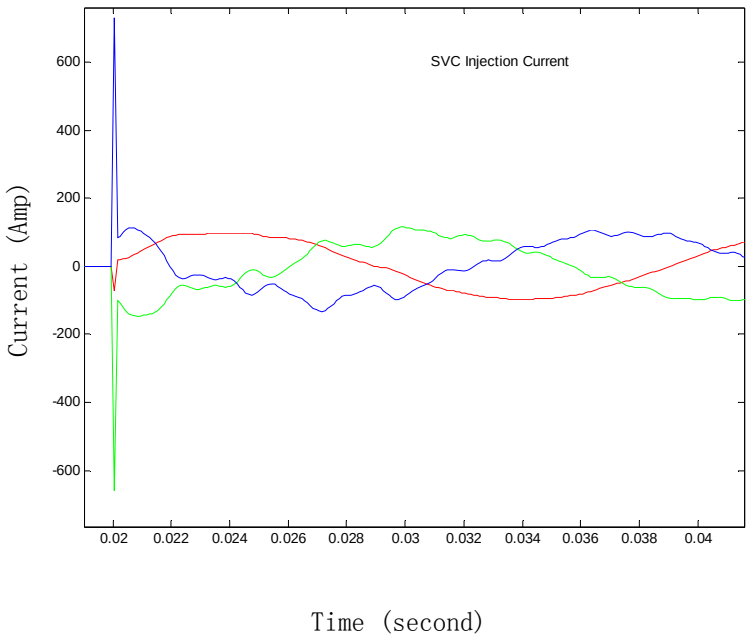

(b) SVC Injection Current

Figure 5.2: Benchmark Waveforms of Interface Bus Voltage and SVC Injection Current

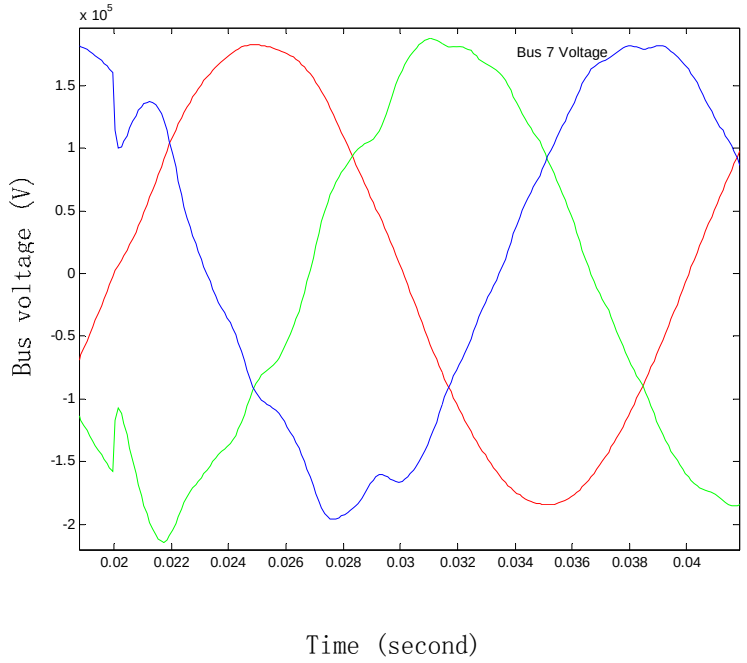

(a) Bus 7 Voltage

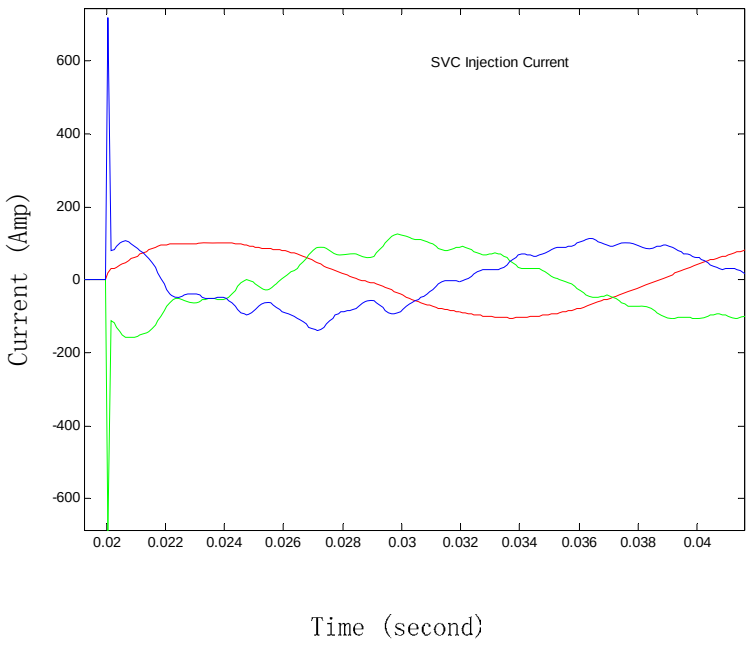

(b) SVC Injection Current

Figure 5.3: Waveforms of Interface Bus Voltage and SVC Injection Current In the Case of Frequency Dependent Equivalent

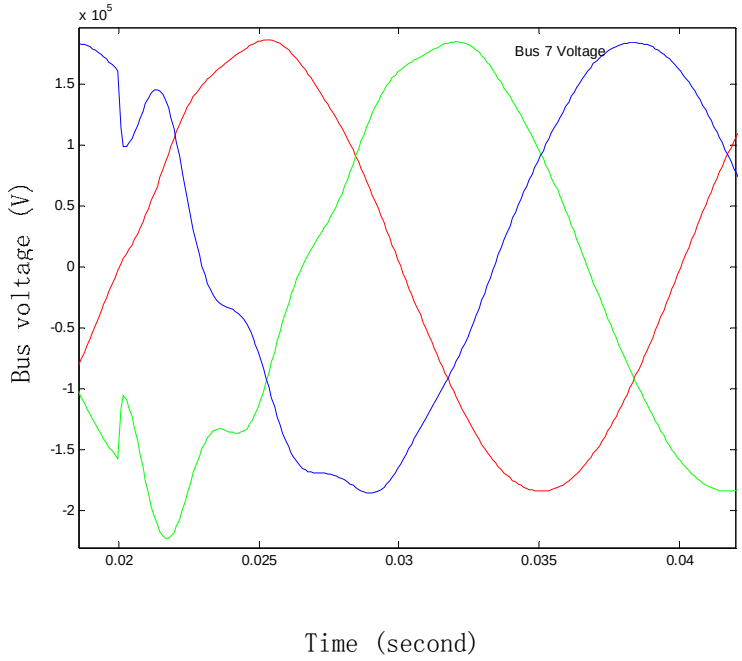

(a) Bus 7 Voltage

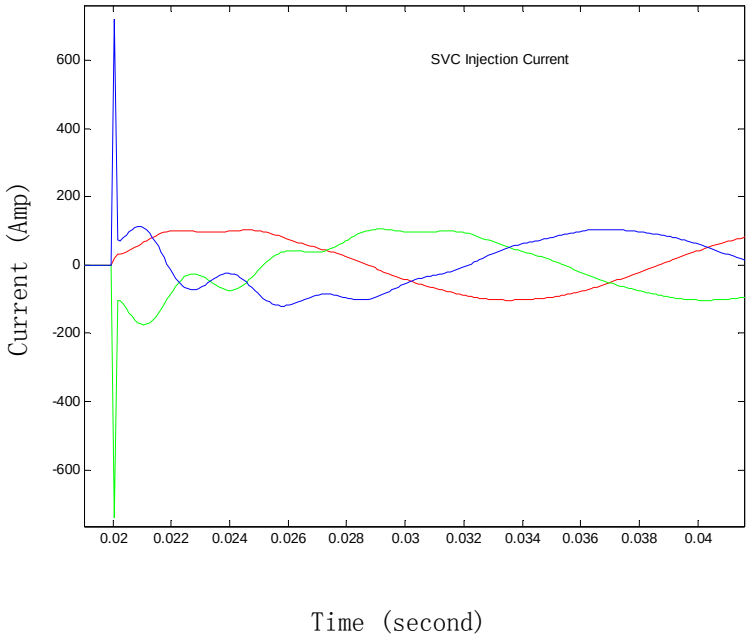

(b) SVC Injection Current

Figure 5.4: Waveforms of Interface Bus Voltage and SVC Injection Current In the Case of Simple Equivalent

The TS simulator models the external system, which is linear and is described as a complex impedance at the fundamental frequency. Internal connections of components, such as transformer windings, are not specified explicitly. For symmetrical disturbances which occurr in the detailed system, how the windings are connected does not matter, but for the asymmetrical disturbances, it does. For general purposes, the frequency dependent equivalent must reflect the internal connections and coupling between phases of the network components. Consequently the RLC equivalent circuit must include mutual coupling between phases.

As described in Chapter 4, the Prony method was used to derive the equivalent of the external system for the hybrid simulation. The equivalent can be determined prior to the simulation since the external network parameters are fixed and, once the simulation begins the equivalent circuit does not change. However the current source in the Norton equivalent is updated at every interchange, as determined by generators in the external system.

Consider, for example, a sub-transient model of the generator which has been shown in chapter 3:

$$\begin{cases} v_d = -ri_d + E_d'' + x_q'' i_q \\ v_q = -ri_q + E_q'' - x_d'' i_d \end{cases}$$

$$\begin{cases} pE_q'' = \dfrac{1}{T_{d0}''}\left[-E_q'' - \left(x_d' - x_d''\right)i_d + E_q'\right] \\ pE_d'' = \dfrac{1}{T_{q0}''}\left[-E_d'' + \left(x_q' - x_q''\right)i_q + E_d'\right] \\ pE_q' = \dfrac{1}{T_{d0}'}\left[-E_q' - \left(x_d - x_d'\right)i_d + E_{fd}\right] \\ pE_d' = \dfrac{1}{T_{q0}'}\left[-E_d' + \left(x_q - x_q'\right)i_q\right] \end{cases}$$

$$\begin{cases} p\delta = (\omega - 1)\omega_0 \\ p\omega = \dfrac{1}{M}\left[P_m - E_d'' i_d - E_q'' i_q - \left(x_q'' - x_d''\right)i_d i_q\right] \end{cases}$$

If the sub-transient model is used in the TS simulator, where the d-axis sub-transient parameters are equal to the q-axis sub-transient parameters, the equivalent circuit of the generator can be represented as shown in Figure 5.5.

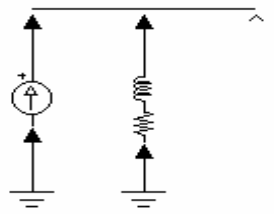

Figure 5.5: Equivalent Circuit of a Thermal Generator

The value of the equivalent current source is a function of generator state variables and sub-transient parameters and the equivalent internal impedance is $jx_d^{''}$.

$$I_x + jI_y = \left(\frac{E_q^{''} \sin\delta}{x_d^{''}} - \frac{E_d^{''} \cos\delta}{x_q^{''}} \right) + j\left(-\frac{E_d^{''} \sin\delta}{x_q^{''}} - \frac{E_q^{''} \cos\delta}{x_d^{''}} \right) \tag{5.1}$$

For the classical model, we have the same equivalent circuit as shown in Figure 4.4. The value of equivalent current source is a function of generator state variables and transient parameter and the equivalent internal impedance is $jx_d^{'}$.

$$I_x + jI_y = \left(\frac{E^{'} \sin\delta}{x_d^{'}} \right) + j\left(\frac{-E^{'} \cos\delta}{x_d^{'}} \right) \tag{5.2}$$

If the transient model is used the d and q axis transient parameters of the generator differ significantly, and there is no corresponding similar circuits such as those of the preceding two models. The generator can only be represented by a pure current source instead of the combination of a current source and an internal impedance. The current source magnitude can be evaluated from the following equation.

$$I = \frac{P_t - jQ_t}{\overline{V}_t} \tag{5.3}$$

The current source parameters in the Norton equivalent can be obtained

through the following matrix manipulation.

$$\begin{bmatrix} Y_{ee} & Y_{eb} \\ Y_{be} & Y_{bb} \end{bmatrix} \begin{bmatrix} V_e \\ V_b \end{bmatrix} = \begin{bmatrix} I_e \\ I_b \end{bmatrix}$$

$$Y_{ee}V_e + Y_{eb}V_b = I_e$$

$$Y_{eb}V_e + Y_{bb}V_b = I_b$$

$$V_e = Y_{ee}^{-1}I_e - Y_{ee}^{-1}Y_{eb}V_b$$

$$Y_{be}Y_{ee}^{-1}I_e - Y_{be}Y_{ee}^{-1}Y_{eb}V_b + Y_{bb}V_b = I_b$$

$$\left(Y_{bb} - Y_{be}Y_{ee}^{-1}Y_{eb}\right)V_b = I_b - Y_{be}Y_{ee}^{-1}I_e$$

where *e* stands for network nodes and *b* for boundary nodes.

The current source parameter in phasor form is $I_b - Y_{be}Y_{ee}^{-1}I_e$. During transients, generator rotor angles are in the process of changing, which affects the injection current, and the current source parameters in turn. Therefore, the current source needs to be updated at every interchange.

Because the frequency dependent equivalent circuit can be determined prior to the simulation, the only variable needed by the EMT simulator at every interchange is the current source value.

V.3 MODELING OF THE DETAILED SYSTEM

In the TS simulator, an equivalent is required to represent the detailed system. There are several different ways to represent the detailed system in the TS program. One way referred to as *system-level modeling*, is to treat the detailed system at the system level where all components in the detailed system are represented by their conventional transient stability model: HVDC links and FACTS devices, for example, would be represented by quasi steady-state model. The model is based on the expected performance of the devices and is usually tailored for a particular disturbance. Any non-expected failures, such as valve commutation failure, cannot be adequately represented.

Device-level modeling models the detailed system based on the boundary waveforms. The method is not concerned with how many components the detailed system has, and what they are, etc. It treats any situation in the same way, modeling the detailed system based on the interface voltage waveforms and the injection current waveforms from the detailed system. This treatment avoids the limitation faced by the system-level modeling.

Generally, the waveforms are distorted during transients, consisting of fundamental components, harmonics, dc-offsets, and other sequence components. In transient stability analysis, harmonics and dc-offset are not considered, thus only fundamental components remain. For symmetrical disturbances the fundamental component only comprises the positive-sequence, consequently the model of the detailed system is determined by the positive-sequence fundamental components of the voltages and currents.

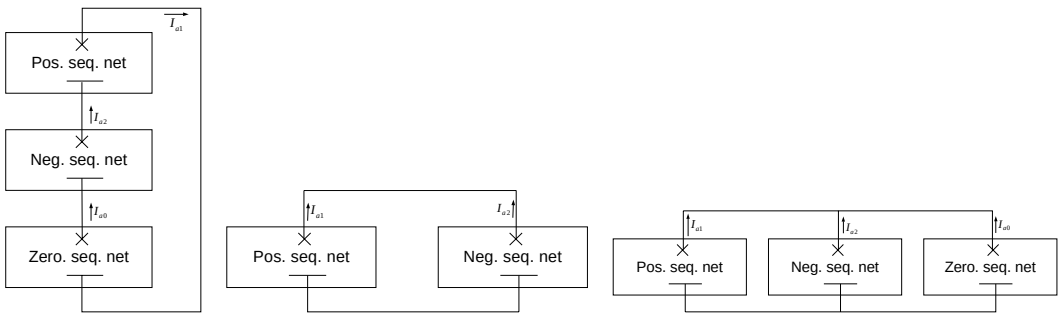

(a) Single line-to-ground fault (b) Double line-to-line fault (c) Double line-to-ground fault

Figure 5.6: Simulation of Asymmetrical Fault

TS simulators deal with symmetrical disturbances by representing the system as a single-phase equivalent, and this is not suitable for the direct solution of asymmetrical disturbances. Asymmetrical disturbances can be analyzed by appropriately interconnecting the positive-, negative-, and zero-sequence networks at fault point in a way where the topology is determined by the type of fault, as shown in Figure 5.6. For a single line-to-ground fault, the three sequence networks are connected in series. For a line-to-line fault, the fault is simulated by connecting

negative-sequence network between the fault point and the reference bus. For a double line-to-ground fault, the three sequence networks are connected in parallel.

The TS simulator handles the effect of negative- and zero-sequence networks on swing curves by building an equivalent impedance of negative- and/or zero-sequence networks and inserting them into the positive-sequence network. From the positive-sequence network point of view, the equivalent impedance can be expressed in terms of the positive-sequence current (I_1) and the positive-sequence bus voltage (V_1), as shown in Figure 5.7. For any fault, the impedance of the equivalent is always equal to V_1/I_1.

In hybrid simulation the positive-sequence network can be divided into two parts, consistent with the partition of the external system and the detailed system. For symmetrical disturbances, there are no negative- and zero-sequence networks. The detailed system alone is represented by the interface bus positive-sequence component voltage ($V_{\text{int}\,erface}$) and the positive-sequence component current ($I_{\text{int}\,erface}$) as shown in Figure 5.8(a). For asymmetrical disturbances, the fault point is always located in the detailed system, thus the voltage $V_{\text{int}\,erface}$ and the current $I_{\text{int}\,erface}$ can represent the detailed system plus the combination of the negative- and zero-sequence networks, as shown in Figure 5.8(b).

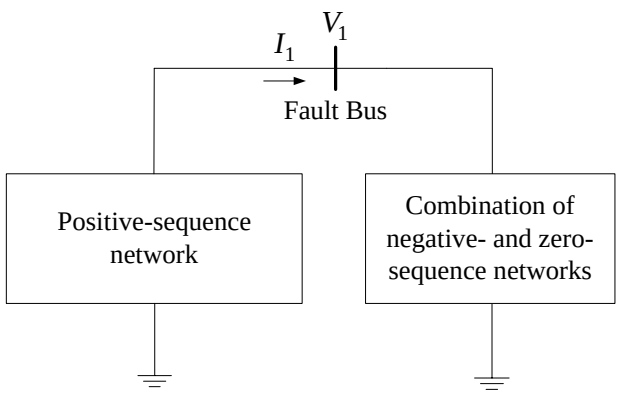

Figure 5.7: Sequence Networks Representation in Conventional TS Simulators

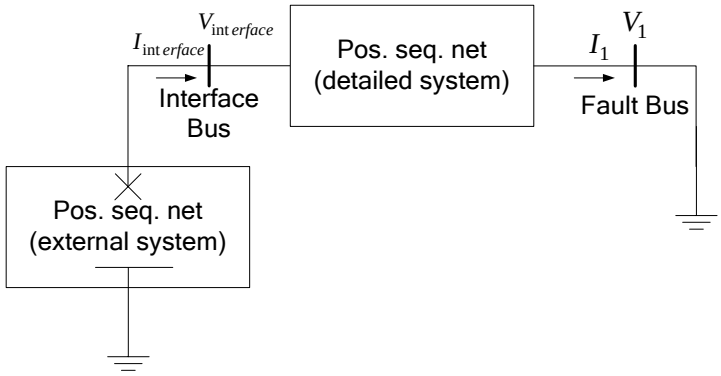

(a) symmetrical

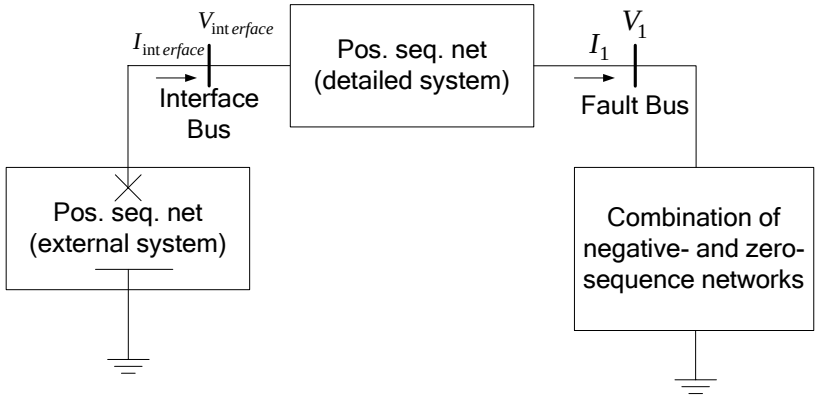

(b) asymmetrical

Figure 5.8: Positive-Sequence Representation in Hybrid Simulation

For application in a hybrid simulator it is not necessary to explicitly interconnect the zero and negative sequence networks. Instead, the equivalent of the negative and zero sequence components will be provided by the EMT simulation and passed to the TS simulator as an equivalent positive sequence component through the interface. Therefore, for any kind of disturbance, the positive-sequence fundamental components of voltages and currents are needed by the TS simulator.

The positive-sequence fundamental components can be extracted from the distorted boundary waveforms. The two conventional extraction methods are least squares curve-fitting and digital Fourier transformation, as discussed in Appendix D. It was found that the two methods have similar performance, as demonstrated by the following example.

For the following three-phase typical SVC current waveforms, as shown in Figure 5.9, the two methods are used to extract the fundamental components. The results are shown in Figure 5.10.

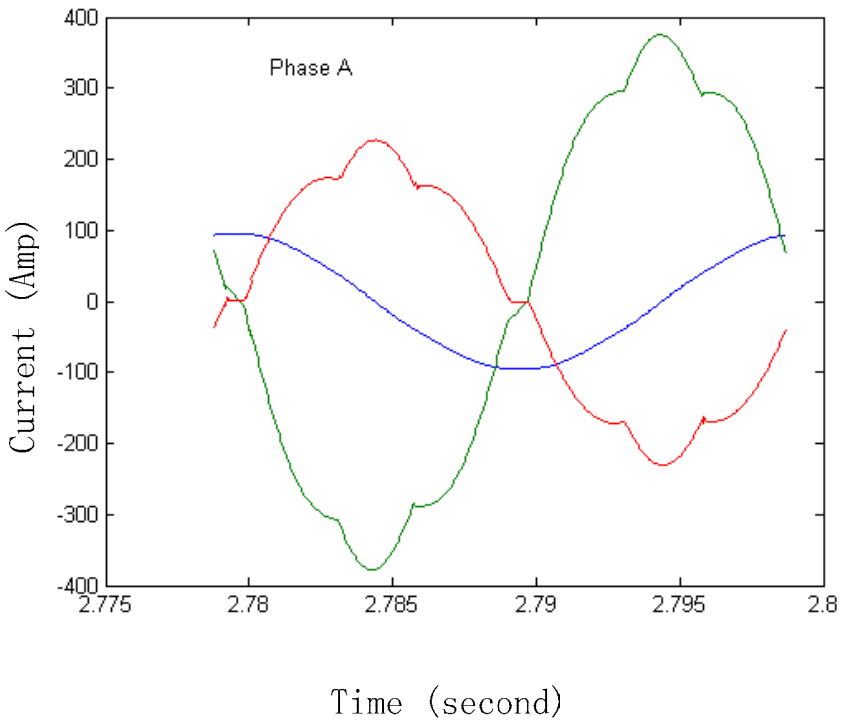

(a) Phase A

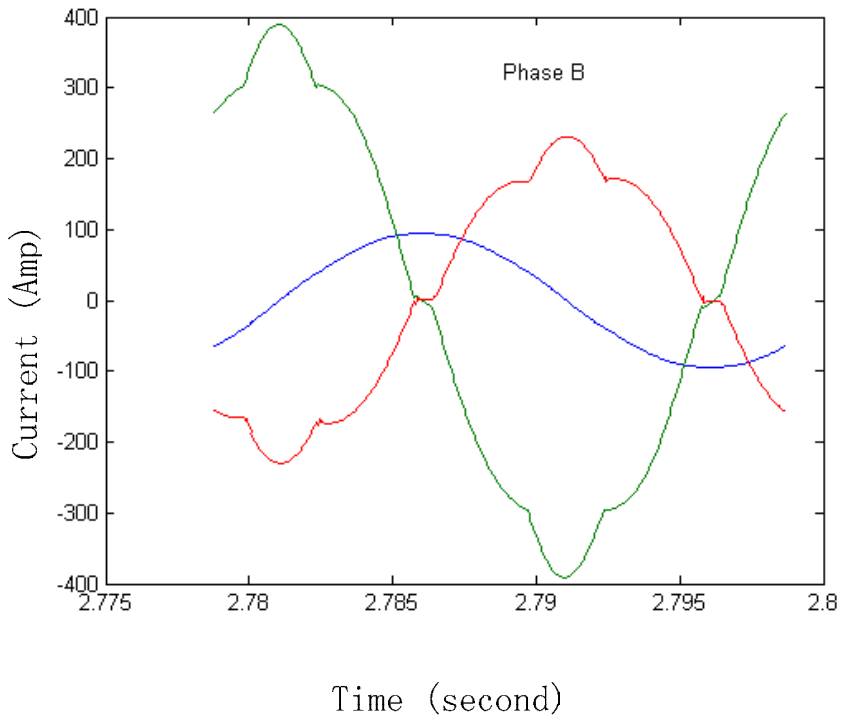

(b) Phase B

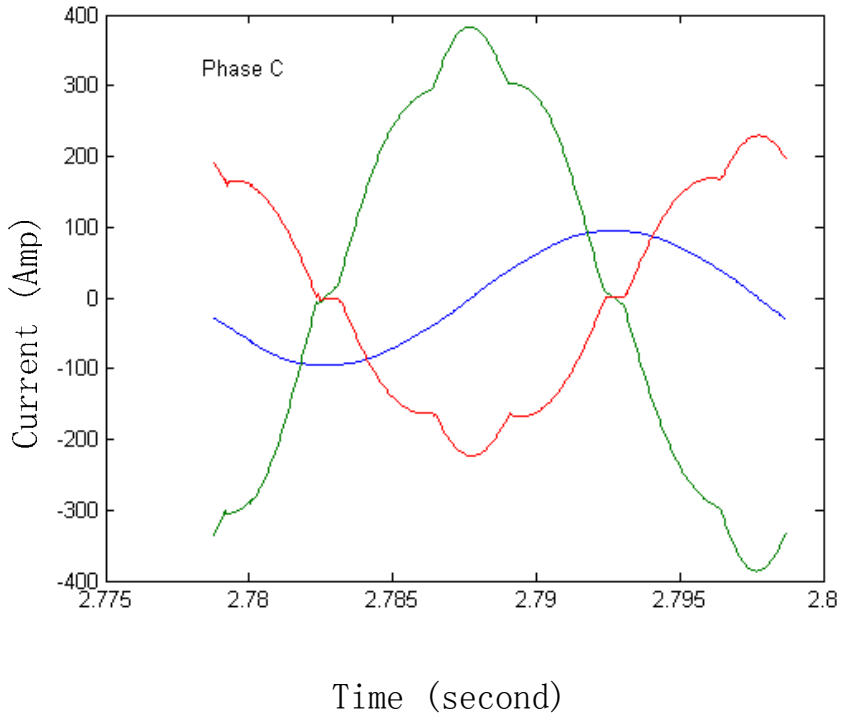

(c) Phase C

Figure 5.9: Three-Phase Distorted SVC Current Waveforms

	Digital Fourier analysis		Least squares method	
	a	*b*	*a*	*b*
Ia:	-30.878645	-135.873448	-30.8786	-135.8734
Va:	185643.7	-42415.07	185643.0	-42415.00
Ib:	135.787209	38.603276	135.7872	38.6033
Vb:	-55918.9	181974.2	-55919.0	181974.0
Ic:	-104.9086	97.27015	-104.9086	97.2701
Vc:	-129724.85	-139559.156	-129725.0	-139559.0

All results were obtained from the same randomly chosen data

where ***a*** and ***b*** represent the real and imaginary parts

Figure 5.10: Extraction Results from Digital Fourier Analysis and Least Squares Method

The results show that from the same randomly chosen data the two methods obtain the same results. In this thesis, the least-squares curve fitting method was used to do the extraction. The equation used is listed below.

$$\begin{bmatrix}\theta_0\\ \theta_1\end{bmatrix}=\begin{bmatrix}\sum_{i=0}^{k-1}\cos^2\omega t_i & \sum_{i=0}^{k-1}\cos\omega t_i\sin\omega t_i\\ \sum_{i=0}^{k-1}\cos\omega t_i\sin\omega t_i & \sum_{i=0}^{k-1}\sin^2\omega t_i\end{bmatrix}\begin{bmatrix}\sum_{i=0}^{k-1}y(t_i)\cos\omega t_i\\ \sum_{i=0}^{k-1}y(t_i)\sin\omega t_i\end{bmatrix} \tag{5.4}$$

where θ_0 and θ_1 are the real and imaginary part of phasor, $y(t_i)$ is date sample of the EMT solution, ω is angular speed.

The boundary condition includes two variables, the interface bus voltage and the injection current from the detailed system. Therefore there are totally four forms of the equation of the detailed system, i.e. current source, voltage source, impedance and power.

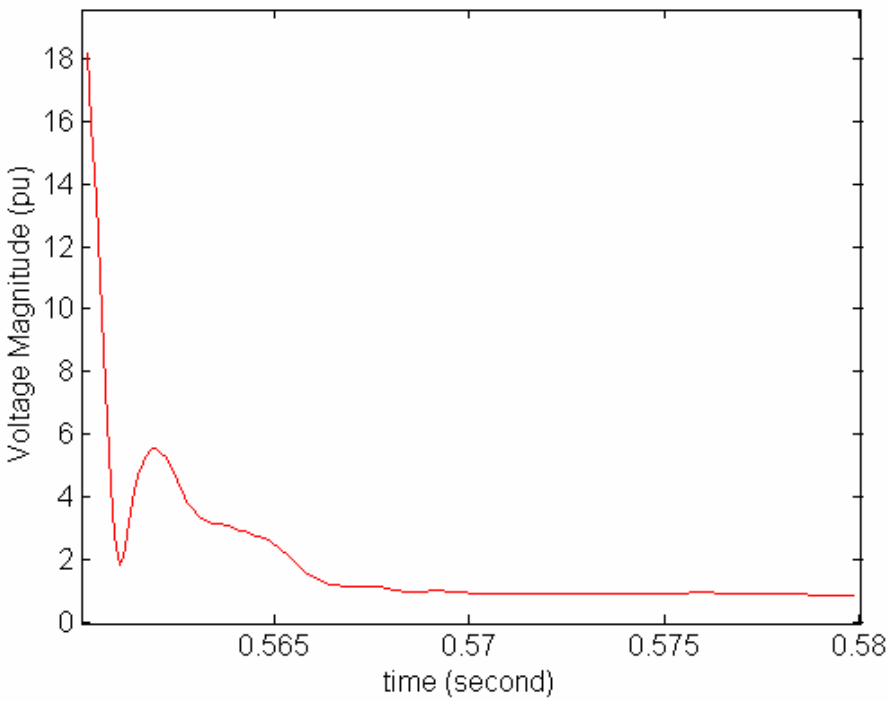

Figure 5.11: Typical Extraction Curve

The extraction is performed on the data samples between two successive interchanges. One issue that has to be solved is how to ensure the credibility of the results. The finally adopted approach is to check whether the extraction is successful is to fit the curves by using the accumulated samples as the simulation progresses within one period. If the results converge to a constant value, as shown in Figure 5.11, the results are assumed to be creditable.

V.4 INTERFACE LOCATION

The choice of the location of the interface bus is at first glance obvious: for an HVDC system it could be the filter bus, and for a FACTS device, it could be the terminals of the device. However, there may be other considerations which would lead to a different location. In fact, the choice of the interface location has a very close relation with the modeling of equivalents of both the external and detailed systems.

V.4.1 CONVENTIONAL APPROACH – WAVEFORMS DISTORTION

There were two different approaches to choose the interface location as proposed in [89-95], which discusses the issue of location with the purpose of making sure that the waveforms from the EMT simulator are the correct shape.

For the first hybrid described by Heffernan et al [89-91], the intention was to model the AC and DC solutions separately. The point of interface location was consequently the converter bus terminal, as shown in Figure 5.12. A fundamental frequency equivalent was used to represent the stability program in the detailed solution and vice versa. The advantage of this choice is that the scale of the detailed system can be reduced to a minimum.

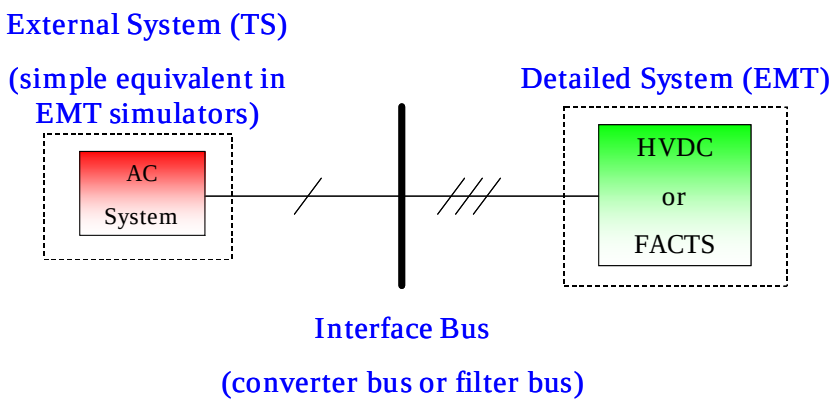

Figure 5.12: Interface Location

Reeve et al [92-93] later correctly pointed out that the major drawback of the detailed solution is in not seeing a true picture of the external system, since the equivalent circuit is fundamental frequency based. A simple fundamental frequency equivalent circuit is insufficient to present the correct impedance of the external system at other frequencies to the converter. The countermeasure proposed is to represent more of the external system in detail through use of the extended interface bus, as shown in Figure 5.13. Therefore, the waveforms at the interfacing buses become more close to the actual waveforms, and the detailed solution is more credible. This will also facilitate data transfer as the waveforms on the extended interface bus are less distorted. However, exactly how far should the interface location be extended is hard to predict and depends on the phase imbalance and waveform distortion.

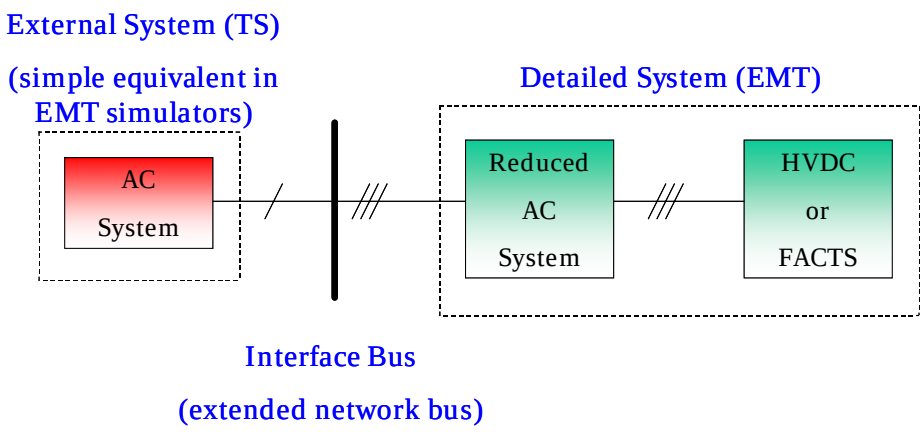

Figure 5.13: Extended Interface Location

As more components are involved in the detailed solution, the complexity of interfacing increases generally. Anderson et al [94,95] proposed that a frequency dependent equivalent circuit should be employed instead of a simple one. The frequency dependent equivalent can provide an accurate picture of the system impedance across its frequency spectra. Correct waveforms can be obtained at the interfacing buses without the effort of extending the interface location. The use of a frequency dependent equivalent avoids the necessity to extend the interface bus.

V.4.2 ALTERNATIVE APPROACH – EXTRACTION QUALITY

Previously the main concern in determining the interface location is the consideration of the effects of waveform distortion on the detailed system equivalent modeling. However, with the use of a frequency dependent equivalent, this consideration has become less important, and instead, the quality of the variables transferred across the interface bus from the EMT to TS has now become more of a concern.

The positive-sequence fundamental components of the distorted waveforms produced by the EMT simulation have to be extracted. In case the number of data samples within one cycle is not sufficient for the extraction when the degree of distortion is too high, the interface location has to be extended. The quality of extraction can be assessed by continuously monitoring the curve fittings using the accumulated samples as the simulation progresses within one time period. If the results converge to consistent values, the number of data samples is sufficient and the extraction is credible. This approach can be used as a simple assessment criterion for determining the optimum interface location.

As discussed in section 3, the equivalent of the detailed system in the TS simulator needs both the interface bus voltage and the injection current from the detailed system in phasor form. Their extraction qualities are affected by the presence of dc-offset in current waveforms.

V.4.3 EFFECTS OF HARMONICS AND DC OFFSET

In this thesis the least-squares curve-fitting method was used to do the extraction, and the period immediately after network disturbances was chosen as the worst condition to test the method. If the method can work under such condition, it can work for the whole simulation.

Following a disturbance the bus voltage waveforms are generally distorted by

many harmonics, while the current waveforms contain an extra component, a quasi-dc offset. The extraction methods, such as curve fitting method, can effectively extract the fundamental component from harmonics, but the capability to deal with time-variant dc offset is quite poor. This situation can be illustrated by the following example.

On a 39-bus-10-machine system (shown in Appendix B), a three-phase solid fault was applied at bus 38, from 0.5 to 0.54 second. The detailed system contains the lines between bus 36, 38 and 39, and generator 9 as well as the transformer associated with it. The interfacing location is at bus 36, and the voltage and current waveforms at the bus are shown in Figure 5.14.

Figure 5.14, which shows the bus 36 voltages and current injections, demonstrates that the bus voltages include many harmonics while the line currents contain significant dc offsets. Figures 5.15-5.20 show the extractions from phase voltages and currents for the cycle right after the fault is applied (0.5-0.52 second). It is obvious that the curve-fitting method can effectively extract the fundamental components from harmonics, but it works quite poorly in the cases with dc offsets.

V.4.4 CHOOSE OF TRANSFER VARIABLES

To build the equivalent of the detailed system in the TS simulator, we need to extract the phasor values of the bus voltages and currents. However, owing to the existence of dc offsets, the phasor value of the current cannot be extracted accurately from the EMT simulation output. In fact, the presence of dc offset is always a problem, especially for relays. Some recent literature [98,99] discusses how to deal with the dc offset.

For hybrid simulation, especially in real-time operation mode, the dc offset must be filtered out very quickly. An alternative approach is illustrated in Figure 5.21.

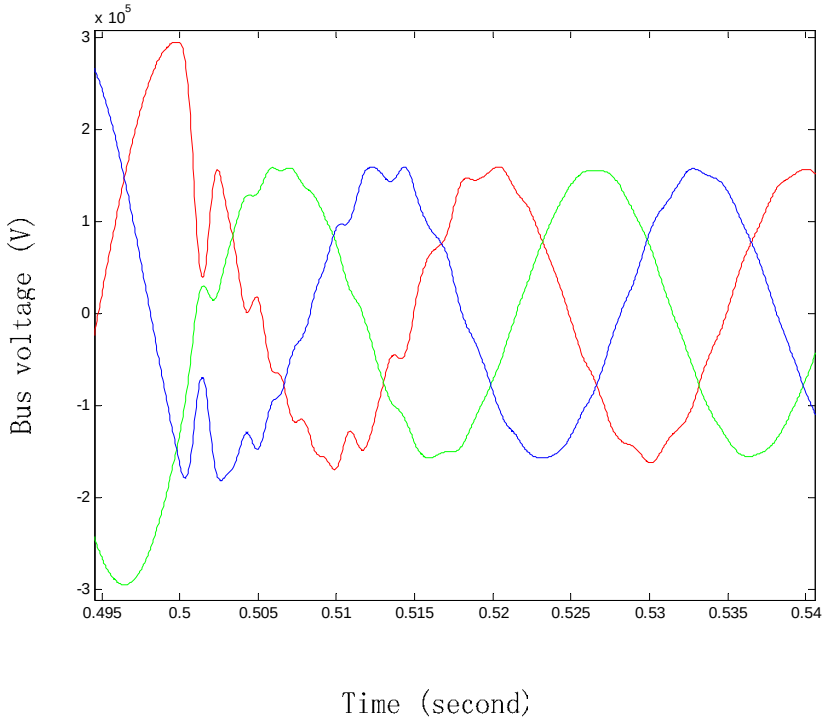

(a) Bus voltage waveforms

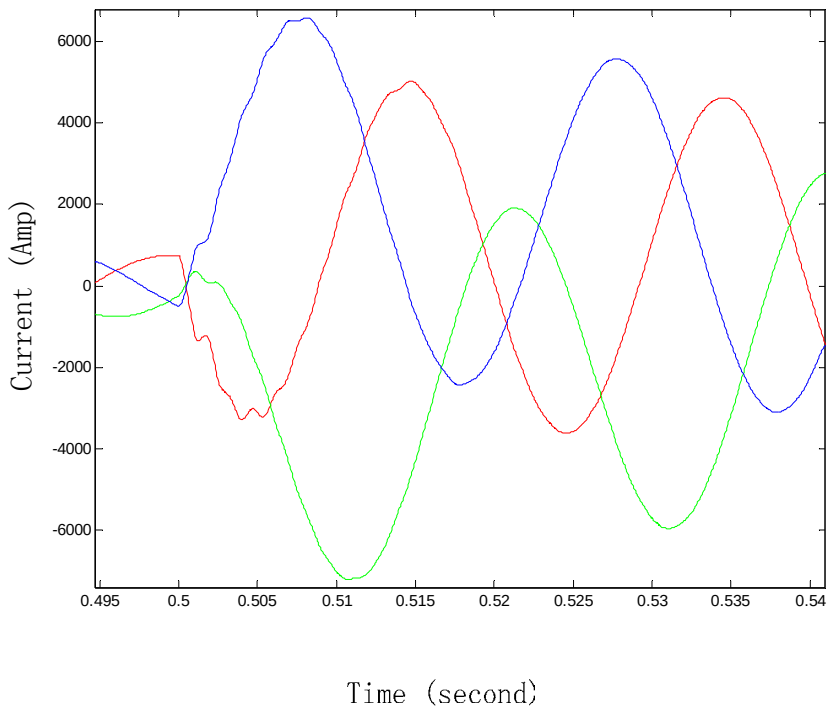

(b) Line current waveforms

Figure 5.14: Busbar No 36 Voltage and Injection Current from Detailed System

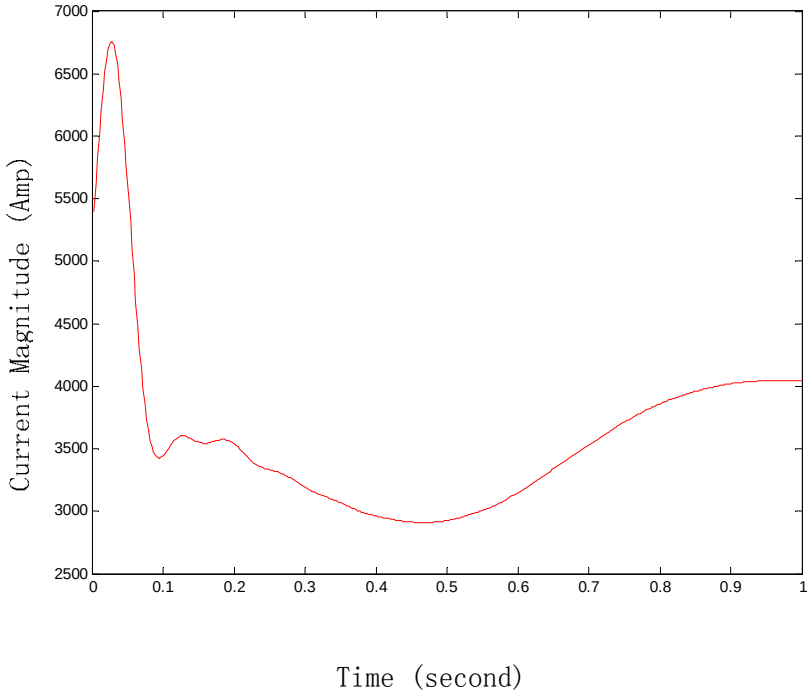

(a) Magnitude

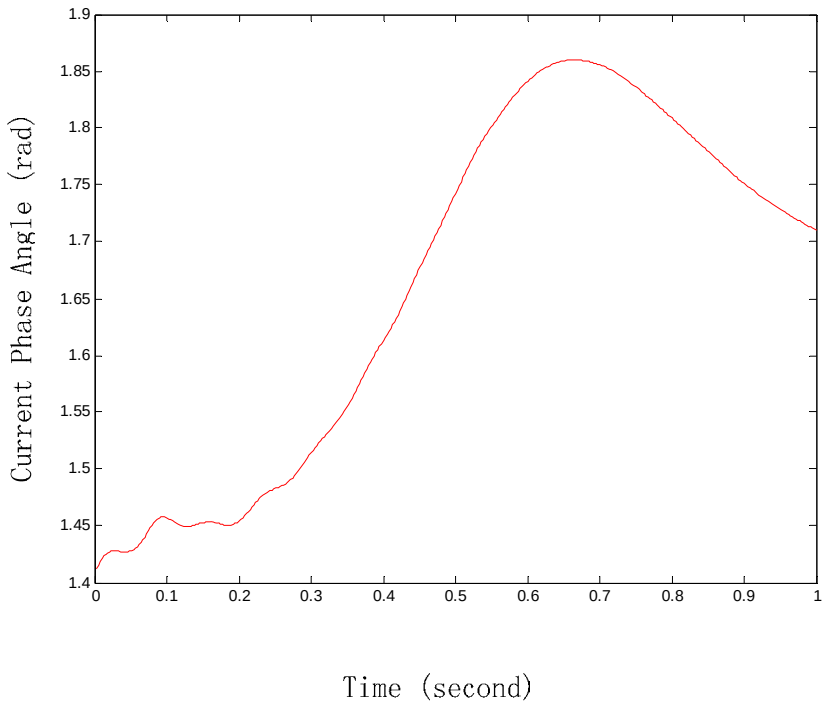

(b) Phase Angle

Figure 5.15: Phase A Current Extraction: Magnitude and Phase Angle

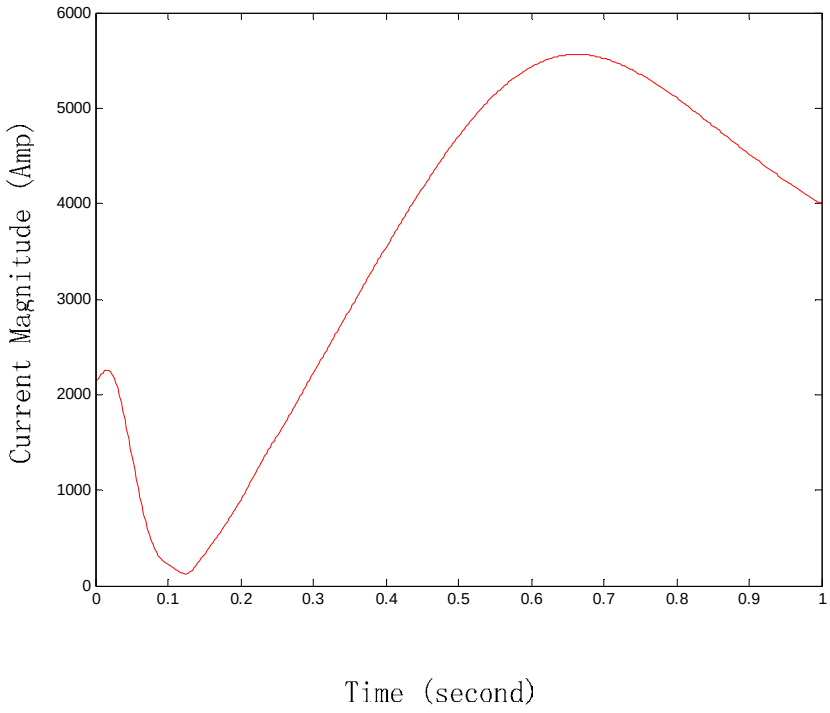

(a) Magnitude

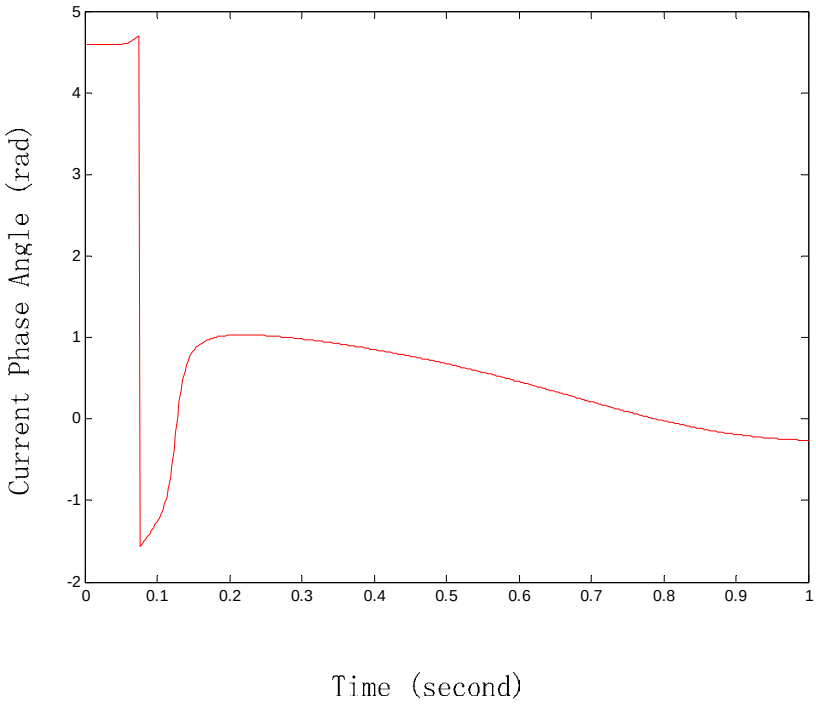

(b) Phase Angle

Figure 5.16: Phase B Current Extraction: Magnitude and Phase Angle

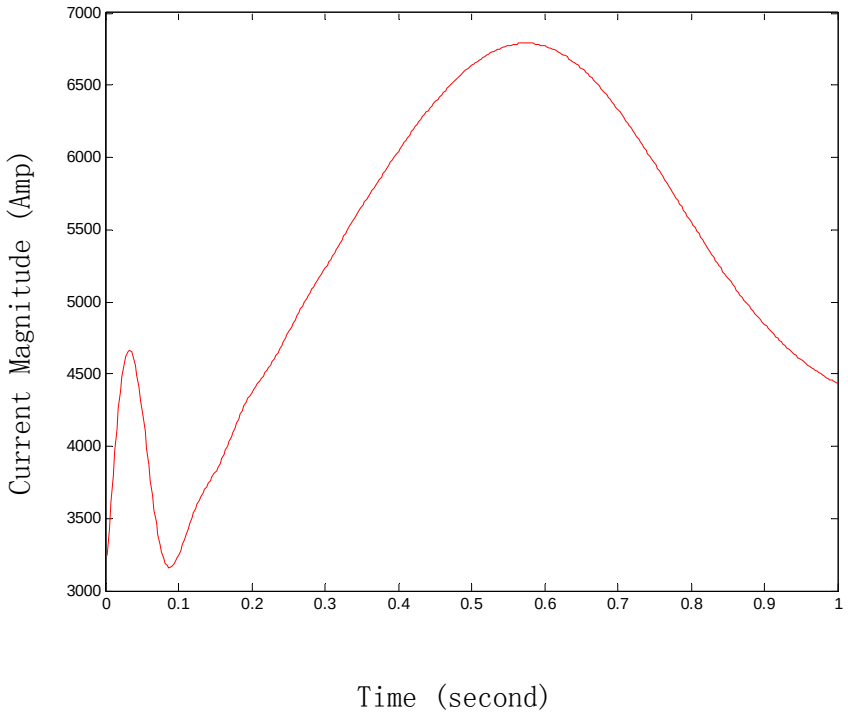

(a) Magnitude

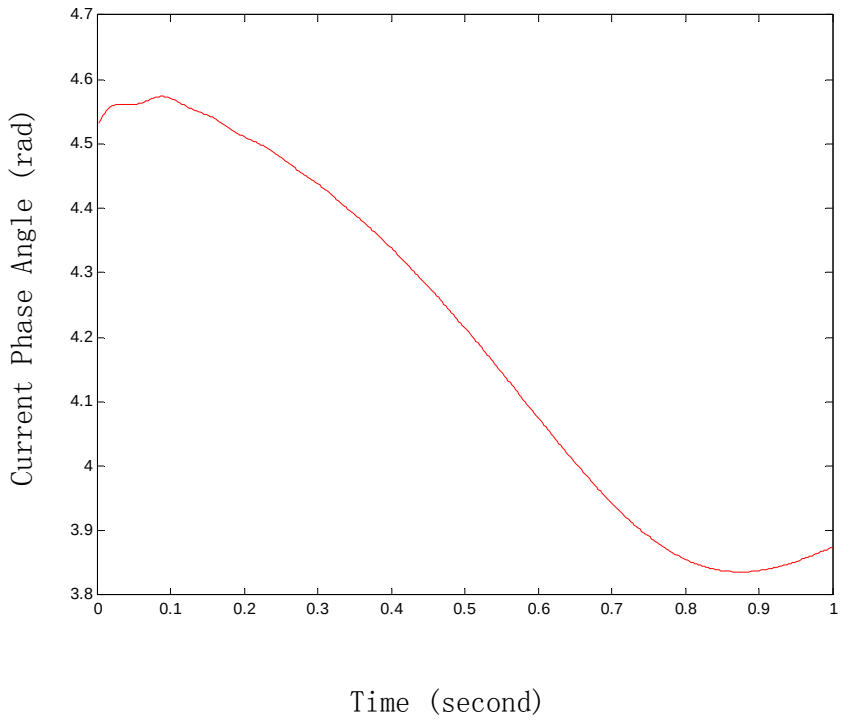

(b) Phase Angle

Figure 5.17: Phase C Current Extraction: Magnitude and Phase Angle

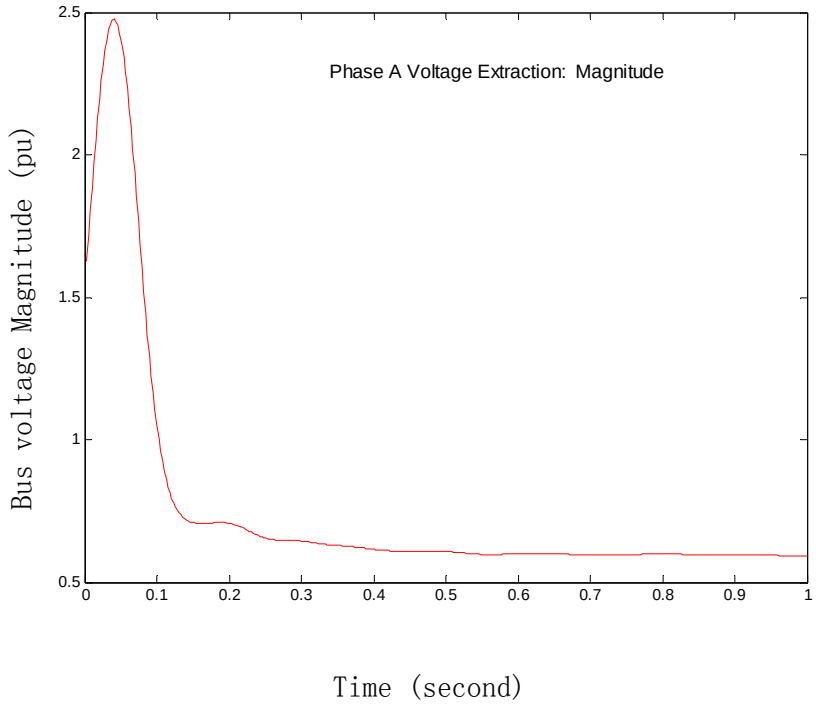

(a) Magnitude

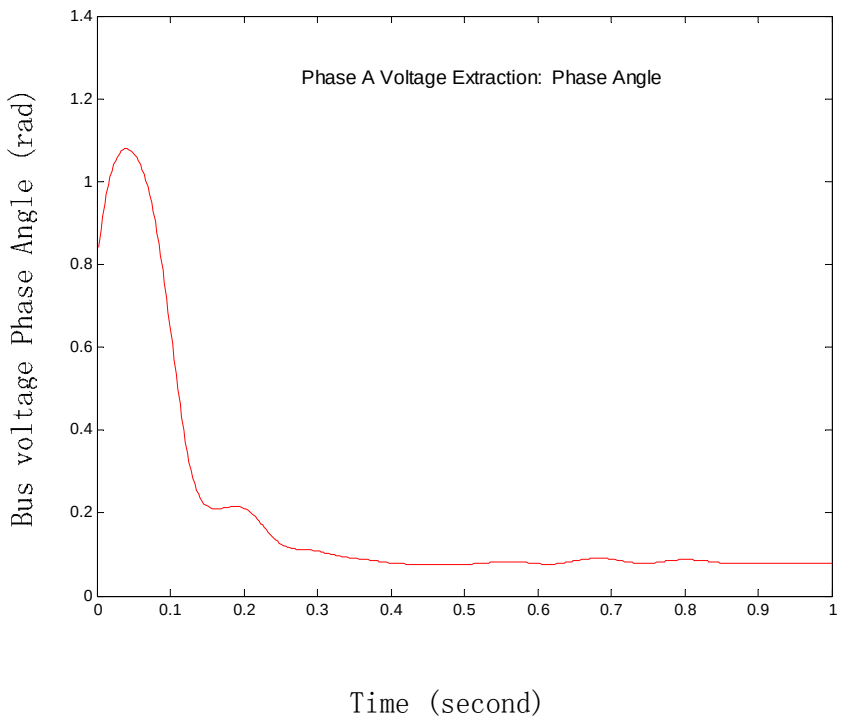

(b) Phase Angle

Figure 5.18: Phase A Voltage Extraction: Magnitude and Phase Angle

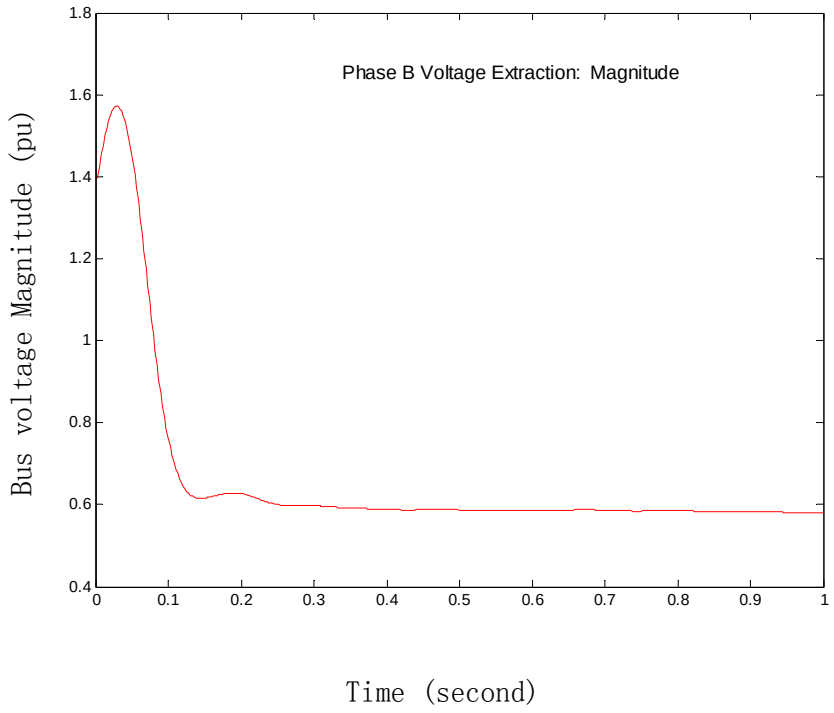

(a) Magnitude

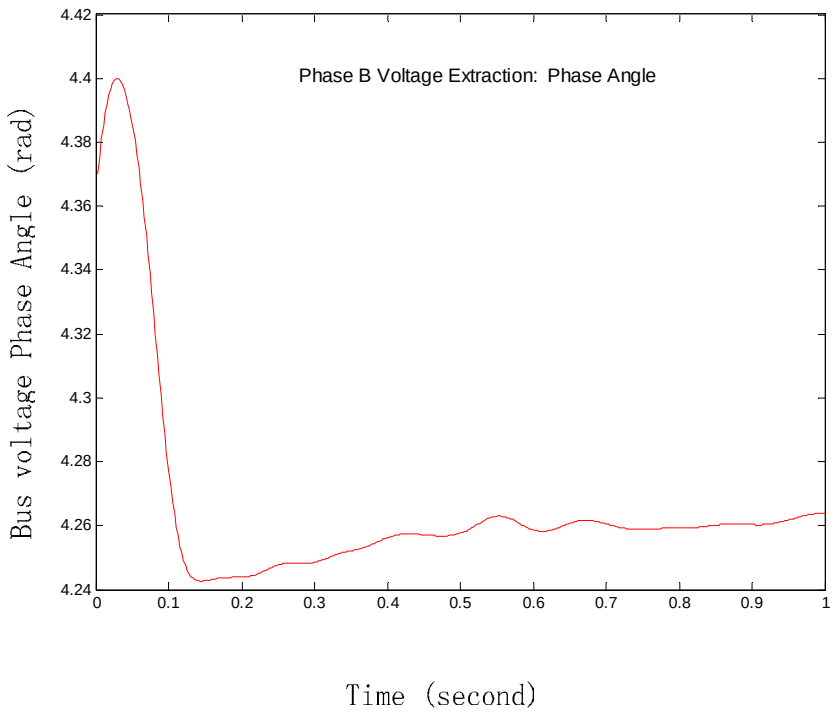

(b) Phase Angle

Figure 5.19: Phase B Voltage Extraction: Magnitude and Phase Angle

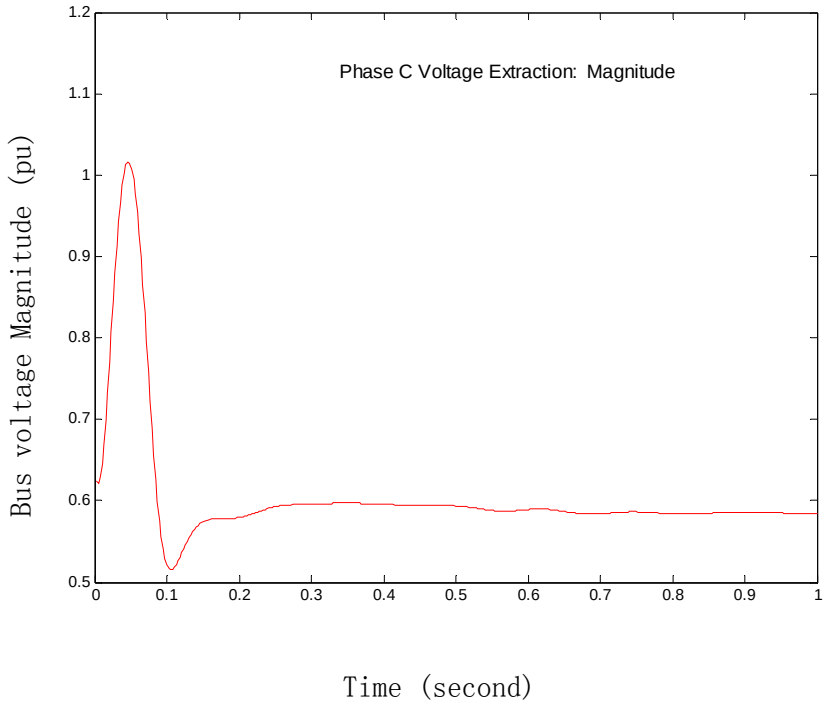

(a) Magnitude

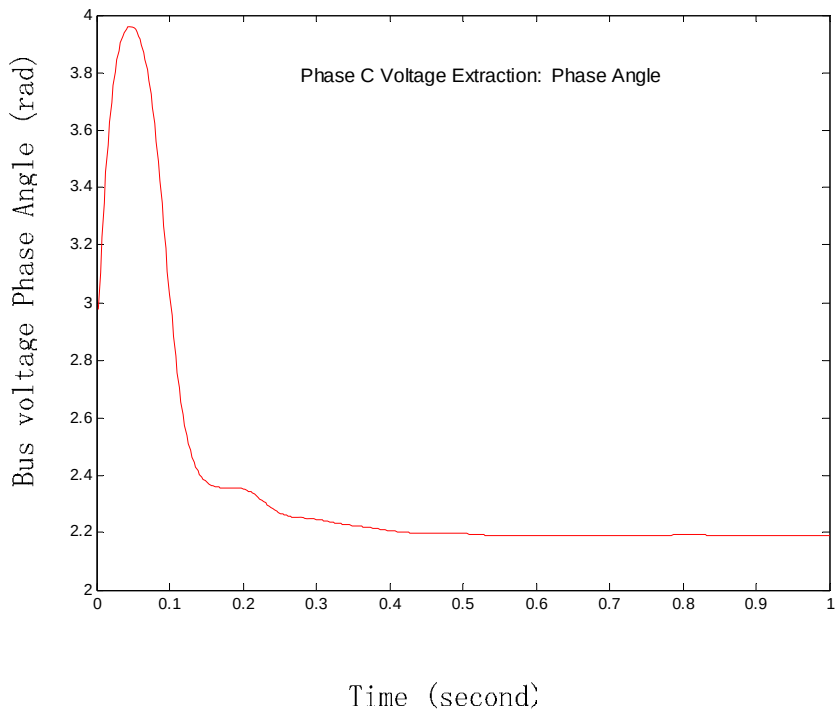

(b) Phase Angle

Figure 5.20: Phase C Voltage Extraction: Magnitude and Phase Angle

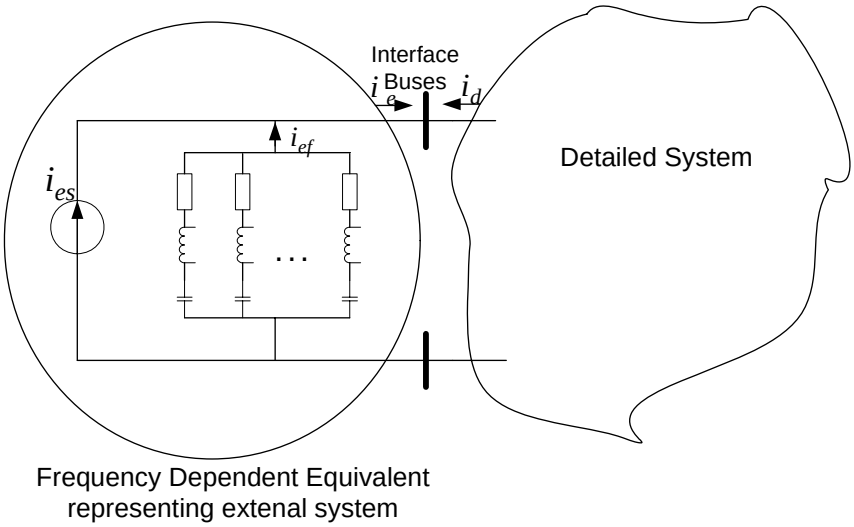

Figure 5.21: Alternative Approach Dealing With Injection Current From Detailed System

At the interface bus the absolute value of the current injected to the bus from the detailed system (i_d) must be equal to that from the external system (i_e) at any time. Any component included in the current i_d must be included in the current i_e. The current i_e can be divided into two parts, i.e. the current from the current source (i_{es}) and the current from the frequency dependent equivalent (i_{ef}). The current i_{es} is three-phase positive-sequence fundamental frequency based, and this means that all non-fundamental components are only included in the current i_{ef}. The fundamental component of the current I_{ef} can be easily filtered out under the knowledge of the impedance of the frequency dependent equivalent and the fundamental component of the interface bus voltage, $I_{ef} = V_{interface\_bus} / Z_{fden}$.

The impedance of the frequency dependent equivalent can be obtained before simulation from the TS simulator, and its value does not change during the simulation. From the Figure 5.18-5.20, the fundamental component of the interface bus voltage can be effectively extracted by curve-fitting method even under the worst distortion condition. Thus, the fundamental component of the current i_d can be calculated without dealing with the dc offset.

The extraction on the bus voltage works well except for the period during which the network disturbance is cleared. In the TS simulator, the breakers in

different phases are assumed to be open simultaneously, which is not true in the real case: current is not interrupted until it reaches a natural zero crossing. Thus for a three-phase fault, three breakers do not interrupt at the same time, but sequentially as shown in Figure 5.22.

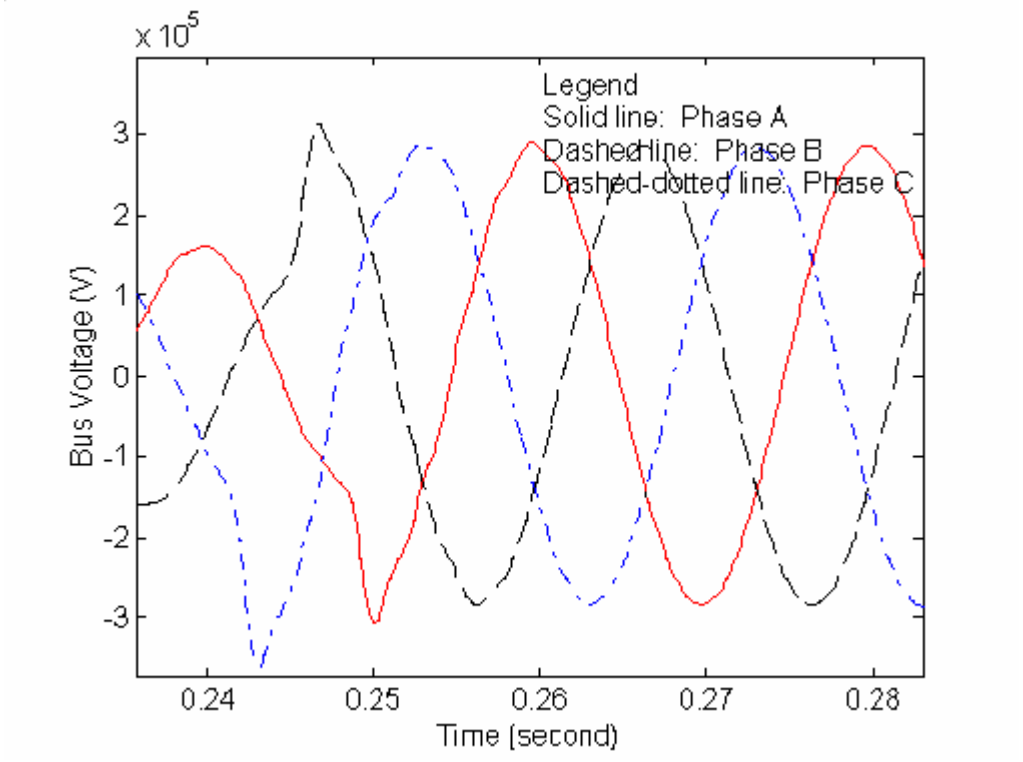

Figure 5.22: Bus Voltage Waveforms after Fault Clearing

As shown, the breaker in phase c turns off first, then phase b and then phase a. The breaker in phase a almost switches off in the middle of the period from 0.24 to 0.26 second. But in the TS simulator, it is assumed that three breakers turn off simultaneously, at 0.24 second.

Because of the different switching times, the bus voltage waveform changes do not occur at the specified time, which causes a problem with the extraction process. Figures 5.23-5.25 show the three-phase bus voltage extraction curves. Curves of phase c show the best extraction while curves of phase a show the worst. This is reasonable since the breaker in phase c acts first and the breaker in phase a acts last.

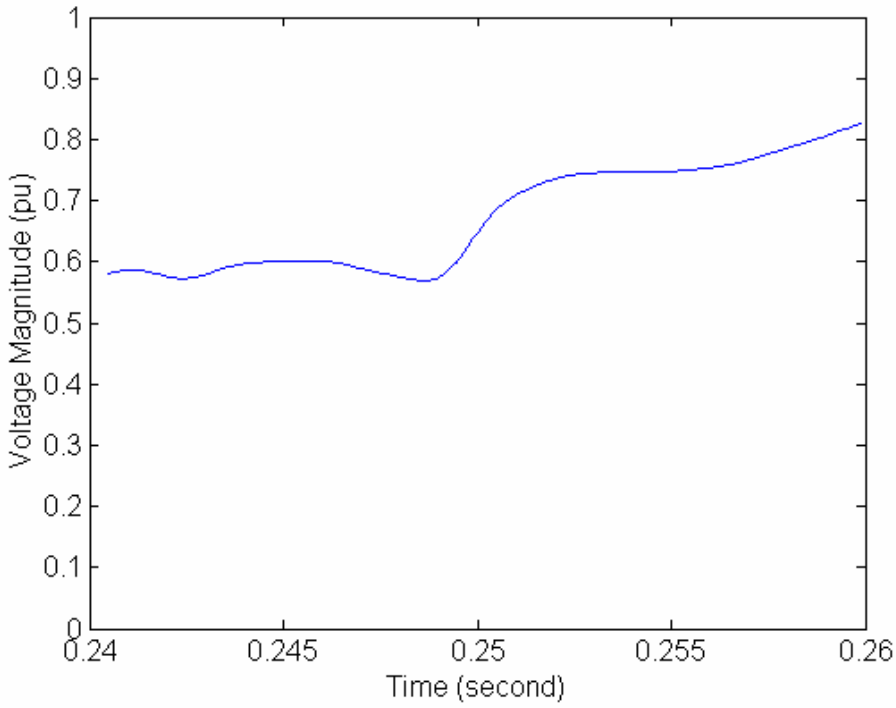

(a) Magnitude

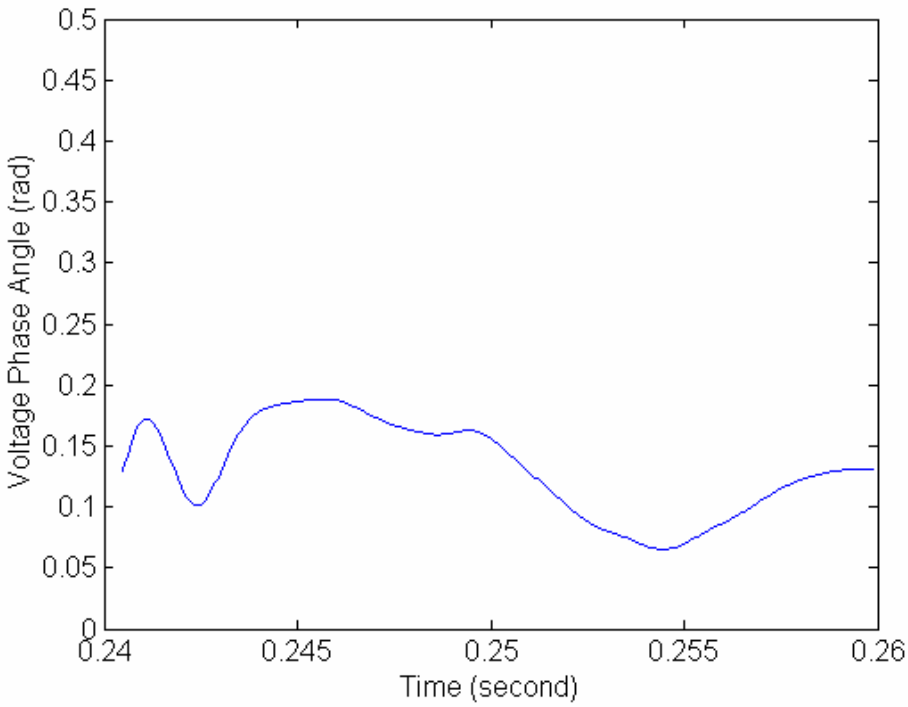

(b) Phase Angle

Figure 5.23: Bus Voltage Phase A Extraction Curves

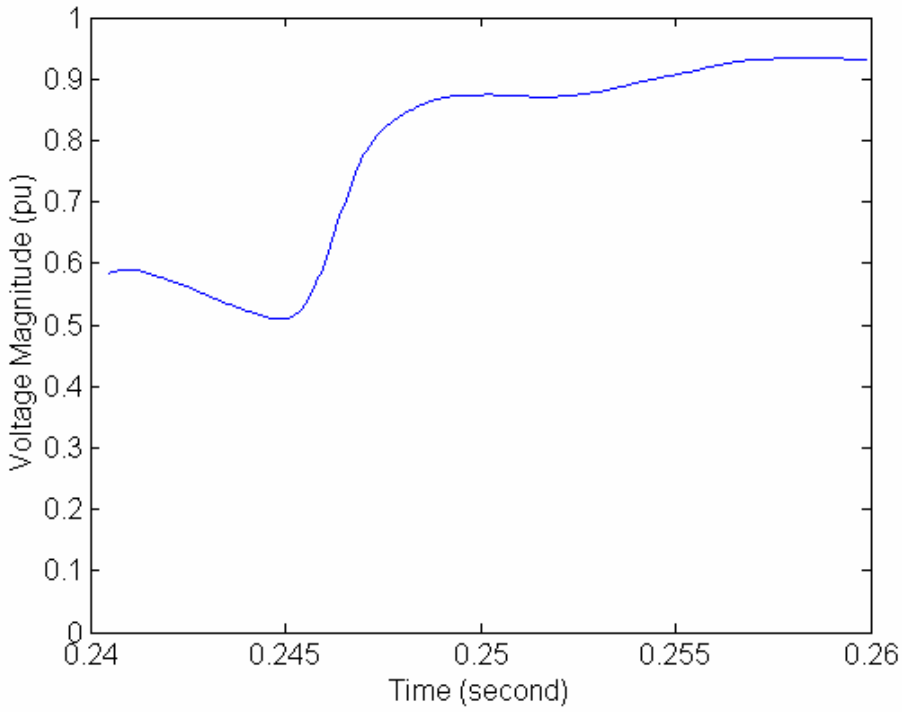

(a) Magnitude

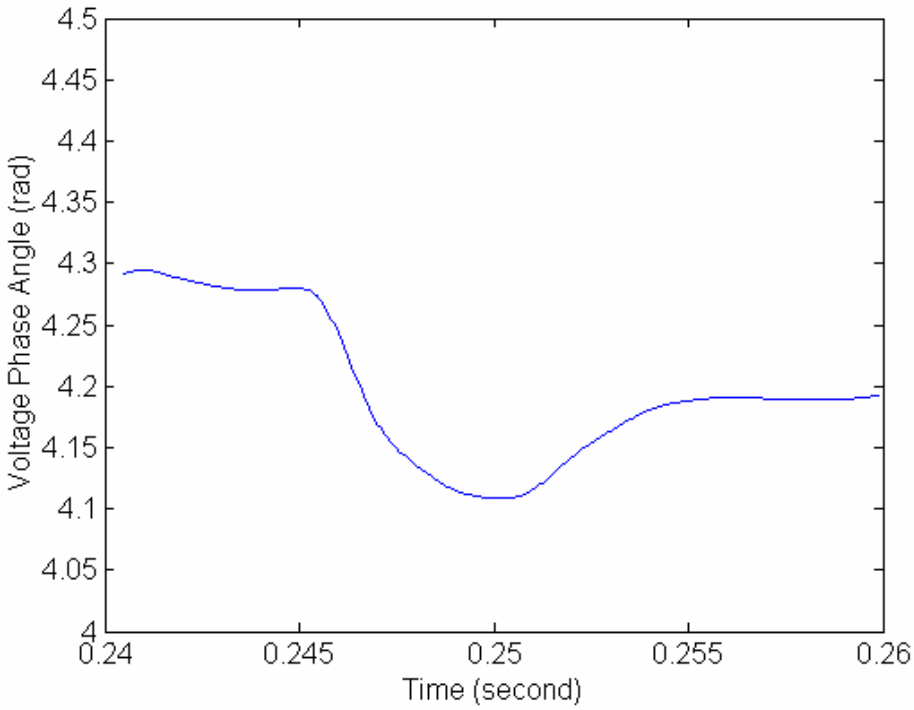

(b) Phase Angle

Figure 5.24: Bus Voltage Phase B Extraction Curves

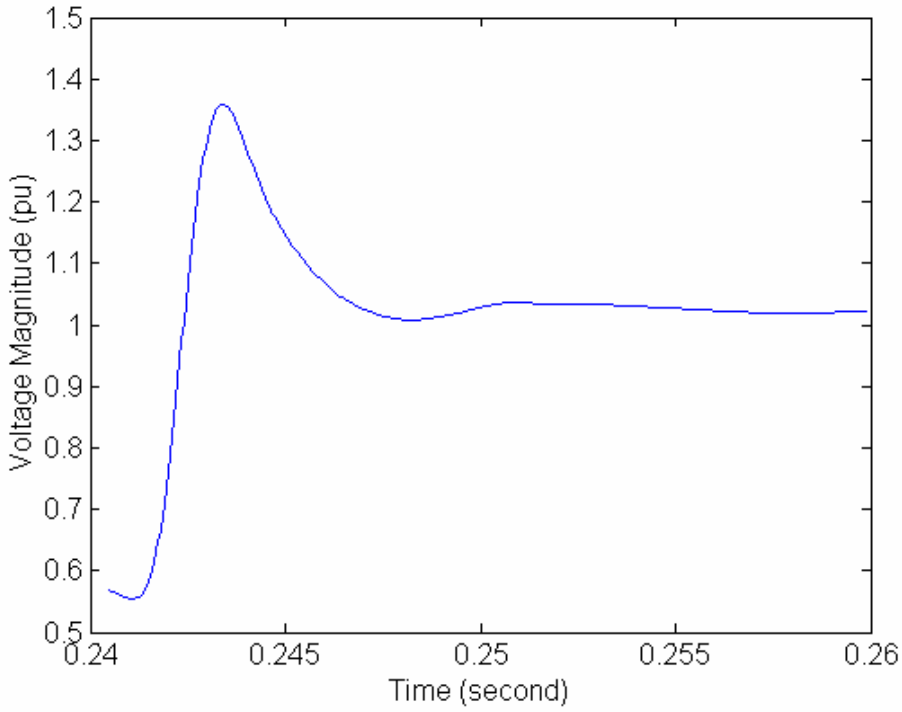

(a) Magnitude

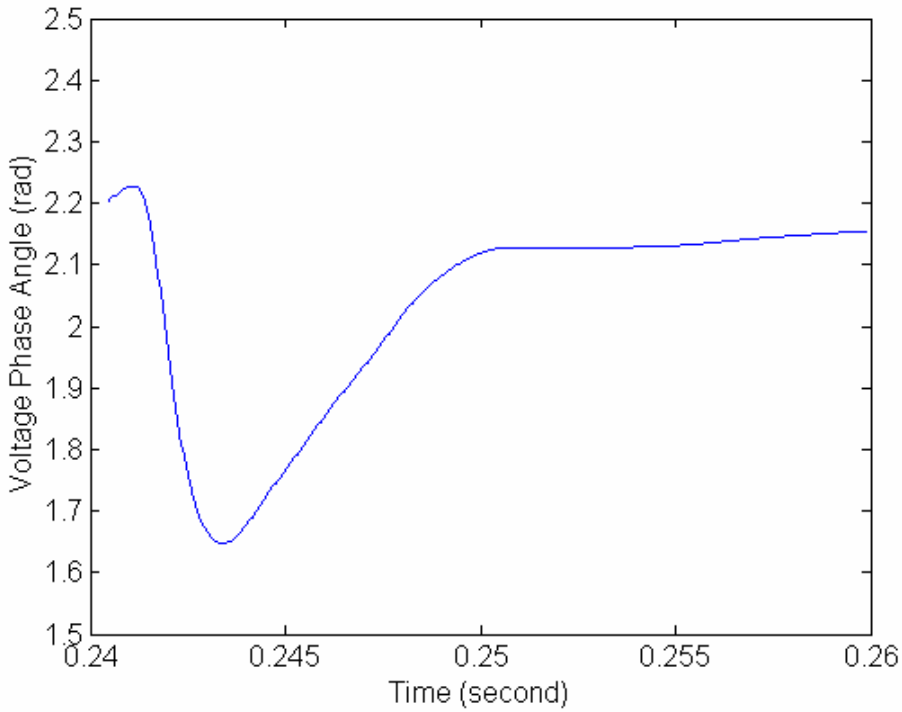

(b) Phase Angle

Figure 5.25: Bus Voltage Phase C Extraction Curves

The difficulty in the extraction cannot be overcome by extending the interface buses. However since, typically, the duration of the fault is relatively short, the inaccuracy caused generally has a very little impact on the overall simulation and it is not normally necessary to extend the interface buses. This is demonstrated by case studies presented in Chapter 6.

V.5 INTERFACE PROTOCOL

While the integration step in the TS simulator is in the order of milliseconds, it is in the order of microseconds in the EMT simulator. An interaction protocol, as a result, has to be defined to allow the simulators to coordinate the execution sequences and work cooperatively as a single simulation tool. Information exchanging is usually carried out at each TS simulator time step and synchronizes with the Norton equivalent updates from the EMT simulation.

V.5.1 HYBRID SIMULATION INTERACTION SCHEME

The following interaction scheme is similar to the ones outlined in [89-95], but has been modified to correspond to a one-cycle integration time step to match the requirements for the implicit trapezoidal integration method as used in the TS simulator. The basis of this scheme is illustrated in Figure 5.26 and can be described as follow.

1. Both the EMT and TS simulators started from the same time T0 and proceeded to time T1.
2. The current sources in the Norton equivalents for the external system are derived from the TS simulation results at T1, and are transferred to the EMT simulator.
3. Using the latest Norton equivalent obtained at T1, the EMT simulator executes from T1 to T2.
4. EMT simulator results from T1 to T2 are processed by using a curve fitting

method to obtain the phasor values of the powers (P and Q) corresponding to time T2.

5. TS simulator uses the P and Q from the EMT simulator to do the calculation for the interval T1 to T2.
6. The above procedure is repeated for the next cycle.

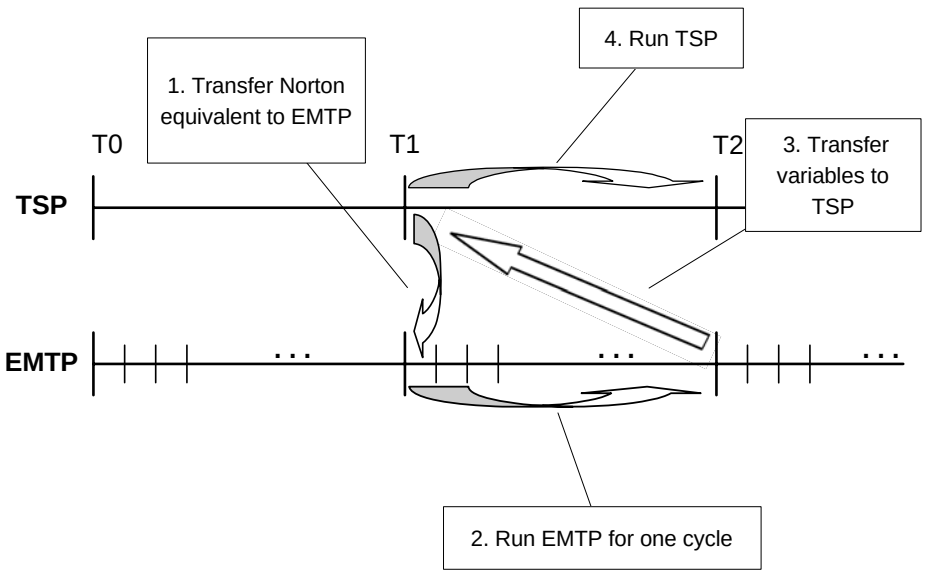

Figure 5.26: Interaction Protocol

In the Norton equivalent, the frequency of the current source is at the system frequency (50 or 60 Hz), being consistent with conventional TS simulator assumption. The values of P and Q are calculated based on the positive-sequence interface voltages and currents.

V.5.2 FREQUENCY MISMATCH DURING TRANSIENTS

The above-described scheme is designed for the ideal case with fixed system frequency. When the system frequency is 50 Hz, the EMT simulation time step is 50μs and TS simulation time step is 20ms, information exchange will take place once every 400 EMT simulation time steps (1 TS steps = 400 EMT steps). However, this is inadequate in practice when there are system frequency variations, since frequency

mismatch will occur if information exchanging is scheduled with fixed time interval.

During transients, the phasor of current source in Norton equivalent is normally not the same at each hybrid simulation time steps ($I_1 \neq I_2, \theta_1 \neq \theta_2$). For instance, at the beginning of one time step, EMT and TS simulators proceed from the same boundary condition I_1, θ_1 as illustrated in Figure 5.27. Upon the completion of the step, the TS simulator updates the current source to I_2, θ_2, which means the next hybrid simulation step should start from I_2, θ_2. However, after 400 EMT steps, the EMT simulator finishes its execution at $I_2^{'}, \theta_2^{'}$ instead. There is a gap if $\theta_2 > \theta_2^{'}$ (or overlap if $\theta_2 < \theta_2^{'}$). Without any remedy to this, magnitude and phase discontinuities will be introduced to the result under the transient conditions.

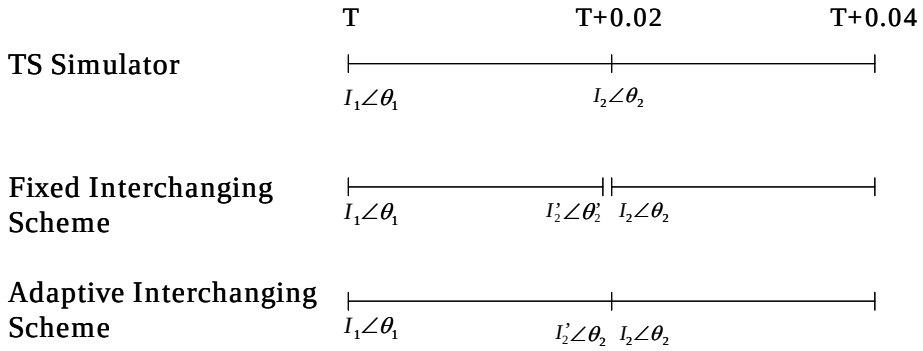

Figure 5.27: Adaptive Interchanging Scheme

The effect of these discontinuities is demonstrated in the interface bus voltage waveforms shown in Figure 5.28, where there was an interchange at 2.8 second. It is obvious, as shown in Figure 5.28(a), that the transients caused by the step magnitude change can be reasonably ignored, whilst the phase discontinuity can produce a spurious transient, as shown in Figure 5.28(b), which in turn causes a significant distortion and unbalance in voltage waveforms.

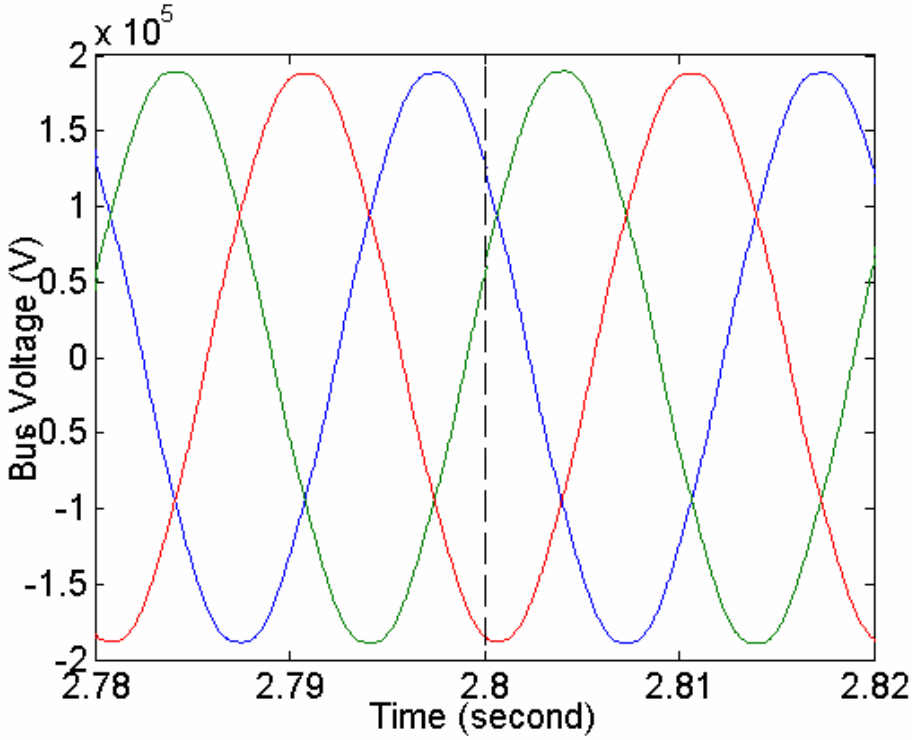

(a) Magnitude Discontinuity

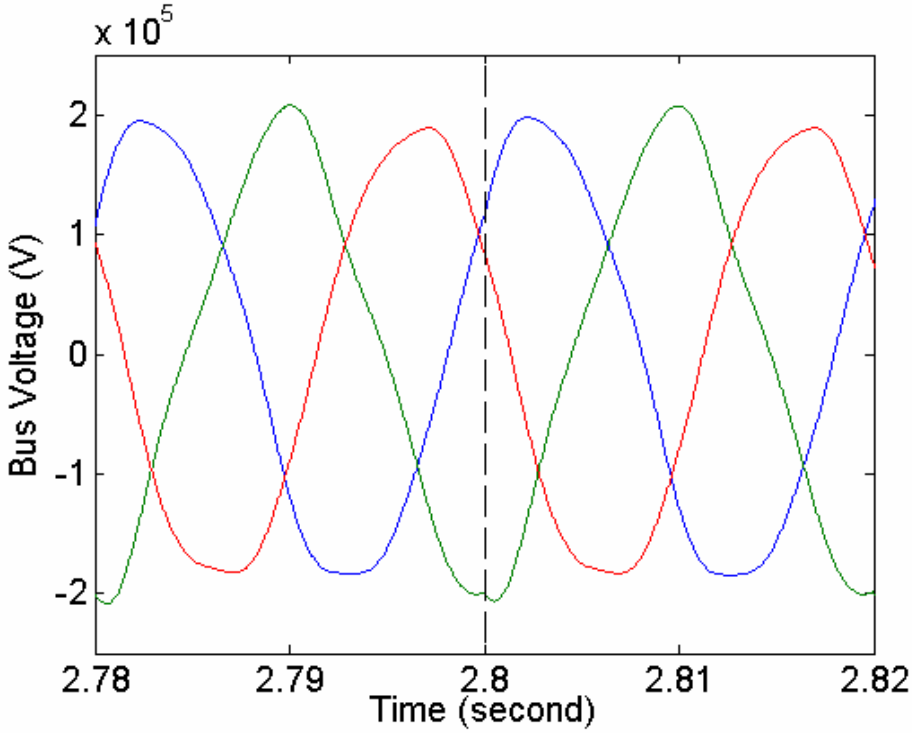

(b) Phase Discontinuity

Figure 5.28: Effects of Discontinuities on the Interface Bus Voltages

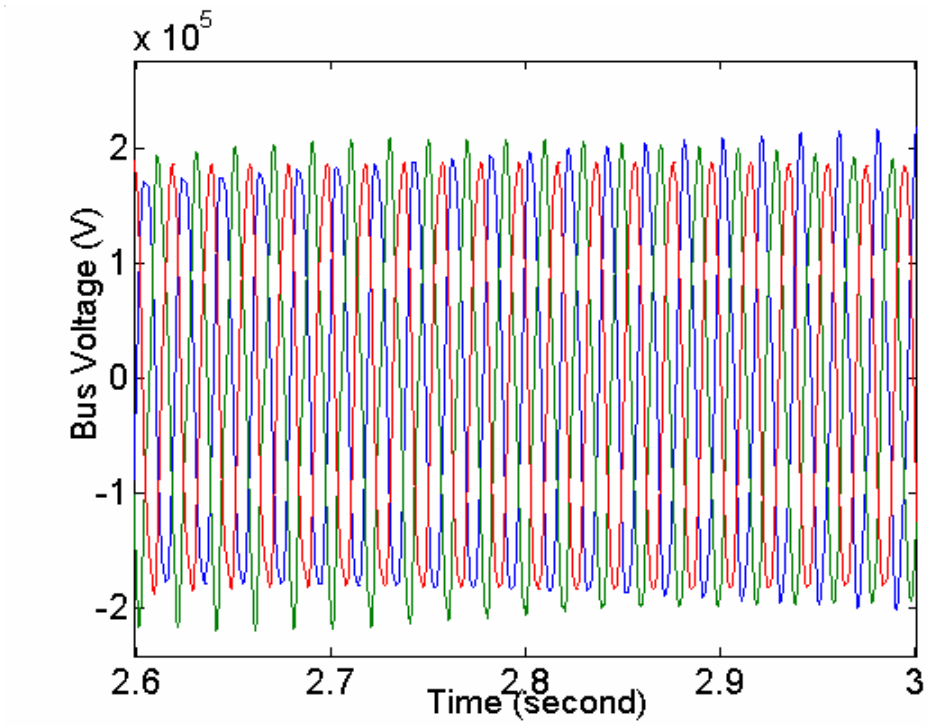

(a) Fixed Schedule

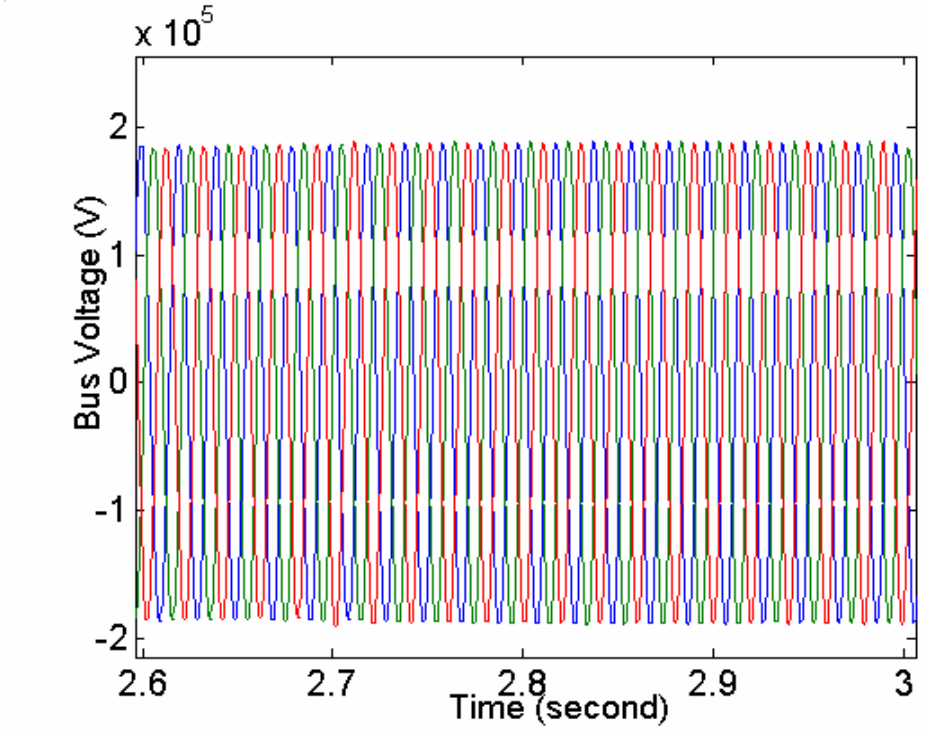

(b) Adaptive Schedule

Figure 5.29: Effects of Fixed and Adaptive Interchange Schedule

Since the phase discontinuity is the cause of the waveform distortion and unbalancing, the remedy is to adaptively adjust the EMT simulator process to "match" the phase difference caused by the frequency variation as illustrated in Figure 5.27. This means the interchange points are not fixed at every 400 EMT steps as described in the case above; rather, the interchange intervals will be extended or shrank to "catch up" with the phase angle, thus eliminating the discontinuity. The success of this method is demonstrated in Figure 5.29. As expected, without any countermeasure, the waveforms from the EMT simulator are heavy unbalanced as shown in Figure 5.29(a). However, with the adaptive interchange schedule, the waveforms are sinusoidal and balanced as shown in Figure 5.29(b).

V.5.3 FREQUENCY DRIFT IN STEADY-STATE

The EMT and TS simulators are of two different types. They adopt different modeling techniques and different solution engines. Therefore, it is impossible for them to generate the same answers on the same network. There must be some differences, more or less. The difference can be observed in the steady-state simulation.

(a) TSP

Voltage (pu): $1.0457\angle 5.1982^{o}$

Power (pu): -1.75582+j0.76614

(b) Hybrid Simulation

Voltage (pu): $1.04434\angle 5.4321^{o}$

Power (pu): -1.75737+j0.79508

Figure 5.30: Simulation Results in Steady-State

To illustrate the difference, a test on 39-bus system was made. The diagram of the 39-bus system is shown in Appendix B. The system was partitioned into an external and a detailed system along bus 36. The interface bus voltage and the injected power in phasor form from the detailed system to the external system in the

steady-state are listed in Figure 5.30(a). For the hybrid simulation, even if the external system is not replaced by an equivalent in the EMT simulator, the interface bus voltage and the injected power in phasor form extracted from the EMT solutions have some minor differences, as listed in Figure 5.30(b).

The difference can cause frequency drift in steady-state in hybrid simulation, even the value is minor. Let's continue the test, to simulate the steady-state for 4 seconds using hybrid simulation without any countermeasure to the difference. The swing curves of generators are shown in solid line in Figures 5.31-5.38.

As illustrated from the figures, the difference does cause transients even in steady state. It is obvious that the difference caused by the interchanging has to be eliminated; otherwise an extra error will be introduced in results.

The remedy to this problem is not unique. In our hybrid simulation, speed governors were added to generators in steady-state until the transients were decreased to a minimum. The swing curves with the countermeasures are also shown in Figures 5.31-5.38, in dashed lines. Generally, the approach can improve the steady state condition, and thus reduce the error introduced during transients.

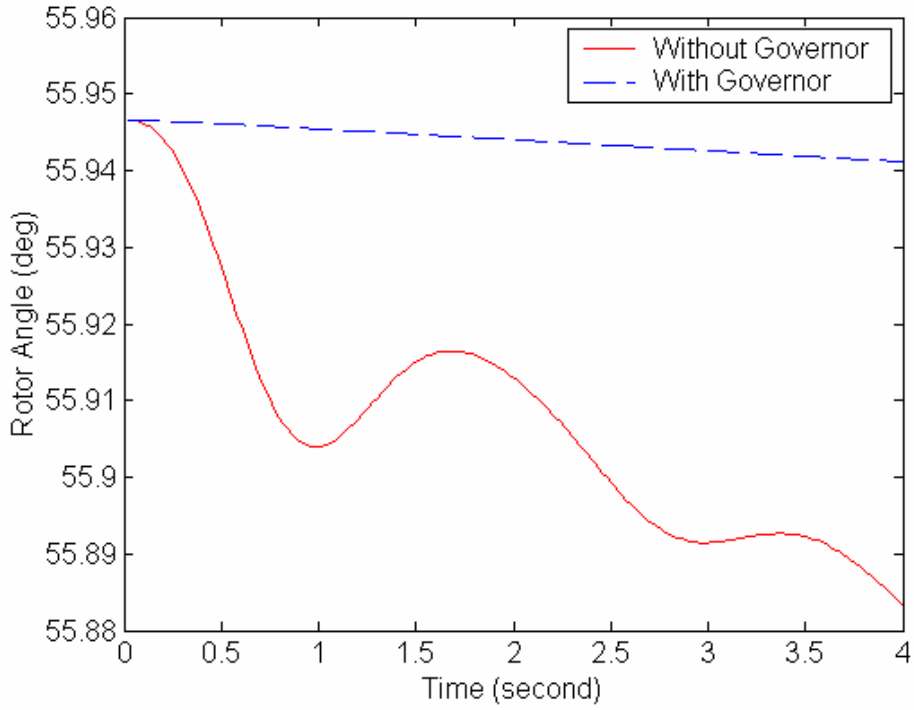

Figure 5.31: Generator 2 Swing Curves

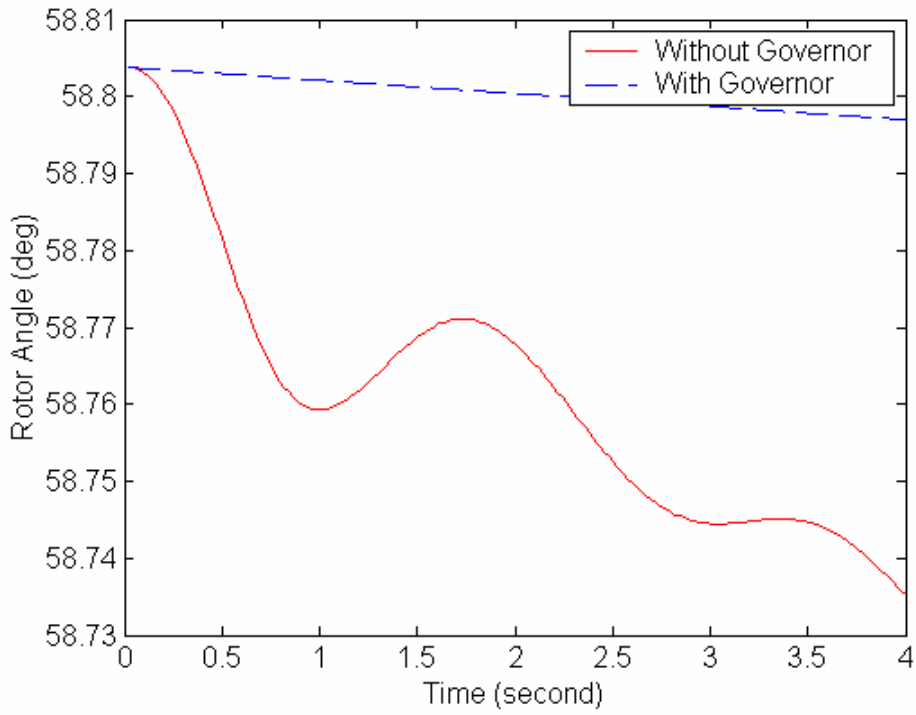

Figure 5.32: Generator 3 Swing Curves

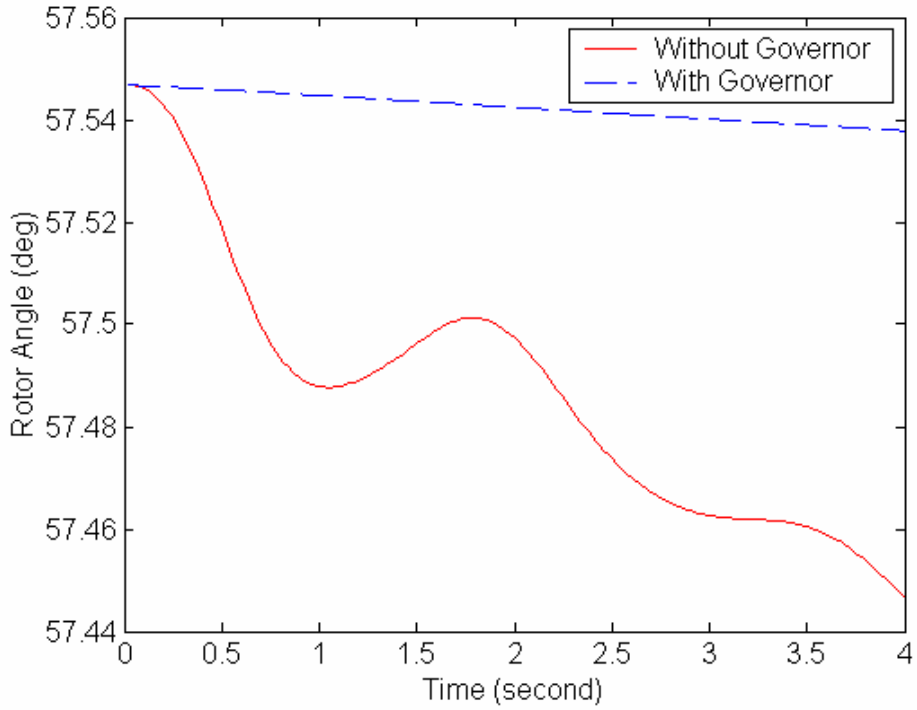

Figure 5.33: Generator 4 Swing Curves

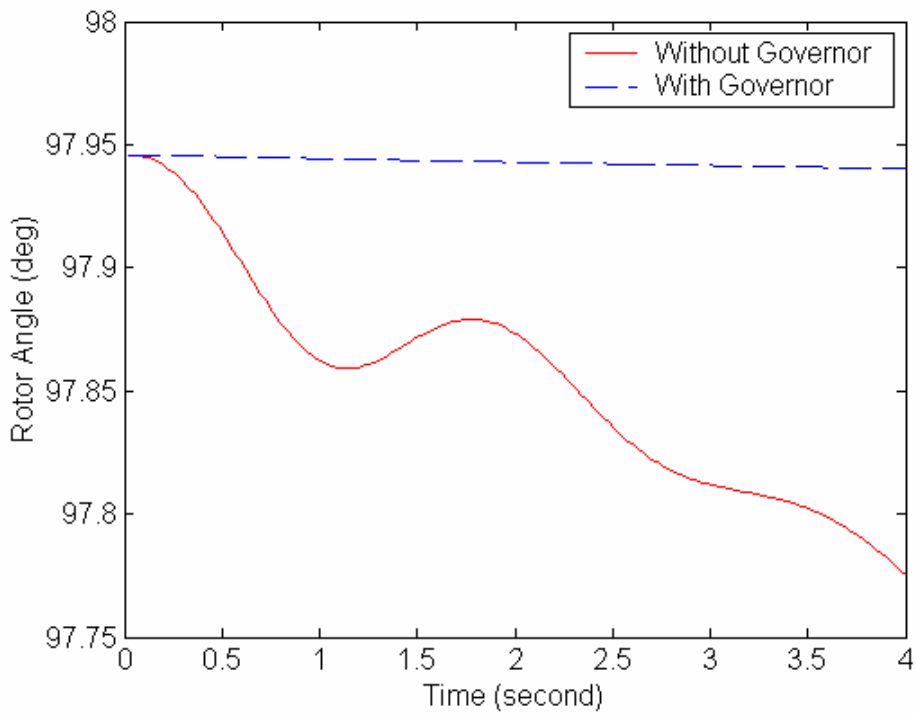

Figure 5.34: Generator 5 Swing Curves

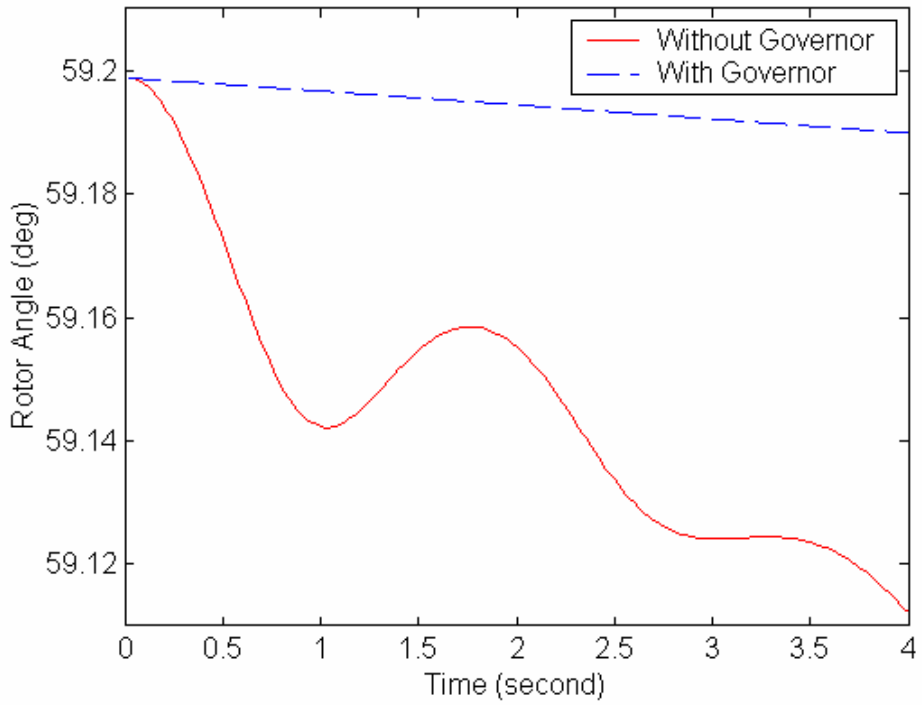

Figure 5.35: Generator 6 Swing Curves

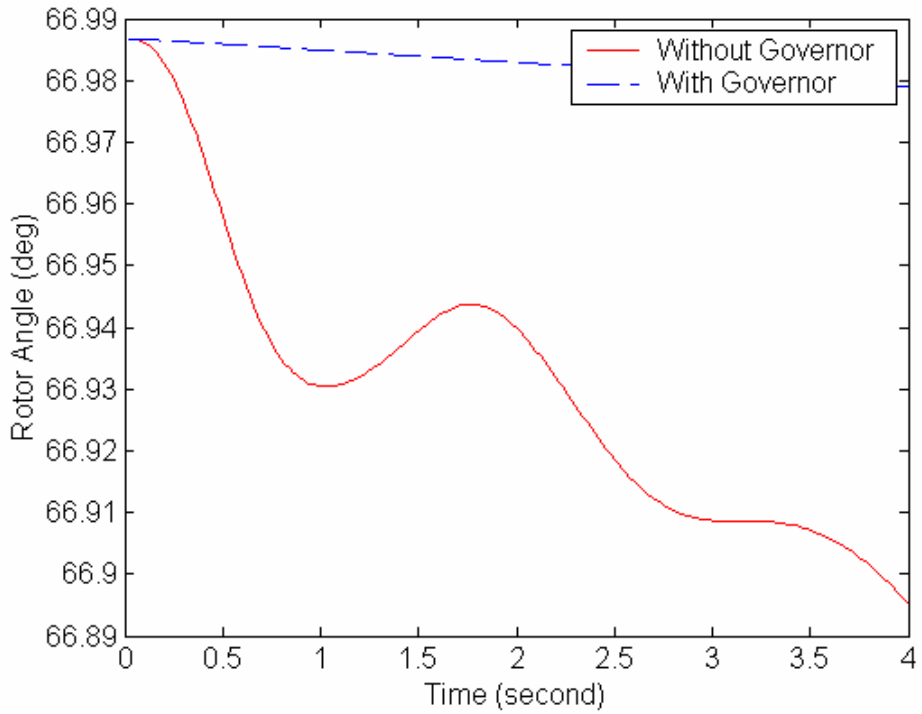

Figure 5.36: Generator 7 Swing Curves

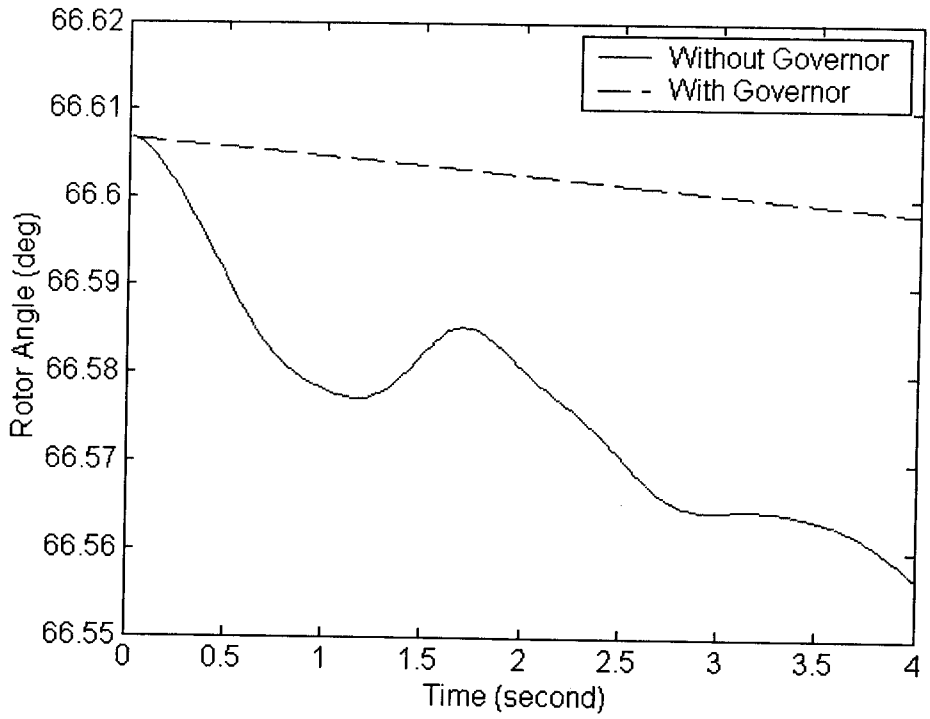

Figure 5.37: Generator 8 Swing Curves

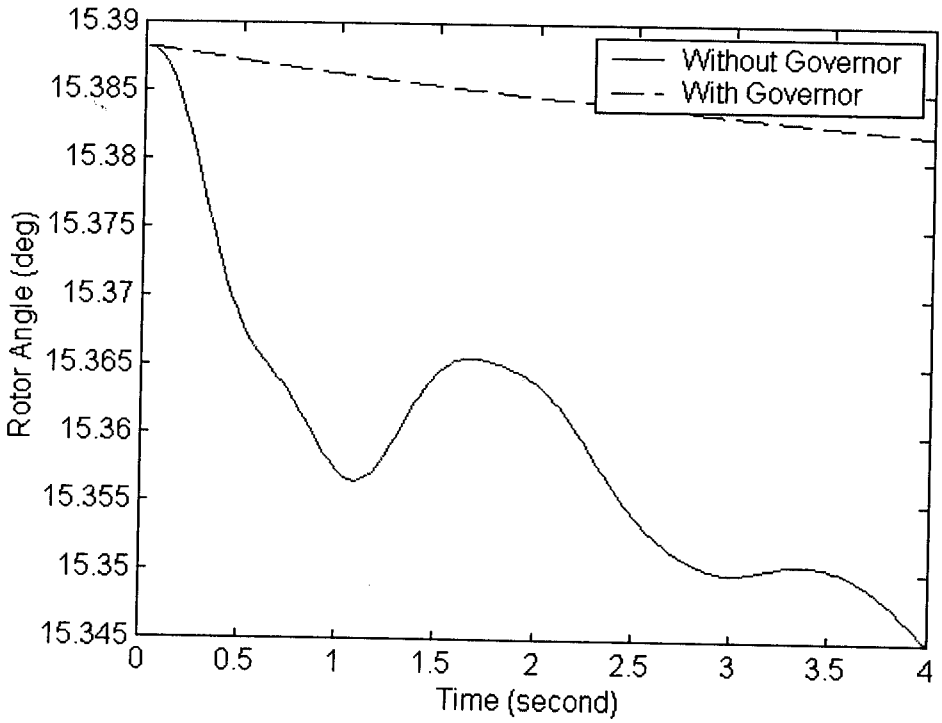

Figure 5.38: Generator 10 Swing Curves

V.6 CONCLUSION

In this chapter, issues relating to proper interfacing have been discussed in detail. In order to ensure the correct shape of waveforms in the EMT simulator a frequency dependent equivalent was required in the EMT simulator to represent the external system. The effect of the frequency dependent equivalent was demonstrated by an example on a 9-bus system, compared with a simple equivalent.

The choice of variables transferred from the EMT simulator to the TS simulator was discussed. For any disturbance, the detailed system can be represented in terms of positive-sequence interface bus voltage and the positive-sequence injection current from the detailed system, which are extracted by using a curve-fitting method.

The choice of interface location has been determined with the purpose of generating correct waveforms from the EMT simulator. With the use of the frequency dependent equivalent, the correct waveform is of less concern. From the TS point of view, the interface location is a factor of consideration to extract the variables from the EMT solutions. To overcome the difficulty in the extraction of the fundamental frequency component of the injection current in the presence of time-variant dc offset, an alternative approach was proposed.

An interaction protocol, which corresponds to a one-cycle integration time step and a match of the requirements for the implicit trapezoidal integration method used in the TS simulator, was proposed in the chapter. In the implementation of the protocol, frequency mismatch, which was explained in details, can cause heavy waveform distortion. Remedy to the problem was to adopt adaptive interfacing scheme, instead of fixed interfacing scheme.

Chapter VI HYBRID SIMULATION – PERFORMANCE EVALUATION

VI.1 INTRODUCTION

In the last Chapter, issues related to the development of hybrid simulation were analyzed theoretically. In this Chapter, a number of case studies were carried out on two systems, i.e. 9-bus-3-machine system and 39-bus-10-machine system, to prove the analyses made in the last Chapter.

The real power of the hybrid simulation lies in its simulation speed on large-scale network while providing detailed solutions to concerned components under a variety of disturbances. But the premise is the hybrid simulation can give creditable results. Theoretical issues on how to make sure the correctness of the results have been discussed. In this Chapter, all analyses will be implemented on the case studies. The emphasis is to check whether the results of the hybrid simulation are creditable.

Hybrid simulators should be able to solve system transients covering a large bandwidth: from electromagnetic transients associated with the devices, to swing curves for the system as a whole. Consequently two approaches were used to assess the hybrid simulation: one is to check the waveform immediately after a disturbance or clearing of a disturbance (determined by the EMT simulation), while the other is to assess the system transient stability, mainly through the machine rotor angle swings and frequency deviations (determined by the TS simulation).

Firstly, comparisons were made between DCG/EMTP, BPA, and a conventional TS simulator developed by the author. The purpose of the comparison is to validate the TS simulator, taking the EMTP as the benchmark.

A hybrid simulator was implemented on a digital electromagnetic transients simulator, known as HYPERSIM using the User Code Block (UCB) facility. The interface itself was implemented as a UCB which is in turn interfaced with the TS

simulator. The performance of the hybrid simulator was assessed from both EMT and TS point of views.

Finally some cases simulating a commutation failure between valves in an SVC model were performed. This kind of disturbance cannot be correctly simulated by conventional transient stability simulators because of limited capability of the simulators, and is one of the advantages of hybrid over conventional simulation.

VI.2 PERFORMANCE COMPARISON BETWEEN EMT AND TS SIMULATORS

In the hybrid simulator built within the HYPERSIM environment, an in-house conventional TS simulation developed by the author [103] was used to simulate the external system.

The validation of the simulator was made on the 39-bus system as shown in Appendix B. Disturbances, including three-phase-ground fault, single-phase-ground fault, double-line fault, double-line-ground fault, were applied at bus 38, from 0.2 to 0.24 second. The commercial software, known as BPA, was used as the benchmark. DCG/EMTP was also added to the comparison, providing a visual comparison to illustrate the differences resulting from the different modeling techniques.

For the compatibility of the results from different types of simulators, all loads in the system were modeled using the simplest constant impedance model. For the generator, subtransient models were used in the TS simulators. Exciters and prime movers were not taken into consideration.

Generator swing curves for various types of fault are shown as follow:

Three-Phase-to-Ground Fault:

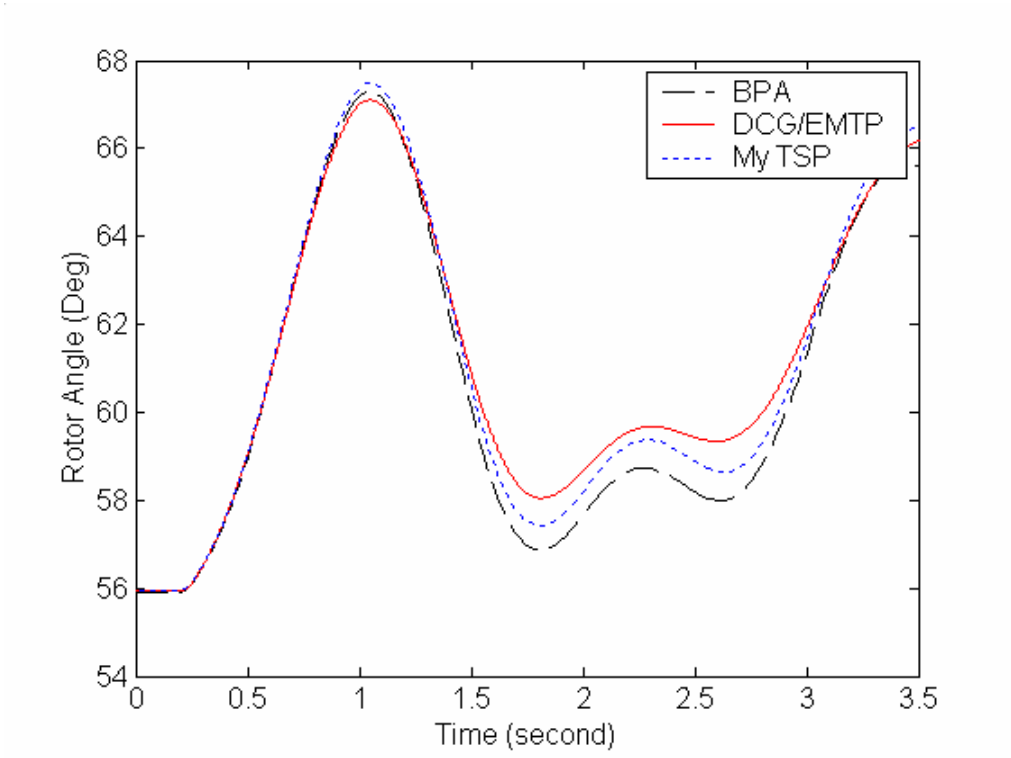

Figure 6.1: Generator 2 Swing Curves Comparison under Three-Phase-to-Ground Fault

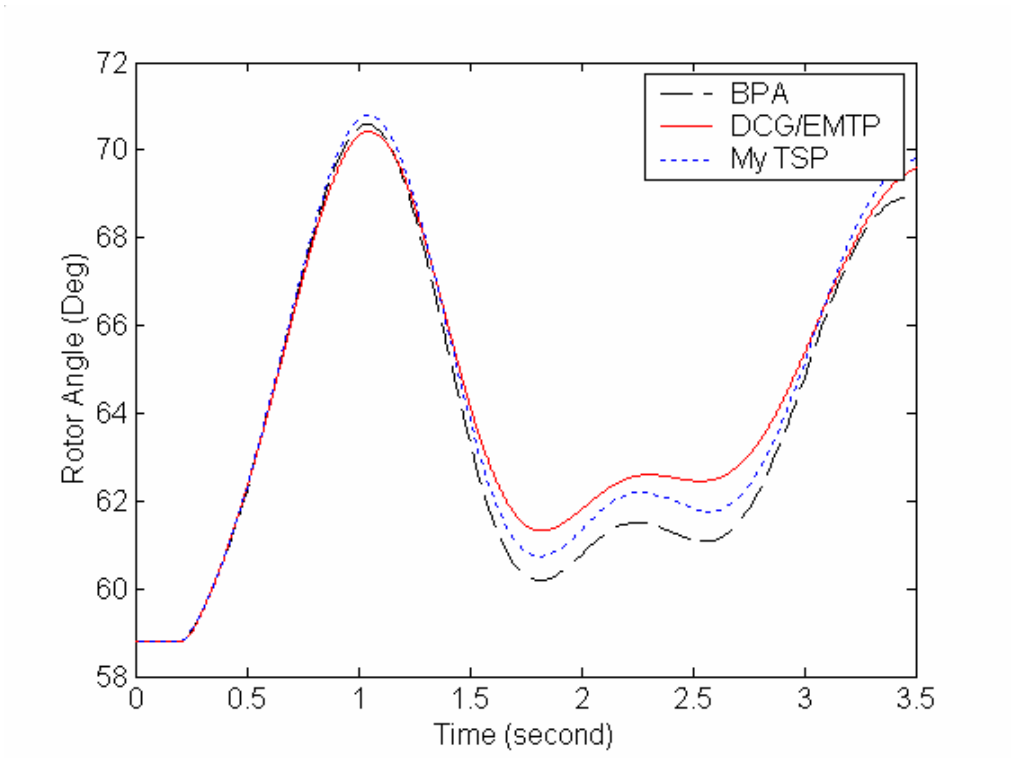

Figure 6.2: Generator 3 Swing Curves Comparison under Three-Phase-to-Ground Fault

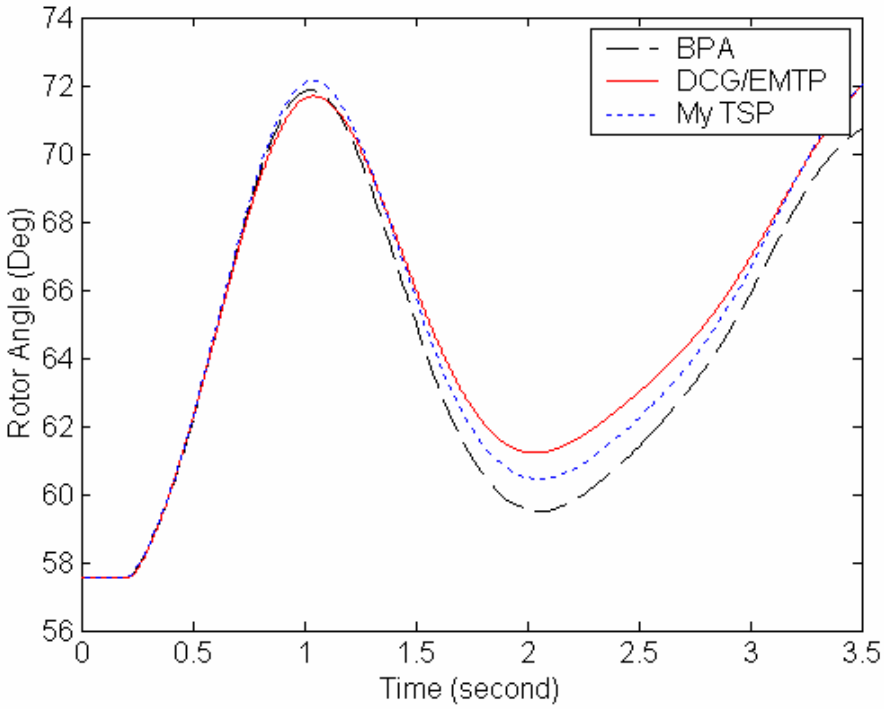

Figure 6.3: Generator 4 Swing Curves Comparison under Three-Phase-to-Ground Fault

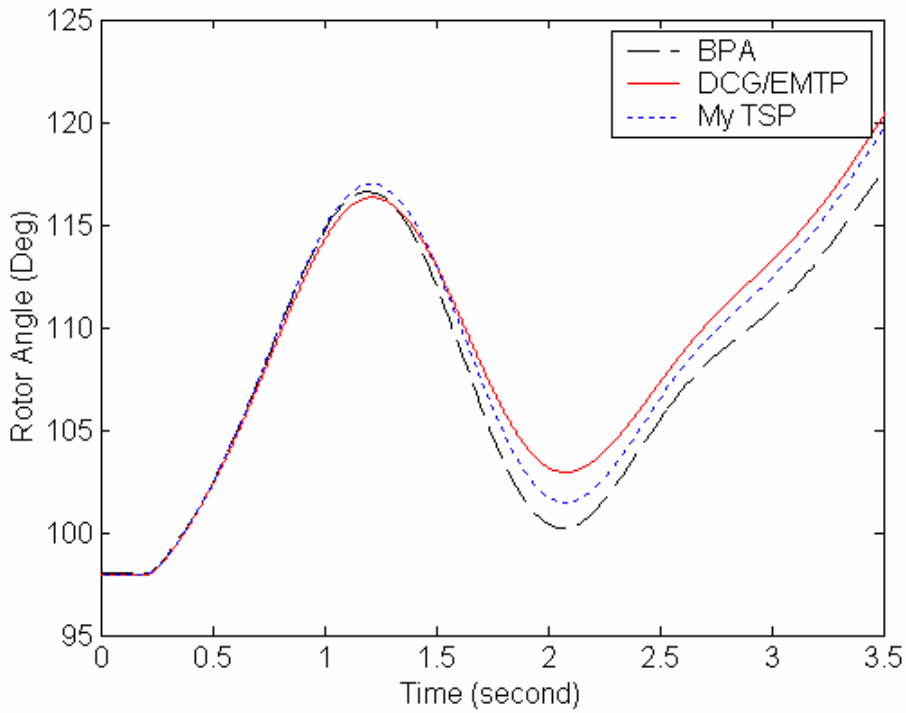

Figure 6.4: Generator 5 Swing Curves Comparison under Three-Phase-to-Ground Fault

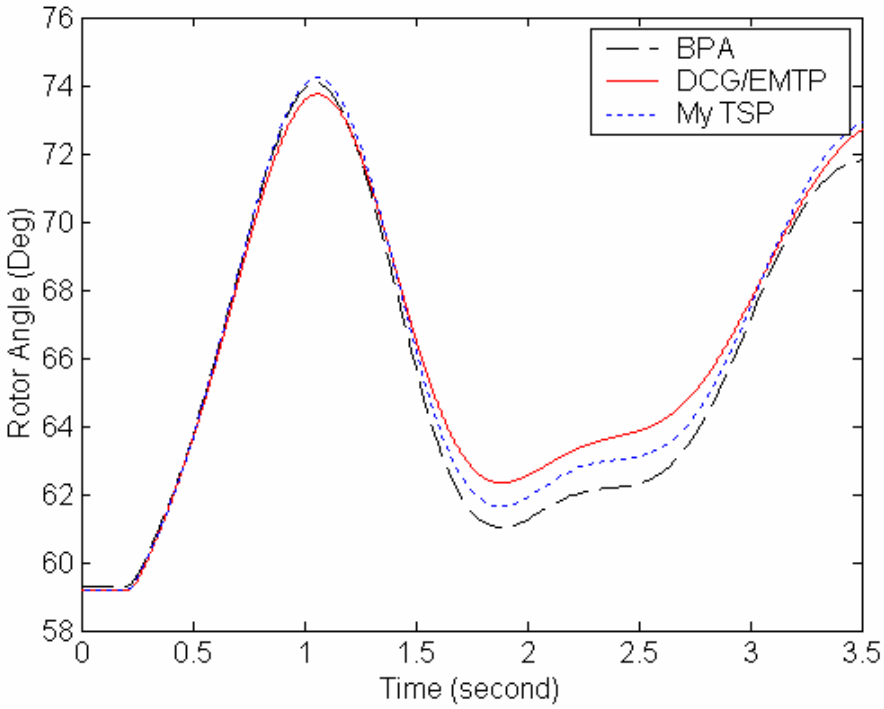

Figure 6.5: Generator 6 Swing Curves Comparison under Three-Phase-to-Ground Fault

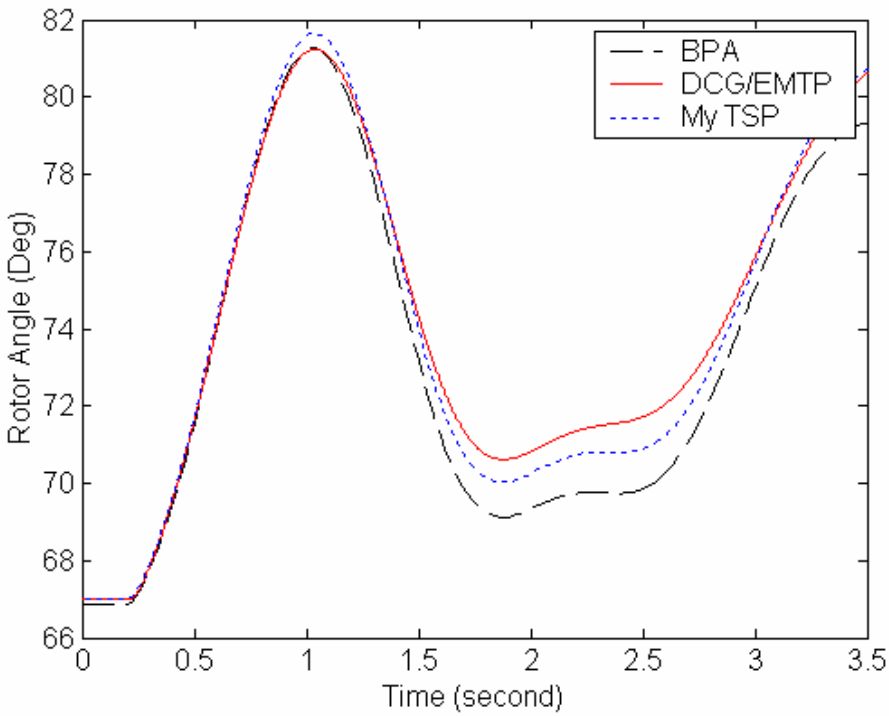

Figure 6.6: Generator 7 Swing Curves Comparison under Three-Phase-to-Ground Fault

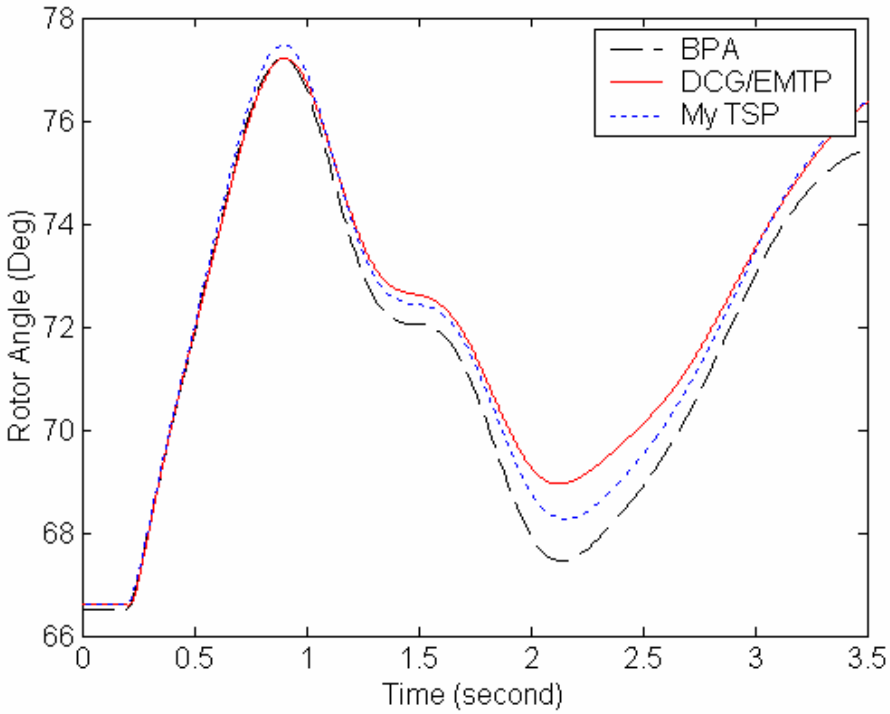

Figure 6.7: Generator 8 Swing Curves Comparison under Three-Phase-to-Ground Fault

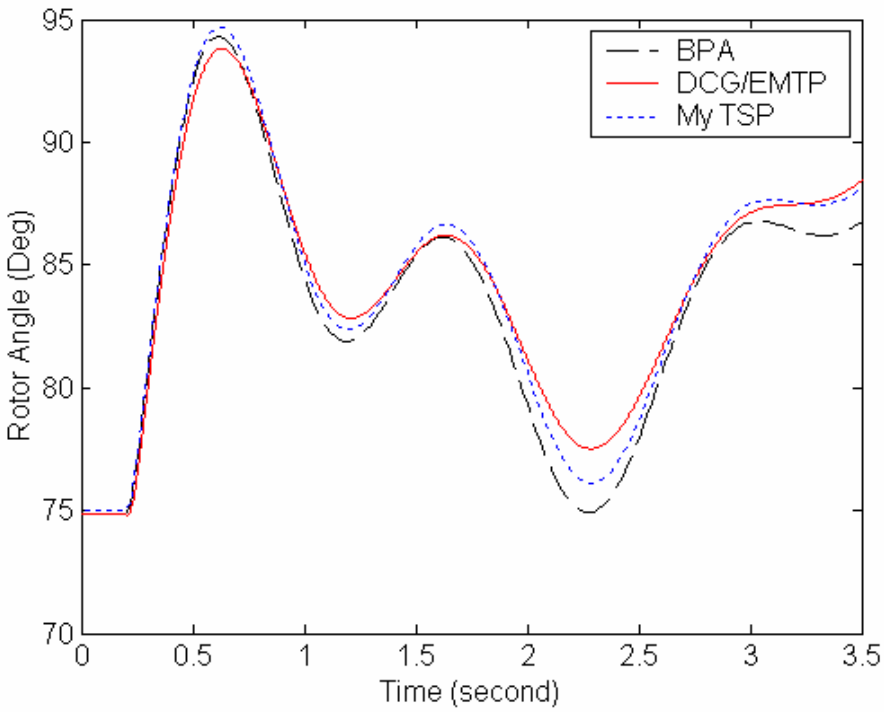

Figure 6.8: Generator 9 Swing Curves Comparison under Three-Phase-to-Ground Fault

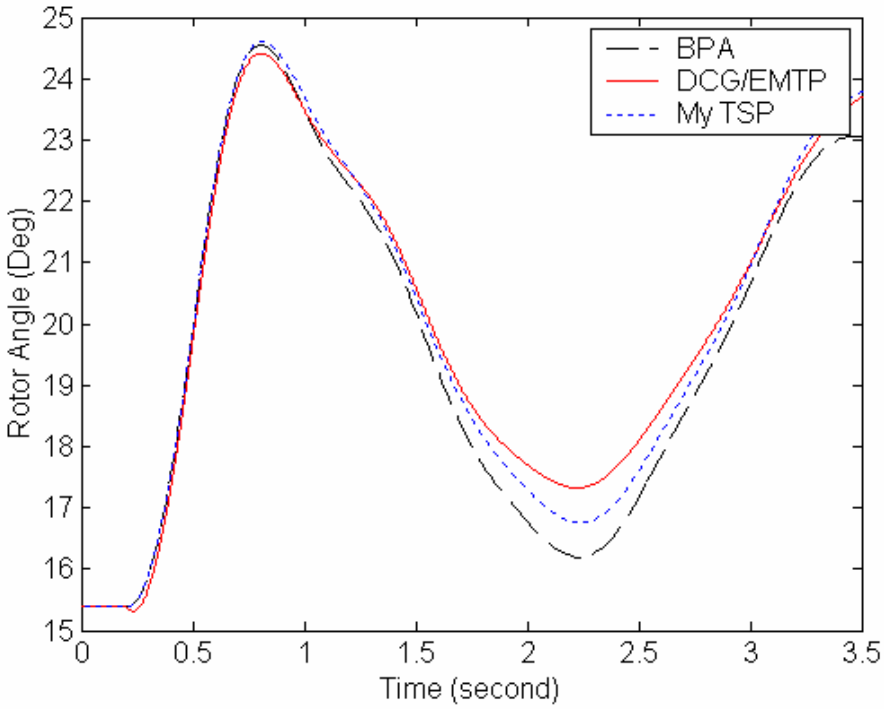

Figure 6.9: Generator 10 Swing Curves Comparison under Three-Phase-to-Ground Fault

Single-Phase-to-Ground Fault:

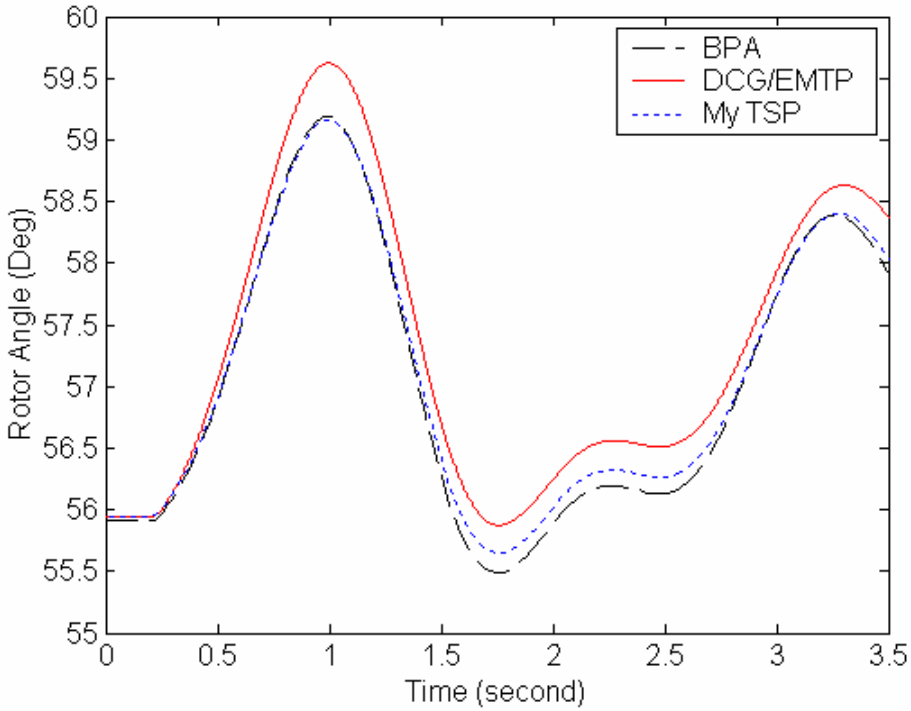

Figure 6.10: Generator 2 Swing Curves Comparison under Single-Phase-to-Ground Fault

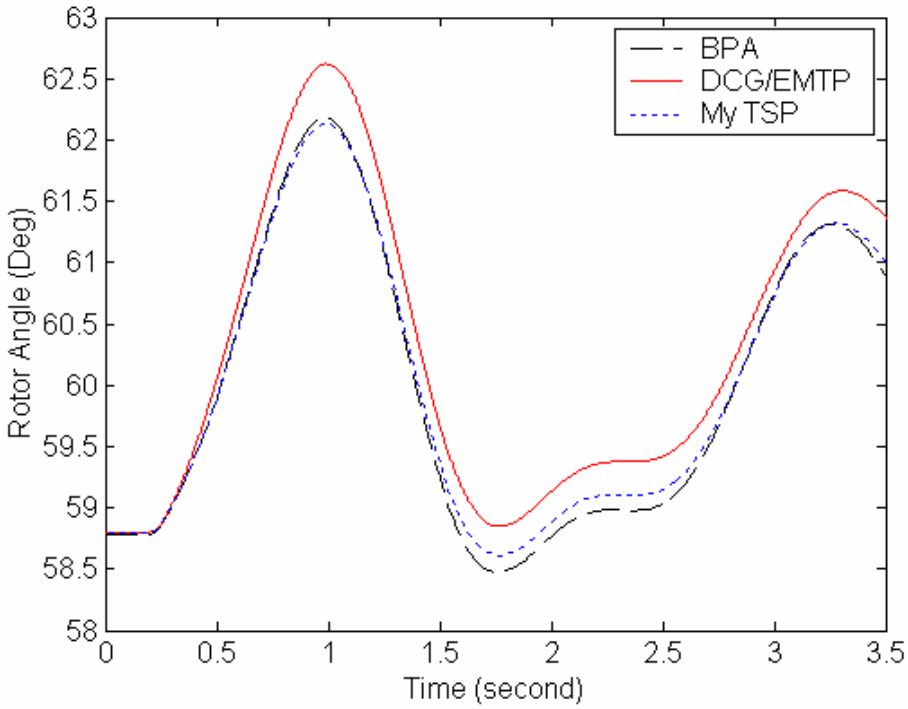

Figure 6.11: Generator 3 Swing Curves Comparison under Single-Phase-to-Ground Fault

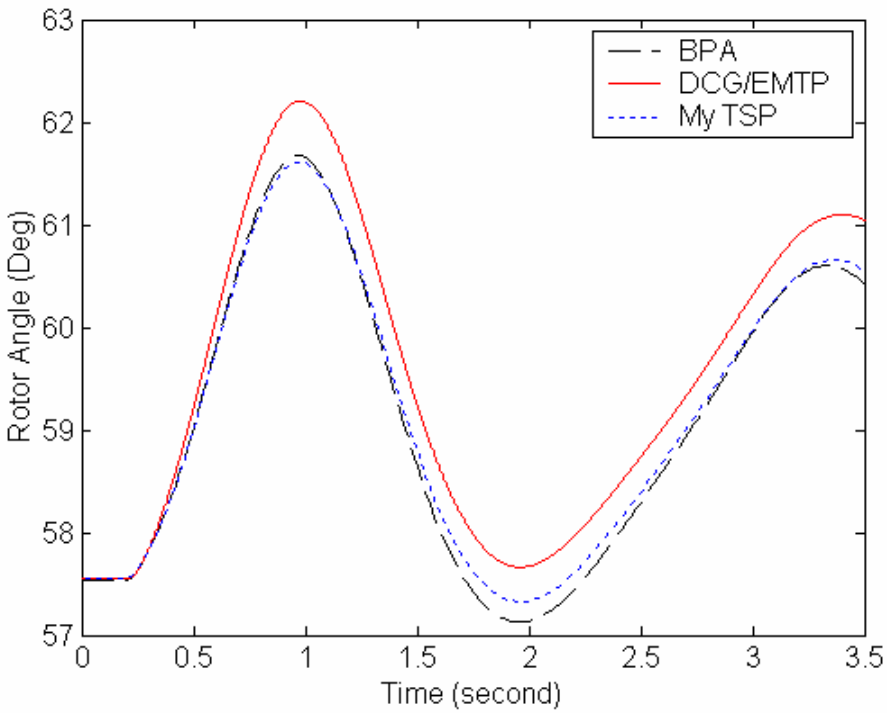

Figure 6.12: Generator 4 Swing Curves Comparison under Single-Phase-to-Ground Fault

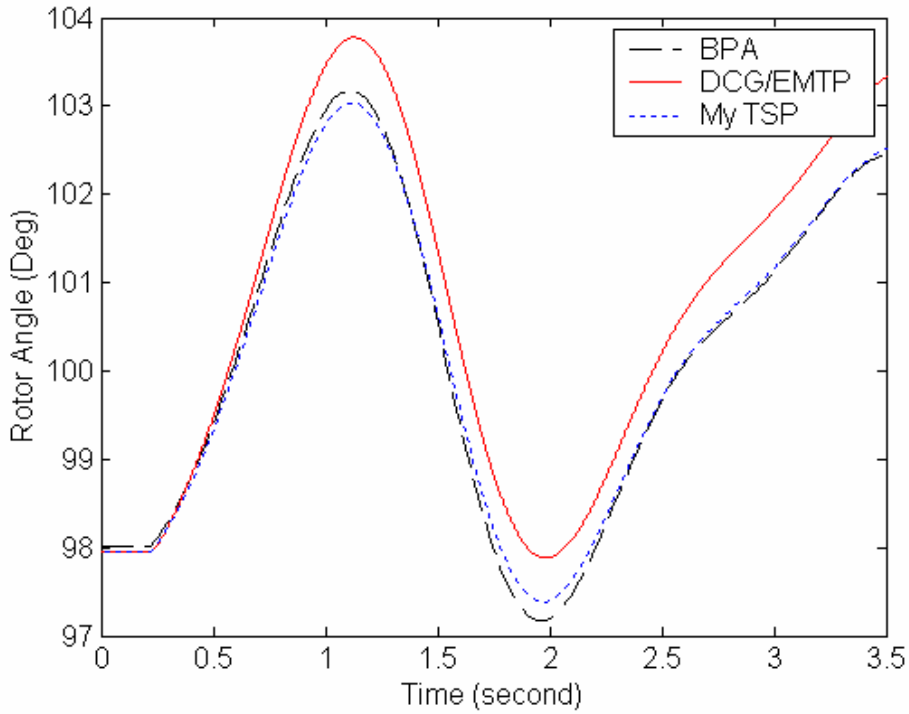

Figure 6.13: Generator 5 Swing Curves Comparison under Single-Phase-to-Ground Fault

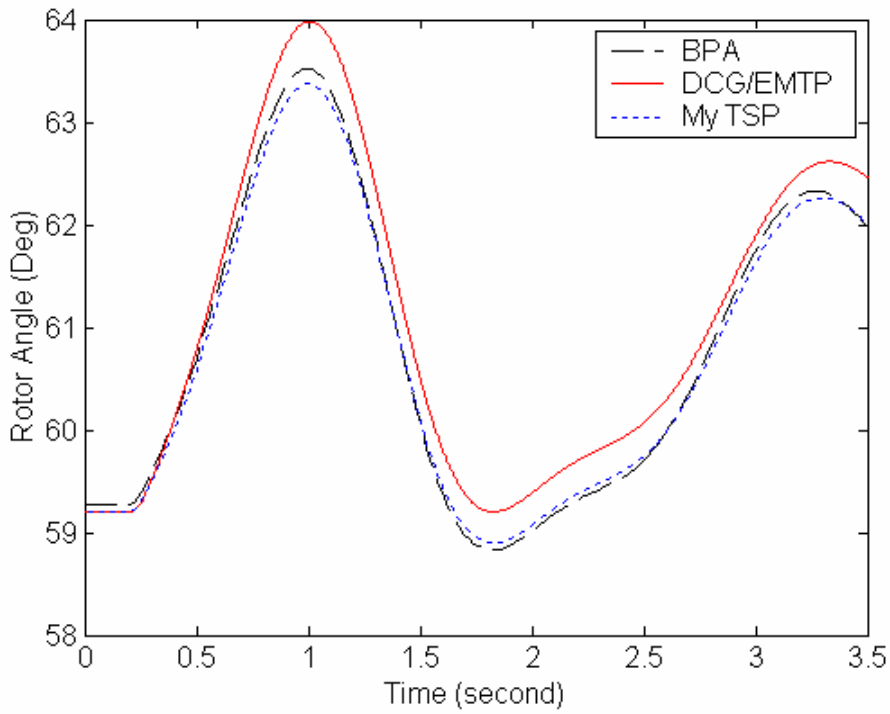

Figure 6.14: Generator 6 Swing Curves Comparison under Single-Phase-to-Ground Fault

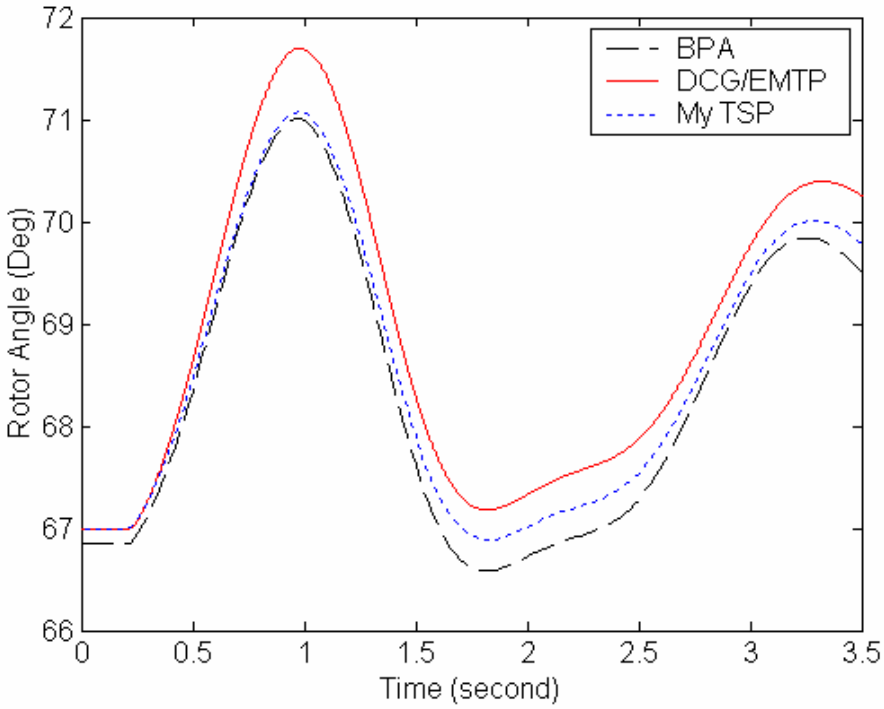

Figure 6.15: Generator 7 Swing Curves Comparison under Single-Phase-to-Ground Fault

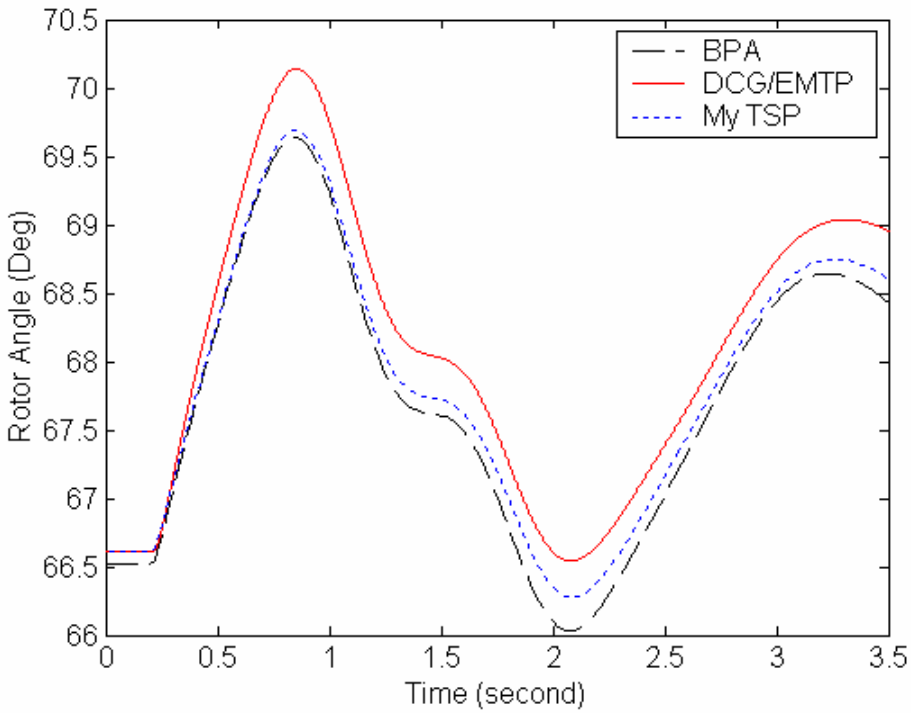

Figure 6.16: Generator 8 Swing Curves Comparison under Single-Phase-to-Ground Fault

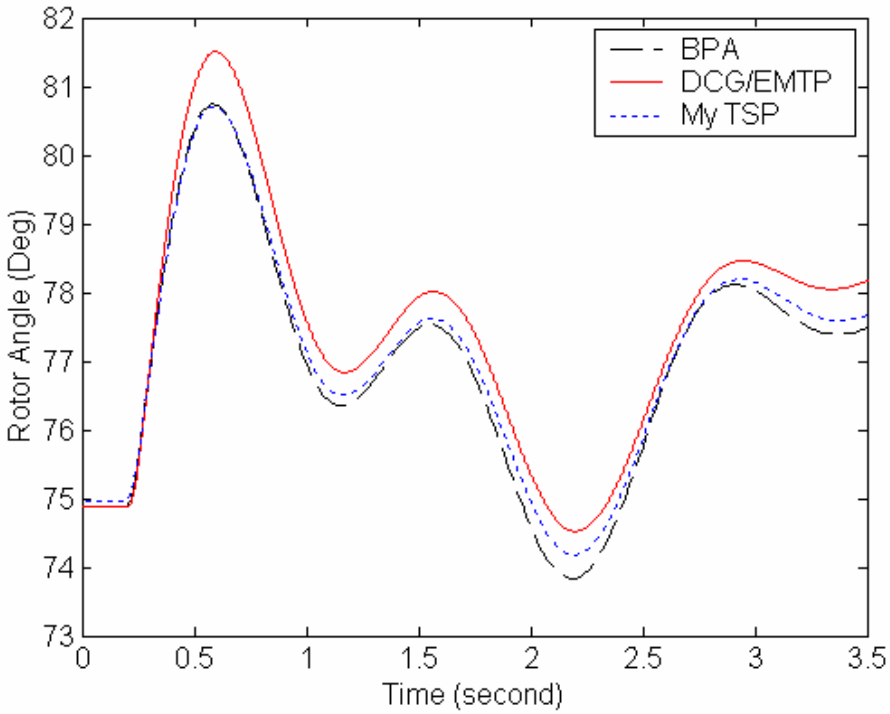

Figure 6.17: Generator 9 Swing Curves Comparison under Single-Phase-to-Ground Fault

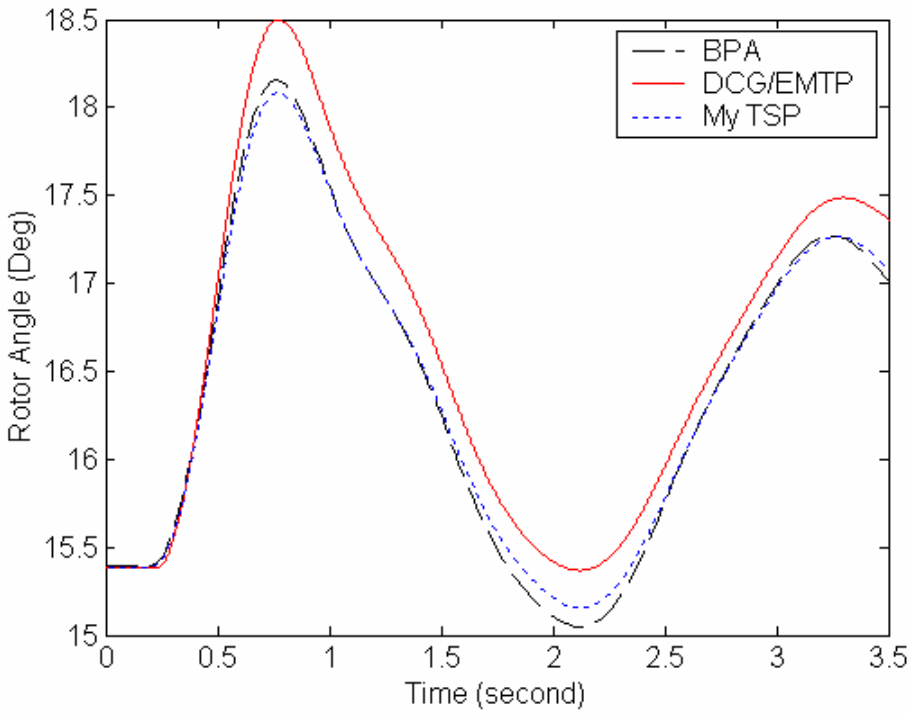

Figure 6.18: Generator 10 Swing Curves Comparison under Single-Phase-to-Ground Fault

Double-Line Fault:

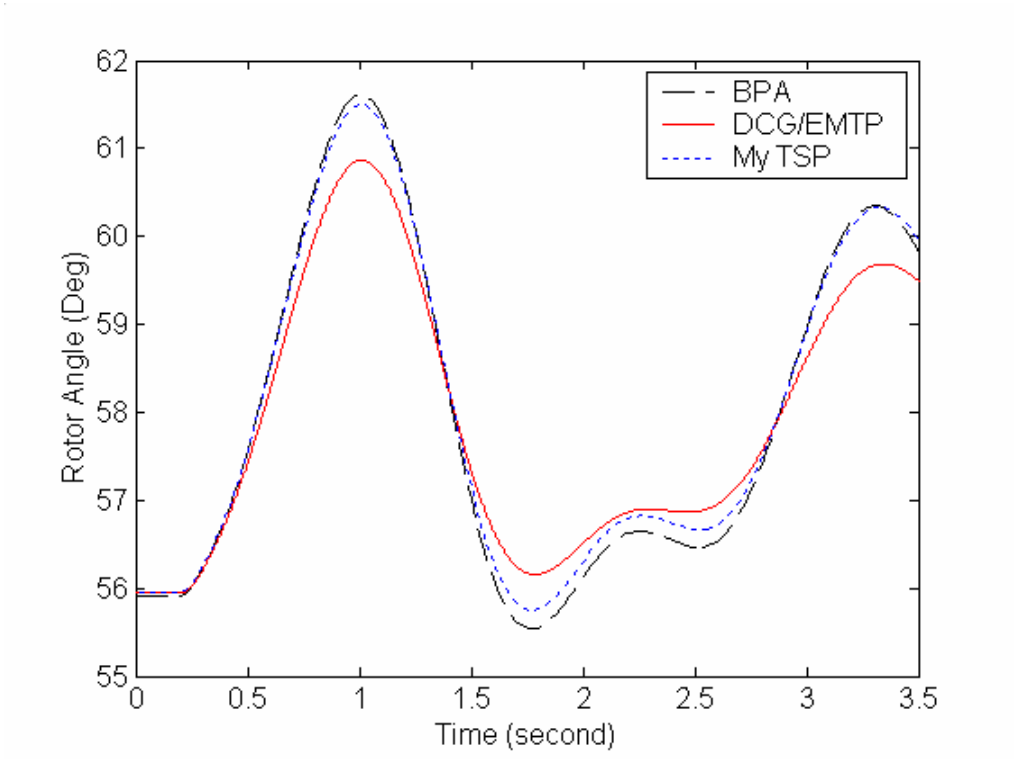

Figure 6.19: Generator 2 Swing Curves Comparison under Double-Ground Fault

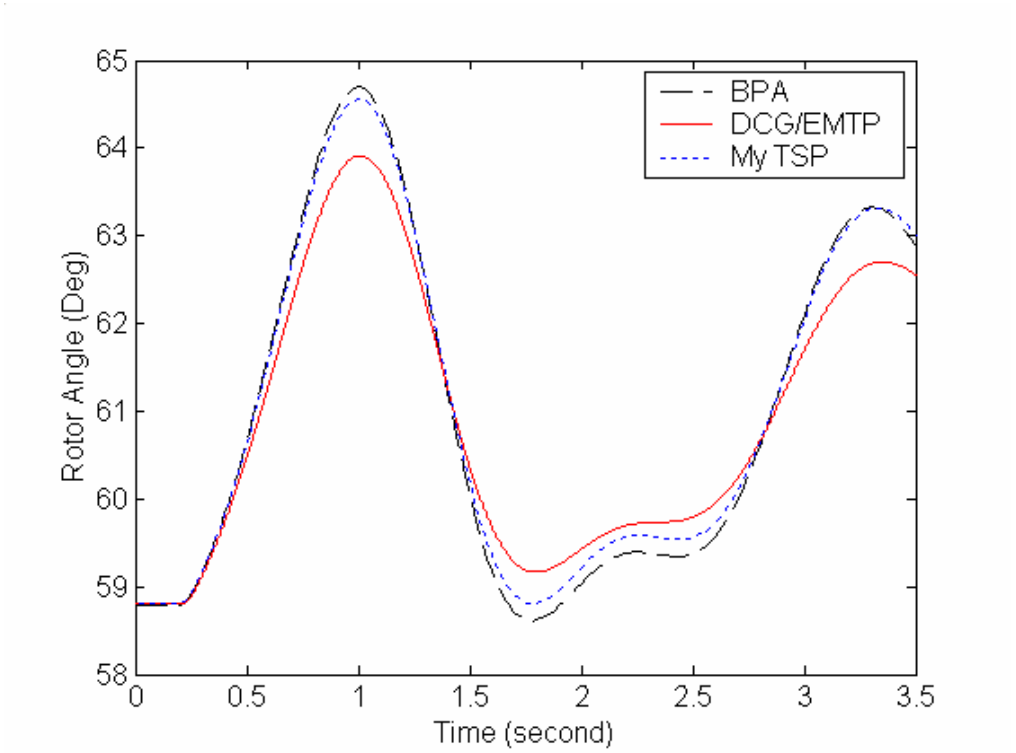

Figure 6.20: Generator 3 Swing Curves Comparison under Double -Ground Fault

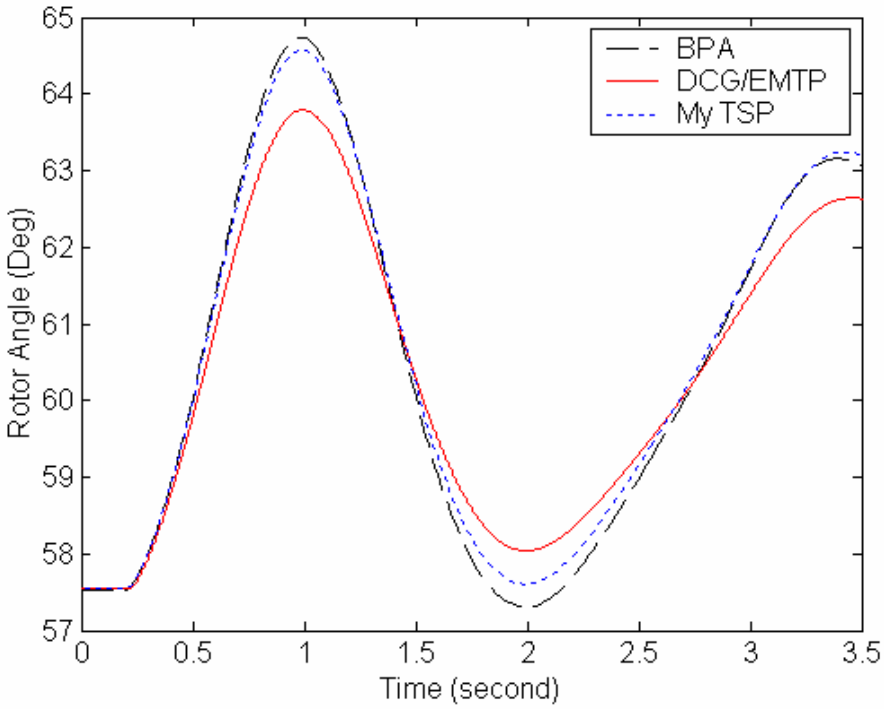

Figure 6.21: Generator 4 Swing Curves Comparison under Double -Ground Fault

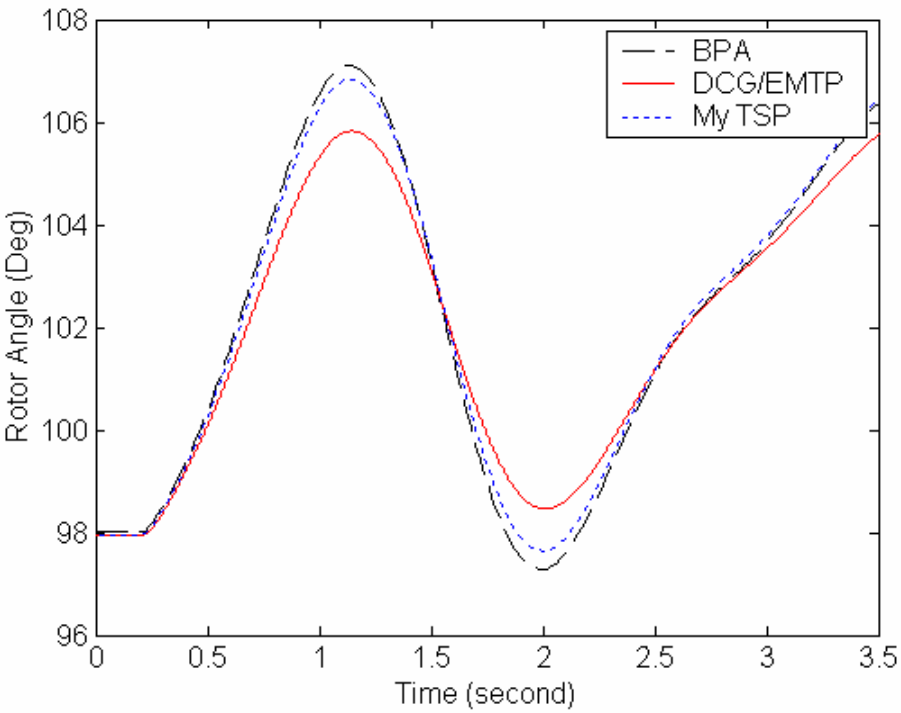

Figure 6.22: Generator 5 Swing Curves Comparison under Double -Ground Fault

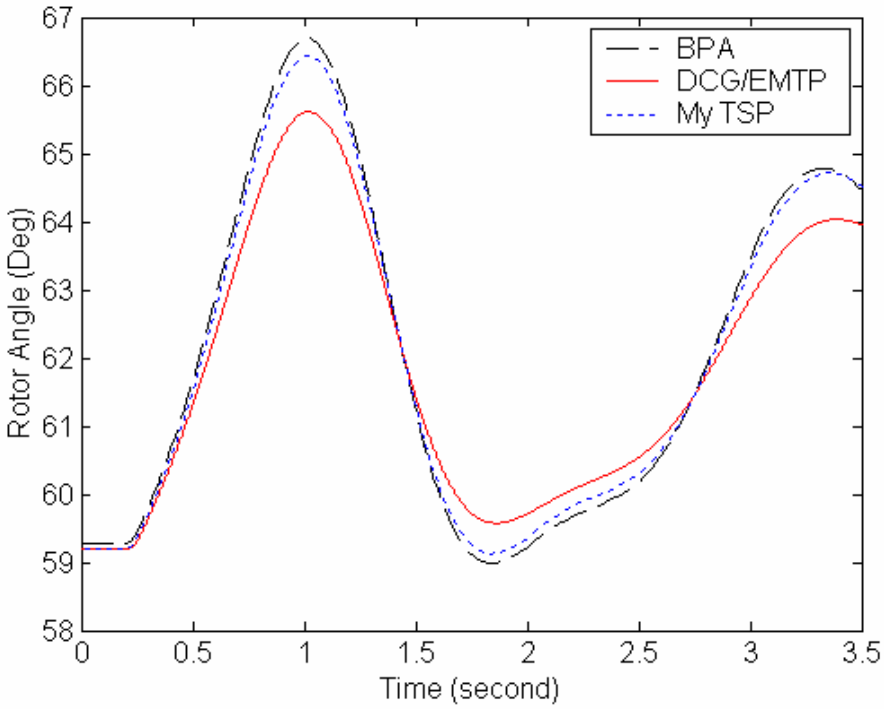

Figure 6.23: Generator 6 Swing Curves Comparison under Double -Ground Fault

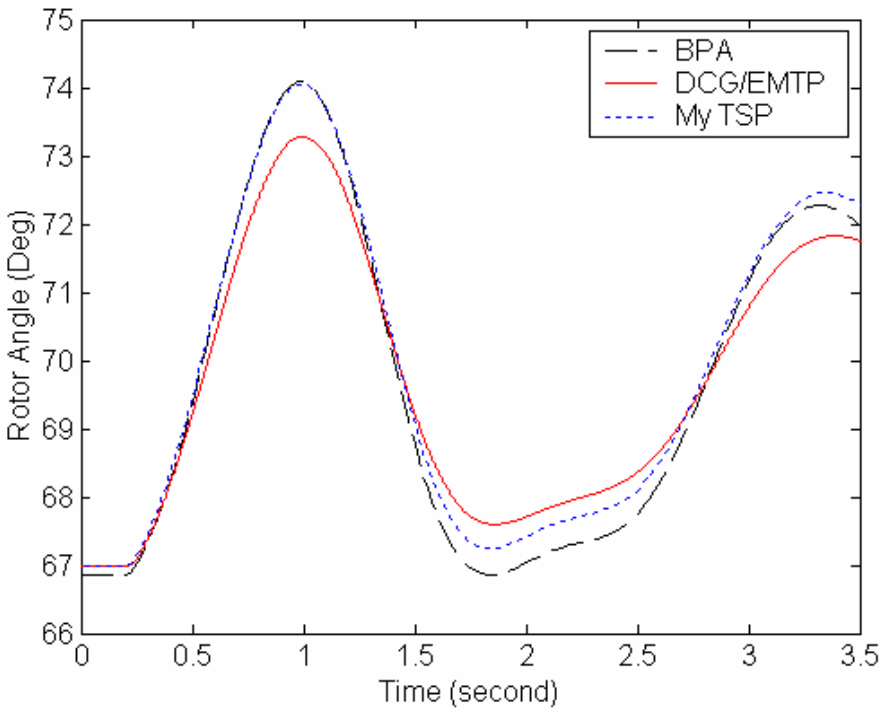

Figure 6.24: Generator 7 Swing Curves Comparison under Double -Ground Fault

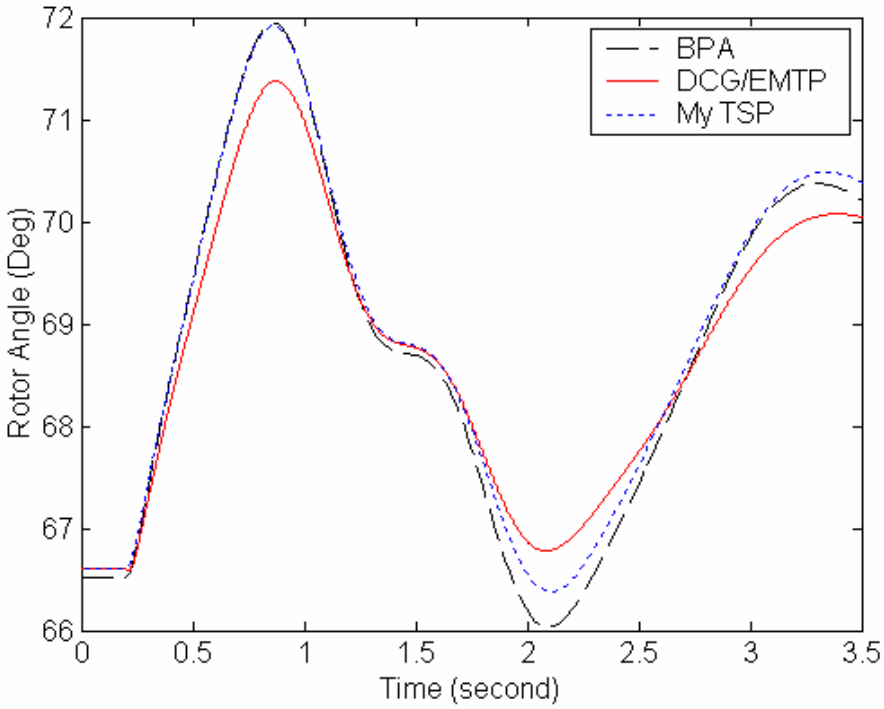

Figure 6.25: Generator 8 Swing Curves Comparison under Double -Ground Fault

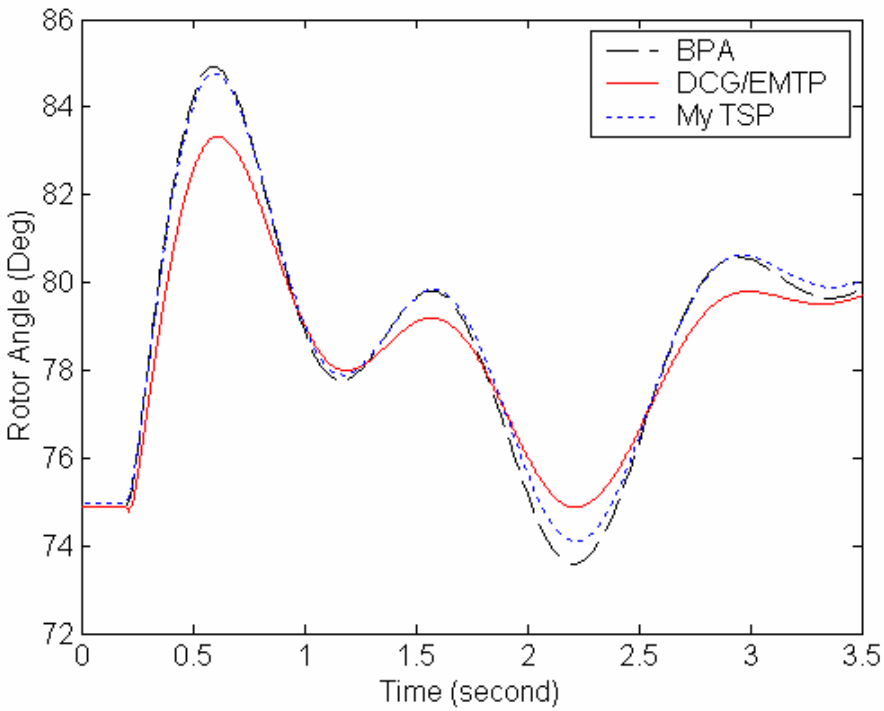

Figure 6.26: Generator 9 Swing Curves Comparison under Double -Ground Fault

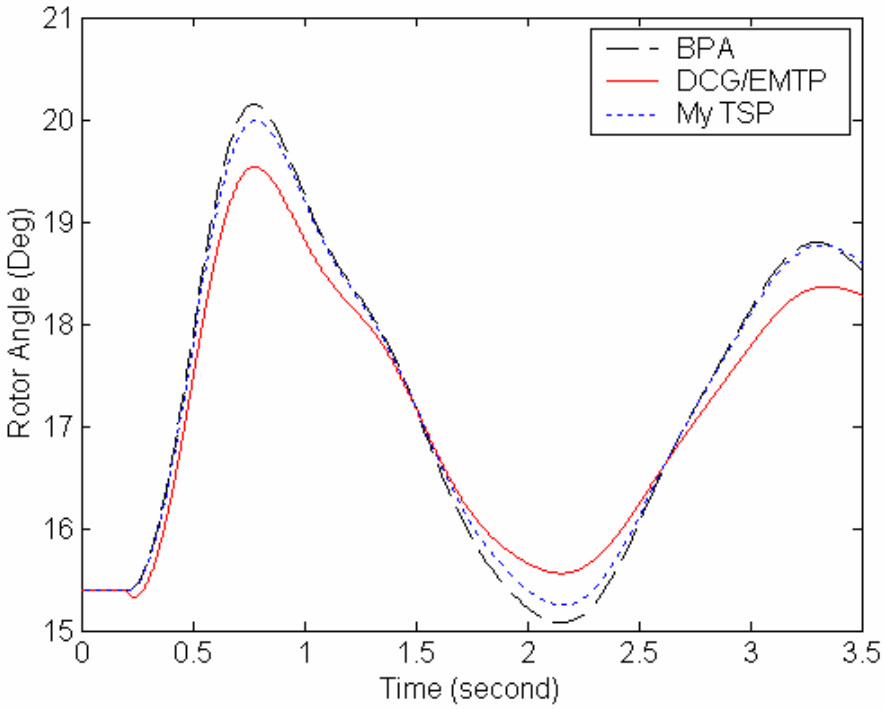

Figure 6.27: Generator 10 Swing Curves Comparison under Double -Ground Fault

Double-Line-to-Ground Fault:

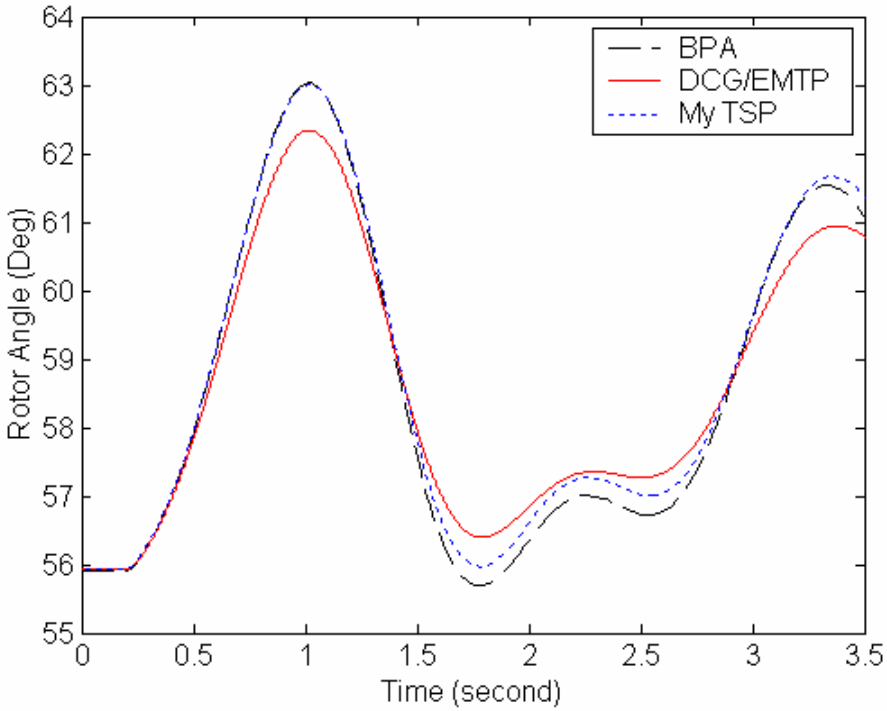

Figure 6.28: Generator 2 Swing Curves Comparison under Double -Ground Fault

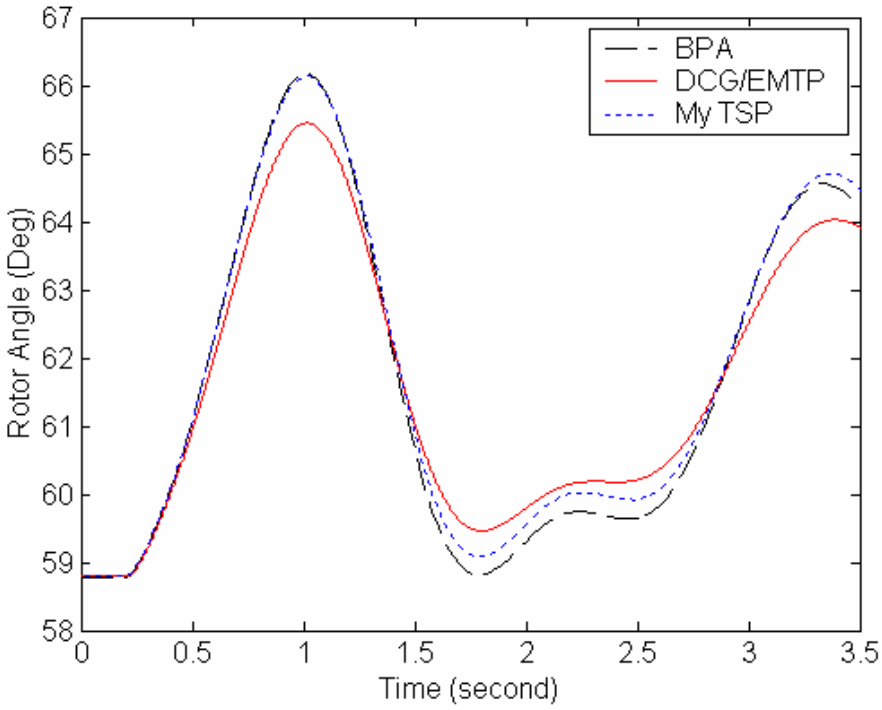

Figure 6.29: Generator 3 Swing Curves Comparison under Double -Ground Fault

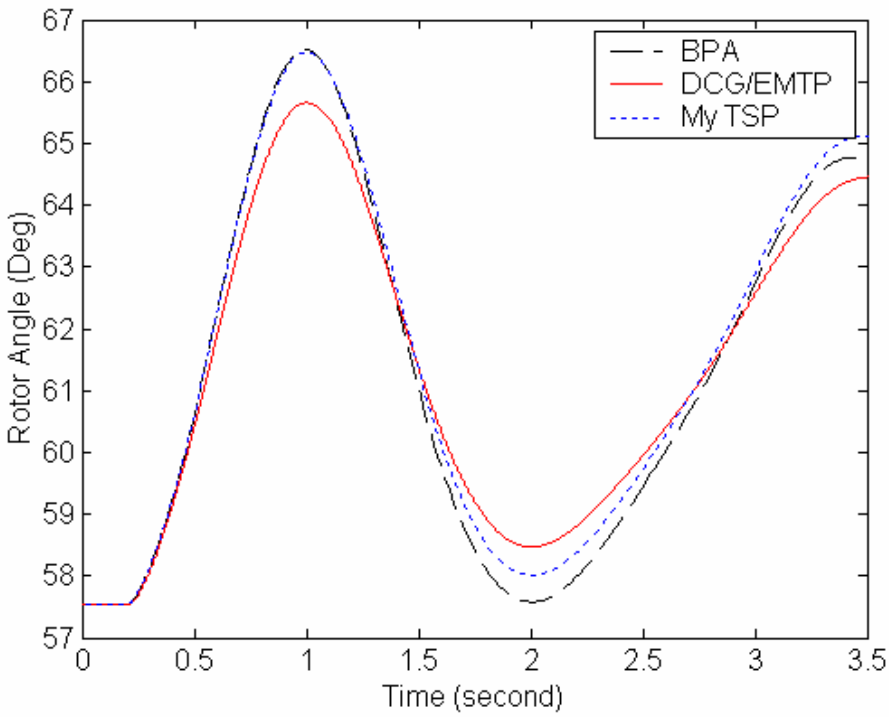

Figure 6.30: Generator 4 Swing Curves Comparison under Double -Ground Fault

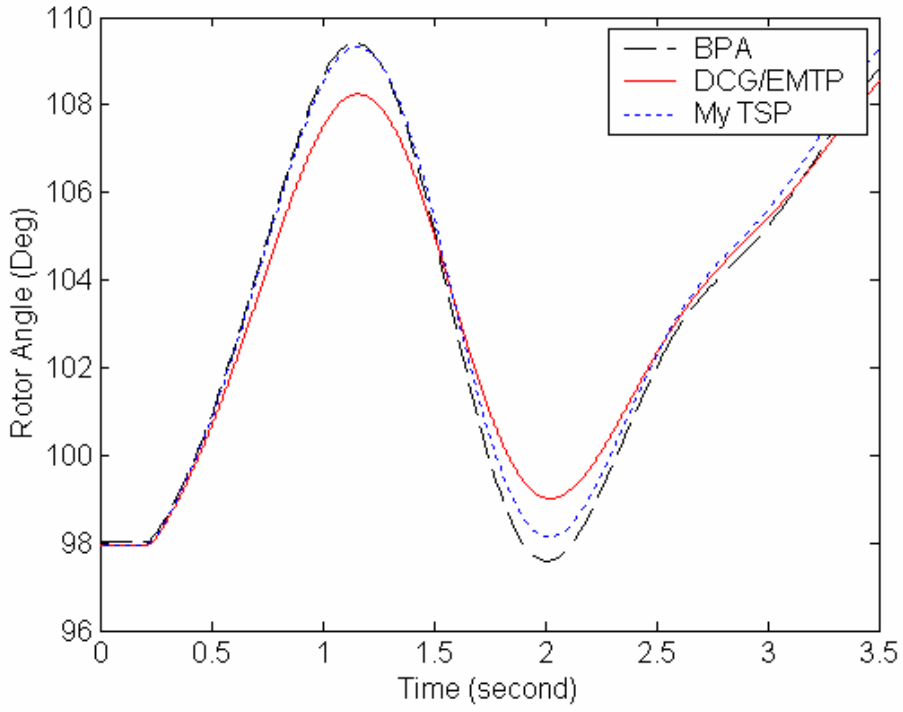

Figure 6.31: Generator 5 Swing Curves Comparison under Double -Ground Fault

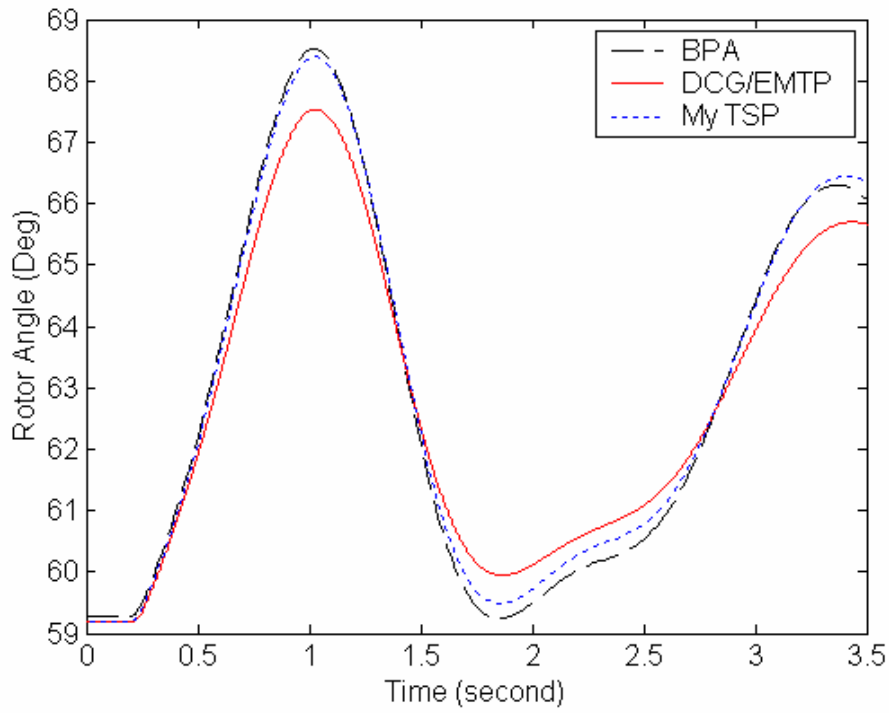

Figure 6.32: Generator 6 Swing Curves Comparison under Double -Ground Fault

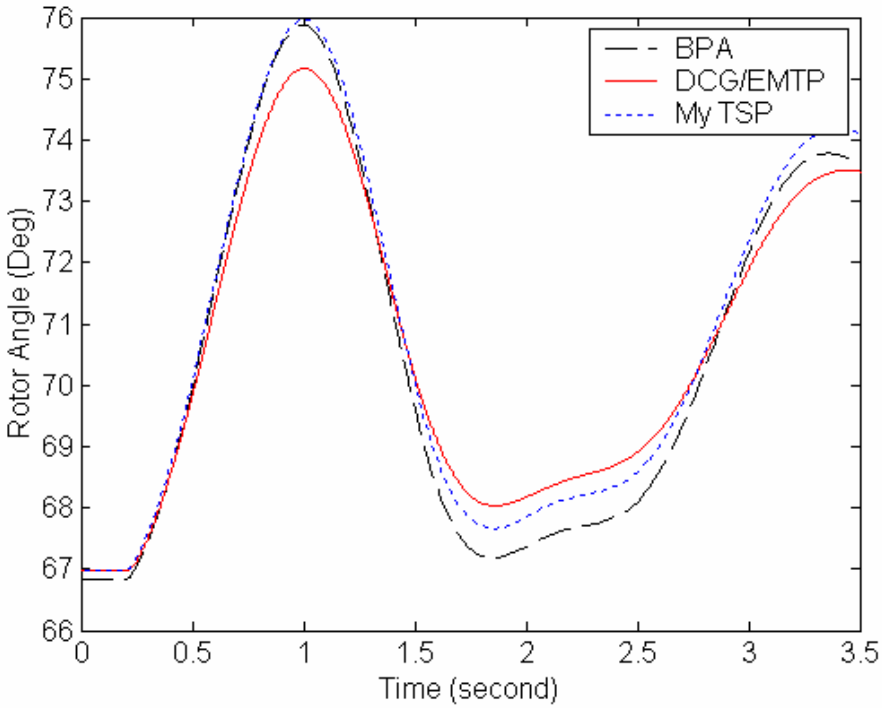

Figure 6.33: Generator 7 Swing Curves Comparison under Double -Ground Fault

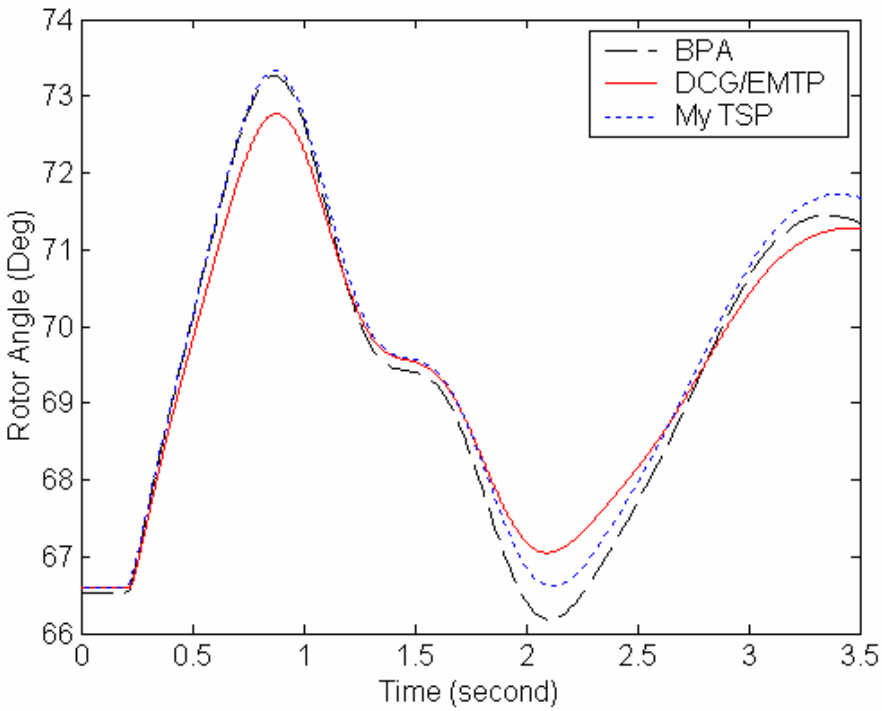

Figure 6.34: Generator 8 Swing Curves Comparison under Double -Ground Fault

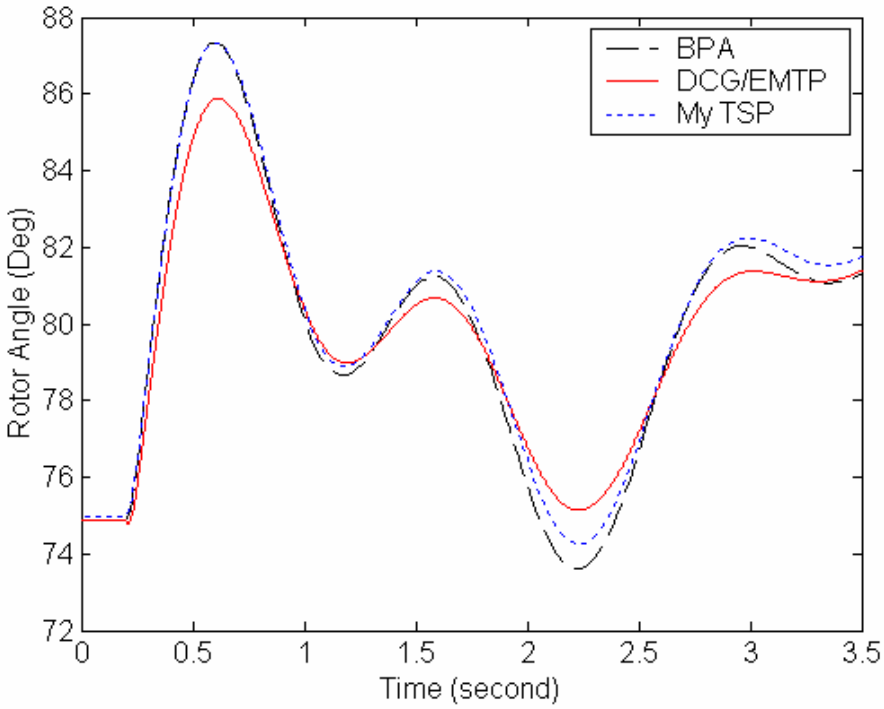

Figure 6.35: Generator 9 Swing Curves Comparison under Double -Ground Fault

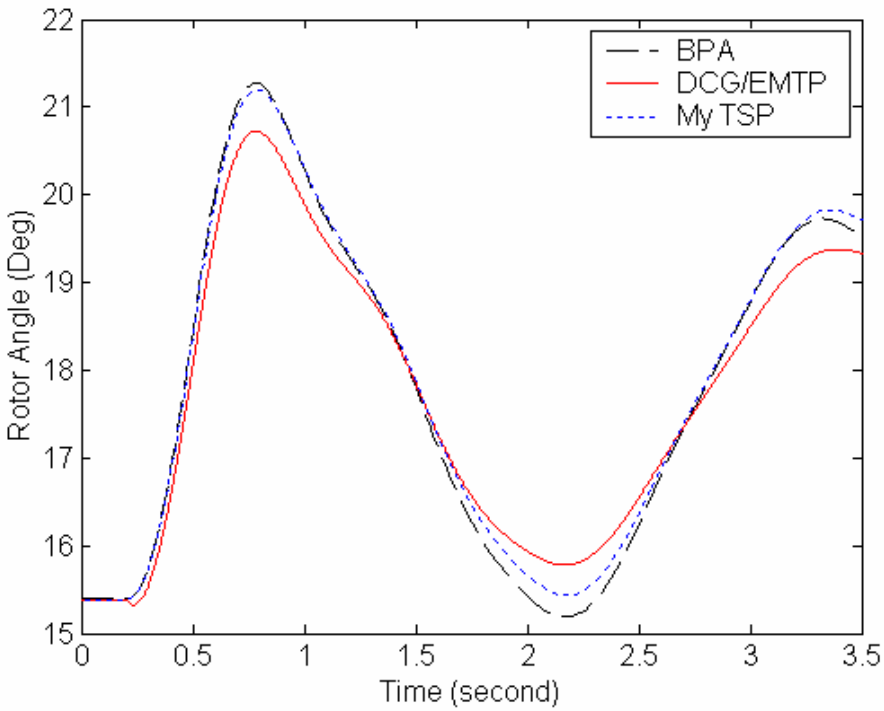

Figure 6.36: Generator 10 Swing Curves Comparison under Double -Ground Fault

From the above curves, it can be observed that the in-house TS simulator

developed by the author is creditable. It is noticed that there are differences between the results from DCG/EMTP and BPA. These differences can be attributed to the differences in the modeling of machines in the EMT simulator and the TS simulator: the foundations of the modeling of generators in the TS simulator adopt many assumptions and methods that have resulted from years of experience. Notwithstanding the small differences in the results, it can be concluded that DCG/EMTP and BPA behave basically in the same way.

VI.3 ELECTROMAGNETIC TRANSIENT ASSESSMENT

A hybrid simulator was implemented on a digital electromagnetic transients simulator, known as HYPERSIM using the User Code Block (UCB) facility. The interface itself is implemented as a UCB which is in turn interfaced with the TS simulator.

HYPERSIM simulates the detailed system, while the embedded TS simulator takes charge of the external system. Throughout the test, the integration time steps of the TS simulator and HYPERSIM are fixed to 50μs and 20ms respectively. In HYPERSIM, the external system was replaced by a frequency dependent equivalent. At each interchange, the EMT simulator transfers power and reactive power, calculated from positive-sequence fundamental frequency component of interface bus voltage, and the TS simulator transfers the three-phase positive-sequence fundamental frequency current source.

In this chapter, the purpose of case studies is to evaluate the performance of hybrid simulation: to check whether the results of hybrid simulation are creditable. The interaction protocol of the hybrid simulation is a serial implementation. The feature of the implementation, in short, is when one simulator is running the other is idle. The detailed steps are listed below, referring to Fig 4.26:

1. Both the EMT and TS simulators started from the same time T0 and proceeded to time T1.

2. The Norton equivalents for the external system are derived from the TS simulation results at T1, and are transferred to the EMT simulator.
3. Using the latest Norton equivalent obtained at T1, the EMT simulator executes from T1 to T2, while the TS simulator is idle.
4. EMT simulator results from T1 to T2 are processed by using a curve fitting method to obtain the phasor values of the powers (P and Q) corresponding to time T2.
5. TS simulator uses the P and Q from the EMT simulator to do the calculation for the interval T1 to T2, while the EMT simulator is idle.
6. The above procedure is repeated for the next cycle.

Hybrid simulators should be able to solve system transients covering a large bandwidth: from electromagnetic transients associated with the devices, to swing curves for the system as a whole. Consequently two approaches were used to assess the hybrid simulation: one is to check the waveform immediately after a disturbance or clearing of a disturbance (determined by the EMT simulation), while the other is to assess the system transient stability, mainly through the machine rotor angle swings and frequency deviations (determined by the TS simulation). In this section, emphasis was placed on the waveform check. For evaluation of electromagnetic transients the response for the first few cycles immediately after disturbances and clearing of the disturbances are of most interest.

For the evaluation of the performance of the hybrid simulation for fast transients, a modified 9-bus 3-machine WSCC test system was used, as shown in Figure 6.37. The modification added to the original WSCC system is the addition of a 130MVAr SVC at bus 7. This SVC, which also includes a transformer, filter banks and terminal bus, forms the detailed system. The detailed system is modeled in HYPERSIM using its built-in TSC/TCR type SVC model. Bus 7 was selected as the interface bus in order to minimize the size of the detailed system. The main WSCC

network was the external system. The hybrid simulation built in HYPERSIM for 9-bus system was shown in Figure 6.38.

For the benchmark case the network as a whole was simulated in the HYPERSIM platform with a time step of 50μs.

The fault scenario is as follows: at 0.2 second the SVC connects to the network (symmetrical disturbance), at 0.5 second a phase (B)-to-phase (C) fault is applied to bus 7 (asymmetrical disturbance), and after three cycles, at 0.56 second, the fault is cleared. In this test, bus 7 is not only the interface bus, but also the fault bus. This is most severe test for the performance of the frequency dependent equivalent.

Figures 6.39, 6.41,and 6.43 are voltage and current waveforms from hybrid simulation, and Figures 6.40, 6.42, and 6.44 are voltage and current waveforms from HYPERSIM. For the case of the frequency dependent equivalent circuits, the waveforms from the hybrid simulation are valid, even though the interface bus happens to be the disturbance bus. This is consistent with the analysis we made in the section 5 of the Chapter 4, i.e. the waveforms of the EMT simulator are not a consideration when choosing interface location in the case of frequency dependent equivalent.

In general, the hybrid simulation can indeed produce outputs matching closely with the results from a full EMT simulation. The use of frequency dependent equivalent can successfully emulate the external system with full fidelity, and hence can account for the propagation of harmonics into the external system.

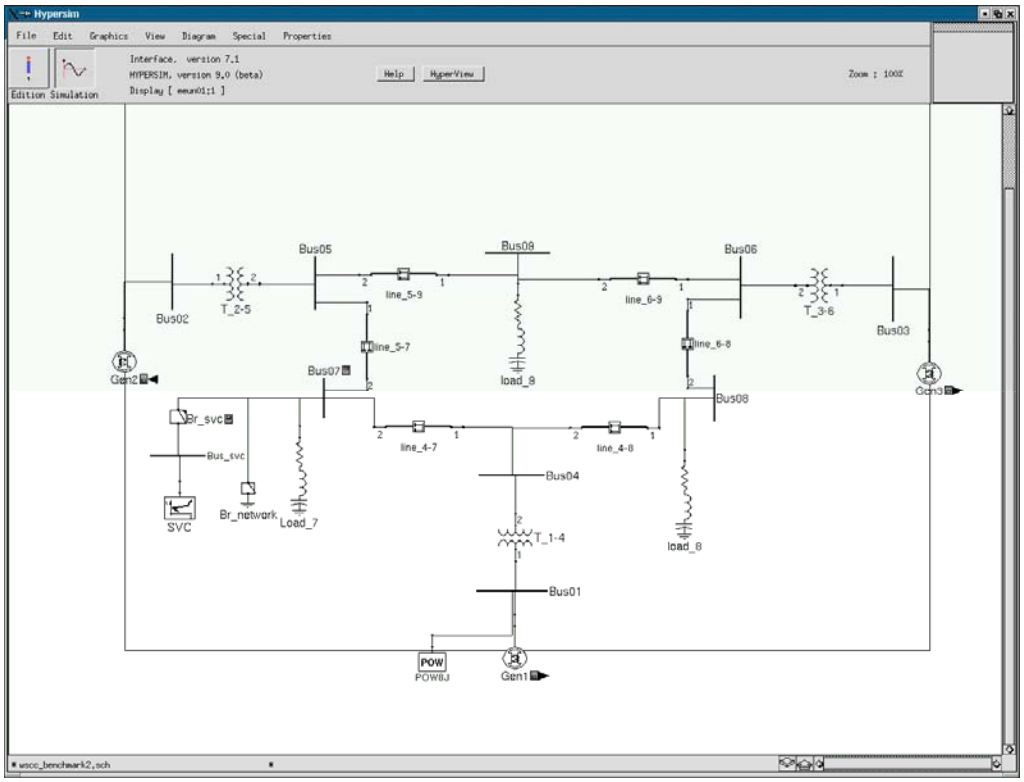

Figure 6.37: Modified 9-Bus System

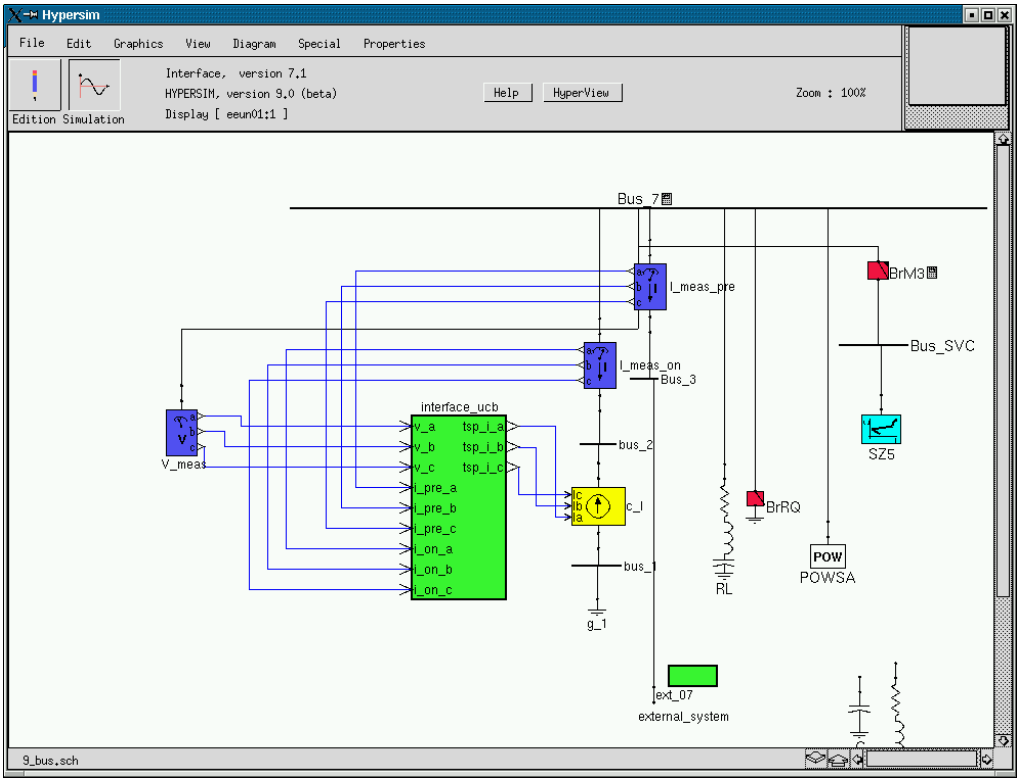

Figure 6.38: Diagram of Hybrid Simulator for 9-Bus System

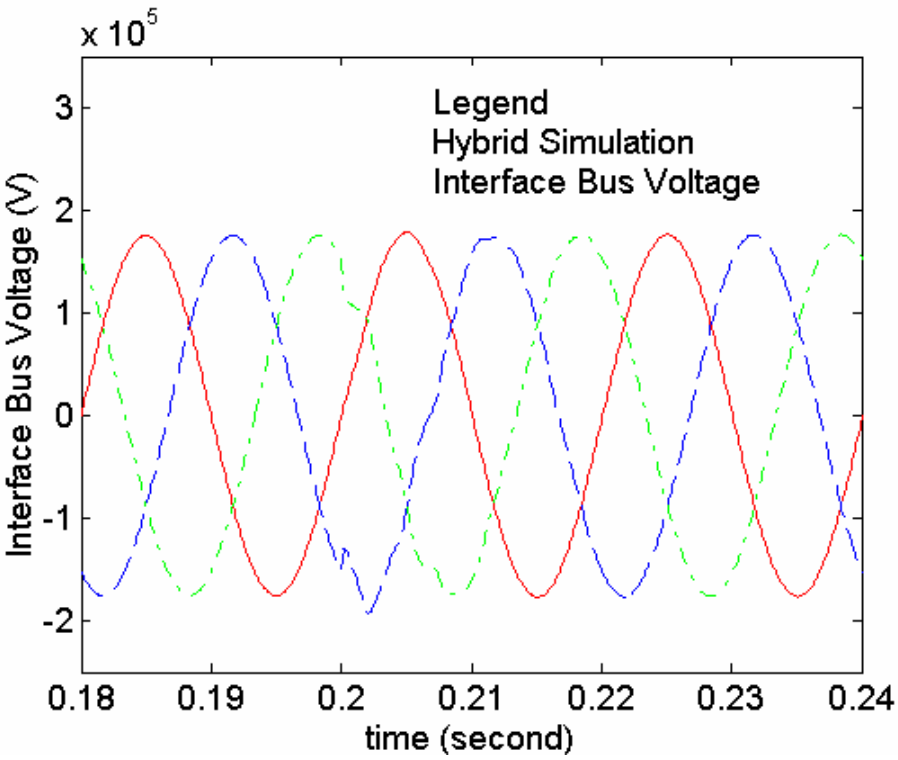

(a) Voltage

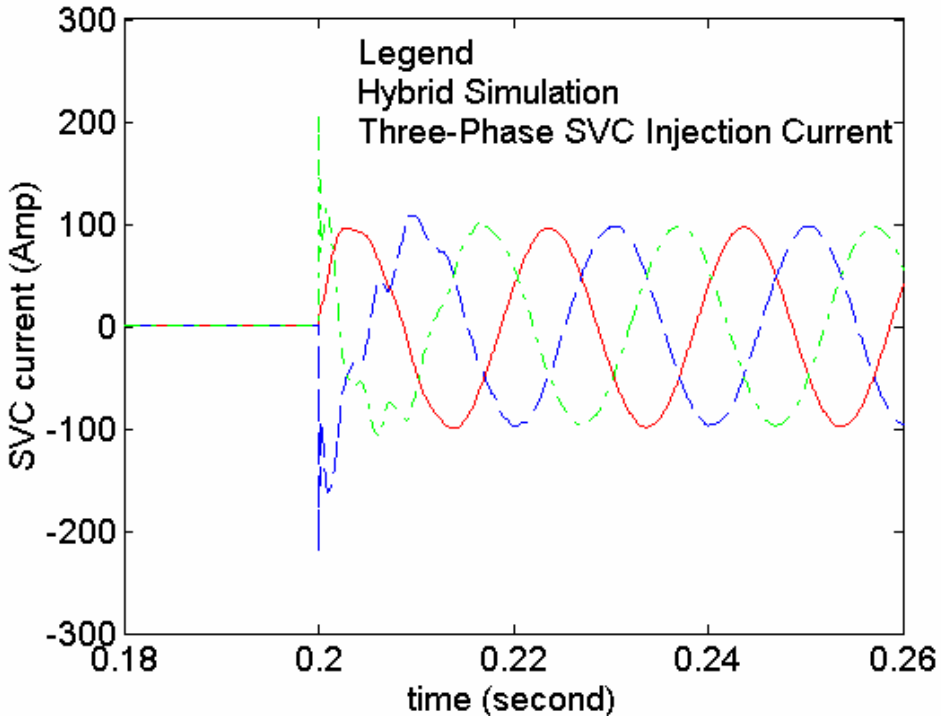

(b) Current

Figure 6.39: Waveforms from Hybrid Simulation When SVC Connected

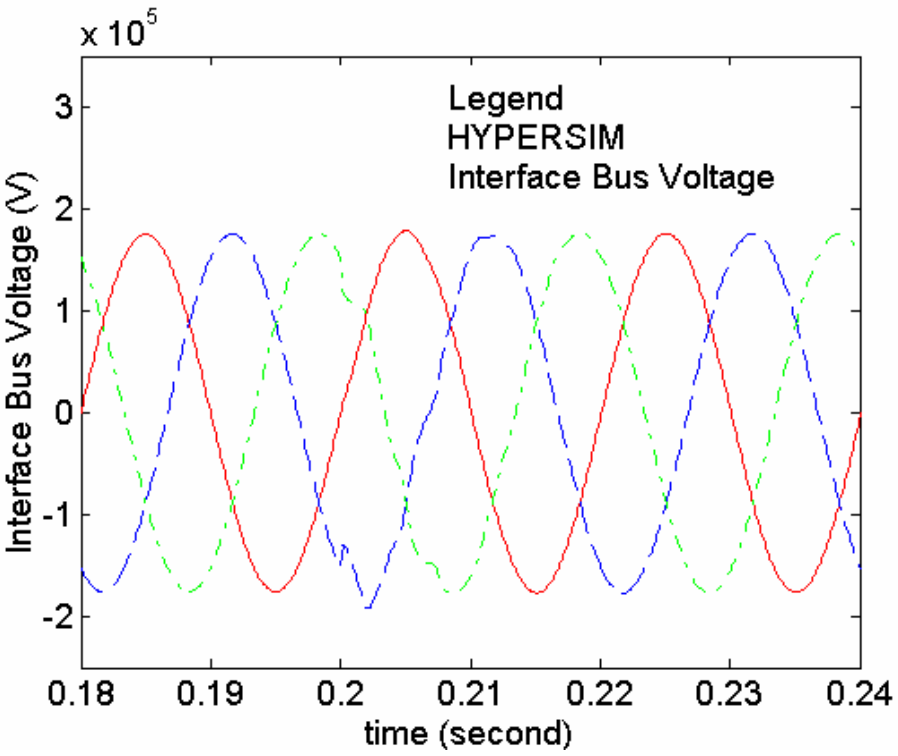

(a) Voltage

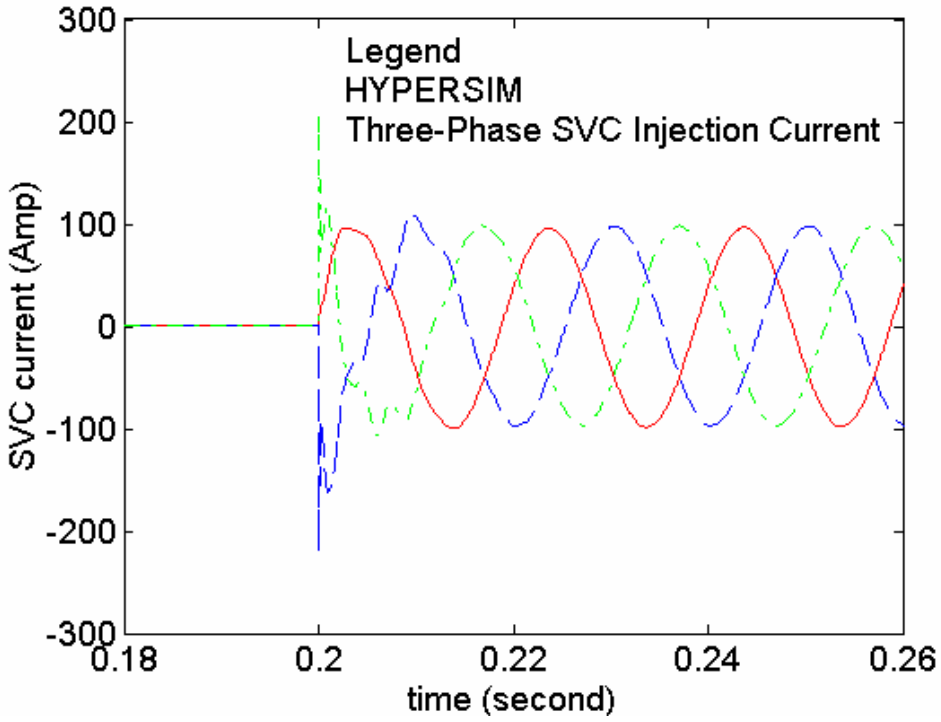

(b) Current

Figure 6.40: Waveforms from Full EMT Simulation When SVC Connected

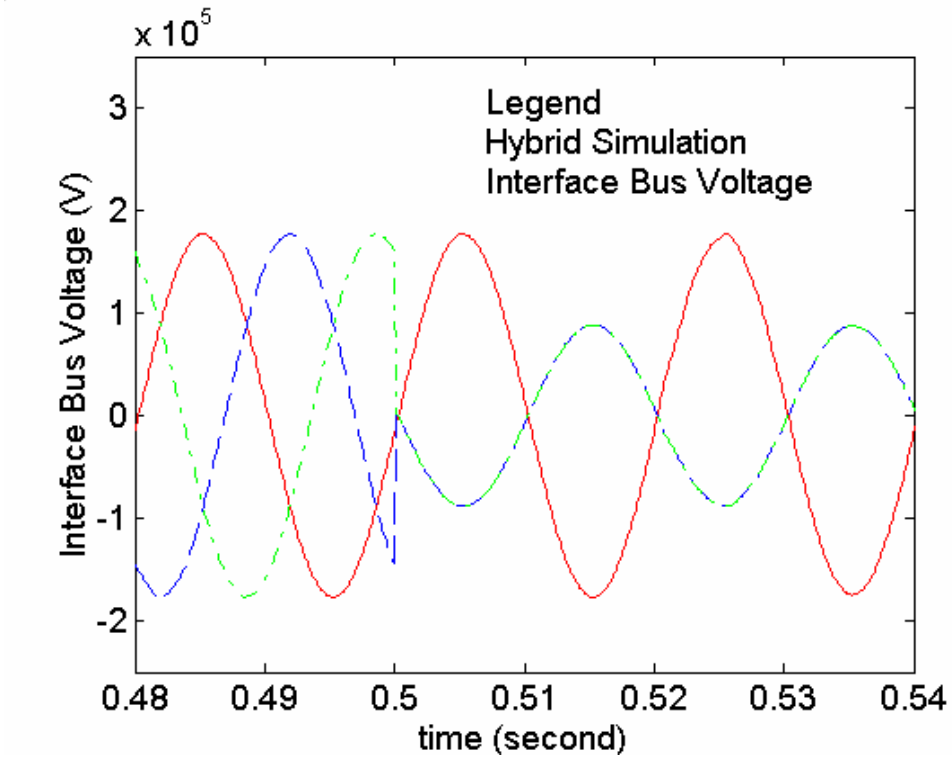

(a) Voltage

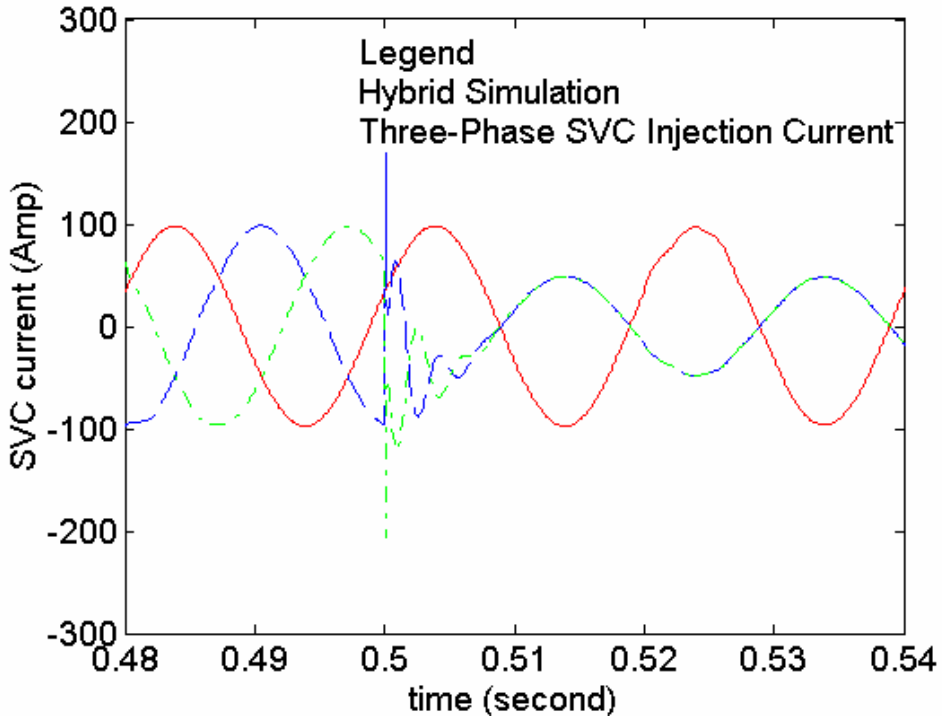

(b) Current

Figure 6.41: Waveforms from Hybrid Simulation under Fault

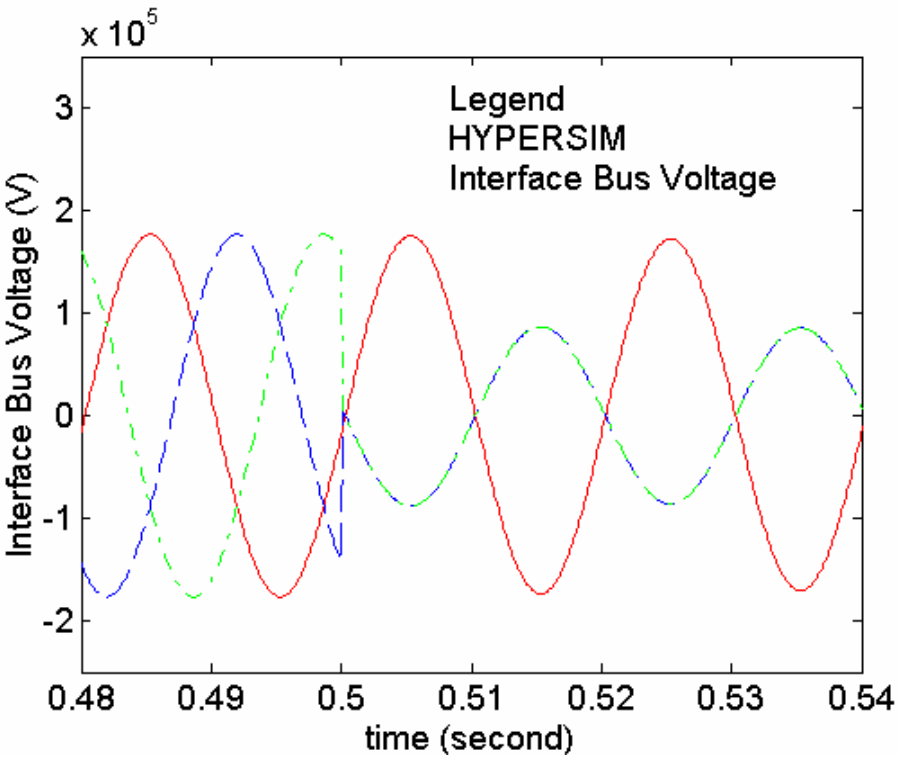

(a) Voltage

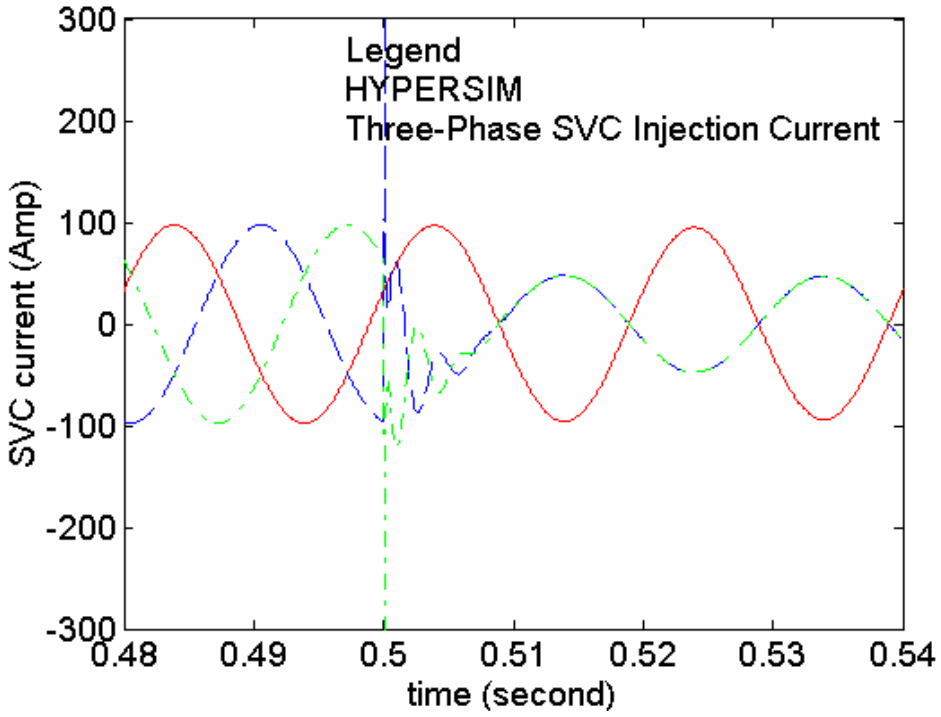

(b) Current

Figure 6.42: Waveforms from Full EMT Simulation Under Fault

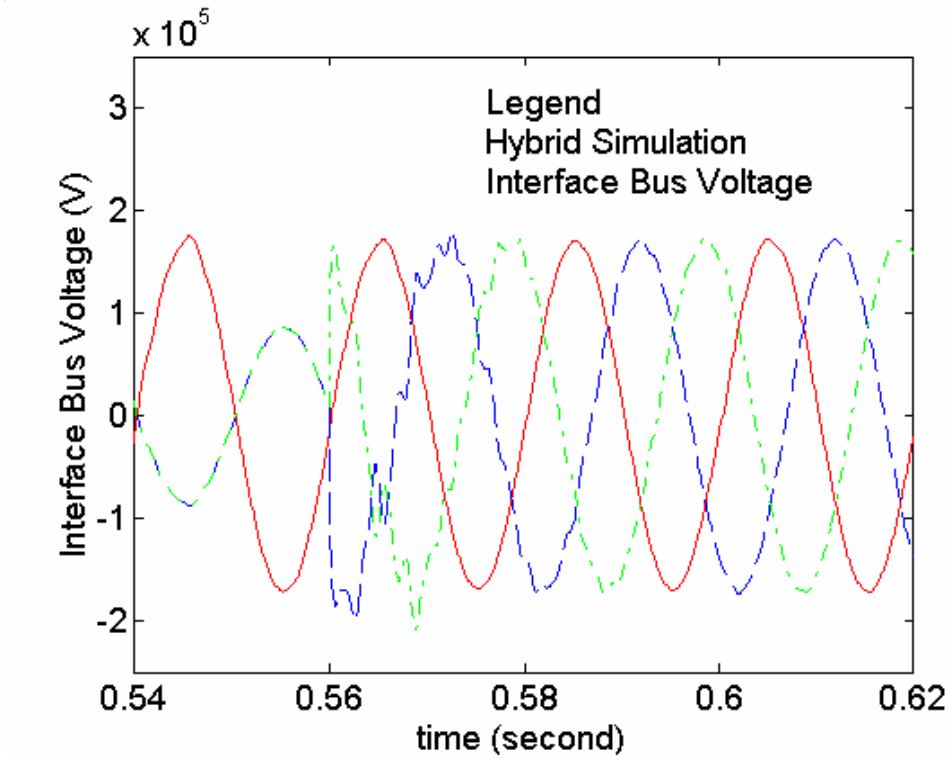

(a) Voltage

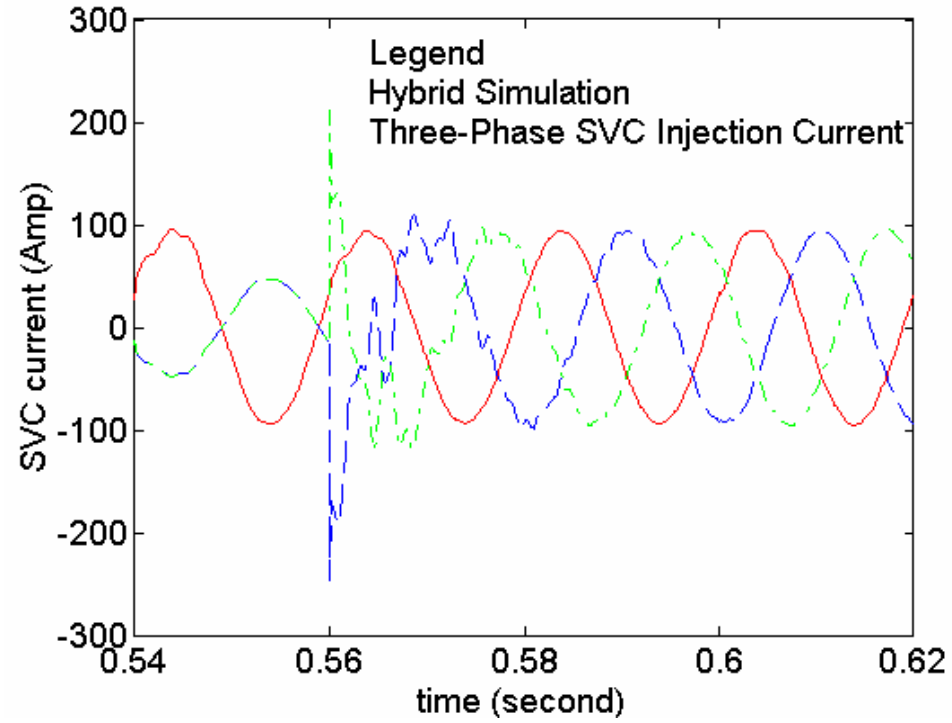

(b) Current

Figure 6.43: Waveforms from Hybrid Simulation after Fault Cleared

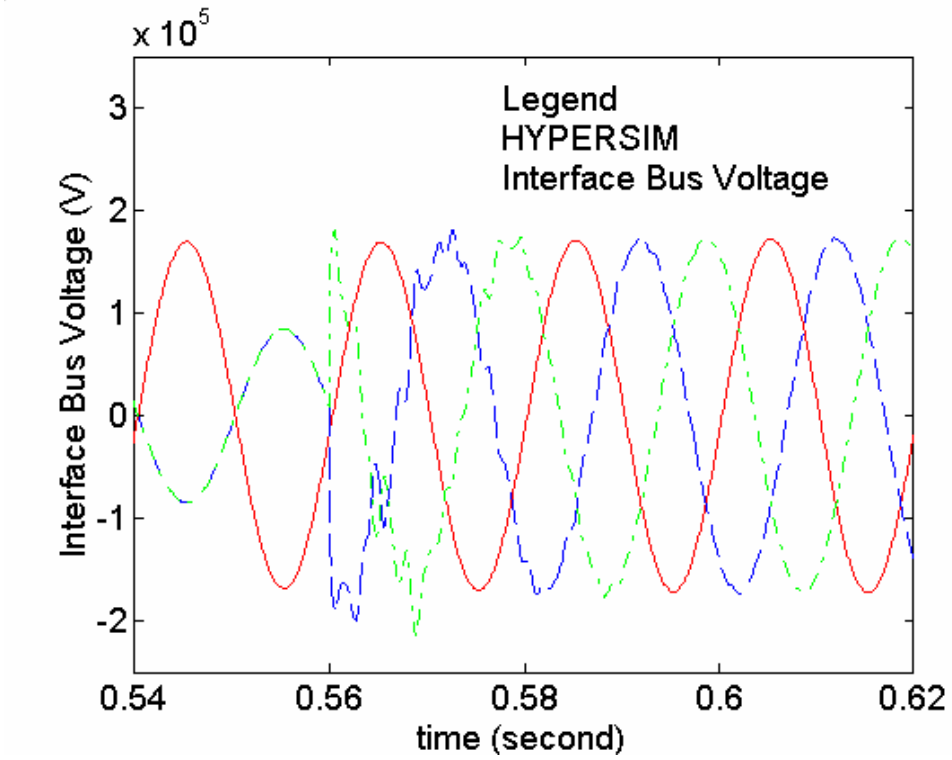

(a) Voltage

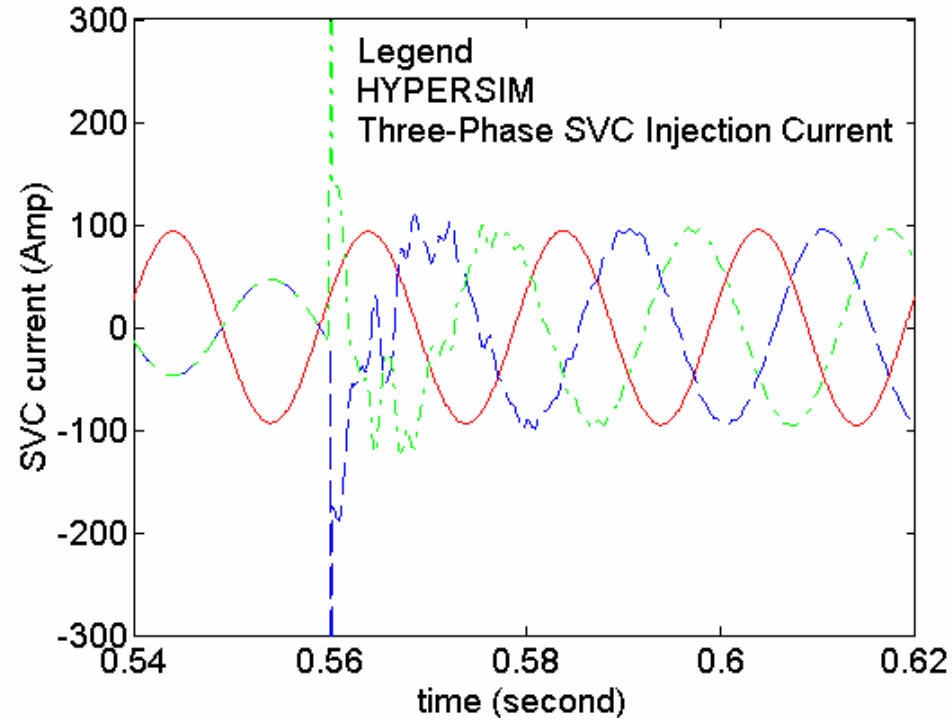

(b) Current

Figure 6.44: Waveforms from Full EMT Simulation after Fault Cleared

VI.4 TRANSIENT STABILITY ASSESSMENT

In this section assessment of hybrid simulation will be given from the transient stability point of view, i.e. rotor angle and/or speed curves of generators. Because part of system is represented at the device level, we would expect that the transient stability results from the hybrid simulation theoretically would be better than those obtained with the pure TS simulator, agreeing better with the results obtained when the whole system is simulated by the EMT simulator. However this is not always true: the TS and EMT simulators are of two different kinds. When they interface, some extra errors will be introduced, such as frequency mismatch during transient and frequency drift in steady state. Even some remedies can decrease their effect on the system transient, they do have some impact, and their effect cannot be measured quantitatively, even though can be analyzed qualitatively.

The assessment from the TS point of view was performed on both 39-bus system and 9-bus system. HYPERSIM simulates the detailed system, while the embedded TS simulator takes charge of the external system. Throughout the test, the integration time steps of the TS simulator and HYPERSIM are fixed to 50μs and 20ms respectively. In HYPERSIM, the external system was replaced by a frequency dependent equivalent. At each interchange, the EMT simulator transfers power and reactive power, calculated from positive-sequence fundamental frequency component of interface bus voltage, and the TS simulator transfers the three-phase positive-sequence fundamental frequency current source.

Firstly, the assessment was performed on 9-bus system. The detailed system description is the same as that in the last section. Four faults were simulated, one symmetrical and three asymmetrical. For the purpose of assessing the accuracy of the hybrid simulator, one benchmark case was prepared, which was based on the DCG/EMTP with the full system wholly modeled in detail. The EMTP representation with detailed machine model is used as the reference.

The following three figures show the rotor speed curves when a three-phase-to-ground fault was applied at bus 7, from 0.5 to 0.56 second.

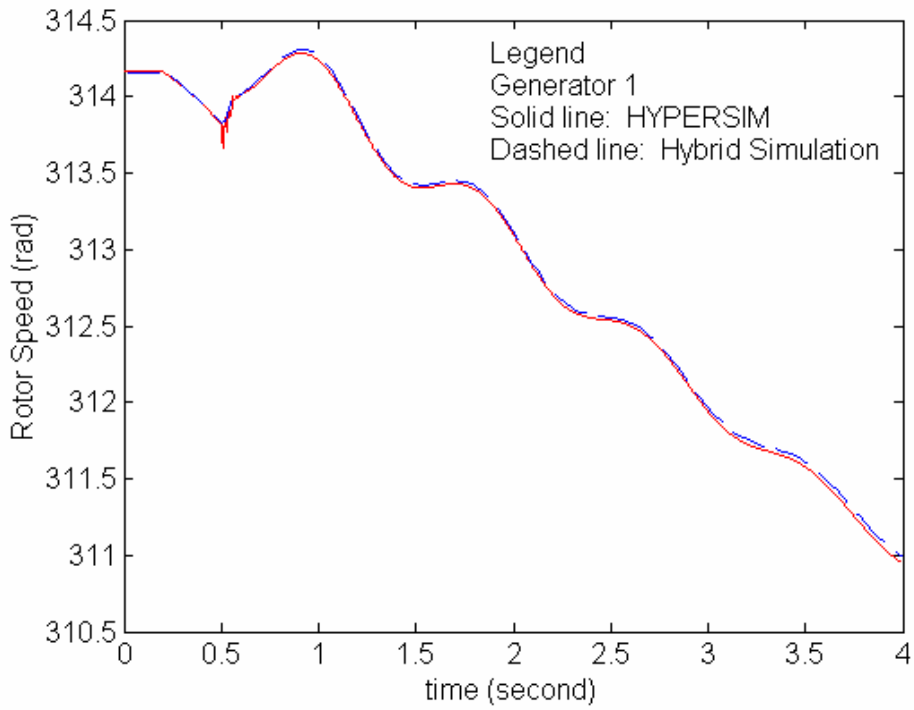

Figure 6.45: Generator 1 Rotor Speed Curves under Three-Phase-Grounded Fault

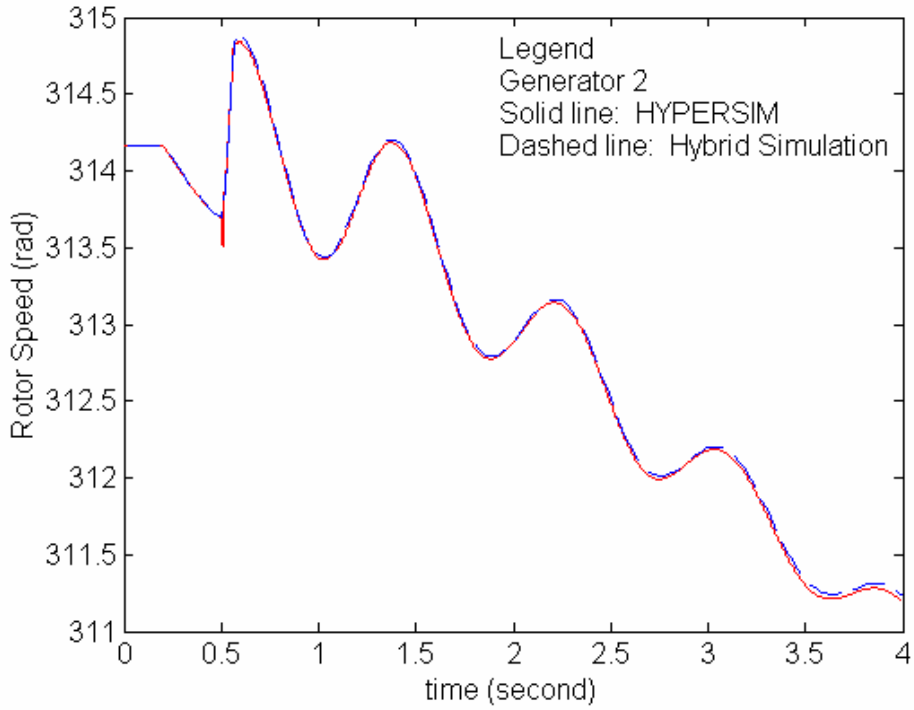

Figure 6.46: Generator 2 Rotor Speed Curves under Three-Phase-Grounded Fault

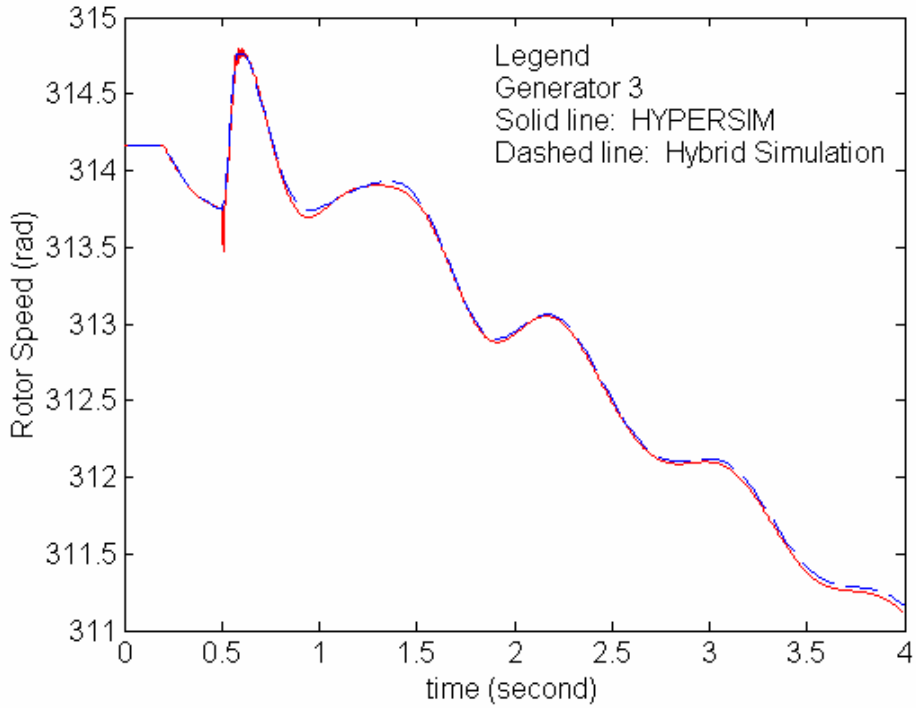

Figure 6.47: Generator 3 Rotor Speed Curves under Three-Phase-Grounded Fault

The following three figures show the rotor speed curves when a single-phase-to-ground fault was applied at bus 7, from 0.5 to 0.56 second.

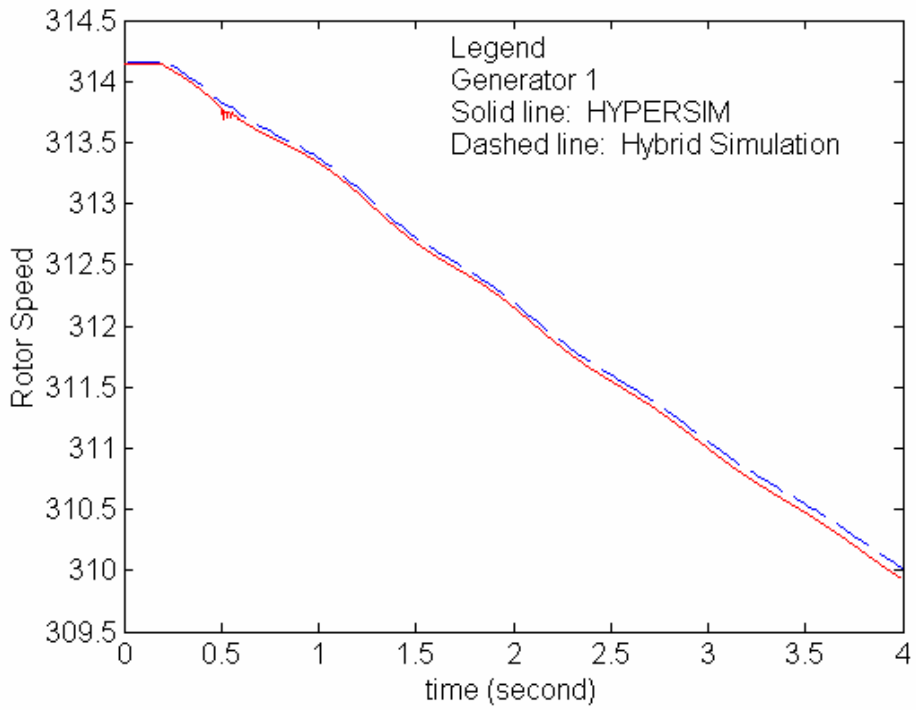

Figure 6.48: Generator 1 Rotor Speed Curves under Single-Phase-Grounded Fault

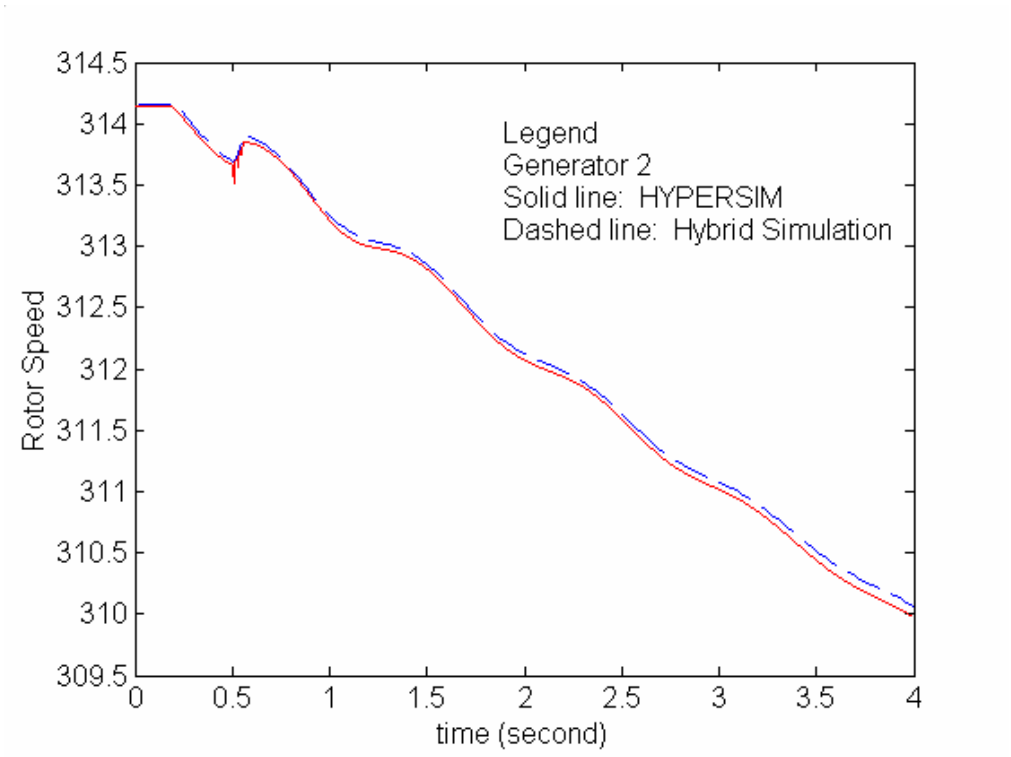

Figure 6.49: Generator 2 Rotor Speed Curves under Single-Phase-Grounded Fault

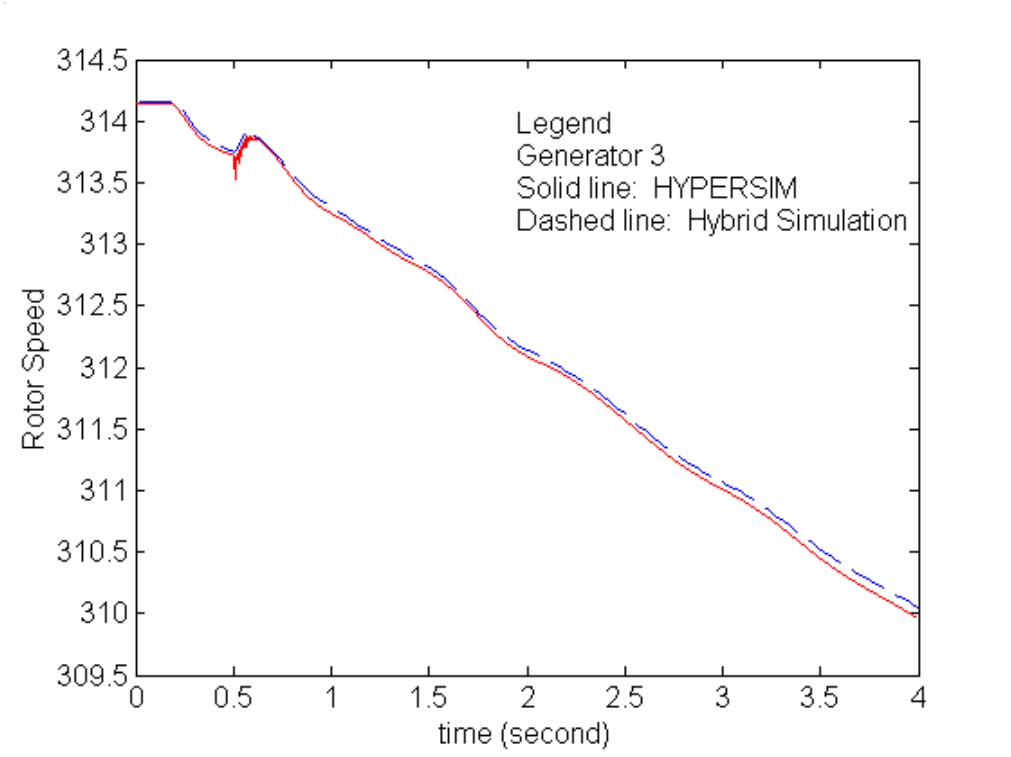

Figure 6.50: Generator 3 Rotor Speed Curves under Single-Phase-Grounded Fault

The following three figures show the rotor speed curves when a line-to-line fault was applied at bus 7, from 0.5 to 0.56 second.

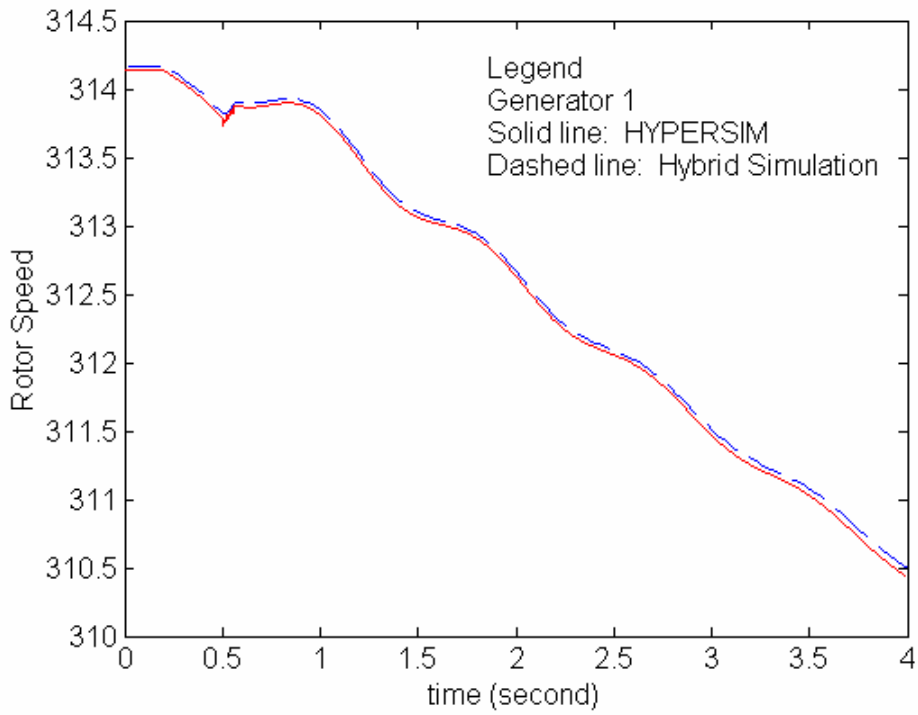

Figure 6.51: Generator 1 Rotor Speed Curves under Line-to-Line Fault

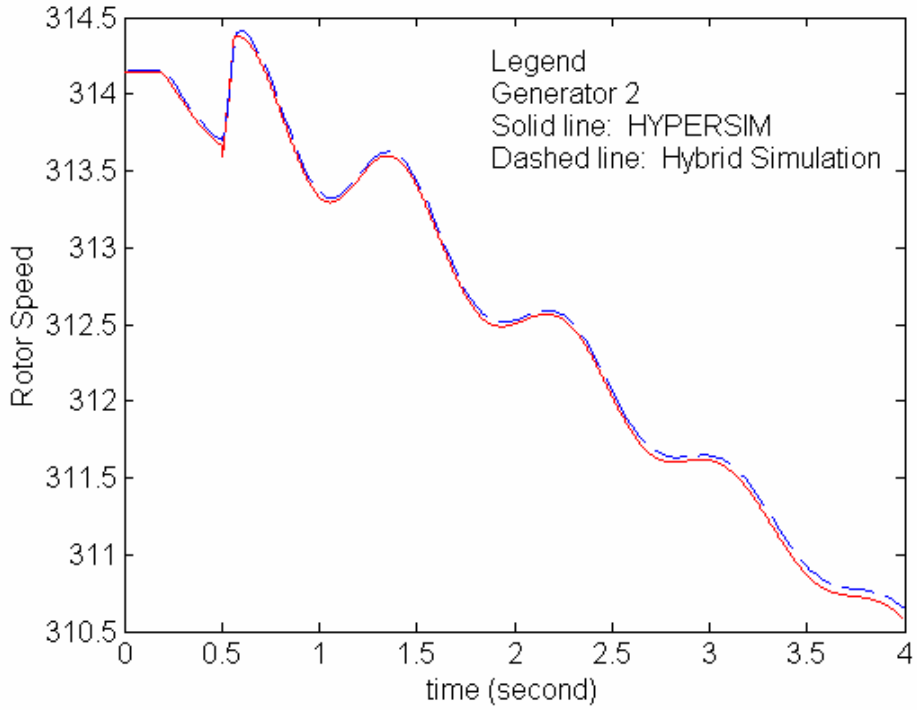

Figure 6.52: Generator 2 Rotor Speed Curves under Line-to-Line Fault

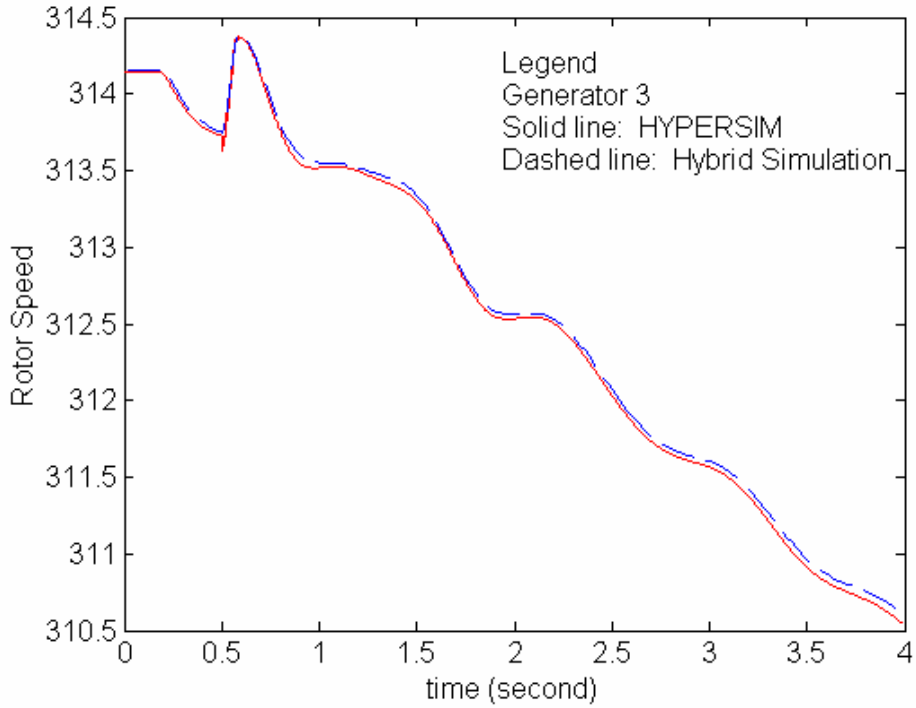

Figure 6.53: Generator 3 Rotor Speed Curves under Line-to-Line Fault

The following three figures show the rotor speed curves when a line-line-to-ground fault was applied at bus 7, from 0.5 to 0.56 second.

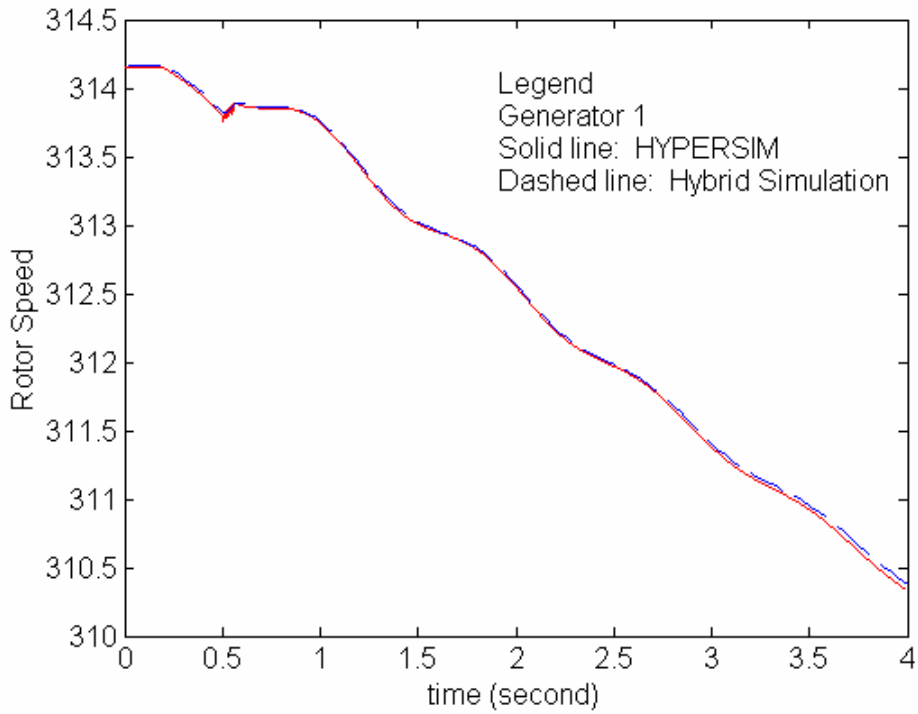

Figure 6.54: Generator 1 Rotor Speed Curves under Line-Line-Grounded Fault

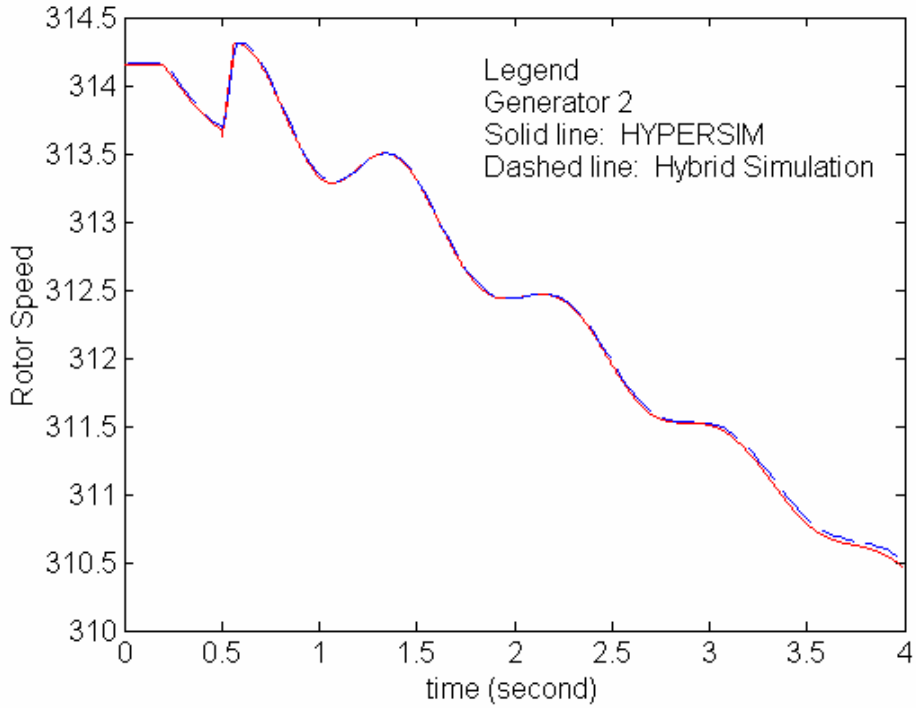

Figure 6.55: Generator 2 Rotor Speed Curves under Line-Line-Grounded Fault

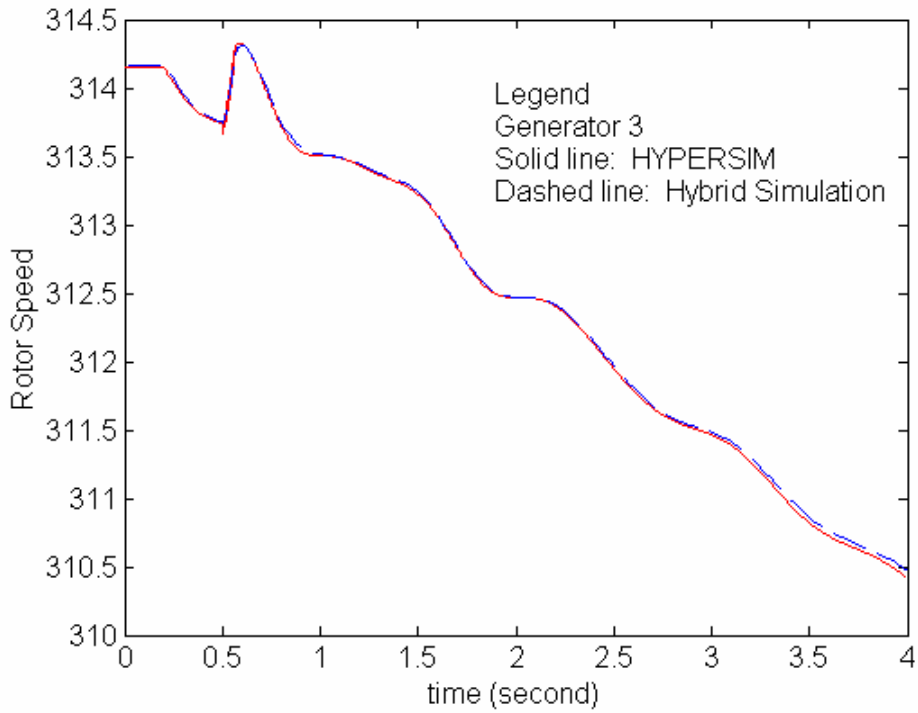

Figure 6.56: Generator 3 Rotor Speed Curves under Line-Line-Grounded Fault

On 39-bus system as shown in Appendix B, the network was partitioned into two parts along bus 36 with the detailed system consisting of generator 9 and components between bus 9 and 36. The generator 9 was replaced by a voltage source. The diagram of hybrid simulation on 39-bus system was shown in Figure 6.57.

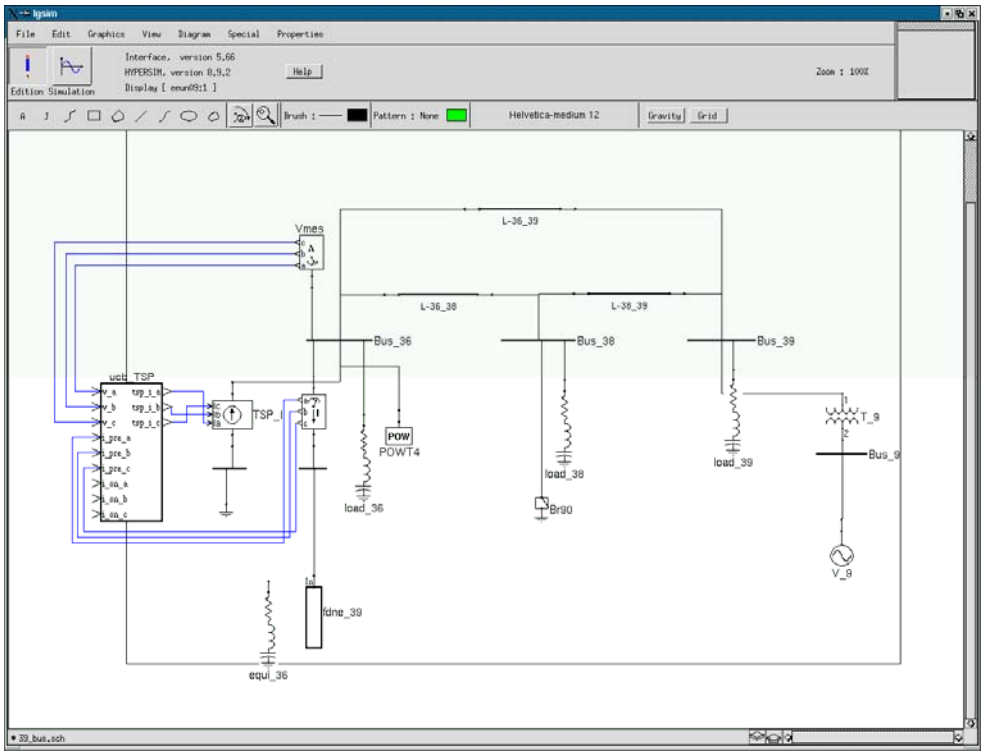

Figure 6.57: Diagram of Hybrid Simulation on 39-Bus System

A symmetrical fault and a single-phase-grounded fault on bus 38, from 0.2 to 0.24 second, were studied. Visual comparisons were made between hybrid simulation and DCG/EMTP, which was taken as benchmark, additionally with swing curves from a transient stability program. Figures 6.58 to 6.65 are swing curves under the three-phase-grounded fault.

From the figures, we can observe that system transient stability can be correctly predicted by hybrid simulation for both stable (on 39-bus system) and unstable (on 9-bus system) cases. The curves from the hybrid simulation are not necessary in between the curves from EMTP and the curves from TSP. But the profiles are in correct shape.

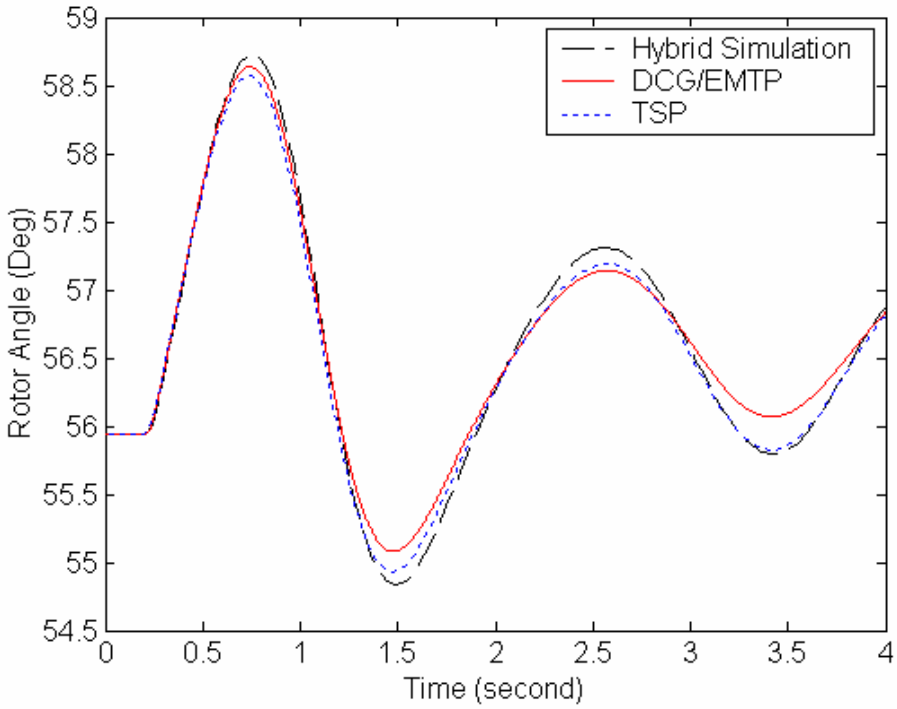

Figure 6.58: Generator 2 Rotor Angle Curve under Three-Phase-Grounded fault

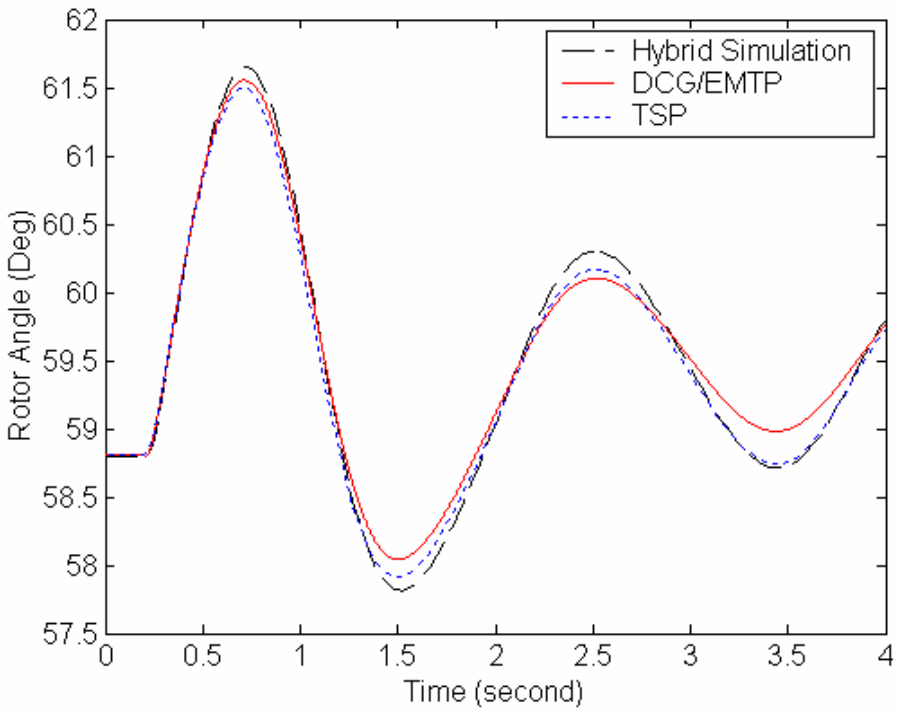

Figure 6.59: Generator 3 Rotor Angle Curve under Three-Phase-Grounded fault

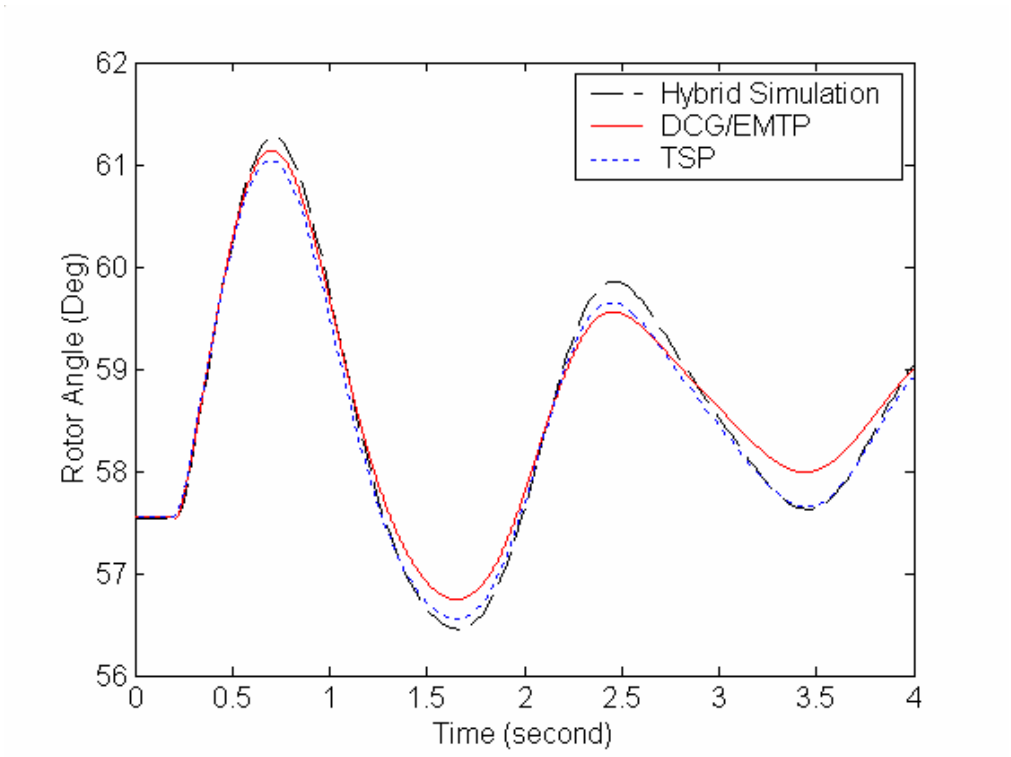

Figure 6.60: Generator 4 Rotor Angle Curve under Three-Phase-Grounded fault

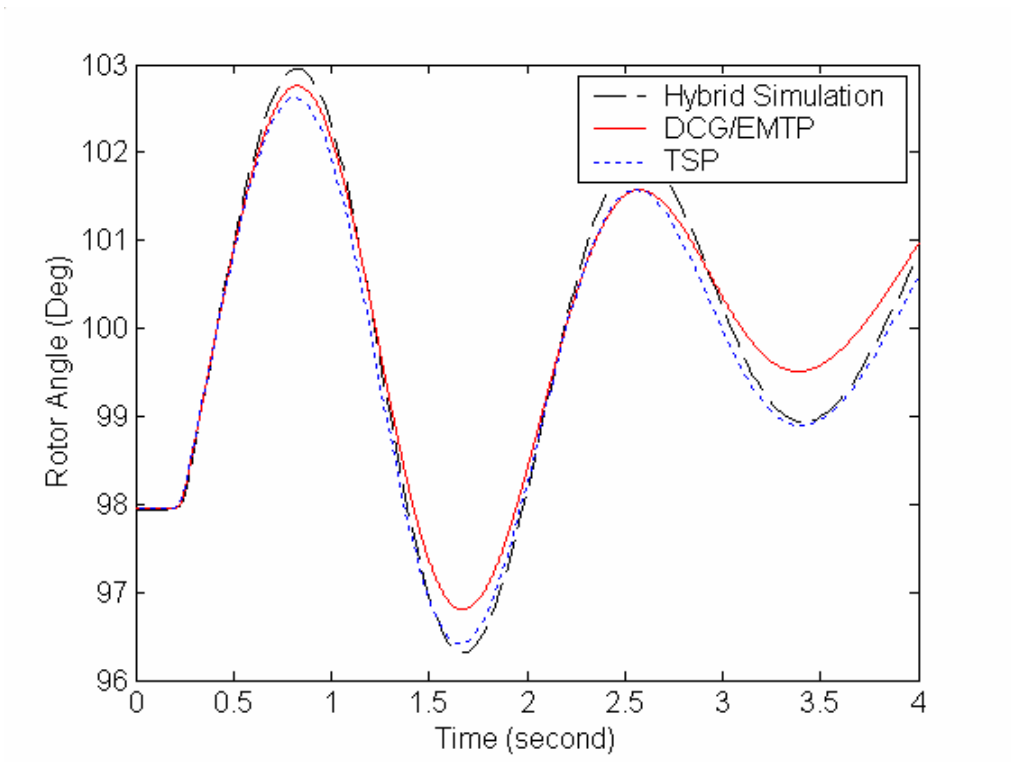

Figure 6.61: Generator 5 Rotor Angle Curve under Three-Phase-Grounded fault

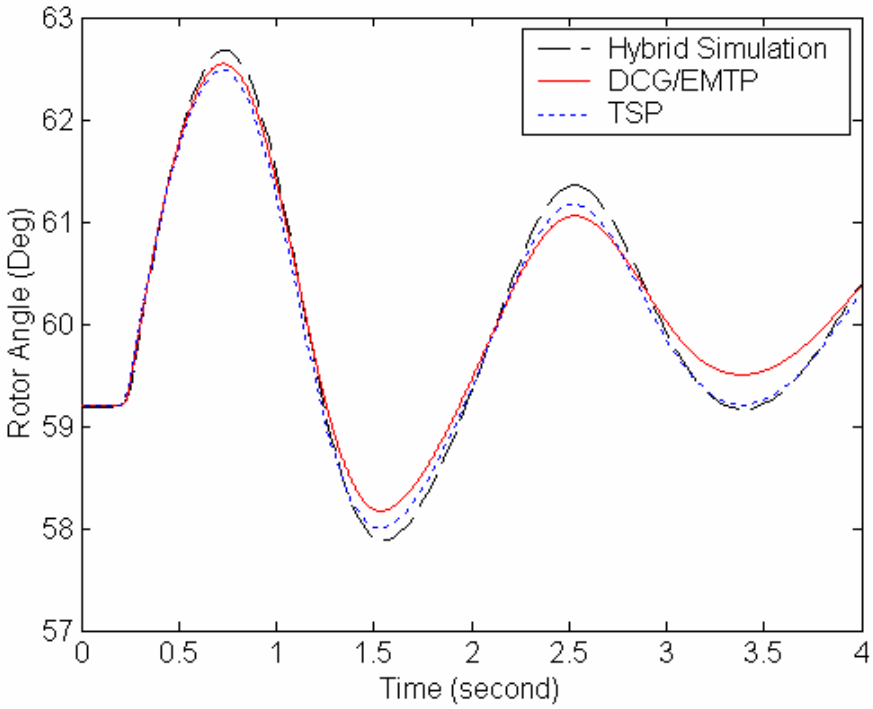

Figure 6.62: Generator 6 Rotor Angle Curve under Three-Phase-Grounded fault

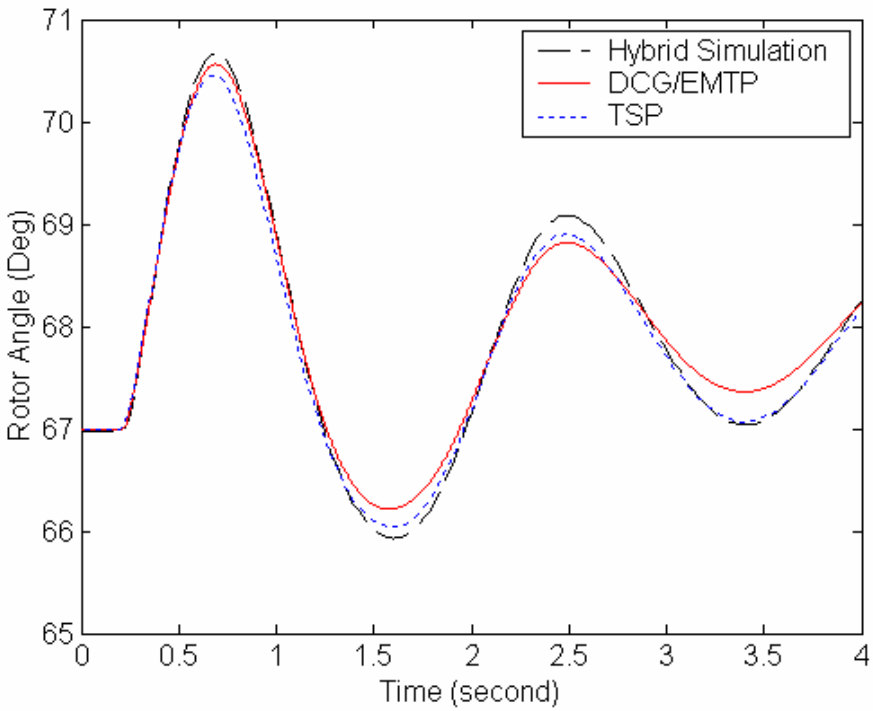

Figure 6.63: Generator 7 Rotor Angle Curve under Three-Phase-Grounded fault

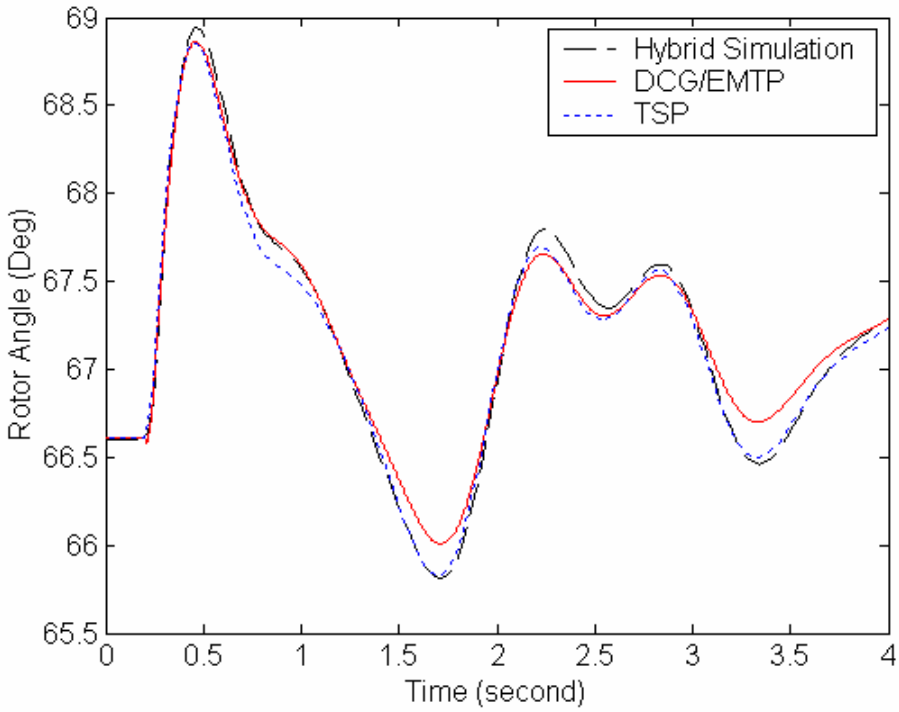

Figure 6.64: Generator 8 Rotor Angle Curve under Three-Phase-Grounded fault

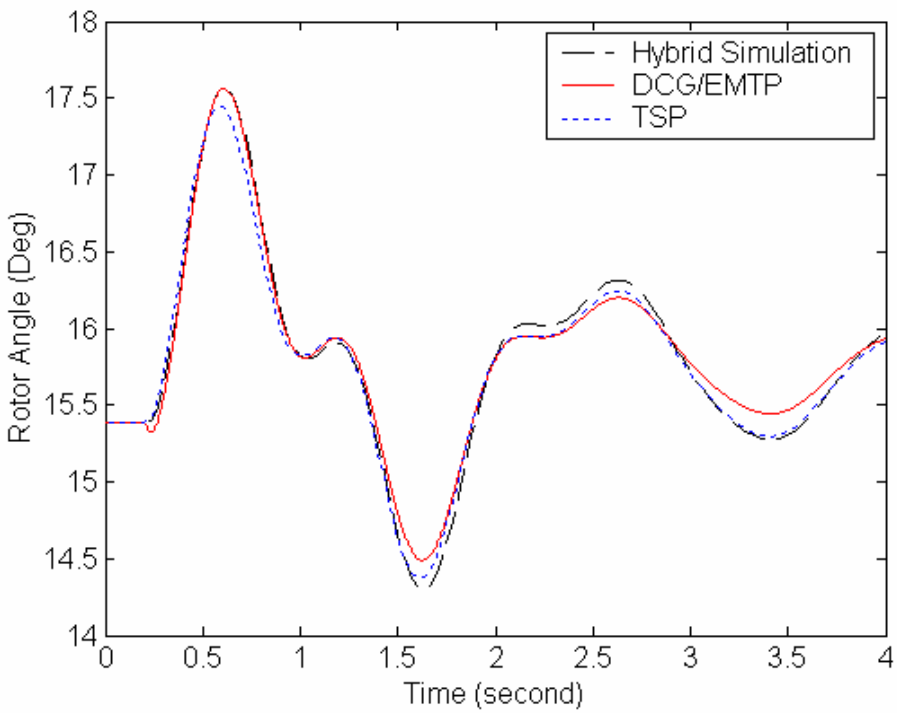

Figure 6.65: Generator 10 Rotor Angle Curve under Three-Phase-Grounded fault

Figures 6.66 to 6.73 are swing curves under the single-phase-grounded fault.

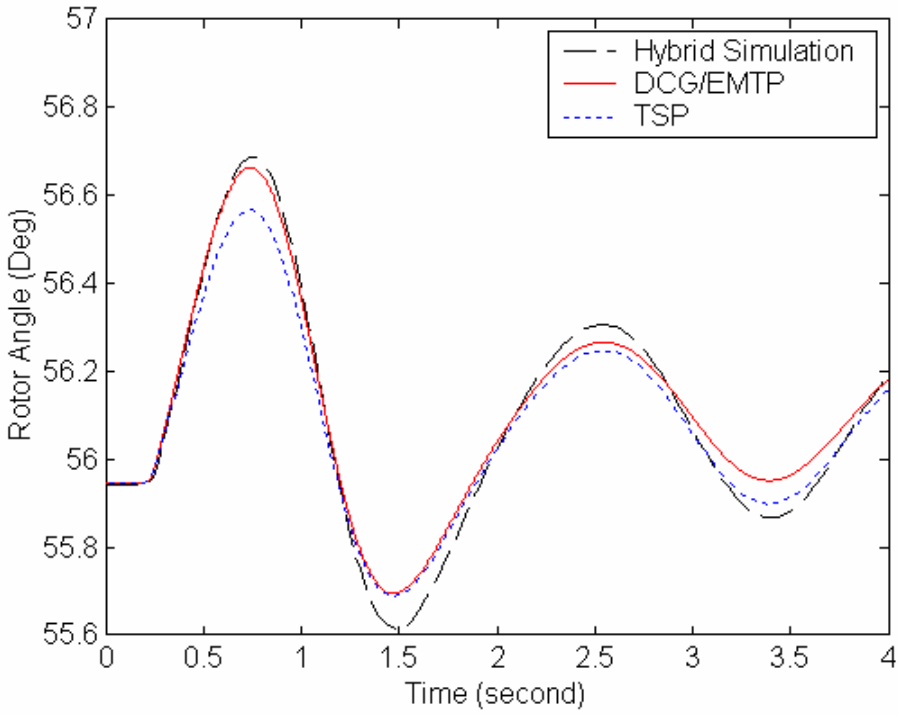

Figure 6.66: Generator 2 Rotor Angle Curve under Single-Phase-Grounded fault

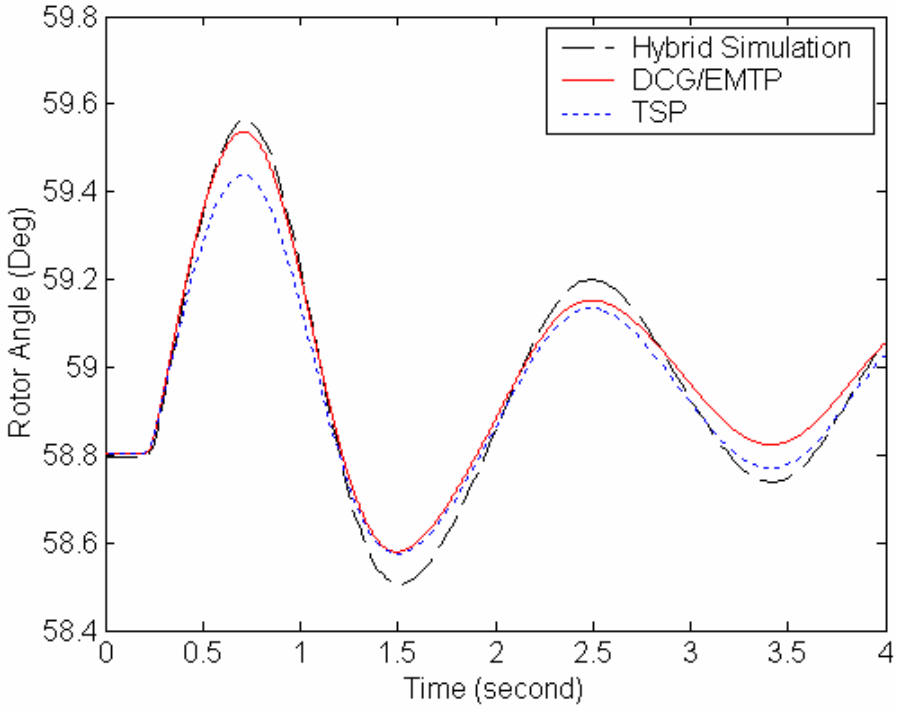

Figure 6.67: Generator 3 Rotor Angle Curve under Single-Phase-Grounded fault

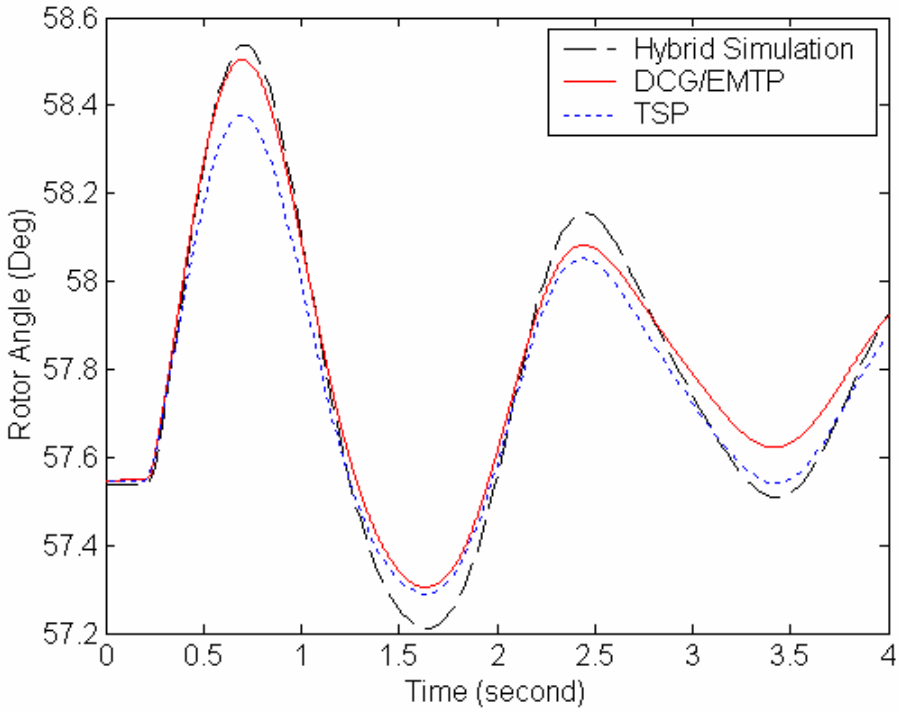

Figure 6.68: Generator 4 Rotor Angle Curve under Single-Phase-Grounded fault

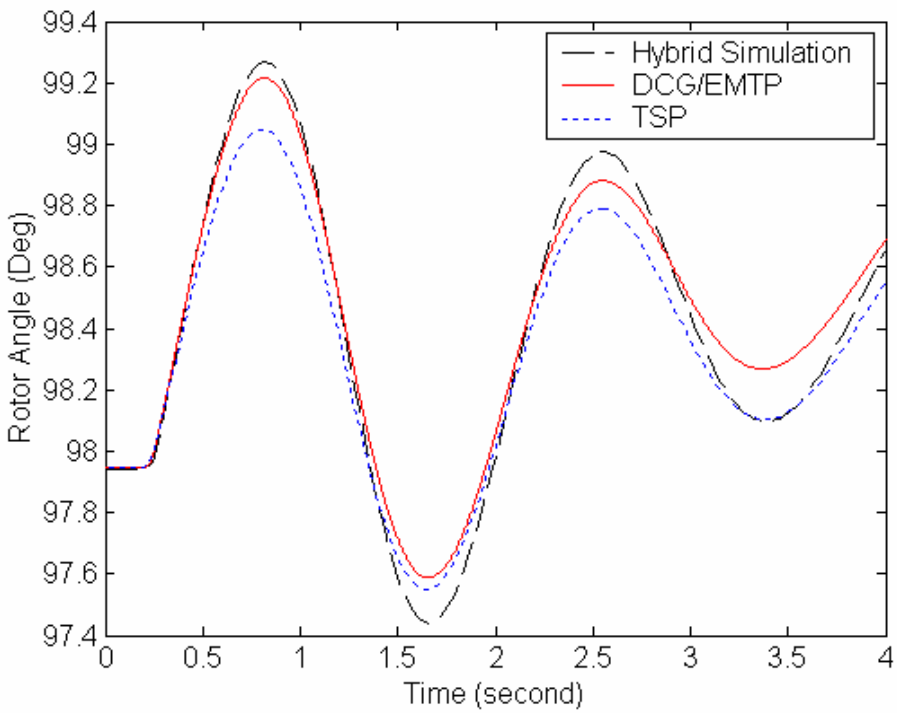

Figure 6.69: Generator 5 Rotor Angle Curve under Single-Phase-Grounded fault

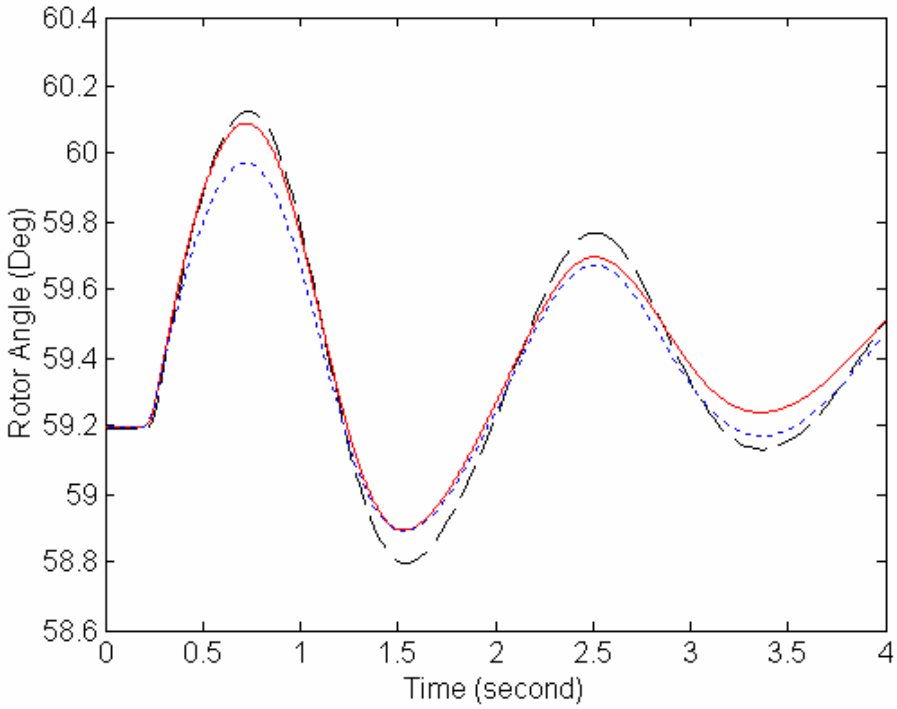

Figure 6.70: Generator 6 Rotor Angle Curve under Single-Phase-Grounded fault

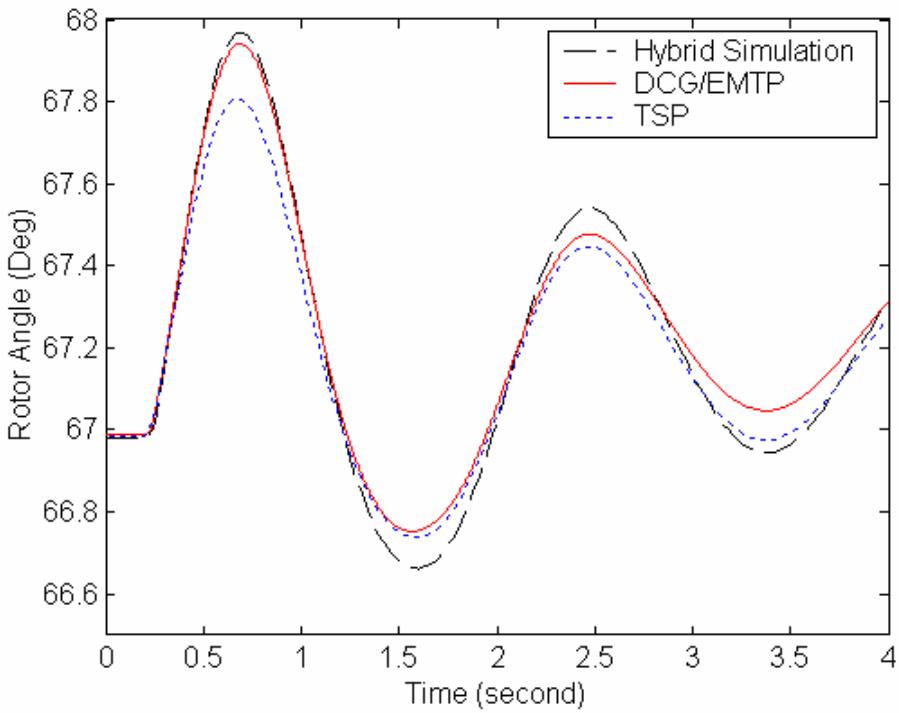

Figure 6.71: Generator 7 Rotor Angle Curve under Single-Phase-Grounded fault

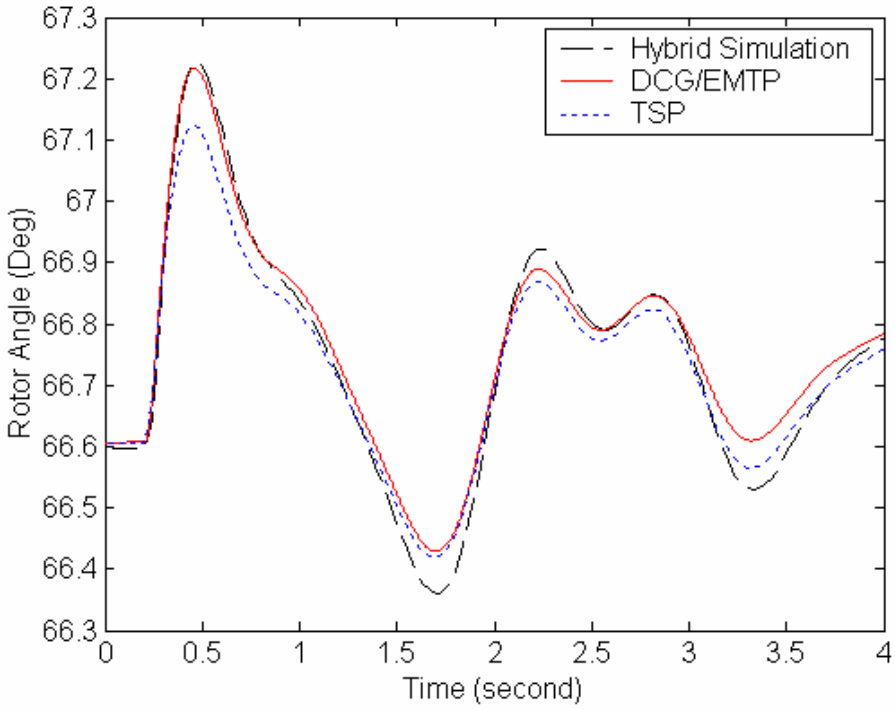

Figure 6.72: Generator 8 Rotor Angle Curve under Single-Phase-Grounded fault

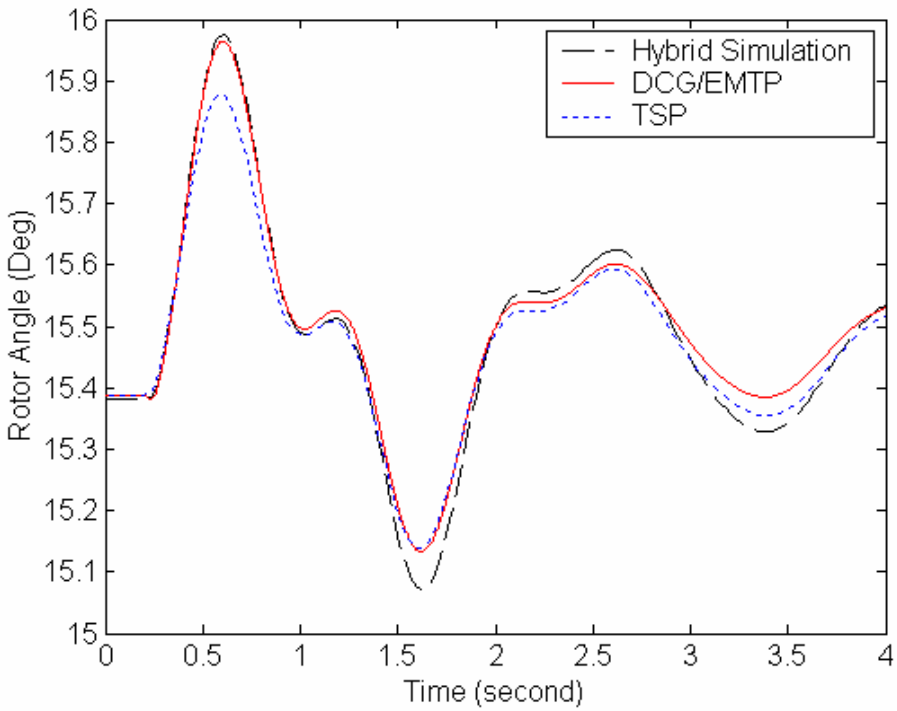

Figure 6.73: Generator 10 Rotor Angle Curve under Single-Phase-Grounded fault

The figures in this section prove that the theoretical analysis made in Chapter 5 are correct. The equivalence of the detailed system based on positive-sequence variables is acceptable.

VI.5 ADVANTAGES OVER CONVENTIONAL TRANSIENT STABILITY SIMULATORS

Providing detailed simulation results for the key components is one of the advantages of the hybrid simulation over conventional transient stability simulators. As FACTS devices and HVDC links are used more and more widely in modern power systems, studies of their impact on network stability become more urgent. Conventional transient stability simulators have a very poor capability to model the devices and links. Generally speaking, the models of the devices and links in the simulators are tailored to specified disturbance under particular circumstance. For the disturbances like commutation failures between valves, the simulators cannot deal with them.

Because of the limited modeling capability, power electronic devices and control systems can only be represented as modified steady-state models in conventional transient stability simulators. The limitation does not exist in the hybrid simulation. As a system operation tool, the hybrid simulation offers extended contingency lists (such as mal-function of power electronic devices) for dynamic security assessment.

In Chapter 5, it has already been pointed out that for any type of disturbance in the detailed system the TS simulator only needs positive-sequence fundamental frequency variables. The statement is also applicable to disturbances such as commutation failures.

The extended contingency capability of the hybrid simulation can be demonstrated by the following example. On 39-bus system, an additional FC/TCR type of SVC was attached to bus 36, as shown in Figure 6.74. The three TCR

branches are connected in delta. For simplicity, the SVC connects to the bus directly, not through a transformer. The SVC can provide a maximum of 100 MVAr reactive power, capacitive and inductive respectively.

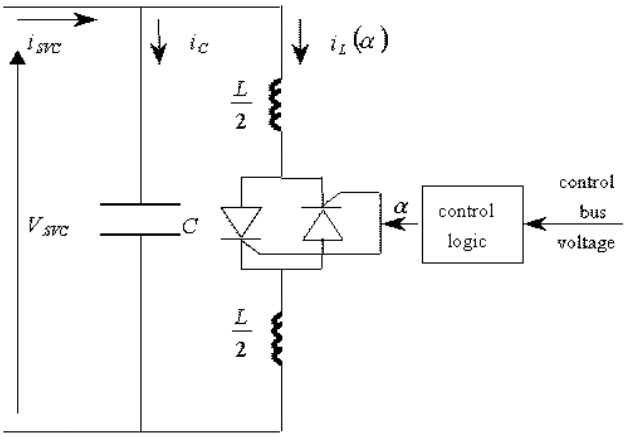

Figure 6.74: Diagram Structure of FC/TCR type of SVC

The breaker connecting SVC closes when the original 39-bus system works at steady state. After some seconds, the whole system reaches to a new steady state operating point, then a single-phase-grounded fault occurs at 0.2 seconds and clears at 0.22 seconds. When the fault occurs, two valves in one branch of TCRs block permanently. Figures 6.75-6.82 show eight generators' visually compared swing curves from the hybrid simulation and DCG/EMTP benchmarks. Among DCG benchmarks, two cases, including SVC working normally and abnormally, are simulated. Thus the effect of valves' blocking can be clearly observed. Traditional TS simulators do not have appropriate modeling techniques to represent the blocking so that there are no swing curves from TS simulators presented.

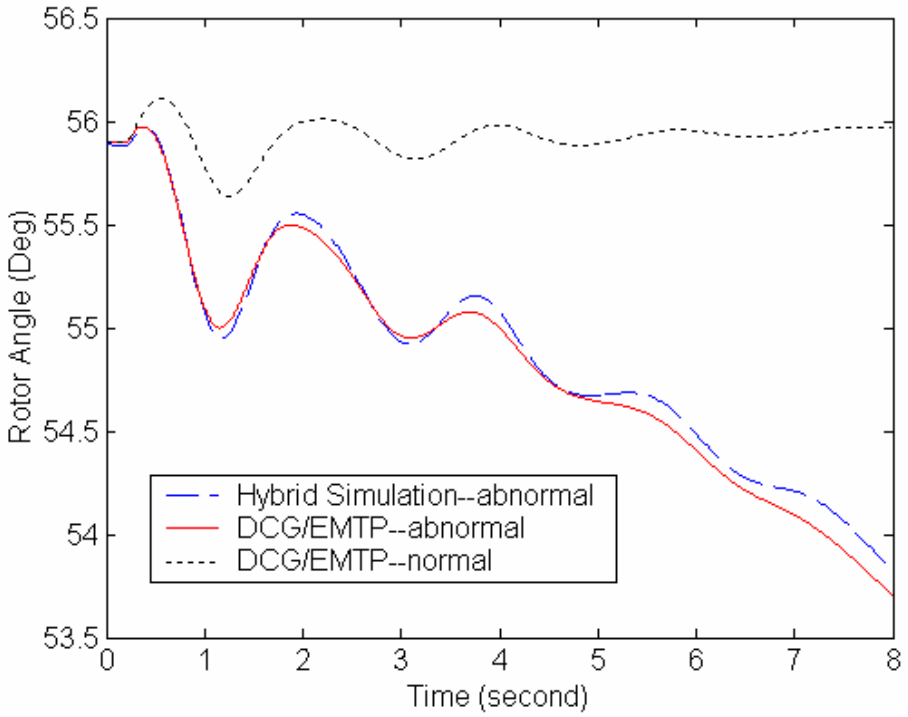

Figure 6.75: Generator 2 Swing Curves

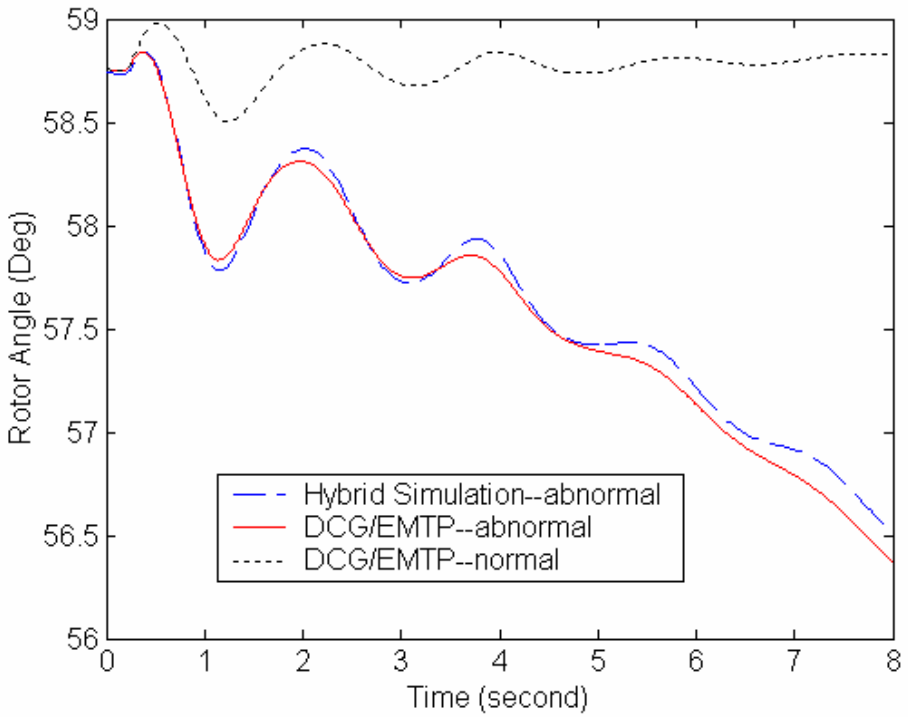

Figure 6.76: Generator 3 Swing Curves

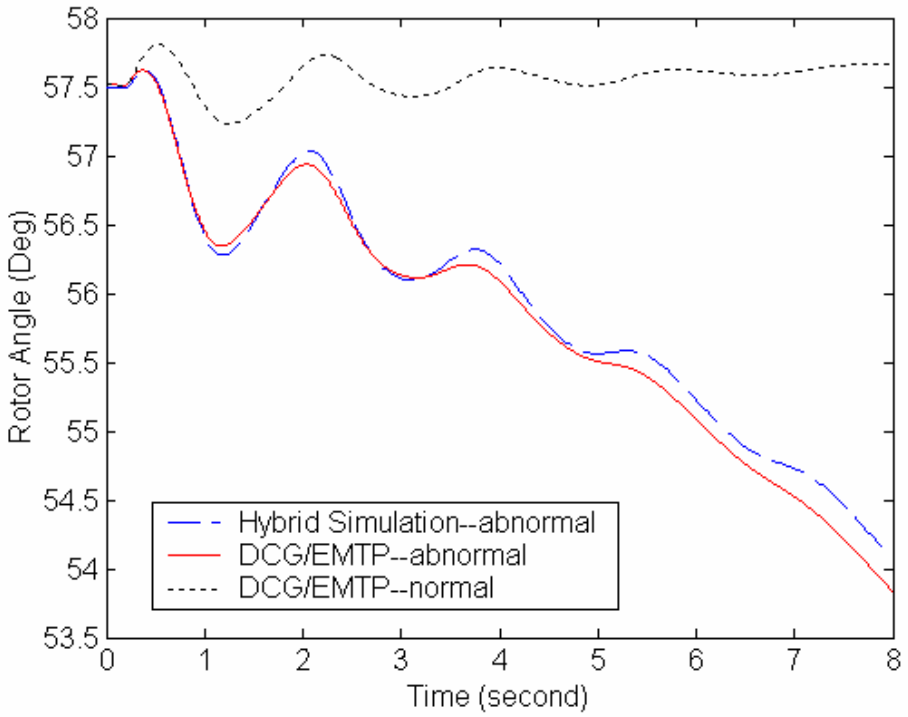

Figure 6.77: Generator 4 Swing Curves

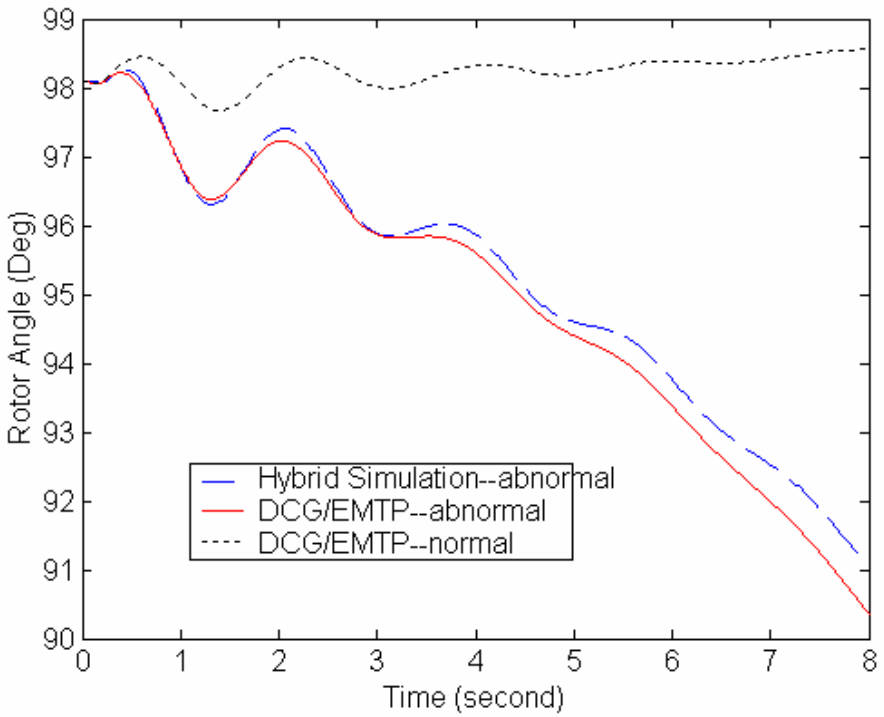

Figure 6.78: Generator 5 Swing Curves

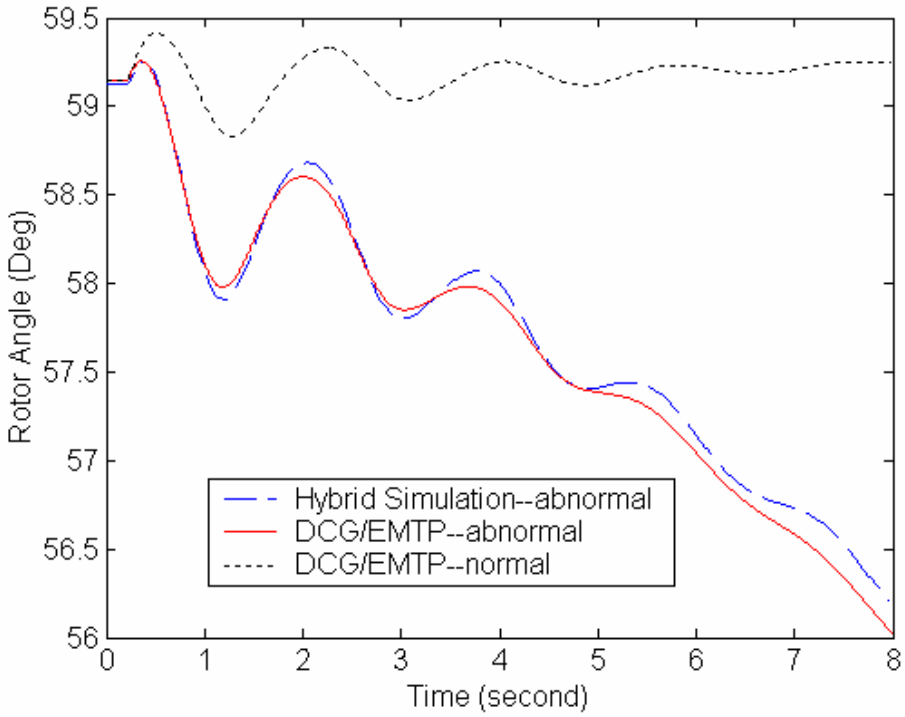

Figure 6.79: Generator 6 Swing Curves

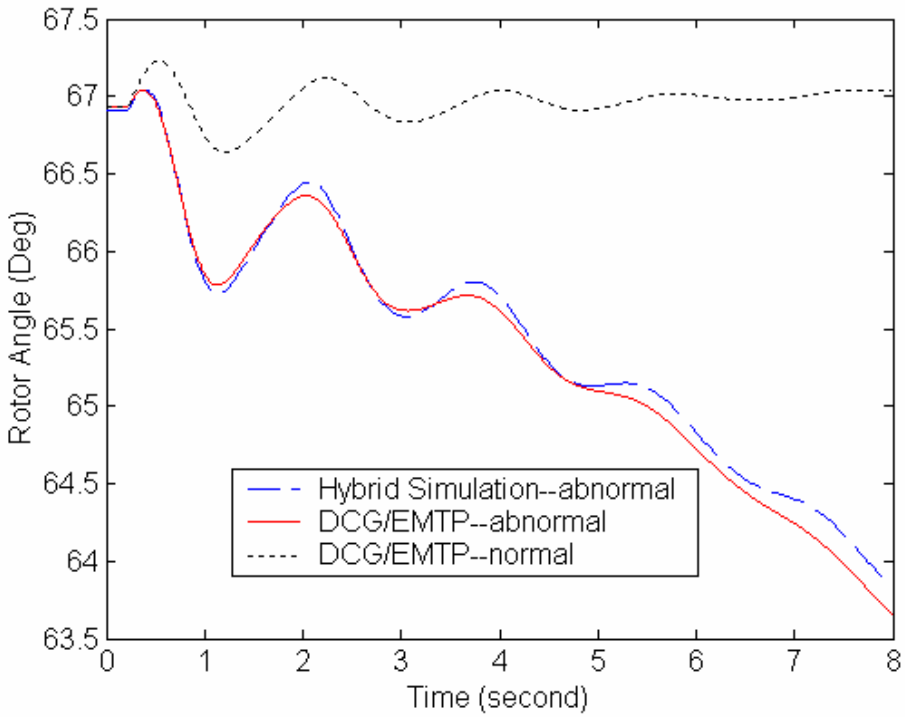

Figure 6.80: Generator 7 Swing Curves

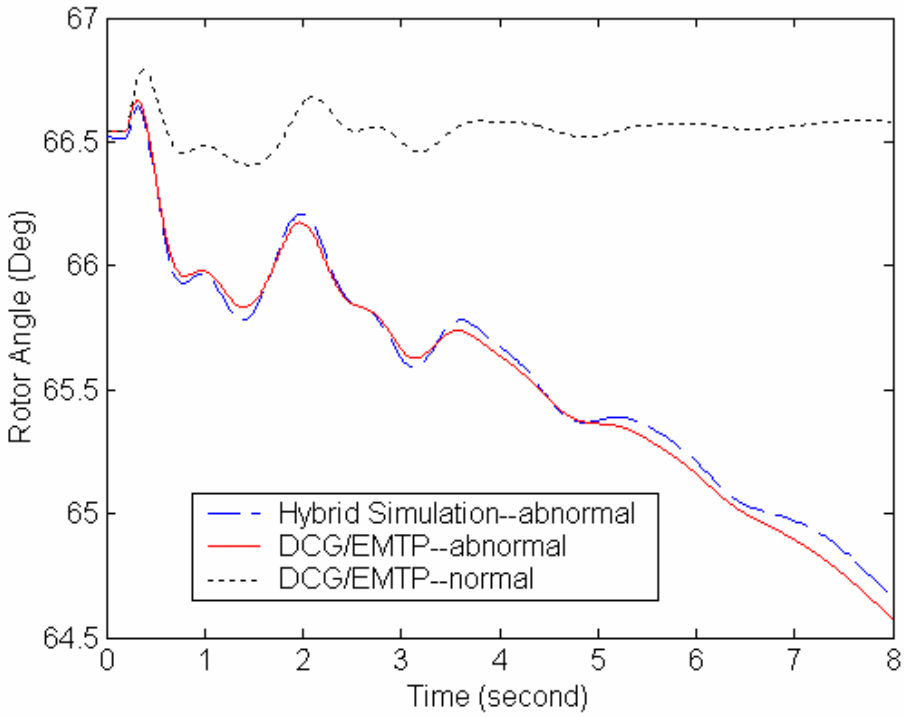

Figure 6.81: Generator 8 Swing Curves

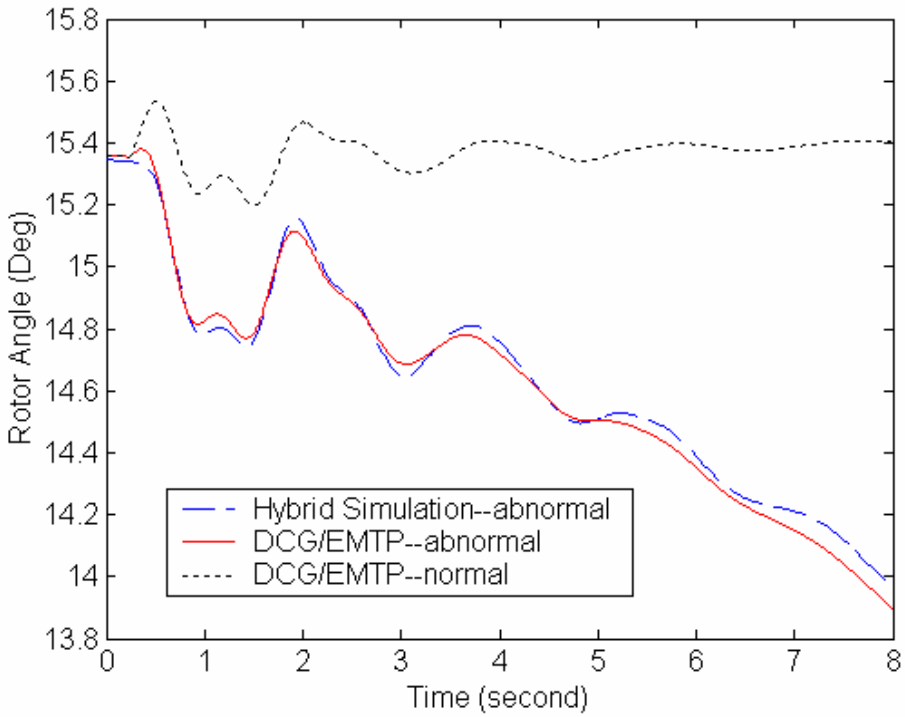

Figure 6.82: Generator 10 Swing Curves

From the figures, it can be concluded that the hybrid simulation can predict the system transient stability correctly for the disturbances that conventional transient stability simulators cannot handle. Conventional transient stability simulators have limitations to simulate the above case. No modeling can effectively reflect mal-function of power electronic in transient stability programs; however, the hybrid simulation can deal with any kind of disturbance.

This ability is important for modern large-size power systems characterized by applications of FACTS devices and HVDC links. Electromagnetic transient simulators are not practical study tools for modern power system because of their high computation resource demands. Conventional transient stability simulators have limitation in modeling. The hybrid simulation provides a practical solution to this problem.

VI.6 CONCLUSION

This chapter presents a number of case studies to support the analyses made in Chapter 4, and to demonstrate that the hybrid simulation can provide results covering transients from components' broadband three-phase waveforms to system swing curves. The hybrid simulator performance was evaluated from both electromagnetic transients and transient stability points of view.

In the hybrid simulation developed in this thesis, a conventional TS simulator was used, in-house developed by the author, and verified by examples shown in section 2. Additionally, some visual comparisons between EMT and TS simulators were made. There are some minor differences between them, caused by the simplifications in machine modeling made in the TS simulator. Notwithstanding, both kinds of simulators can correctly predict system transient stability.

A hybrid simulator was implemented on a digital electromagnetic transients simulator, known as HYPERSIM using the User Code Block (UCB) facility. The interface itself is implemented as a UCB which is in turn interfaced with the TS

simulator. HYPERSIM simulates the detailed system, while the embedded TS simulator takes charge of the external system.

The evaluation was performed from two aspects, i.e. from both EMT and TS points of view. The electromagnetic transients assessment was made on 9-bus system. The emphasis was placed on the waveforms immediately after disturbances and clearing of disturbances. From the figures it can be concluded that the use of frequency dependent equivalents can ensure the correctness of waveforms from the EMT simulator.

The transient stability assessment was made on 9-bus system and 39-bus system. The disturbances applied on 9-bus system caused the system to be unstable, while the 39-bus system remained stable for the applied faults. In both cases the hybrid simulator can correctly predict the swing curves.

Finally, a number of mal-function disturbances of power electronics were studied. For the disturbances, conventional transient stability simulators cannot provide effective modeling. Hybrid simulation provides a practical solution to the disturbances for modern large-size power system.

From all the case studies presented, it can be concluded that the hybrid simulator can indeed provide correct results over a broad range of frequencies.

Chapter VII PARALLEL HYBRID SIMULATION

VII.1 INTRODUCTION

For the hybrid simulator to run in real time the EMT simulator must run uninterruptedly while the TS simulator runs in parallel and updates the Norton equivalent periodically. This means that the hybrid simulator must use a parallel implementation of interaction protocol. In Chapters 5 and 6 the feasibility of hybrid simulation based on serial implementation of interaction protocol was demonstrated. To the best knowledge, all the achievements in hybrid simulation published so far are based on the serial implementation. The feature of the serial implementation is, in short words, that when one simulator runs the other is idle. In this chapter a new parallel implementation of interaction protocol which makes real-time hybrid simulation feasible is presented. In parallel mode, the EMT simulator runs continually.

The difficulty faced by the parallel implementation is that the accurate variables needed by the TS simulator are available only when the EMT simulator finishes its computation between two successive interchanging. By building a prediction scheme into the TS simulator, a successful parallel implementation developed. Some case studies are shown to demonstrate the feasibility and efficiency of the method.

VII.2 PARALLEL IMPLEMENTATION OF INTERFACE PROTOCOL

Under the serial implementation, when the EMT simulator is running, the TS simulator is idle, and vice versa. Under the parallel implementation, the EMT simulator must run continuously. At each interchanging the TS simulator updates the current source in the Norton equivalent.

Refering to Figure 7.1(a), the total simulation time from T0 to T1 (the same from T1 to T2, and so on) is the addition of the EMT simulation time and the TS simulation time, as shown in Figure 7.1(b). The EMT simulator starts to run first; after it finishes its computation for one period, the appropriate variables are transferred to the TS simulator which then begins to execute; the final step is to update the current source in the Norton equivalent. The sequence of executions fits the requirements of both simulators in off-line mode.

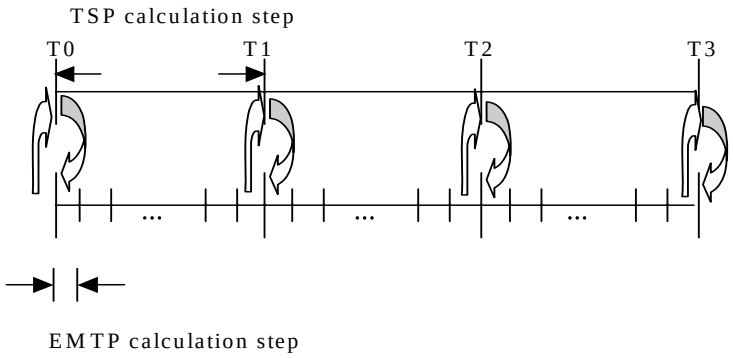

(a) Hybrid Simulation

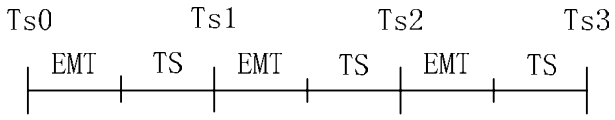

(b) Simulation Time in Serial Implementation

(c) Simulation Time in Parallel Implementation

Figure 7.1: Simulation Time of Hybrid Simulation for Different Implementations

Under the parallel implementation, the total simulation time from T0 to T1 (and so on) is the EMT simulation, as shown in Figure 7.1(c), because the TS simulator runs in parallel with the EMT simulator. The implementation can be outlined as follows, referring to Figure 7.2:

Suppose the hybrid simulator has finished its computation from T0 to T1.

(i) The equivalents of the external system are obtained from the TS simulator at T1 and are transferred to the EMT simulator.

(ii) Using the equivalent obtained at T1 from the TS simulator, the EMT simulator is executed from T1 to T2, meanwhile the TS simulator run from T1 to T2 in some way.

(iii) Before the EMT simulator reaches T2, the TS simulator finishes its computation and updates the current source in Norton equivalent.

(iv) The above procedure is repeated.

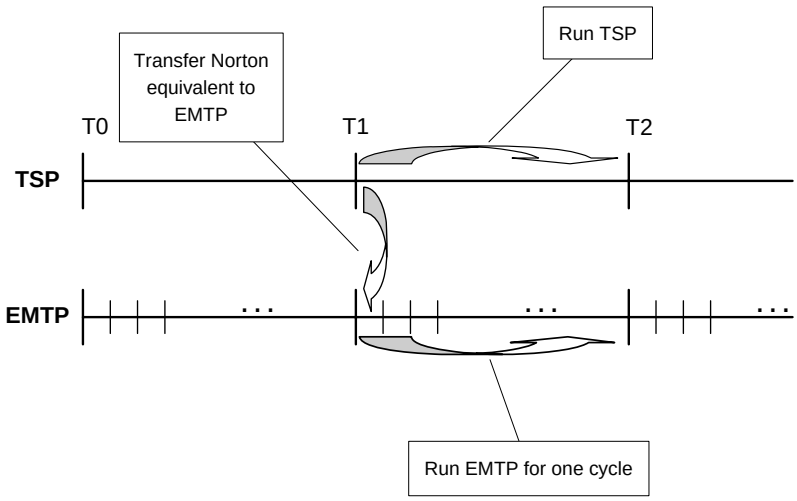

Figure 7.2: Parallel Implementation of Interaction Protocol

As shown in Figure 7.2, while the EMT simulator is running, the TS simulator runs as well. Here raises the difficulty faced by the implementation, i.e. the TS simulator cannot run without the variables transferred from the EMT simulator. However, the accurate variables are available only when the EMT simulator finishes its computation. Thus the time left for the TS simulator from the beginning of computation to the update of the current source is zero, because the EMT simulator needs to continue its computation uninterruptedly.

The solution to the problem is to build a prediction scheme in the TS simulator. The success of the solution has a very close relation with the extraction quality issue discussed in Chapter 5.

VII.3 PREDICTION SCHEME IN TRANSIENT STABILITY SIMULATORS

TS and EMT simulators are both based on step-by-step time-domain solutions, but they use rather different solution algorithms. Owing to the large time step inherent with TS simulators, their solution algorithm relies on an iterative approach, whereby the bus voltages are predicted, and injection currents from the machines are calculated, the bus voltages are correspondingly calculated and compared with the predicted values, and the process is repeated to convergence. With the EMT solution algorithm, on the other hand, the time step is usually small enough such that a linear approximation of the bus voltages is sufficient and iteration is not required.

Therefore, the ideal process of both simulators under the parallel implementation can be illustrated by Figure 7.3.

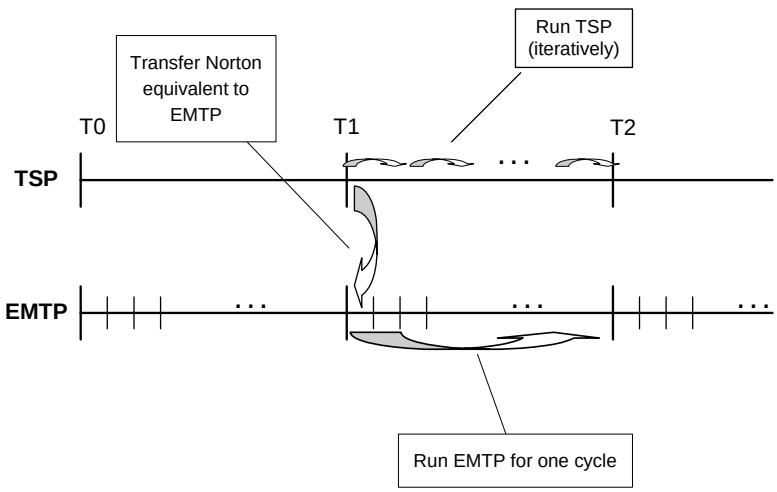

Figure 7.3: Ideal Process Under Parallel Implementation

At the completion of the first iteration of the TS simulator, the EMT has finished some steps, and some data samples are available. The available data can be used to predict the actual values of variables which are available only when the EMT

simulator completes its computation for one period. Thus the second iteration can use the predicted variables to do the calculation. As more iterations complete, more data become available and can be used for the prediction. This can be illustrated by Figure 7.4(a).

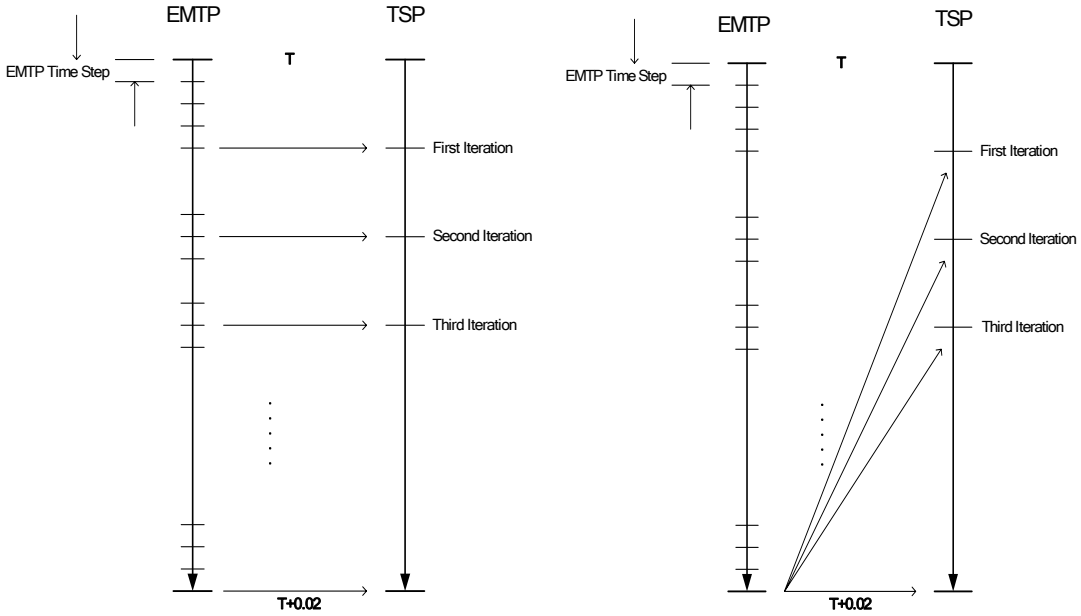

(a) Parallel Implementation (b) Serial Implementation

Figure 7.4: Diagram for Different Implementation

For convenience, serial implementation was sketched in Figure 7.4(b). We can see that in serial implementation each iteration uses variables extracted from a complete set of data, while in parallel implementation most iterations use part of the data. Thus, the prediction is the key factor for the parallel implementation. If the prediction can be made with reasonable accuracy, the parallel implementation can generate the same results as the serial implementation.

The variables transferred from the EMT simulator to the TS simulator are based on the extraction from the interface bus voltages. The method to check whether the extraction is creditable is the convergence of the extraction. The typical extraction curve has been shown in Chapter 5. For the convenience of the following discussion, the curve is shown in Figure 7.5 again.

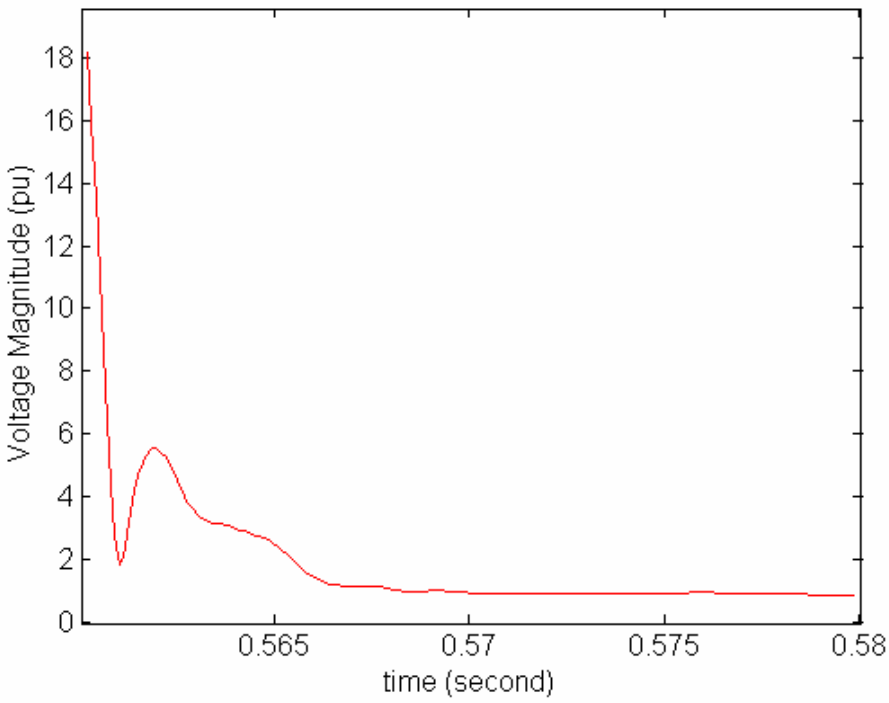

Figure 7.5: Typical Extraction Curve

For parallel implementation, if the extraction curve converges very quickly, that means more iterations of the TS simulator use accurate predicted variables, and the results are more accurate. Fortunately, commonly used extraction method, such as curve-fitting method, can effectively extract variables from distorted waveforms, as shown in Figure 7.5. Thus the parallel implementation of interaction protocol based on the prediction scheme can provide the accuracy very similar to those produced by serial implementation.

For practical implementation, one issue that has to be addressed is how to initialize the process, since there is no history data available for the first prediction. Consequently in actual implementation the first iteration is postponed for a short delay corresponding to the beginning of the interaction interval while the EMT simulator produces some data. Another issue is that towards the end of the interaction interval, there should be some time left for the TS simulator to update the current sources in the Norton equivalent in preparation for the coming interchange. The actual implementation of the parallel protocol is as illustrated in Figure 7.6.

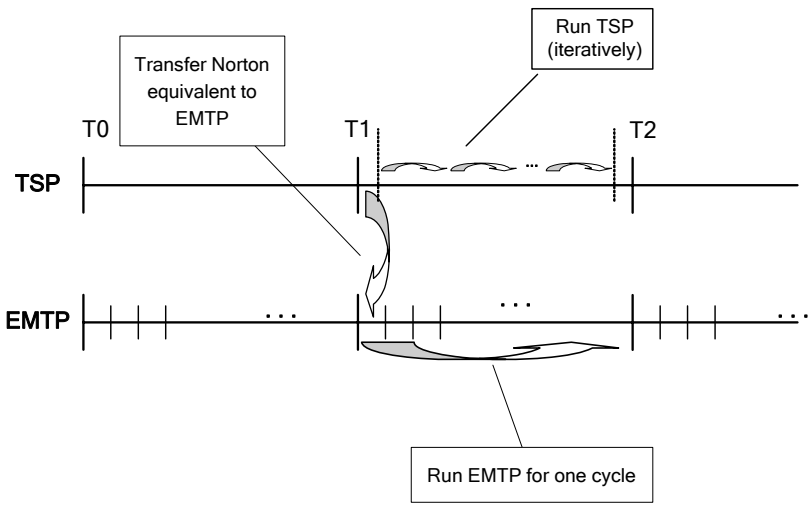

Figure 7.6: Actual Process Under Parallel Implementation

VII.4 PERFORMANCE STUDY

In this section, a detailed performance study of the parallel protocol is presented. Based on the proposed parallel implementation scheme, a parallel hybrid simulator prototype was built to run on a dual Xeon 2.4GHz parallel computer running RedHat 7.3 with Kernel 2.4.20 and RTAI 24.1.11 real-time extension. Multi-threaded technique was used for the implementation of the parallel interaction protocol. A master thread is created to coordinate the EMT and TS simulation threads and each simulation thread runs on a dedicated processor. For simplicity, a fixed number of EMT time steps is used to represent the short period needed in the beginning and end of the each TS time step, as illustrated in Figure 7.6. For the current implementation, the number of time steps is set to 20. Thus the TS simulator starts its iteration in each time step after the EMT simulator has completed its first 20 time steps, and it ends the iteration when the EMT simulator still has 20 time steps to go before the end of each period. When the TS simulator finishes one iteration, it fetches the updated variables from the EMT simulator from the remote processor. The number of iterations performed depends on the calculation speed of the processor, and will vary depending on the computing platform. As an alternative platform, the parallel hybrid simulation was also tested on an SGI Origin 2100 8-

processor computer with IRIX64. Table 7.1 shows the performance of the parallel hybrid simulator running on the Linux and IRIX64 platforms.

OS Platform	Processor Type	The number of iterations (communication) performed
IRIX 6.5	MIPS R12000 350MHz	10
Red Hat Linux 7.3	Intel Xeon 2.6GHz	17

Table 7.1: Parallel Hybrid Simulation Performance in Linux and IRIX64 Platform

The case study was performed on 39-bus system, as shown in Appendix A2. Bus 36 was chosen as the interface bus, and the detailed system includes the part of network between bus 36 and bus 9. Generator 9 is replaced by a voltage source, and the external system is represented by a frequency dependent equivalent in the EMT simulator. The detailed system is viewed as a variable load based on positive-sequence fundamental component interface voltage. The EMT simulator uses 50 microseconds as integration time step, while in the TS simulator is 20 milliseconds.

Figure 7.7-7.17 show the results for the three-phase solid fault applied at bus 38 from 0.2 to 0.24 second. For the validation of the accuracy of the parallel implementation, the results are compared with corresponding results of serial (non-real-time) implementation. In addition a benchmark case was used to validate the hybrid simulation, in which the network as a whole was modeled in DCG/EMTP.

Since the hybrid simulator includes two distinct types of simulator, it should be able to correctly simulate both electromagnetic and electromechanical transients.

Figure 7.7-7.14 show the rotor speed curves of generator 2, 4, 5, 8 and 10, respectively. Clearly, curves produced by the parallel implementation compare very well with those from the series implementation, and they both match the benchmark case well. This shows that the proposed parallel protocol based simulation results compare well with those of the conventional serial approach.

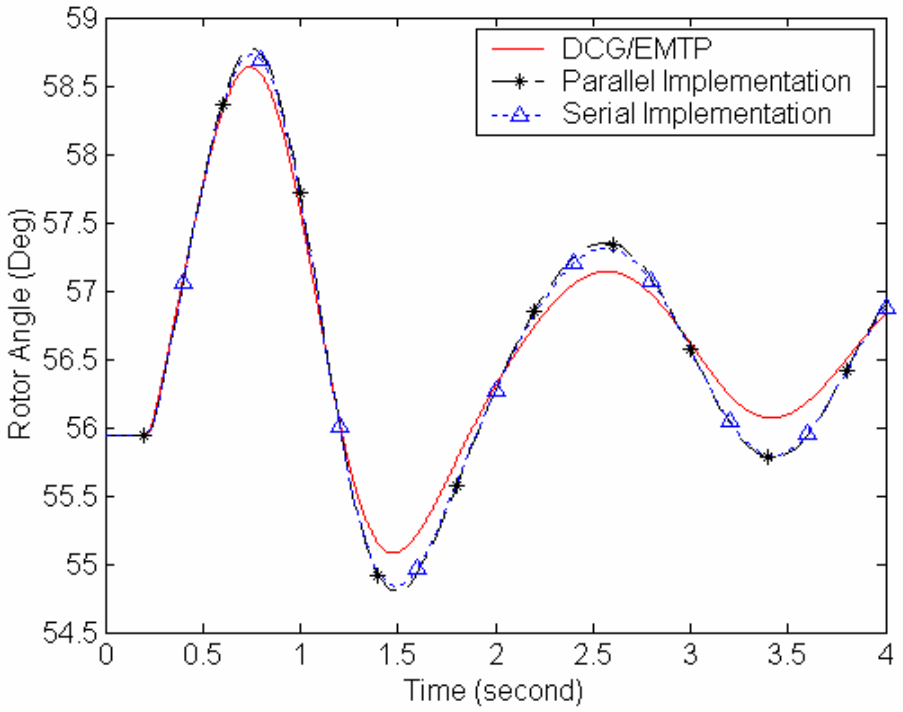

Figure 7.7: Generator 2 Swing Curves

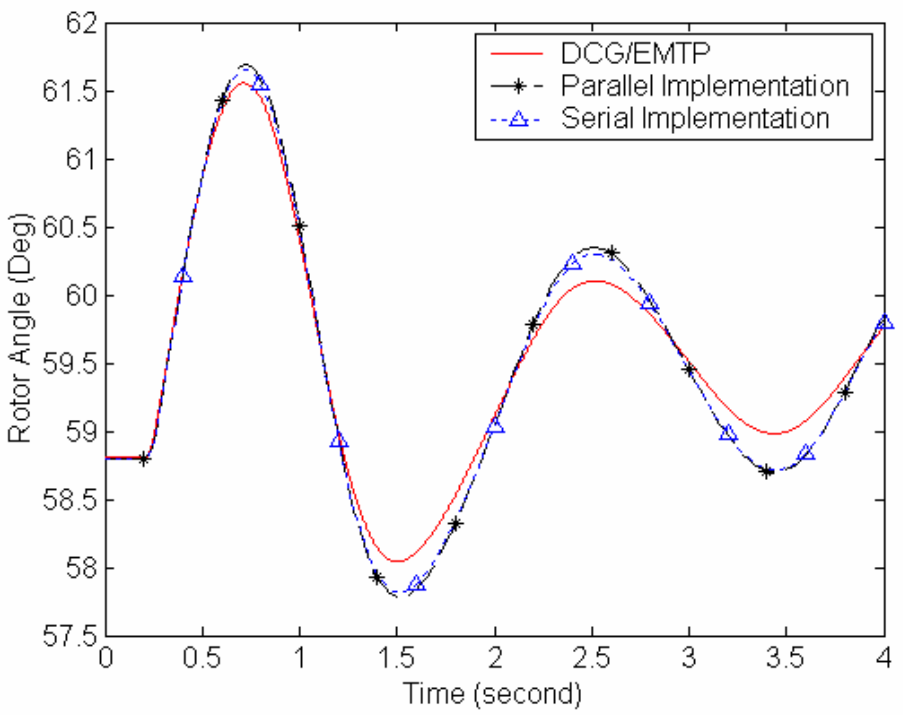

Figure 7.8: Generator 3 Swing Curves

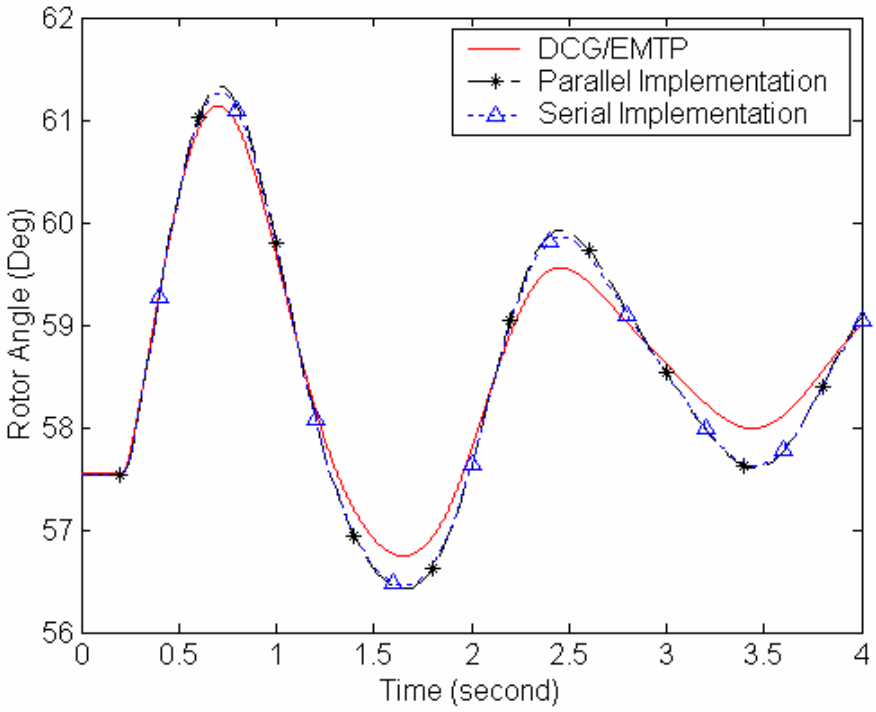

Figure 7.9: Generator 4 Swing Curves

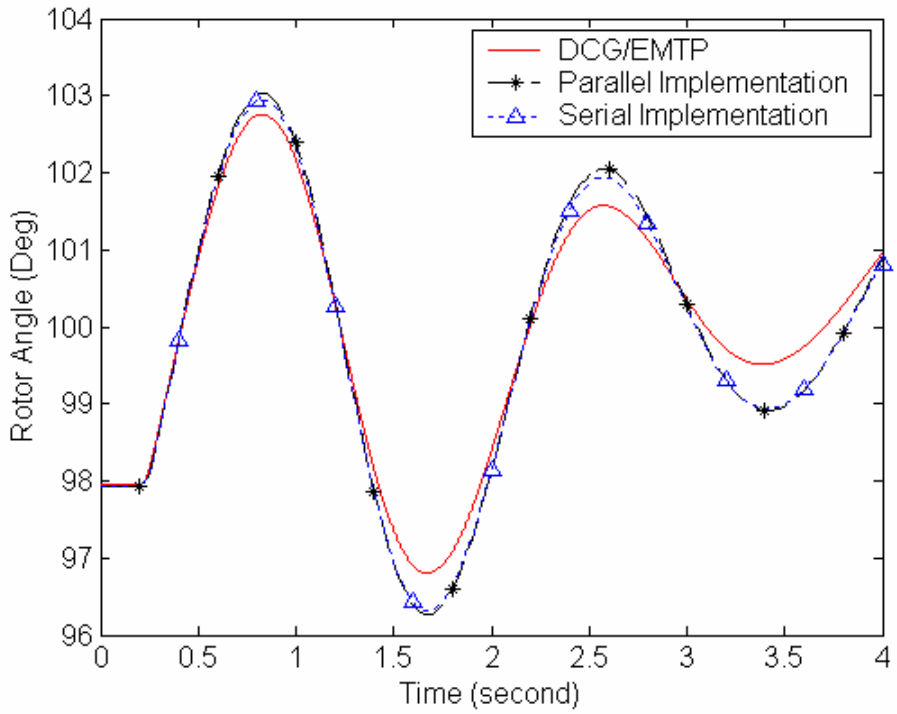

Figure 7.10: Generator 5 Swing Curves

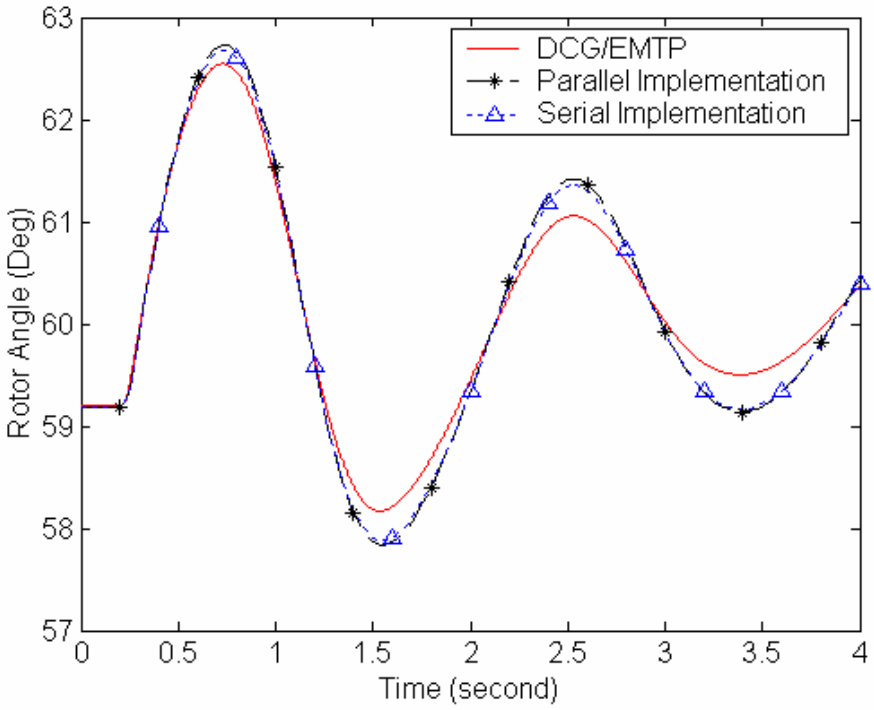

Figure 7.11: Generator 6 Swing Curves

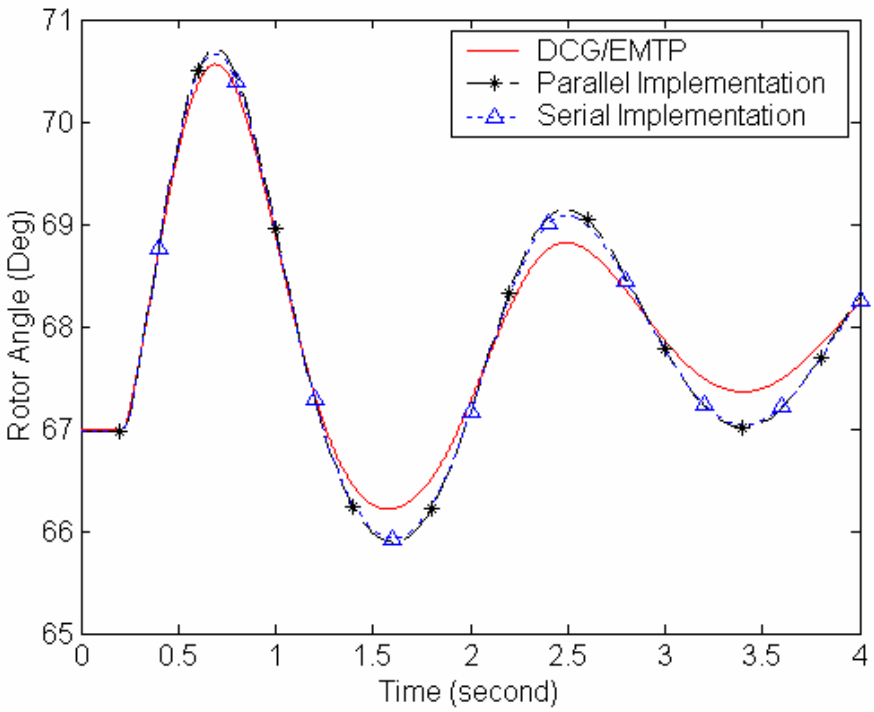

Figure 7.12: Generator 7 Swing Curves

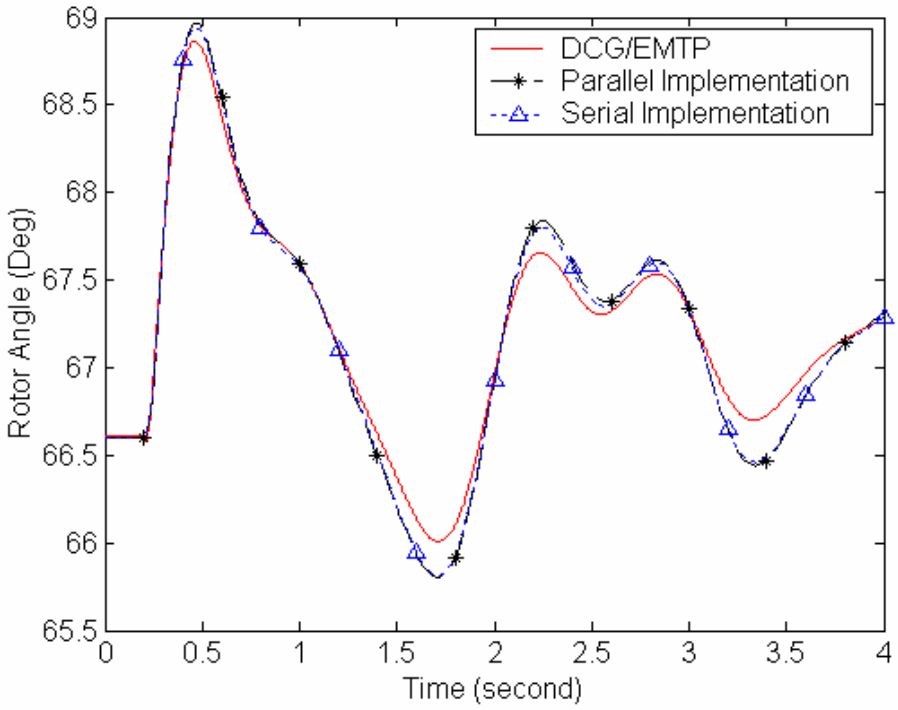

Figure 7.13: Generator 8 Swing Curves

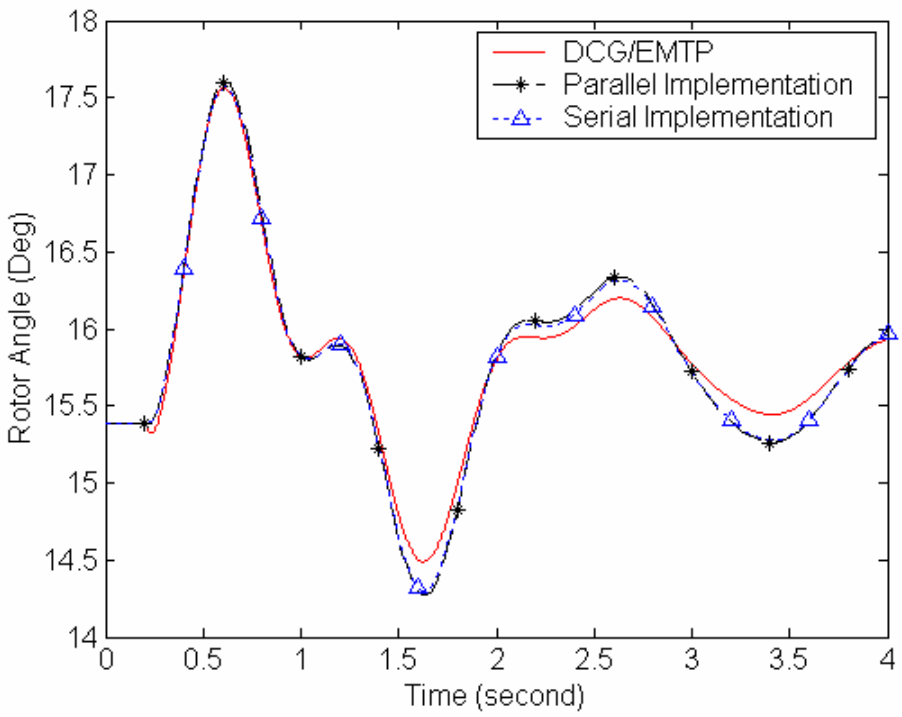

Figure 7.14: Generator 10 Swing Curves

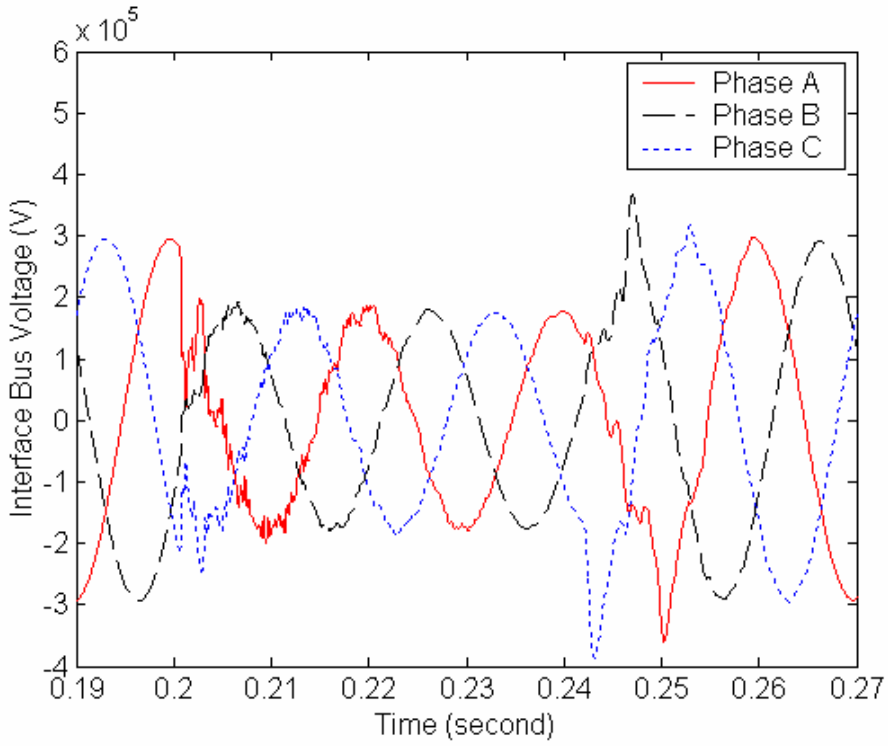

Figure 7.15: Interface Bus voltage from Benchmark

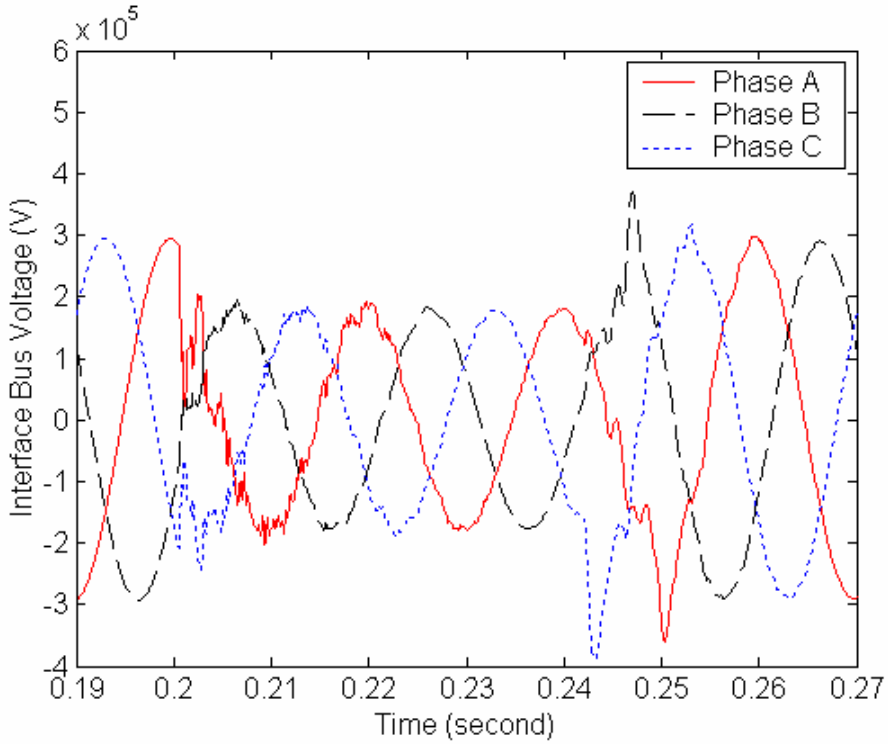

Figure 7.16: Interface Bus voltage from Serial Implementation

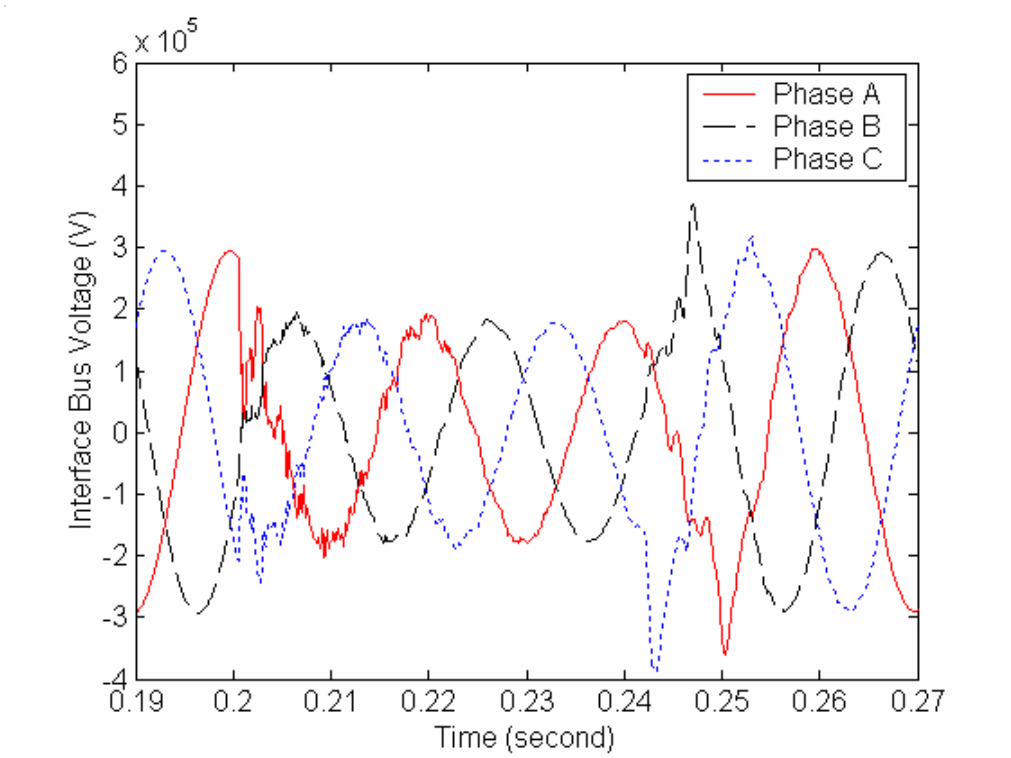

Figure 7.17: Interface Bus voltage from Parallel Implementation

Figure 7.15-7.17 show interface bus phase a, b and c voltage waveforms. The use of a frequency dependent equivalent leads to very good results, matching the benchmark case solutions very closely. This demonstrates that the hybrid simulation can produce solutions compatible with full EMTP simulation, but with much lower computational effort.

A preliminary implementation of the parallel hybrid simulation has also been carried out using a fully digital real-time electromagnetic transients simulator called HYPERSIM. Both the TS simulator and the parallel interface protocol were implemented as a User Code Block (UCB) of HYPERSIM. With the task mapping facility, the detailed EMT network will be automatically partitioned in subsystems for parallel distribution over a farm of processing units. For the current implementation, UCB is considered as a subsystem as well and will be distributed to a separate processing unit for parallel execution. Figure 7.18 shows the parallel execution of the HYPERSIM based hybrid simulation with time step of 120ms.

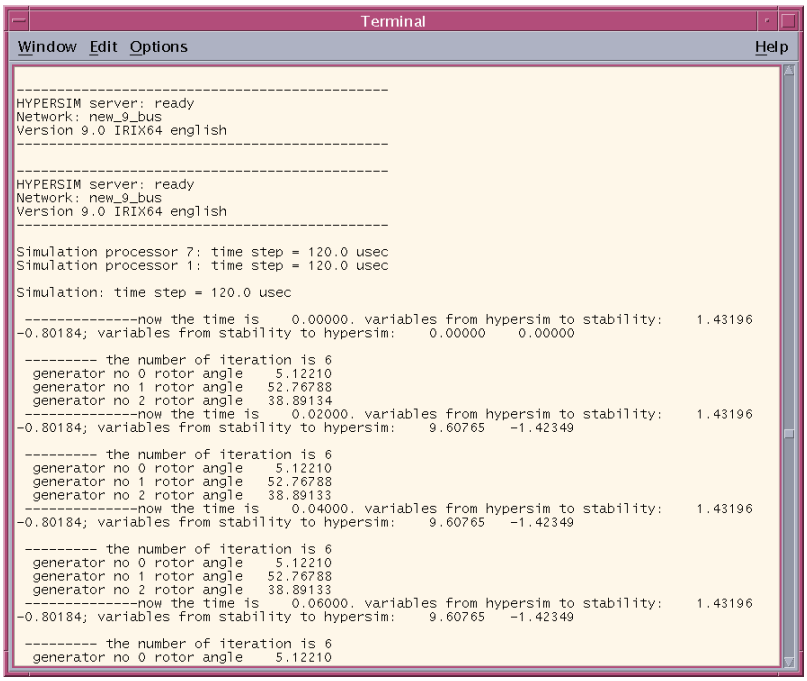

```
Terminal
Window  Edit  Options                                                    Help

-----------------------------------------------
HYPERSIM server: ready
Network: new_9_bus
Version 9.0 IRIX64 english
-----------------------------------------------

-----------------------------------------------
HYPERSIM server: ready
Network: new_9_bus
Version 9.0 IRIX64 english
-----------------------------------------------

Simulation processor 7: time step = 120.0 usec
Simulation processor 1: time step = 120.0 usec

Simulation: time step = 120.0 usec

 --------------now the time is    0.00000. variables from hypersim to stability:    1.43196
-0.80184; variables from stability to hypersim:    0.00000    0.00000

 --------- the number of iteration is 6
  generator no 0 rotor angle    5.12210
  generator no 1 rotor angle   52.76788
  generator no 2 rotor angle   38.89134
 --------------now the time is    0.02000. variables from hypersim to stability:    1.43196
-0.80184; variables from stability to hypersim:    9.60765   -1.42349

 --------- the number of iteration is 6
  generator no 0 rotor angle    5.12210
  generator no 1 rotor angle   52.76788
  generator no 2 rotor angle   38.89133
 --------------now the time is    0.04000. variables from hypersim to stability:    1.43196
-0.80184; variables from stability to hypersim:    9.60765   -1.42349

 --------- the number of iteration is 6
  generator no 0 rotor angle    5.12210
  generator no 1 rotor angle   52.76788
  generator no 2 rotor angle   38.89133
 --------------now the time is    0.06000. variables from hypersim to stability:    1.43196
-0.80184; variables from stability to hypersim:    9.60765   -1.42349

 --------- the number of iteration is 6
  generator no 0 rotor angle    5.12210
```

Figure 7.18: Preliminary Real-Time Test Results

VII.5 CONCLUSION

The promise of hybrid simulation is the ability to simulate very large-size networks with TS-like speed, while delivering EMT-like accuracy on key components. The approach is to partition the whole network into two parts, one for TS simulator and one for EMT simulator. An interaction protocol coordinates two communications between the two simulators. While much work has been reported on the development of hybrid simulation based on serial implementation of protocol, these hybrid simulators cannot function in real time.

This chapter proposes a parallel implementation for interaction protocol which allows real-time solution. The protocol relies on a prediction scheme to allow the EMT simulator to run continually, which is a basic requirement of real-time operation. A real-time hybrid simulator running on both dual-Xeon Linux and SGI Origin 2100 system has been built to demonstrate the real-time operation of the proposed parallel interaction protocol. Case studies showed very good comparison between the parallel and series protocols, as well as with an EMTP benchmark.

Chapter VIII CONCLUSIONS

In this research the issues and difficulties related to the interface of two very different programs were studied and overcome. EMT simulators are normally aimed at detailed studies of relatively small networks: they can accurately model power system components (including nonlinearities) such as power electronic systems and their associated control systems at the device level; however, the mandatory small time step results in a computationally intensive simulator, impracticable for the simulation of very large systems. On the other hand, TS simulators are aimed at solving the electromechanical equations of very large systems, where precision related to the wave shape of the voltage and current waveforms is not an issue. TS programs use relatively large time steps, and are computationally very efficient. However the large time steps do not allow modelling of power electronic systems at the device level: FACTS equipment and HVDC converters have to be represented as relatively simple mathematical models. Consequently it is not practicable to study such contingencies as unbalanced and/or mal-operation of power electronic equipment in a TS program.

Hybrid simulation, which includes both EMT and TS simulators within an integrated analysis tool, is a significant step towards the realization of a powerful digital power system simulator, capable of efficient simulation of large size networks, while providing accurate representation of highly nonlinear components, such as FACTS devices and HVDC links. In this research a functional hybrid simulator was developed based on a novel interface between an EMT simulator and a comprehensive TS simulator. Real-time operation was realized using an original predictive parallel interaction protocol.

The EMT and TS simulators each take responsibility for one part of power systems, called the detailed system and the external system respectively. In the EMT simulator the external network is represented as a Norton equivalent, including a

dynamically controlled current source and a frequency dependent equivalent derived using the Prony method, and initialized before the simulation. The impedance parameters do not change during the simulation while the controlled current source is updated at each interchange. However, simple update of the current source at regular interval would cause phase discontinuity and hence waveform distortion and unbalancing. Instead, the interchange intervals should be adjusted dynamically to eliminate any phase discontinuity.

In the TS simulator, an equivalent must be presented to represent the effect of the detailed system on system stability. For the best representation of the detailed system, the equivalent needs to be extracted from boundary voltage and current waveforms, and the equivalent must be based on power frequency because the TS simulator only takes power frequency components into account. For any kind of disturbance occurring in the detailed system, the TS simulator only uses positive-sequence fundamental frequency components.

Generally, the equivalent of the detailed system needs both interfacing bus voltages and injection current from the detailed system in phasor form. Because of the presence of dc-offset in the current waveforms during transients, conventional methods, such as curve-fitting, cannot give credible extraction results. An alternative approach to derive the value of current was developed. The value can be calculated based on the interfacing bus voltage and power frequency impedance of the frequency dependent equivalent.

The communication between the detailed and external systems is maintained through a well-defined common interfacing location. It was shown that the variables transferred from the TS to EMT do not heavily dependent on the interface location. The equivalent of the detailed system is extracted from the waveforms at the interfacing location. If the waveforms are excessively distorted, the extraction may fail. For such case, the interfacing location must be extended to alleviate the distortion.

Both the EMT and TS simulators proceed in parallel and communicate with each other at specified time intervals and in specified order. Since the two simulators have differences in integration time step and component modelling techniques, an interaction protocol is needed in order to coordinate the variables transferred between the two simulators. For convenience, the integration step of the TS simulator is a multiple of the time step used in the EMT and variables interchange takes place only at common periodic time points.

Two protocol implementations have been developed in this work, namely serial and parallel. In the serial mode, when one simulator is running, the other is idle. This makes it impossible for any real-time applications since the total computation time for the hybrid simulation would equal to the sum of both the EMT and TS simulators computation time. In the parallel mode which allows for real-time operations, the two simulators run in parallel: the TS simulator updates variables when the EMT simulator is running. The problem of obtaining accurate extraction results owing to the incomplete set of data from the running EMT simulator was overcome through the use of a prediction scheme incorporated in the TS simulator.

Several case studies based on a 39 bus system were presented which verified the theoretical analysis related to hybrid simulation. Performance studies of the hybrid simulation were made based on serial implementation and visual comparisons were made between the hybrid simulation and DCG/EMTP, which was taken as benchmark. Comparison results show that the hybrid simulation can generate fully creditable results for both device-level waveforms and system swing curves.

Based on parallel implementation of protocol, a parallel hybrid simulation was built to run and test on two different multi-processor computer platforms, namely a dual-Xeon Linux workstation and a Silicon Graphics (SGI) multi-processor server. System swing curves were visually compared between the parallel implementation, the serial implementation and the benchmark. Comparison results showed that the parallel implementation can totally ensure the correctness of simulation results.

REFERENCE

1. Hermann W. Dommel, *Digital Computer Solution of Electromagnetic Transients in Single- and Multiphase Networks*, IEEE on Pas, Vol. PAS-88, No. 4, April 1969, pp 388-397

2. Hermann W. Dommel, *Electromagnetic Transient Programs (EMTP) Theory Book*, Bonneville Power Administration, 1987

3. R.H. Park, *Two-Reaction Theory of Synchronous Machines – Generalized Method of Analysis – Part I,* AIEE Trans., Vol. 48, pp. 716-727, 1929; *Part II,* Vol. 52, pp. 352-355, 1933

4. IEEE Working Group Report, *Recommended Phasor Diagram for Synchronous Machines*, IEEE Trans on PAS, Vol PAS-88, No 11, Nov 1969, pp 1593-1969

5. P. M. Anderson, B. L. Agrawal, and J. E. Van Ness, S*ubsynchronous Resonance in Power Systems,* IEEE Press 1990

6. IEEE Subsynchronous Resonance Task Force of the Dynamic System Performance Working Group Power System Engineering Committee, *First Benchmark Model for Computer Simulation of Subsynchronous Resonance,* IEEE Trans on PAS, Vol. PAS-96, No. 5, Sep/Oct 1977, pp 1565-1572

7. IEEE Committee Report, *First Supplement to A Bibliography for the Study of Subsynchronous Resonance between Machines and Power Systems,* IEEE Trans on PAS, Vol. PAS-98, No. 6, Nov/Dec 1979, pp 1872-1875

8. IEEE Subsynchronous Resonance Task Force of the Dynamic System Performance Working Group Power System Engineering Committee, *Proposed Terms and Definition for Subsynchronous Oscillations,* IEEE Trans on PAS, Vol. PAS-99, No. 2, March/April 1980, pp 506-511

9. IEEE Subsynchronous Resonance Task Force of the Dynamic System Performance Working Group Power System Engineering Committee, *Second Benchmark Model for Computer Simulation of Subsynchronous Resonance,* IEEE Trans on PAS, Vol. PAS-104, No. 5, May 1985, pp 1057-1066

10. IEEE std 115-1983, *IEEE Guide: Test Procedures for Synchronous Machines*

11. IEEE std 115-1995, *IEEE Guide: Test Procedures for Synchronous Machines*

12. I. M. Canay, *Determination of Model Parameters of Synchronous Machines,* IEE Proc., Vlo. 130, Pt. B, No. 2, March 1983, pp 86-94

13. R. P. Schulz, W. D. Jones, D. N. Euart, *Dynamic Models of Turbine Generators Derived from Solid Rotor Equivalent Circuits,* IEEE Trans on PAS, Vol. PAS-92, May/June 1973, pp 926-933

14. IEEE std 115A-1987, *IEEE Standard Procedures for Obtaining Synchronous Machine Parameters by Standstill Frequency Response Testing*

15. G. Gross, M. C. Hall, *Synchronous Machine and Torsional Dynamics Simulation in the Computation of Electromagnetic Transients,* IEEE Trans on PAS, Vol. PAS-97, No. 4, July/Aug 1978, pp 1074-1086

16. Alan Budner, *Introduction of Frequency-Dependent Line Parameters into an Electromagnetic Transients Program,* IEEE Trans on PAS, Vol. PAS-89, No. 1, Jan 1970, pp 88-97

17. J. K. Snelson, *Propagation of Traveling Waves on Transmission Lines Frequency Dependent Parameters,* IEEE Trans on PAS, Vol. PAS-91, Fan/Feb 1972, pp 85-91

18. R. P. Wasley, S. Selvavinayagamoorthy, *Approximate Frequency-Response Values for Transmission-Line Transient Analysis,* Proc IEE, Vol. 121, No. 4, April 1974, pp 281-286

19. W. Scott Meyer, H. W. Dommel, *Numerical Modeling of Frequency-*

Dependent Transmission-Line Parameters in an Electromagnetic Transients Program, IEEE Trans on PAS, Vol. PAS-93, Sep/Oct 1974, pp 1401-1409

20. A. Semlyen, A. Dabuleanu, *Fast and Accurate Switching Transient Calculation on Transmission Lines with Ground Return Using Recursive Convolutions,* IEEE Trans on PAS, Vol. PAS-94, No. 2, March/April 1975, pp 561-571

21. A. Ametant, *A Highly Efficient Method for Calculating Transmission Line Transients,* IEEE Trans on PAS, Vol. PAS-95, No. 5, Sep/Oct 1976, pp 1545-1551

22. J. R. Marti, *Accurate Modeling of Frequency-Dependent Transmission Lines in Electromagnetic Transient Simulations,* IEEE Trans on PAS, Vol. PAS-101, No. 1, Jan 1982, pp 147-155

23. L. Marti, *Low-Order Approximation of Transmission Lines Parameters for Frequency-Dependent Models,* IEEE Trans on PAS, Vol. PAS-102, No. 11, Nov 1983, pp 3582-3589

24. A. M. Gole, V. K. Sood, *A Static Compensator Model for Use with Electromagnetic Transients Simulation Programs,* IEEE Trans on PD, Vol. 5, No. 3, July 1990, pp 1398-1407

25. J. M. Zavahir, J. Arrillaga, N. R. Watson, *Hybrid Electromagnetic Transient Simulation with the State Variable Representation of HVDC Converter Plant,* IEEE Trans on PD, Vol. 8, No. 3, July 1993, pp 1591-1597

26. Dragan Jovcic, Nalin Pahalawaththa, Mohamed Zavahir, *Analytical Modeling of HVDC-HVAC Systems,* IEEE Trans on PD, Vol. 14, No. 2, April 1999, pp 506-511

27. Fernando L. Alvarado, Robert H. Lasseter, Juan J. Sanchez, *Testing of Trapezoidal Integration with Damping for the Solution of Power Transient Problems,* IEEE Trans on PAS, Vol. PAS-102, No. 12, Dec 1983, pp 3783-

3790

28. J. R. Marti, Jiming Lin, *Suppression of Oscillation in the EMTP*, IEEE Trans on PS, Vol. 4, No. 2, May 1989, pp 739-747

29. Jiming Lin, J. R. Marti, *Implementation of the CDA Procedure in the EMTP*, IEEE Trans on PS, Vol. 5, No. 2, May 1990, pp 394-402

30. Neville R. Watson, Garth D. Irwin, *Electromagnetic Transient Simulation of Power System Using Root-Matching Techniques*, IEE, Proc-Gener, Transm. Distrib, Vol. 145, No. 5, Sep 1998, pp 481-486

31. Neville R. Watson, Garth D. Irwin, *Comparison of Root-Matching Techniques for Electromagnetic Transient Simulation*, IEEE Trans on PD, Vol. 15, No. 2, April 2000, pp 629-634

32. J. M. Smith, *Mathematical Modeling and Digital Simulation for Engineers and Scientists*, Wiley, New York, 1977

33. Van-Que Do, Alpha Oumar Barry, *A Real-Time Model of the Synchronous Machine Based on Digital Signal Processors*, IEEE Trans on Applied Superconductivity, Vol. 3, No. 1, March 1993, pp 60-66

34. Y. Maharsi, V. Q. Do, V. K. Sood, S. Casoria, J. Belanger, *HVDC Control System Based on Parallel Digital Signal Processors*, IEEE Trans on PS, Vol. 10, No. 2, May 1995, pp 995-1001

35. Harbans Nakra, R. Lewis Vaughan, Charles Gagnon, Andre Venne, *Real-Time Simulator for Power System Dynamics Studies*, IEEE Trans on PS, Vol. 10, No. 2, May 1995, pp 1063-1070

36. D. A. Woodford, A. M. Gole, R. W. Menzies, *Digital Simulation of DC Links and AC Machines*, IEEE Trans on PAS, Vol. PAS-102, No. 6, June 1983, pp 1616-1623

37. D. A. Woodford, T. Ino, M. Mathur, A. Gole, R. Wierckx, *Validation of*

Digital Simulation of HVDC Transients by Field Tests, IEE Conf. Publication on AC and DC Power Transmission, 1985, pp 377-381

38. R. Kuffel, J. Giesbrecht, T. Maguire, R. P. Wierckx, P. McLaren, *RTDS-A Fully Digital Power System Simulator Operating in Real Time,* IEEE Catalogue No. 95TH8130, pp498-503

39. Pierre Mercier, Charles Gagnon, Michel Tetreault, Michel Toupin, *Real-Time Digital Simulation of Power Systems at Hydro-Quebec,* ICDS'95, Texas, April 1995, pp 9-12

40. Norman Balabanian, Theodore A. Bickart, *Electrical Network Theory,* John Wiley & Sons, Inc, 1969

41. A.O. Barry, F. Guay, S. Guerette, P. Giroux, *Digital Real-Time Simulation for Distribution Systems,* Transmission and Distribution Construction, Operation and Live-Line Maintenance Proceedings. 2000 IEEE ESMO - 2000 IEEE 9th International Conference on , 8-12 Oct. 2000, pp. 252 - 258

42. Prabha Kundur, *Power System Stability and Control,* McGraw-Hill, 1994

43. Paul M. Anderson, A. A. Fouad, *Power System Control and Stability,* IEEE Press, 1994

44. Peter W. Sauer, M. A. Pai, *Power System Dynamics and Stability,* Prentice-Hall Inc, 1998

45. Hingorani, Narain G., *Understanding FACTS: concepts and technology of flexible AC transmission system* , New York : IEEE Press, c2000

46. R. Mohan Mathur, Rajiv K. Varma, *Thyristor-Based FACTS Controllers for Electrical Transmission Systems,* A John Wiley & Sons, Inc, IEEE Press 2002

47. Philip Moore, Peter Ashmole, *Tutorial: Flexible AC Transmission Systems,* Power Engineering Journal, Dec 1995, pp 282-286

48. Philip Moore, Peter Ashmole, *Tutorial: Flexible AC Transmission Systems*

Part 2 Methods of Transmission Line Compensation, Power Engineering Journal, Dec 1996, pp 273-278

49. Philip Moore, Peter Ashmole, *Tutorial: Flexible AC Transmission Systems Part 3 Conventional FACTS Controllers,* Power Engineering Journal, Aug 1997, pp 177-183

50. Philip Moore, Peter Ashmole, *Tutorial: Flexible AC Transmission Systems Part 4 Advanced FACTS Controllers,* Power Engineering Journal, April 1998, pp 95-100

51. J. Arrillaga, *High voltage direct current transmission,* London: Institution of Electrical Engineers, c1998

52. *FACTS Application,* technical report 96TP116-0, IEEE PES, 1996

53. Claudio A. Canizares, *Power Flow and Transient Stability Models of FACTS Controllers for Voltage and Angle Stability Studies,* PES Winter Meeting, Vol. 2, 23-27, Jan 2000, pp. 1447-1454

54. Edward Wilson Kimbark, *Power System Stability Volume III-Synchronous Machines,* John Wiley & Sons Inc, 1956

55. G. Shackshaft, *Effect of Oscillatory Torques on the Movement of Generator Rotors,* Proc. IEE, Vol. 117, No. 10, Oct 1970, pp 1969-1974

56. Ronald G. Harley, B. Adkins, *Calculation of the Angular Back Swing Following a Short Circuit of a Loaded Alternator,* Proc. IEE, Vol. 117, No. 2, Feb 1970, pp 377-386

57. D. B. Mehta, B. Adkins, *Transient Torque and Load Angle of a Synchronous Generator Following Several Types of System Disturbance,* Proc. IEE, Vol. 107, No. 31, Feb 1960, pp 61-74

58. Brian Stott, *Power System Dynamic Response Calculations,* Proc of IEEE, Vol. 67, No. 2, Feb 1979, pp 219-241

59. J. Fong, C. Pottle, *Parallel Processing of Power System Analysis Problems Via Simple Parallel Microcomputer Structure,* IEEE Trans on PAS, Vol. PAS-97, No. 5, Sep/Oct 1978, pp 1834-1841.

60. Fernando L. Alvarado, *Parallel Solution of Transient Problems by Trapezoidal Integration,* IEEE Trans on PAS, Vol. PAS-98, No. 3, May/June 1979, pp 1080-1090

61. L. Elder, M. J. Metcalfe, *An Efficient Method for Real-Time Simulation of Large Power System Disturbance,* IEEE Trans on PAS, Vol. PAS-101, No. 2, Feb 1982, pp 334-339

62. M. Rafian, M. J. H. Sterling, M. R. Irving, *Parallel Processor Algorithm for Power System Simulation,* IEE Proc, Vol. 135, Pt. C, No. 4, July 1988, pp 285-290

63. M. A. Pai, S. K. Ghoshal, A. Kulkarni, *A Predictor Corrector Algorithm in the Parallel Solution of Power System Dynamics,* Power Symposium, 1990, Proc of Twenty-Second Annual North American, 15-16 Oct 1990, pp 118-125

64. Jian Sheng Chai, Anjan Bose, *Bottlenecks in Parallel Algorithm for Power System Stability Analysis,* IEEE Trans on PS, Vol. 8, No. 1, Feb 1993, pp 9-15

65. K. W. Chan, A. R. Daniels, R. W. Dunn, T. Berry, *A Partitioning Algorithm for Parallel Processing of Large Power Systems Network Equation,* IEE 2nd International Conference on APSCOM, Dec 1993, HK, pp 893-898

66. K. W. Chan, R. W. Dunn, A. R. Daniels, *Efficient Heuristic Partitioning Algorithm for Parallel Processing of Large Power Systems Network Equations,* IEE Proc.-Gener. Transm. Distrib., Vol. 142, No. 6, Nov 1995, pp 625-630

67. K. W. Chan, A. R. Edwards, R. W. Dunn, A. R. Daniels, *Real-Time Electromechanical Transient Simulator for On-Line Applications,* First International Conference on Digital Power System Siulators-ICDS'95, College

Station, Texas, U.S.A., April 5-7, 1995, pp 259-263

68. Thomas L. Baldwin, Lamine Mili, Arun G. Phadke, *Dynamic Ward Equivalent for Transient Stability Analysis*, IEEE Trans on PS, Vol. 9, No. 1, Feb 1994, pp 59-67

69. A. M. Miah, *Simple Dynamic Equivalent for Fast Online Transient Stability Assessment*, IEE Proc.-Gener. Transm. Distrib., Vol. 145, No. 1, Janv 1998, pp 49-55

70. A. S. Morched, J. H. Ottevangers, L. Martf, *Multi-Port Frequency Dependent Network Equivalents for the EMTP*, IEEE Trans on PD, Vol. 8, No. 3, July 1993, pp 1402-1412

71. A. S. Morched, V. Brandwajn, *Transmission Network Equivalents for Electromagnetic Transients Studies*, IEEE Trans on PAS, Vol. PAS-102, No. 9, Sep 1983, pp 2984-2994

72. N. R. Watson, J. Arrillaga, A. P. B. Joosten, *A.C. System Equivalents for the Dynamic Simulation of HVDC Convertors*, IEE Conference Publication, No. 255, Sep 1985, pp 394-399

73. Mehdi Vakilian, Addas Ketabi, *A Method for Reduction of Power System Transient Model*, Transmission and Distribution Donference, 1999, IEEE, Vol. 1, pp 198-205

74. Ali Abur, Harinderpal Singh, *Time Domain Modeling of External Systems for Electromagnetic Transients Programs*, IEEE Trans on PS, Vol. 8, No. 2, May 1993, pp 671-678

75. Harinderpal Singh, Ali Abur, *Multi-Port Equivalencing of External Systems for Simulation os Switching Transients*, IEEE Trans on PD, Vol. 10, No. 1, Jan 1995, pp 374-382

76. J. F. Hauer, *Application of Prony Analysis to the Determination of Modal*

Content and Equivalent Models for Measured Power System Response, IEEE Trans on PS, Vol. 6, No. 3, Aug 1991, pp 1062-1068

77. H. Okamoto, A. Kurita, J. J. Sanchez-Gasca, K. Clark, N. W. Miller, J. H. Chow, *Identification of equivalent Linear Power System Models from Electromagnetic Transient Time Domain Simulation using Prony's Method*, , Proceeding of the 35th Conference on Decision and Control, Kobe, Japan, December 1996, pp. 3857-3863

78. Jun-Hee Hong, Jong-Keun Park, *A Time-Domain Approach to Transmission Network Equivalents Via Prony Analysis for Electromagnetic Transients Analysis*, IEEE Trans on PS, Vol. 10, No. 4, Nov 1995, pp 1789-1797

79. J. J. Sanchez-Gasca, K. Clark, N. W. Miller, H. Okamoto, A. Kurita, J. H. Chow, *Identifying Linear Models from Time Domain Simulations*, IEEE Computer Applications in Power, Volume: 10 , Issue: 2 , April 1997, pp 26-30

80. Matlab 6.5 On Line Help, Mathworks Inc., 1992.

81. L. A. Snider, *Application of Real Time Simulators for the Study of Interconnected Power Systems*, Invited Paper, Plenary Session of EMPD'95, Singapore, Oct 1995

82. L. A. Snider, Charles Gagnon, Ghyslain Cloutier, *Real-time Power System Simulators: Contribution to the Successful Development of Complex Power Systems*, APSCON-97, Hong Kong, Nov 1997, pp 389-395

83. D. Jakominich, R. Krebs, D. Retzmann, A. Kumar, *Real Time Digital Power System Simulator Design Considerations and Relay Performance Evaluation*, IEEE Trans on PD, Vol. 14, No. 3, July 1999, pp 773-780

84. Kevin K. W. Chan, Laurence A. Snider, *Electromagnetic Electromechanical Hybrid Real-time Digital Simulator for the Study and Control of Large Power Systems*, Power System Technology, 2000. Proceedings, Powercon 2000,

International Conference on, Vol. 2, 4-7, Dec 2000, pp 783-788

85. Kevin K. W. Chan, Laurence A. Snider, *Development of a Hybrid Real-time Fully Digital Simulator for the Study and Control of Large Power Systems,* APSCOM-2000, Hong Kong, Oct 2000, pp 527-531

86. L.A. Snider, H.T. Su, K.W. Chan, Do Van Que, *Development of a Broadband Real-Time Fully Digital Simulator for the Study and Control of Large Power Systems,* Trans on IMACS on Mathematics and Computers in Simulation

87. J. Reeve, S. P. Lane-Smith, J. M. Wikston, *Incorporation of FACTS into Transients Programs for System Simulation,* International Conference on AC and DC Power Transmission, Sep 1991, pp 379-383

88. John Reeve, S. P. Lane-Smith, *Integration of Real-Time Controls and Computer Programs for Simulation of Direct Current Transmission,* IEEE Trans on PD, Vol. 5, No. 4, Nov 1990, pp 2047-2053

89. M. D. Heffernan, K. S. Turner, J. Arrillaga and C. P. Arnold, *Computation of AC-DC System Disturbance. Part I Interactive Coordination of Generator and Convertor Transient Models*, IEEE Trans on PAS, Vol. PAS-100, No. 11, pp.4341-4348, November 1981

90. K. S. Turner, M. D. Heffernan, C. P. Arnold and J. Arrillaga, *Computation of AC-DC System Disturbance. Part II Derivation of Power Frequency Variables from Convertor Transient Response*, IEEE Trans on PAS, Vol. PAS-100, No. 11, pp.4349-4355, November 1981

91. K. S. Turner, M. D. Heffernan, C. P. Arnold and J. Arrillaga, *Computation of AC-DC System Disturbance. Part III Transient Stability Assessment*, IEEE Trans on PAS, Vol. PAS-100, No. 11, pp.4356-4363, November 1981

92. J. Reeve and R. Adapa, *A New Approach to Dynamic Analysis of AC Networks Incorporating Detailed Modeling of DC System. Part I Principles and Implementation*, IEEE Trans on PD, Vol. 3, No. 4, pp. 2005-2011, October

1988

93. J. Reeve and R. Adapa, *A New Approach to Dynamic Analysis of AC Networks Incorporating Detailed Modeling of DC System. Part II Application to Interaction of DC and Weak AC Sysrem*, IEEE Trans on PD, Vol. 3, No. 4, pp. 2012-2019, October 1988

94. G. W. J. Anderson, N. R. Watson, C. P. Arnold and J. Arrillaga, *A New Hybrid Algorithm for Analysis of HDVC and FACTS Systems*, Proc. of EMPD'95, Vol. 2, pp. 462-467, 1995

95. M. Sultan, J. Reeve and R. Adapa, *Combined Transient and Dynamic Anaysis of HVDC and FACTS Systems*, IEEE Trans. on PD, Vol. 13, No. 4, pp. 1271-1277, October 1998

96. B. Kasztenny and M. Kezunovic, *A Method for Linking Different Modeling Techniques for Accurate and Efficient Simulation*, IEEE Trans on PS, Vol. 15, No. 1, pp. 65-71, February 2000

97. Hiroto Inabe, Tomoyuki Futada, Haruyuki Horii, and Kenichi Inomae, *Development of an Instantaneous and Phasor Analisys Combined Type Real-Time Digital Power System Simulator,* International Conference on Power Systems Transient----IPST 2003 in New Orleans, USA

98. Soon-Ryul Nam, Sang-Hee Kang, Jong-Keun Park, *An Analytic Method for Measuring Accurate Fundamental Frequency Components*, IEEE Trans on PD, Vol. 17, No. 2, April 2002, pp. 405-411

99. Yong Guo, Mladen Kezunovic, Deshu Chen, *Simplified Algorithms for Removal of the Effect of Exponential Decaying DC-Offset on the Fourier Algorithm*, IEEE Trans on PD, Vol. 18, No. 3, July 2003, pp. 711-717

100. Gerald, Curtis F., *Applied Numerical Analysis*, Addison-Wesley Pub Co., C1994

101. Louis L. Scharf, *Statistical Signal Processing*, Addison-Wesley Pub Co, 1990

102. John Harris, *Handbook of Mathematics and Computational Science*, Springer, New York, c1998

103. S. Hongtian, D. Z. Fang, S. Wennan, H. F. Wang, *Constant Jacobian Matrix and its Application to Fast Trajectory of Power Systems*, IEE Proc.-Gener. Trans. Distrib., Vol. 149, No. 2, March 2002, pp. 210-214

104. M. A. Pai, *Energy Function Analysis for Power System Stability*, Kluwer Academic Publisher, c1989

Appendix A ONE-LINE DIAGRAM OF 3-MACHINE-9 BUS SYSTEM [43]

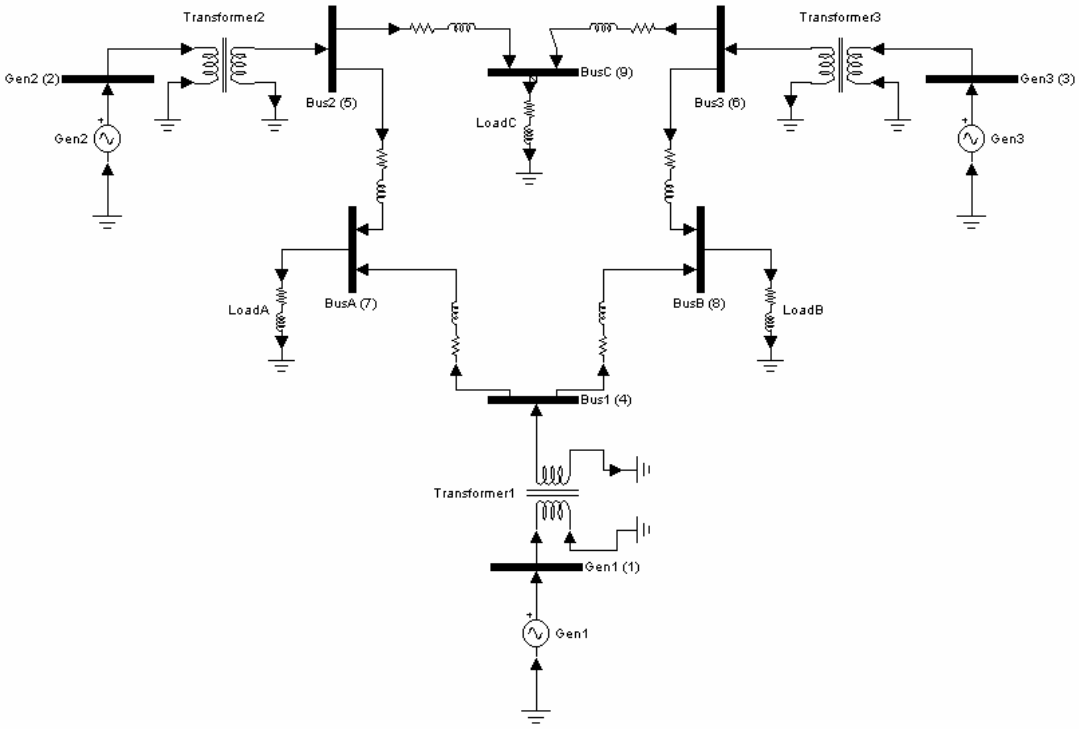

Figure a1: 9-Bus System One-Line Diagram

Table a1: 9-Bus System Load

Bus No	7	8	9
Real power (MW)	125.0	90.0	100.0
Reactive power (MVar)	70.0	40.0	55.0

Table a2: 9-Bus System Load Flow Condition

Bus No	Bus Type
1	Slack Bus (1.0, 0)
2	PV Bus (1.0pu, 1.53pu)
3	PV Bus (1.0pu, 0.7pu)
4	PQ Bus
5	PQ Bus
6	PQ Bus
7	PQ Bus
8	PQ Bus
9	PQ Bus

Table a3: 9-Bus System Transformer

	Transformer 1	Transformer 2	Transformer 3
Primary winding	Delta connection		
Bus No	1	2	3
Base voltage (p-p, kV)	16.5	18.0	13.8
Resistance (Ω)	0	0	0
Reactance (Ω)	0.0784 (0.0288 pu)	0.10125 (0.03125 pu)	0.0558 (0.0293 pu)

Inductance (per winding, mH)	0.74865	0.96687	0.53286
Secondary winding	Wye-ground connection		
Bus No	4	5	6
Base voltage (p-p, kV)	230	230	230
Resistance (Ω)	0	0	0
Reactance (Ω)	15.235 (0.0288 pu)	16.53 (0.03125 pu)	15.5 (0.0293 pu)
Inductance (per winding, mH)	48.4945	52.61662	49.33803
Turn ratio	1:1	1:1	1:1

Table a4: 9-Bus System Transmission Line

Bus1 No	Bus2 No	Base voltage	Resistance (Ω)	Reactance (Ω)	Inductance (mH)	Susceptance (μmho B/2)	Capacitance (μF)
4	7	230 (posi)	5.29 0.01(pu)	44.965 0.085(pu)	143.12804	166.3516 0.088(pu)	0.52951
		(zero)	15.87 0.03(pu)	134.895 0.255(pu)	429.38412	249.52741 0.132(pu)	0.79427
Length=100km, R1=0.0529Ω/km, L1=0.14313*10e-2H/km, C1=1.05904*10e-8F/km Zs1=367.63Ω, velocity1=2.568*10e5km/s, travel time=38.93269*10e-5s R0=0.1587Ω/km, L0=0.42938*10e-2H/km, C0=1.58854*10e-8F/km Zs0=519.9Ω, velocity0=1.21082*10e5km/s, travel time=82.58897*10e-5s							
4	8	230	8.993 0.017(pu)	48.668 0.092(pu)	154.91506	149.33837 0.079(pu)	0.47536
		(zero)	26.979 0.051(pu)	146.004 0.276(pu)	464.74517	224.00756 0.1185(pu)	0.71304
Length=100km, R1=0.08993Ω/km, L1=0.1549*10e-2H/km, C1=0.95072*10e-8F/km, Zs1=403.66Ω, velocity1=2.6057*10e5km/s, travel time=38.3771866*10e-5s R0=0.26979Ω/km, L0=0.46475*10e-2H/km, C0=1.42608*10e-8F/km, Zs0=570.87Ω, velocity0=1.22834*10e5km/s, travel time=81.4103*10e-5s							
5	7	230	16.928 0.032(pu)	85.169 0.161(pu)	271.10135	289.22495 0.153(pu)	0.92063
		(zero)	50.784 0.096(pu)	255.507 0.483(pu)	813.30404	433.83743 0.2295(pu)	1.38095
Length=100km, R1=0.16928Ω/km, L1=0.2711*10e-2H/km, C1=1.84124*10e-8F/km Zs1=383.715Ω, velocity1=1.4154*10e5km/s, travel time=70.65183*10e-5s R0=0.50784Ω/km, L0=0.8133*10e-2H/km, C0=2.76189*10e-8F/km Zs0=542.65Ω, velocity0=0.66722*10e5km/s, travel time=149.8754*10e-5s							
6	8	230	20.631 0.039(p.u)	89.93 0.17(p.u)	286.25608	338.37429 0.179(p.u)	1.07708
		(zero)	61.893 0.117(pu)	269.79 0.51(pu)	858.76824	507.56144 0.2685(pu)	1.61562
Length=100km R1=0.20631Ω/km, L1=0.28626*10e-2H/km, C1=2.15416*10e-8F/km, Zs1=364.54Ω, velocity1=1.27345*10e5km/s, travel time=78.5265*10e-5s R0=0.61893Ω/km, L0=0.85877*10e-2H/km, C0=3.23124*10e-8F/km Zs0=515.53Ω, velocity0=0.60031*10e5km/s, travel time=166.5799*10e-5s							
5	9	230	4.4965 0.0085(p.u)	38.088 0.072(p.u)	121.23787	140.83176 0.0745(p.u)	0.44828
		(zero)	13.4895 0.0255(pu)	114.264 0.216(pu)	363.71361	211.34216 0.1118(pu)	0.67272

Length=80km R1=0.05621Ω/km, L1=0.15155*10e-2H/km, C1=1.1207*10e-8F/km Zs1=367.73Ω, velocity1=2.4265*10e5km/s, travel time=32.969*10e-5s R0=0.16862Ω/km, L0=0.45464*10e-2H/km, C0=1.68181*10e-8F/km Zs0=519.93Ω, velocity0=1.14361*10e5km/s, travel time=69.9539*10e-5s							
6	9	230	6.2951 0.0119(p.u)	53.3232 0.1008(p.u)	169.73302	197.54253 0.1045(p.u)	0.628797
		(zero)	18.8853 0.0357(pu)	159.9696 0.3024(pu)	509.19905	296.40832 0.1568(pu)	0.9435
Length=80km R1=0.07869Ω/km, L1=0.21217*10e-2H/km, C1=1.57195*10e-8F/km Zs1=367.38Ω, velocity1=1.73156*10e5km/s, travel time=46.2*10e-5s R0=0.23607Ω/km, L0=0.6365*10e-2H/km, C0=2.35874*10e-8F/km Zs0=519.47Ω, velocity0=0.81613*10e5km/s, travel time=98.0234*10e-5s							

Table a5: 9-Bus System Generator

	Generator 1	Generator 2	Generator 3
Rated MVA	247.5	192.	128.
Base voltage (kV)	16.5	18.0	13.8
Power factor	1.	0.85	0.85
Type	Hydro	Stream	Stream
Speed (r/min)	180	3600	3600
Inertia constant 2H(s)	47.28	12.8	6.02
X_l (Ω)	(0.0336 pu)	(0.0521 pu)	(0.0742 pu)
X_d (Ω)	(0.146 pu)	(0.8958 pu)	(1.3125 pu)
X_q (Ω)	(0.0969 pu)	(0.8645 pu)	(1.2578 pu)
$X_d^{'}$ (Ω)	(0.0608 pu)	(0.1189 pu)	(0.1813 pu)
$X_q^{'}$ (Ω)	(0.0969 pu)	(0.1969 pu)	(0.25 pu)
$X_d^{''}$ (Ω)	(0.04 pu)	(0.089 pu)	(0.107 pu)
$X_q^{''}$ (Ω)	(0.04 pu)	(0.089 pu)	(0.107 pu)
$T_{d0}^{'}$ (s)	8.96	6.0	5.89
$T_{q0}^{'}$ (s)	0	0.535	0.6
$T_{d0}^{''}$ (s)	0.04	0.033	0.033
$T_{q0}^{''}$ (s)	0.06	0.078	0.07

Note:

1. Reactance values in table 4 are on a 100-MVA base and 230kv voltage base. All time constants are in *s*.
2. All values in table 5 are on 100-MVA base and machines' rated terminal voltage.

Appendix B ONE-LINE DIAGRAM OF NEW-ENGLAND SYSTEM [104]

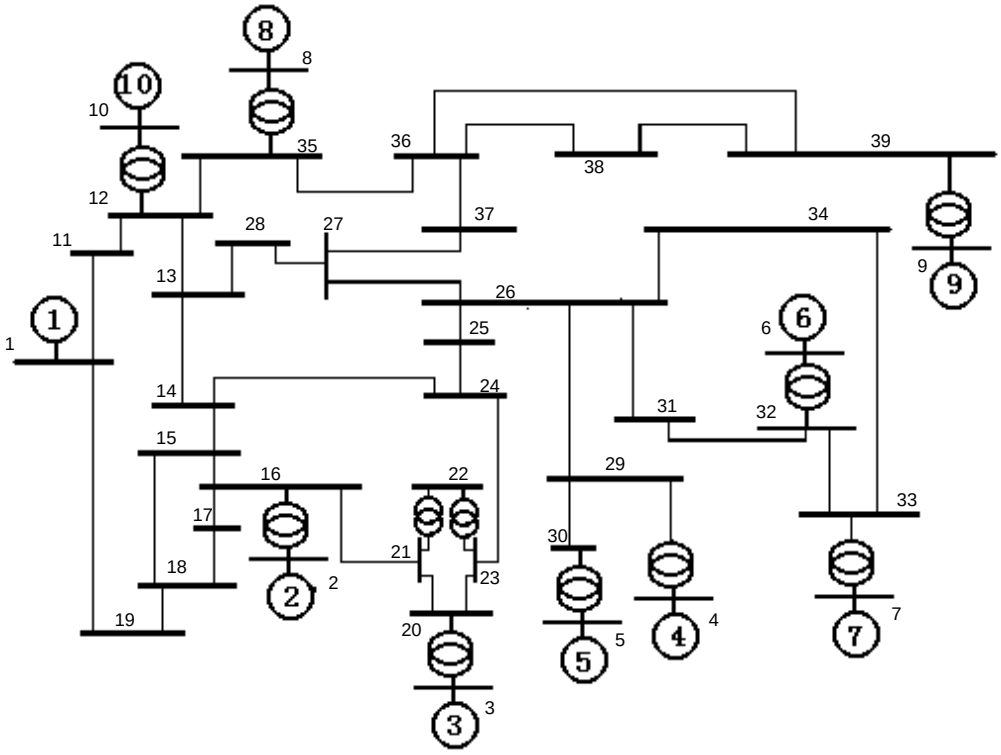

Figure b1: 39-Bus System One-Line Diagram

Table b1: 39-Bus System Load

Bus No	Real power (MW)	Reactive power (Mvar)
1	1104	250
2	9.2	4.6
13	322	2.4
14	500	184
17	233.8	84
18	522	176
22	7.5	88
25	320	153
26	329	32.3
28	158	30
30	628	103
31	274	115
33	247.5	84.6
34	308.6	-92.2
35	224	47.2
36	139	17
37	281	75
38	206	27.6
39	283.5	26.9

Table b2: 39-Bus System Load Flow Condition

Bus No	Bus Type
1	Slack Bus (1.0, 0)
2	PV Bus (0.982pu, 5.63pu)
3	PV Bus (0.9831pu, 6.5pu)
4	PV Bus (0.9972pu, 6.32pu)
5	PV Bus (1.0123pu, 5.08pu)
6	PV Bus (1.0493pu, 6.5pu)
7	PV Bus (1.0635pu, 5.6pu)
8	PV Bus (1.0278pu, 5.4pu)
9	PV Bus (1.0265pu, 8.3pu)
10	PV Bus (1.0475pu, 2.5pu)
11	PQ Bus
12	PQ Bus
13	PQ Bus
14	PQ Bus
15	PQ Bus
16	PQ Bus
17	PQ Bus
18	PQ Bus
19	PQ Bus
20	PQ Bus
21	PQ Bus
22	PQ Bus
23	PQ Bus
24	PQ Bus
25	PQ Bus
26	PQ Bus
27	PQ Bus
28	PQ Bus
29	PQ Bus
30	PQ Bus
31	PQ Bus
32	PQ Bus
33	PQ Bus
34	PQ Bus
35	PQ Bus
36	PQ Bus
37	PQ Bus
38	PQ Bus
39	PQ Bus

Table b3: 39-Bus System Transformer

	Transformer 1	Transformer 2	Transformer 3
Primary winding	Delta conection		
Bus No	2	3	4
Base voltage (p-p, kV)	20.	20.	20.
Resistance (per winding, Ω)	0	0	0.0042
Reactance (Ω)	0.05 (0.0125 pu)	0.04 (0.01 pu)	0.0284 (0.0071 pu)
Inductance (per winding, mH)	0.47745	0.38196	0.2712
Secondary winding	Wye-grounded connection		
Bus No	16	20	29
Base voltage (p-p, kV)	345.	345.	345.
Resistance (per winding, Ω)	0	0	0.41659

Reactance (Ω)	14.87813 (0.0125 pu)	11.9025 (0.01 pu)	8.45078 (0.0071 pu)
Inductance (per winding, mH)	47.35856	37.88683	26.89965
Turn ratio	1:1.07	1:1.07	1:1.07

	Transformer 4	Transformer 5	Transformer 6
Primary winding	Delta connection		
Bus No	5	6	7
Base voltage (p-p, kV)	20.	20.	20.
Resistance (per winding, Ω)	0.0054	0	0.003
Reactance (Ω)	0.036 (0.009 pu)	0.0286 (0.00715 pu)	0.0544 (0.0136 pu)
Inductance (per winding, mH)	0.34377	0.27312	0.51948
Secondary winding	Wye-grounded connection		
Bus No	30	32	33
Base voltage (p-p, kV)	345.	345.	345.
Resistance (per winding, Ω)	0.53561	0	0.29756
Reactance (Ω)	10.71225 (0.009 pu)	8.51029 (0.00715 pu)	16.1874 (0.0136 pu)
Inductance (per winding, mH)	34.09815	27.08909	51.52609
Turn ratio	1: 1.009	1:1.025	1:1

	Transformer 7	Transformer 8	Transformer 9
Primary winding	Delta connection		
Bus No	8	9	10
Base voltage (p-p, kV)	20.	20.	20.
Resistance (per winding, Ω)	0.0036	0.0048	0
Reactance (Ω)	0.0464 (0.0116 pu)	0.0312 (0.0078 pu)	0.0362 (0.00905 pu)
Inductance (per winding, mH)	0.4431	0.29793	0.34569
Secondary winding	Wye-grounded connection		
Bus No	35	39	12
Base voltage (p-p, kV)	345.	345.	345.
Resistance (Ω)	0.35708	0.4761	0
Reactance (Ω)	13.8069 (0.0116 pu)	9.28395 (0.0078 pu)	10.77176 (0.00905 pu)
Inductance (per winding, mH)	43.94873	29.55173	34.28758
Turn ratio	1: 1.025	1: 1.025	1: 1.025

	Transformer 10	Transformer 11	Transformer 12
Primary winding	Wye-grounded connection		
Bus No	22	22	29
Base voltage (p-p, kV)	345.	345.	345.
Resistance (per winding, Ω)	0.9522	0.9522	0.41659
Reactance (Ω)	25.88794 (0.02175 pu)	25.88794 (0.02175 pu)	8.21273 (0.0069 pu)
Inductance (per winding, mH)	82.40386	82.40386	26.14192
Secondary winding	Wye-grounded connection		
Bus No	21	23	30
Base voltage (p-p, kV)	345.	345.	345.
Resistance (per winding, Ω)	0.9522	0.9522	0.41659

Reactance (Ω)	25.88794 (0.02175 pu)	25.88794 (0.02175 pu)	8.21273 (0.0069 pu)
Inductance (per winding, mH)	82.40386	82.40386	26.14192
Turn ratio	1:1.006	1: 1.006	1:1.06

Table b4: 39-Bus System Transmission Line

Bus1 No	Bus2 No	Base voltage	Resistance (Ω)	Reactance (Ω)	Inductance (mH)	Susceptance (μmho B/2)	Capacitance (μF)
1	11	345.	1.19025 0.001 (pu)	29.75625 0.025 (pu)	94.71709	315.05986 0.375(pu)	1.00287
			3.57075 0.003 (pu)	89.26875 0.075 (pu)	284.15126	210.0399 0.25(pu)	0.66858
1	19	345.	1.19025 0.001(p.u)	29.75625 0.025 (p.u)	94.71709	504.09578 0.6(p.u)	1.60459
			3.57075 0.003 (pu)	89.26875 0.075 (pu)	284.15126	336.064 0.4(pu)	1.06972
11	12	345.	4.16588 0.0035 (pu)	48.91928 0.0411 (pu)	155.71489	293.51 0.34935(pu)	0.93427
			12.497625 0.0105 (pu)	146.7578 0.1233 (pu)	467.14466	195.673 0.2329(pu)	0.622847
12	13	345.	1.54733 0.0013 (pu)	17.97278 0.0151 (pu)	57.20912	108.04453 0.1286(pu)	0.34392
			4.641975 0.0039 (pu)	53.918325 0.0453 (pu)	171.62736	72.02968 0.08573(pu)	0.2292776
12	35	345.	8.33175 0.007 (p.u)	10.23615 0.0086(p.u)	32.58268	61.33165 0.073(p.u)	0.19522
			24.99525 0.021 (pu)	30.70845 0.0258(pu)	97.748	40.88777 0.04867(pu)	0.13015
13	14	345.	1.54733 0.0013(p.u)	25.35233 0.0213(p.u)	80.69896	93.00567 0.1107(p.u)	0.29605
			4.641975 0.0039 (pu)	76.057 0.0639(pu)	242.09687	62.00378 0.0738(pu)	0.197364
13	28	345.	1.30928 0.0011(p.u)	15.83033 0.0133(p.u)	50.38949	89.81306 0.1069(p.u)	0.28588
			3.927825 0.0033(pu)	47.491 0.0399(pu)	151.16847	59.875376 0.07127(pu)	0.190589
14	15	345.	0.9522 0.0008(p.u)	15.2352 0.0128(p.u)	48.49515	56.37471 0.0671(p.u)	0.17945
			2.8566 0.0024(pu)	45.7056 0.0384(pu)	145.4854	37.58314 0.04473(pu)	0.119631
14	24	345.	0.9522 0.0008(p.u)	15.35423 0.0129(p.u)	48.87402	58.05503 0.0691(p.u)	0.18479
			2.8566 0.0024(pu)	46.062675 0.0387(pu)	146.622	38.70335 0.046067(pu)	0.1232
15	16	345.	0.23805 0.0002(p.u)	3.09465 0.0026(p.u)	9.85058	18.231464 0.0217(p.u)	0.058033

			0.71415 0.0006(pu)	9.28395 0.0078(pu)	29.55173	12.15431 0.014467(pu)	0.038688
15	18	345.	0.9522 0.0008(p.u)	13.3308 0.0112(p.u)	42.43325	62.00378 0.0738(p.u)	0.19736
			2.8566 0.0024(pu)	39.9924 0.0336(pu)	127.29976	41.33585 0.0492(pu)	0.131576
16	17	345.	0.71415 0.0006(p.u)	10.9503 0.0092(p.u)	34.85589	47.46902 0.0565(p.u)	0.1511
			2.14245 0.0018(p.u)	32.8509 0.0276(pu)	104.5677	31.646 0.03767(pu)	0.100732
16	21	345.	0.83318 0.0007(p.u)	9.76005 0.0082(p.u)	31.0672	58.30708 0.06945(p.u)	0.1856
			2.499525 0.0021(pu)	29.28015 0.0246(pu)	93.2016	38.9 0.0463(pu)	0.12382
17	18	345.	0.4761 0.0004(p.u)	5.47515 0.0046(p.u)	17.42794	32.76623 0.039(p.u)	0.1043
			1.4283 0.0012(pu)	16.42545 0.0138(pu)	52.2838	21.84415 0.026(pu)	0.069532
18	19	345.	2.73758 0.0023(p.u)	43.20608 0.0363(p.u)	137.52921	159.79836 0.1902(p.u)	0.50865
			8.212725 0.0069(pu)	129.618 0.1089(pu)	412.5876	106.5322 0.1268(pu)	0.3391
20	21	345.	0.4761 0.0004(p.u)	5.11808 0.0043(p.u)	16.29134	30.58181 0.0364(p.u)	0.09734
			1.4283 0.0012(pu)	15.3542 0.0129(pu)	48.874	20.38787 0.024267(pu)	0.064897
20	23	345.	0.4761 0.0004(p.u)	5.11808 0.0043(p.u)	16.29134	30.58181 0.0364(p.u)	0.09734
			1.4283 0.0012(pu)	15.3542 0.0129(pu)	48.874	20.38787 0.024267(pu)	0.064897
23	24	345.	1.07123 0.0009(p.u)	12.02153 0.0101(p.u)	38.2657	72.42176 0.0862(p.u)	0.23053
			3.213675 0.0027(pu)	36.064575 0.0303(pu)	114.7971	48.281 0.057467(pu)	0.153684
24	25	345.	2.14245 0.0018(p.u)	25.82843 0.0217(p.u)	82.21443	153.74921 0.183(p.u)	0.4894
			6.42735 0.0054(pu)	77.485 0.0651(pu)	246.6433	102.5 0.122(pu)	0.326266
25	26	345.	1.07123 0.0009(p.u)	11.18835 0.0094(p.u)	35.61362	71.83365 0.0855(p.u)	0.22865
			3.213675 0.0027(pu)	33.56505 0.0282(pu)	106.841	47.8891 0.057(pu)	0.152436
26	27	345.	0.83318 0.0007(p.u)	10.59323 0.0089(p.u)	33.71928	56.37471 0.0671(p.u)	0.17945
			2.499525 0.0021(pu)	31.78 0.0267(pu)	101.1578	37.583 0.04473(pu)	0.11963

26	29	345.	1.9044 0.0016(p.u)	23.20988 0.0195(p.u)	73.87933	127.70426 0.152(p.u)	0.4065
			5.7132 0.0048(pu)	69.63 0.0585(pu)	221.638	85.1362 0.10133(pu)	0.271
26	31	345.	0.9522 0.0008(p.u)	16.06838 0.0135(p.u)	51.14723	107.03634 0.1274(p.u)	0.34071
			2.8566 0.0024(pu)	48.205 0.0405(pu)	153.4417	71.35756 0.08493(pu)	0.227138
26	34	345.	0.35708 0.0003(p.u)	7.02248 0.0059(p.u)	22.35323	28.56543 0.034(p.u)	0.09093
			1.071225 0.0009(pu)	21.0674 0.0177(pu)	67.06	19.0436 0.02267(pu)	0.06062
27	28	345.	0.83318 0.0007(p.u)	9.76005 0.0082(p.u)	31.0672	55.45054 0.066(p.u)	0.1765
			2.499525 0.0021(pu)	29.28 0.0246(pu)	93.2016	36.967 0.044(pu)	0.11767
27	37	345.	1.54733 0.0013(p.u)	20.59133 0.0173(p.u)	65.54422	135.09767 0.1608(p.u)	0.43003
			4.641975 0.0039(pu)	61.774 0.0519(pu)	196.633	90.065 0.1072(pu)	0.286686
31	32	345.	0.9522 0.0008(p.u)	16.6635 0.014(p.u)	53.04157	107.70846 0.1282(p.u)	0.34285
			2.8566 0.0024(pu)	49.9905 0.042(pu)	159.1247	71.8056 0.085467(pu)	0.22856
32	33	345.	0.71415 0.0006(p.u)	11.4264 0.0096(p.u)	36.37136	77.54673 0.0923(p.u)	0.24684
			2.14245 0.0018(pu)	34.2792 0.0288(pu)	109.1141	51.6978 0.06153(pu)	0.16456
33	34	345.	2.61855 0.0022(p.u)	41.65875 0.035 (p.u)	132.60392	151.64881 0.1805(p.u)	0.48271
			7.85565 0.0066(pu)	124.97625 0.105(pu)	397.81176	101.0992 0.12033(pu)	0.32181
35	36	345.	3.8088 0.0032(p.u)	38.44508 0.0323(p.u)	122.37447	215.50095 0.2565(p.u)	0.68596
			11.4264 0.0096(pu)	115.335 0.0969(pu)	367.1234	143.6673 0.171(pu)	0.45731
36	37	345.	1.66635 0.0014(p.u)	17.49668 0.0147(p.u)	55.69365	100.65112 0.1198(p.u)	0.32038
			4.99905 0.0042(pu)	52.49 0.0441(pu)	167.0809	67.101 0.079867(pu)	0.21359
36	38	345.	5.11808 0.0043(p.u)	56.41785 0.0474(p.u)	179.58359	327.74627 0.3901(p.u)	1.04325
			15.354 0.0129(pu)	169.25 0.1422(pu)	538.751	218.4975 0.26007(pu)	0.6955

Length=100km R1=0.0511808Ω/km, L1=179.58359e-5H/km, C1=2.0865e-8F/km Zs1=293.3757Ω, velocity1=1.63364e5km/s, travel time=612.128e-6s R0=0.15354Ω/km, L0=538.751e-5H/km, C0=1.391e-8F/km Zs0=622.343Ω, velocity0=1.15516e5km/s, travel time=865.68e-6s							
36	39	345.	6.78443 0.0057(p.u)	74.39063 0.0625(p.u)	236.79271	432.26213 0.5145(p.u)	1.37593
			20.3533 0.0171(pu)	223.1719 0.1875(pu)	710.378	288.175 0.343(pu)	0.91729
Length=100km R1=0.0678443Ω/km, L1=236.79271e-5H/km, C1=2.75186e-8F/km Zs1=293.34Ω, velocity1=1.2388e5km/s, travel time=807.23e-6s R0=0.203533Ω/km, L0=710.378e-5H/km, C0=1.83458e-8F/km Zs0=622.2665Ω, velocity0=0.875965e5km/s, travel time=1141.56e-6s							
38	39	345.	1.66635 0.0014(p.u)	17.97278 0.0151(p.u)	57.20912	104.59987 0.1245(p.u)	0.33295
			4.99905 0.0042(pu)	53.918 0.0453(pu)	171.627	69.733 0.083(pu)	0.22197
Length=100km R1=0.0166635Ω/km, L1=57.20912e-5H/km, C1=0.6659e-8F/km Zs1=293.1083Ω, velocity1=5.12345e5km/s, travel time=195.1808e-6s R0=0.0499905Ω/km, L0=171.627e-5H/km, C0=0.44394e-8F/km Zs0=621.77Ω, velocity0=3.62281e5km/s, travel time=276.029e-6s							

Table b5: 39-Bus System Generator

	Generator 1 (voltage source)	Generator 2	Generator 3
Rated MVA	100.	100.	100.
Base voltage (kV)	345.	20.	20.
Power factor			
Type			
Speed (r/min)			
Inertia constant 2H(s)	1000.	60.6	71.6
R_a (Ω)	0	0	0
X_l (Ω)	(0.003 pu)	(0.035 pu)	(0.0304 pu)
X_d (Ω)	(0.2pu)	(0.295 pu)	(0.2495 pu)
X_q (Ω)	(0.019pu)	(0.282 pu)	(0.237 pu)
$X_d^{'}$ (Ω)	(0.006pu)	(0.0697 pu)	(0.0531 pu)
$X_q^{'}$ (Ω)	(0.008pu)	(0.17 pu)	(0.0876 pu)
$X_d^{''}$ (Ω)	-	- (0.0369 pu)	- (0.032 pu)
$X_q^{''}$ (Ω)	-	- (0.0369 pu)	- (0.032 pu)
$T_{d0}^{'}$ (s)	7	6.56	5.7
$T_{q0}^{'}$ (s)	0.7	1.5	1.5
$T_{d0}^{''}$ (s)	-	- (0.066)	- (0.057)
$T_{q0}^{''}$ (s)	-	- (0.066)	- (0.057)

	Generator 4	Generator 5	Generator 6
Rated MVA	100.	100.	100.
Base voltage (kV)	20.	20.	20.

Power factor			
Type			
Speed (r/min)			
Inertia constant 2H(s)	59.2	52	79.6
R_a (Ω)	0	0	0
X_l (Ω)	(0.0295 pu)	(0.054 pu)	(0.0224 pu)
X_d (Ω)	(0.262pu)	(0.67 pu)	(0.254 pu)
X_q (Ω)	(0.258pu)	(0.62 pu)	(0.241 pu)
$X_d^{'}$ (Ω)	(0.0436pu)	(0.132 pu)	(0.05 pu)
$X_q^{'}$ (Ω)	(0.166pu)	(0.166 pu)	(0.0814 pu)
$X_d^{''}$ (Ω)	- (0.031)	- (0.0568)	- (0.0236)
$X_q^{''}$ (Ω)	- (0.031)	- (0.0568)	- (0.0236)
$T_{d0}^{'}$ (s)	5.69	5.4	7.3
$T_{q0}^{'}$ (s)	1.5	0.44	0.4
$T_{d0}^{''}$ (s)	- (0.057)	- (0.054)	- (0.073)
$T_{q0}^{''}$ (s)	- (0.057)	- (0.054)	- (0.073)

	Generator 7	Generator 8	Generator 9
Rated MVA	100.	100.	100.
Base voltage (kV)	20.	20.	20.
Power factor			
Type			
Speed (r/min)			
Inertia constant 2H(s)	52.8	48.6	69
R_a (Ω)	0	0	0
X_l (Ω)	(0.0322 pu)	(0.028 pu)	(0.0298 pu)
X_d (Ω)	(0.295pu)	(0.29 pu)	(0.2106 pu)
X_q (Ω)	(0.292pu)	(0.28 pu)	(0.205 pu)
$X_d^{'}$ (Ω)	(0.049pu)	(0.057 pu)	(0.057 pu)
$X_q^{'}$ (Ω)	(0.186pu)	(0.0911 pu)	(0.0587 pu)
$X_d^{''}$ (Ω)	- (0.034 pu)	- (0.03 pu)	- (0.0314)
$X_q^{''}$ (Ω)	- (0.034 pu)	- (0.03 pu)	- (0.0314)
$T_{d0}^{'}$ (s)	5.66	6.7	4.79
$T_{q0}^{'}$ (s)	1.5	0.41	1.96
$T_{d0}^{''}$ (s)	- (0.056)	- (0.067)	- (0.047)
$T_{q0}^{''}$ (s)	- (0.056)	- (0.067)	- (0.047)

	Generator 10		
Rated MVA	100.		
Base voltage (kV)	20.		
Power factor			
Type			

Speed (r/min)			
Inertia constant 2H(s)	84		
R_a (Ω)	0		
X_l (Ω)	(0.0125 pu)		
X_d (Ω)	(0.1pu)		
X_q (Ω)	(0.069pu)		
$X_d^{'}$ (Ω)	(0.031pu)		
$X_q^{'}$ (Ω)	(0.018pu)		
$X_d^{''}$ (Ω)	- (0.0132)		
$X_q^{''}$ (Ω)	- (0.0132)		
$T_{d0}^{'}$ (s)	10.2		
$T_{q0}^{'}$ (s)	0		
$T_{d0}^{''}$ (s)	- (0.1)		
$T_{q0}^{''}$ (s)	- (0.1)		

Note:

1. All per unit values in table 4 are on a 100-MVA base and 345kv voltage base. All time constants are in *s*.
2. All values in table 5 are in 100-MVA power base and machines' rated terminal voltage.

Appendix C NUMERICAL SOLUTION TO ORDINARY DIFFERENTIAL EQUATION [2]

Most components in power system can be expressed by ordinary differential equations in mathematical form. Thus, the issue of solving system variables can be transformed to the issue of solving a set of differential equations. How to obtain stable and accurate resolution is an essential task of simulation. A number of numerical solution techniques for solving ordinary differential equations are available, including closed-form solution, implicit integration, and etc [2].

The appearance and development of computers influences drastically network theory by demanding methods of analysis adapted to the solution of computer-size problems. Traditional methods for hand solution of networks are not necessarily best for use on a computer with networks of much greater size.

In this section, an attempt is made to summarize some of the numerical solution techniques for solving ordinary differential equations suitable for computer-sized problems. Since power system networks are most linear, techniques for linear ordinary differential equations are given special emphasis.

C.1 CLOSED-FORM SOLUTION

Suppose a set of linear differential equations in state-variable form with initial condition,

$$\begin{aligned} &\left[\frac{dx}{dt}\right] = [A][x] + [g(t)] \\ &x(0) = x_0 \end{aligned} \tag{c.1}$$

where A is a constant square matrix, g(t) is a vector of known forcing functions.

The closed-form solution of Eq. (c.1), which carries us from the state of the system at $t-\Delta t$ to that of *t*, is

$$[x(t)] = e^{[A]\Delta t}[x(t-\Delta t)] + \int_{t-\Delta t}^{t} e^{[A](t-u)}[g(u)]du \tag{c.2}$$

where the matrix $e^{[A]\Delta t}$ is called the transient matrix. Eq. (c.2) contains the case where $[x(t)]$ is simply desired as a function of *t* by setting $\Delta t = t$.

The computation task lies in finding this transient matrix. Since there is no closed-form solution for the matrix exponential $e^{[A]\Delta t}$, the way out is to transform this matrix to a diagonal matrix, whose elements can be easily evaluated by using the eigenvalues λ_i of $[A]$ and the matrix of eigenvectors (modal matrix) $[M]$ of $[A]$, and then to transform back again [1].

$$e^{[A]\Delta t} = [M]\left[e^{\Lambda\Delta t}\right][M]^{-1} \tag{c.3}$$

where $e^{[\Lambda]\Delta t}$ is diagonal matrix with elements $e^{\lambda_i \Delta t}$, $[M]$ is eigenvector (modal) matrix of $[A]$, and λ_i is eigenvalues of $[A]$.

With Eq. (c.3), Eq. (c.2) becomes

$$[x(t)] = [M]e^{[\Lambda]\Delta t}[M]^{-1}[x(t-\Delta t)] + \int_{t-\Delta t}^{t} [M]e^{[\Lambda](t-u)}[M]^{-1}[g(u)]du \tag{c.4}$$

The convolution integral in Eq. (c.4) can be evaluated in closed-form for many types of functions [g(t)].

To quote from [1], “Could such a closed-form solution be used in an EMTP? For network of moderate size, it probably could. …If the network contains switches which frequently change their position, then its implementation would probably become vary tricky. Combining it with Bergeron’s method for distributed-parameter lines, or with more sophisticated convolution methods for lines with frequency-dependent parameters, should in principle be possible. Where the method becomes almost unmanageable, or useless, is in network with nonlinear elements. Another difficulty would arise with the state-variable formulation, because Eq. (c.1) cannot be easily assembled by a computer as the node equations used in the EMTP. This difficulty could be overcome, however, since there are ways of using node equations even for state-variable formulations, by distinguishing node types according to the types of branches (R, L, or C) connected to them”.

Laplace transform methods fit into this part discussion since they provide closed-form solutions as well. The Laplace transform of Eq. (c.1) is

$$s[X(s)]-[x(0)]=[A][X(s)]+[G(s)] \tag{c.5}$$

From which the formal solution in the s-domain is obtained as

$$[X(s)]=(s[U]-[A])^{-1}([x(0)]+[G(s)]) \tag{c.6}$$

The computational task in (c.6) is the determination of the inverse of $(s[U]-[A])$. The key to doing this efficiently is again through the eigenvalues and eigenvectors of $[A]$.

The traditional Laplace transform techniques involve ratio of polynomials and the poles and zeros thereof. The task of computing the coefficients of the polynomials in a network function $P(s)/Q(s)$ is not only time-consuming but also prone to serious numerical inaccuracies, especially when the polynomials are of a high degree. To quote from [1] again, "…the polynomial approach is just not matched to the network analysis tasks which the computer is called upon to handle. The eigenvalue approach is much better suited and gives all of the theoretical information that the Laplace transform methods are designated to provide".

C.2 EXPLICIT METHODS

Explicit methods mean the value of the dependent variable [*x*] at any value of *t* is computed from knowledge of the values of [*x*] from the previous time steps. For Eq. (c.1), $[x_t]$ is calculated explicitly by evaluating $\left[\frac{dx}{dt}\right]$ with known [*x*]. These methods are easy to implement for the solution of a complex set of system state equations. The more commonly used explicit methods are Euler, predictor-corrector methods, and Runge-Kutta methods.

Before the three methods are discuss, let's first have a look at the Taylor-series method. This method is not strictly a numerical method, but it is sometimes used in conjunction with the numerical schemes, is of general applicability, and serves as an introduction to the other techniques we will discuss [2].

The matrix exponential $e^{[A]\Delta t}$ can be approximated by a power series, derived from a Taylor series expansion:

$$e^{[A]\Delta t} = [U] + \Delta t[A] + \frac{\Delta t^2}{2!}[A]^2 + \frac{\Delta t^3}{3!}[A]^3 + \frac{\Delta t^4}{4!}[A]^4 + \cdots \tag{c.7}$$

This series is, in effect, the definition of the matrix exponential. Taylor series is a series including infinite terms. When in practical application, we only take s part of them. We normally truncate the Taylor series when the contribution of the last term is negligible to the number of decimal places to which we are working. However, the error of truncation cannot be computed. In fact, the number of Taylor-series terms to be included is a matter of judgment and experience.

C.2.1 EULER METHOD

In Taylor series, if time step is made small enough, only a few terms of the Taylor-series expansion may be needed for good accuracy. The Euler method follows this idea to the extreme for first-order differential equations. It uses only the first two terms of the Taylor series.

For Eq. (c.1), the Euler form can be written as:

$$[x_{n+1}] = [x_n] + \left[\frac{dx}{dt}\right]_{\substack{x=x_n \\ t=t_n}} \Delta t \tag{c.8}$$

Figure c.1 illustrates the principle of applying the Euler method.

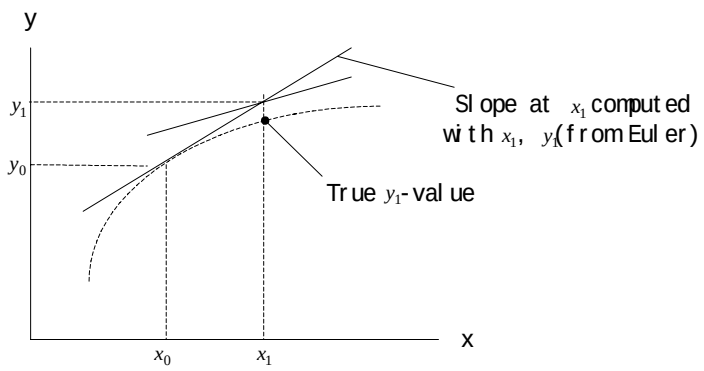

Figure c.1: Illustration of Euler Method

The method considers only the first derivative of [x] and is, therefore, referred to as a first-order method. To give sufficient accuracy for each step, Δt has to be

small. This will increase round-off errors, and the computational effort required will be very high.

C.2.2 MODIFIED EULER METHOD

In the simple Euler method, the slope at the beginning of the interval through the interval is used to determine the increment to the function. This technique would be correct only if the function were linear. What is needed instead is the correct average slope within the interval. This can be approximated by the mean of the slopes at both ends of the interval.

Suppose the arithmetic average of the slopes at the beginning and end of the interval is used to compute x_{n+1}:

$$[x_{n+1}] = [x_n] + \frac{\left[\frac{dx}{dt}\right]_{\substack{x=x_{n+1}\\ t=t_{n+1}}} + \left[\frac{dx}{dt}\right]_{\substack{x=x_n\\ t=t_n}}}{2}\Delta t \qquad \text{(c.9)}$$

Eq. (c.9) should give us an improved estimate for x_{n+1} at t_{n+1}. However, we are unable to employ Eq. (c.9) directly, since the derivative is a function of both *x* and *t* and we cannot evaluate $\left[\frac{dx}{dt}\right]_{\substack{x=x_n\\ t=t_n}}$ with the true value of x_{n+1} unknown. The modified Euler method works around this problem by estimating or predicting a value of x_{n+1} by the simple Euler relation, Eq. (c.8). It then uses this value to compute $\left[\frac{dx}{dt}\right]_{\substack{x=x_n\\ t=t_n}}$, giving an improved estimate (a correct value) for x_{n+1}. Thus, the modified Euler method consists of the following steps [42]:

1. *Predictor step*. By using the derivative at the beginning of the step, the value at the end of the step is predicted

$$[x_{n+1}]^P = [x_n] + \left[\frac{dx}{dt}\right]_{\substack{x=x_n\\ t=t_n}}\Delta t$$

2. *Corrector step*. By using the predicted value of x_{n+1}, the derivative at the end of the step is computed and the average of this derivative and the derivative at the beginning of the step is used to find the corrected value.

$$[x_{n+1}]^C = [x_n] + \frac{\left[\frac{dx}{dt}\right]_{\substack{x=x_{n+1}^P \\ t=t_{n+1}}} + \left[\frac{dx}{dt}\right]_{\substack{x=x_n \\ t=t_n}}}{2}\Delta t$$

Since the value of $\left[\frac{dx}{dt}\right]_{\substack{x=x_{n+1} \\ t=t_{n+1}}}$ was computed using the predicted value, of less than prefect accuracy, we might want to re-correct the x_{n+1} value as many times as will make a significant difference.

The modified Euler method is the simplest of predictor-corrector methods. Among the well known higher order predictor-corrector methods are the Adams-Bashforth method, Milne method, and Hamming method, etc.

C.2.3 RUNGE-KUTTA METHODS

The R-K methods solve a differential equation efficiently and yet are the equivalent of approximating the exact solution by matching the first *n* terms of the Taylor-series expansion. The R-K methods do not require explicit evaluation of derivatives higher than the first. The effects of higher derivatives are included by several evaluations of the first derivative. Depending on the number of terms effectively retained in the Taylor-series, we have R-K methods of different orders. Generally, the increment to the [*x*] is a weighted average of a number of estimates of the increment. We will only consider the second- and forth-order R-K methods, even though there are higher-order methods.

Second-order R-K method is equivalent to considering first and second derivative terms in the Taylor series. A general formula giving the value of [*x*] for the (n+1) step is:

$$\begin{aligned} [x_{n+1}] &= [x_n] + \frac{[K_1 + K_2]}{2} \\ [K_1] &= \left[\frac{dx}{dt}\right]_{\substack{x=x_n \\ t=t_n}} \Delta t \\ [K_2] &= \left[\frac{dx}{dt}\right]_{\substack{x=x_n+K_1 \\ t=t_n+\Delta t}} \Delta t \end{aligned} \tag{c.10}$$

Forth-order R-K method is equivalent to considering up to forth derivative term in the Taylor series expansion. The general formula giving the value of [x] for the (n+1) step is:

$$
\begin{aligned}
&[x_{n+1}] = [x_n] + \frac{1}{6}([K_1] + [2K_2] + [2K_3] + [K_4]) \\
&K_1 = \left[\frac{dx}{dt}\right]_{\substack{x=x_n \\ t=t_n}} \Delta t \\
&K_2 = \left[\frac{dx}{dt}\right]_{\substack{x=x_n+K_1/2 \\ t=t_n+\Delta t/2}} \\
&K_3 = \left[\frac{dx}{dt}\right]_{\substack{x=x_n+K_{12}/2 \\ t=t_n+\Delta t/2}} \\
&K_4 = \left[\frac{dx}{dt}\right]_{\substack{x=x_n+K_3 \\ t=t_n+\Delta t}}
\end{aligned}
\tag{c.11}
$$

The physical interpretation of the above solution is as follows:

K_1 = (slope at the beginning of the time step) Δt

K_2 = (first approximation to slope at midstep) Δt

K_3 = (second approximation to slope at midstep) Δt

K_4 = (slope at the end of step) Δt

Thus the incremental value of [x] is given by the weighted average of estimates based on slopes at the beginning, midpoint, and the end of the time step.

Explicit methods are not easily applied to individual branch equations, which are then assembled into node equations, as applied to the state-variable Eq. (c.1).

C.3 IMPLICIT INTEGRATION METHODS

Let the solution to Eq. (c.1) be written as an integral equation,

$$[x(t)] = [x(t-\Delta t)] + \int_{t-\Delta t}^{t} ([A][x(u)] + [g(u)])du \tag{c.12}$$

Implicit integration methods use interpolation functions for the expression under the integral. Interpolation implies that the functions must pass through the yet unknown points, for Eq. (c.12) at time t.

In developing formulas for numerical integration, we pass a polynomial ($P_n(x)$) through points defined by the function $f(x)$, and then integrate this polynomial approximation to the function. This permits us to integrate a function known only as a table of values. When the values are equispaced, we have the Newton-Gregory forward polynomial [2], so

$$\int_a^b f(x)dx = \int_a^b P_n(x_s)dx \tag{c.13}$$

There are various ways that we can employ Eq. (c.13). The interval of integration (a,b) can match the range of fit of the polynomial, (x_0, x_n). In this case, we get the Newton-Cotes formula; these are a set of integration rules corresponding to the varying degrees of the interpolating polynomial.

C.3.1 TRAPEZOIDAL RULE

The first of the Newton-Cotes formula, based on approximating $f(x)$ on (x_n, x_{n+1}) by a straight line, is called the trapezoidal rule. The familiar and simple trapezoidal rule can also be considered to be an adaptation of the definition of the definite integral as a sum.

From Eq. (c.12), by using linear interpolation on [x] and [g] between t-Δt and t, assuming for the time being that [x] were known at t (which , in reality, is not true, thereby making the method implicit), we get,

$$[x(t)] = [x(t-\Delta t)] + \frac{\Delta t}{2}[A]([x(t-\Delta t) + x(t)]) + \frac{\Delta t}{2}([g(t-\Delta t) + [g(t)]]) \tag{c.14}$$

Linear interpolation implies that the areas under the integral of Eq. (c.12) are approximated by trapezoidal (Figure c.2).

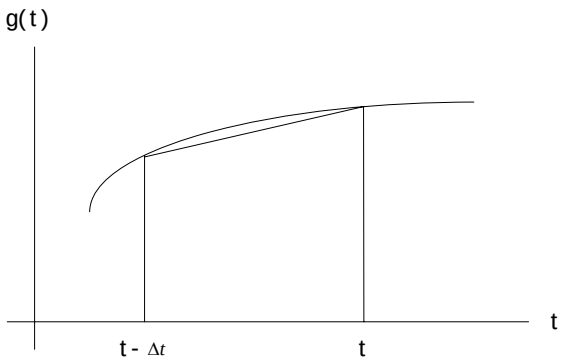

Figure c.2: Illustration of Trapezoidal Rule

The method is identical with using "central difference quotients" in Eq. (c.1)

$$\frac{[x(t)-[x(t-\Delta t)]]}{\Delta t}=[A]\frac{[x(t)+[x(t-\Delta t)]]}{2}+\frac{[g(t)]+[g(t-\Delta t)]}{2} \tag{c.15}$$

The trapezoidal rule of integration is admittedly of lower order accuracy than many other methods. The major drawback of the trapezoidal rule of integration is the danger of numerical oscillation under some circumstances.

C.3.2 BACKWARD EULER METHOD

Backward Euler method falls into the category of implicit numerical analysis because is uses the derivative of [x] with the values of $[x(t)]$ yet unknown. For Eq. (c.1), applying the method, we have

$$[x_{n+1}]=[x_n]+\left[\frac{dx}{dt}\right]_{\substack{x=x_{n+1}\\ t=t+\Delta t}}\Delta t \tag{c.16}$$

We can interpret from difference point of view that the method uses the slope at the end of interval to determine the increment to the function, as compared to Euler and Modified Euler methods. Or we can interpret from integration viewpoint that the function $f(x)$ in the interval (t-Δt, t) just is substituted with a straight line parallel to the axis of independent variable and with a magnitude equal to the value of $f(x)$ at time t.

The backward Euler method produces too much damping. Implicit integration methods can apply to both state-variable equations and individual branch equations, which are then assembled into node equations.

C.4 ERROR PROPAGATION AND NUMERICAL STABILITY

Error and stability are two permanent topics associated with numerical analysis. There are three major error sources in numerical methods, i.e. original data error, round-off error, and truncation error. Here we mainly discuss the errors caused by truncation.

The error in a single step caused by truncation is called local truncation error, since all practical applications of numerical methods to differential equations involve many steps, the accumulation of these errors is termed the global truncation error.

For explicit methods, the local truncation error of Euler method is in the second of time step, expressed as $O(h^2)$, and the global truncation is $O(h)$. The local and global truncation errors of Modified Euler method are $O(h^3)$ and $O(h^2)$ respectively. The second-order R-K method has the same local and global truncation errors as the Modified Euler method. The local and global truncation errors of forth-order R-K method are $O(h^5)$ and $O(h^4)$.

The local and global truncation errors of the trapezoidal rule are $O(h^3)$ and $O(h^2)$.

In the application of numerical integration methods, it is very important to consider the propagation od error, which may cause slight error made early in the process to be magnified at later steps. Numerical stability depends on the propagation of error. If early errors carry through but cause no significant further errors later, the method is said to be numerically stable. If, on the other hand, early errors cause other large errors later, the method is said to be numerically unstable.

Numerical stability is related to the stiffness of the set of differential equations representing the system, that is, the system which the smallest and largest eigenvalues or time constants are orders of magnitude apart. Most power system are probably stiff in that sense.

A fundamental theorem about A-stable states [2]:

Let a multistep method be called A-stable, if, when it is applied to the problem $\left[\frac{dx}{dt}\right] = \lambda[x], \mathrm{Re}(\lambda) < 0$, it is stable for all $\Delta t > 0$.

Then:

1. No explicit linear multistep method is A-stable.
2. No implicit linear multistep method of order greater than two is A-stable.
3. The most accurate A-stable linear multistep method of order two is the trapezoidal rule.

Explicit techniques are inherently unstable. They require a step size tailored to the highest frequency or smallest time constant, even though this mode may produce only negligible ripples, with the overall behavior determined by the larger time constants in stiff system. Even after the fast mode dies out, small time steps continue to be required to maintain numerical stability.

The trapezoidal rule is numerically A-stable. The stiffness of the system being analyzed affects accuracy but not numerical stability. With larger time steps, high frequency modes and fast transients are filtered out, and the solutions for the slower modes are accurate. For systems involving simulations in which time steps are limited by numerical stability considerations rather than accuracy, implicit methods are generally better suited than explicit methods. The trapezoidal rule is widely used in electromagnetic transients simulators.

The trapezoidal rule is a second-order method. Implicit integration methods of higher order have not been widely used for power system applications since they are less numerically stable than the trapezoidal rule.

Appendix D LEAST SQUARE AND DIGITAL FOURIER ANALYSIS

In the development of hybrid simulation, we have to deal with the issue of extracting a value in phasor form from time domain broadband solutions. Both least square method and digital Fourier analysis can do this.

D.1 LEAST SQUARE METHOD

The idea behind least square is to fit a model to measurements in such a way that weighted errors between the measurements and the model are minimized [101].

Let's first illustrate the basic principles of least squares by using linear problems. The linear model says that observations $y = [y_1\ y_2 \cdots y_N]^T$ consist of a model or signal, component $x = [x_1\ x_2 \cdots x_N]^T$, plus an error component $n = [n_1\ n_2 \cdots n_N]^T$:

$$y = x + n \tag{d.1}$$

The signal component obeys the linear equation

$$x = H\theta \tag{d.2}$$

where H is a Nxp matrix and θ is a px1 vector.

$$H = \begin{bmatrix} h_{11} & h_{12} & \cdots & h_{1p} \\ h_{21} & & & \\ \vdots & & & \vdots \\ h_{N1} & & \cdots & h_{Np} \end{bmatrix} = \begin{bmatrix} h_1 & h_2 & \cdots & h_p \end{bmatrix}$$

$$\theta = \begin{bmatrix} \theta_1 & \theta_2 & \cdots & \theta_p \end{bmatrix}^T$$

The vector θ is unknown and is precisely the weights in this linear combination that we wish to determine. The matrix H is known when the mode structure, or dynamics, of a system are known, but unknown otherwise. Call each column a mode of the signal x .

In our later application, it is better to interpret the vector of errors n as errors or residuals in fitting the model $H\theta$ to the data y. Then the equation $y = H\theta + n$ is called an equation error model for the idea model $x = H\theta$. Sometimes $x = H\theta$ is the signal component in a signal-plus-noise model $y = x + n$, where n is additive noise.

Consider the linear model $y = H\theta + n$, for a given estimate of θ, the squared error between *y* and the model $H\theta$ is defined to be,

$$e^2 = (y - H\theta)^T (y - H\theta) = n^T n \tag{d.3}$$

This is minimized to obtain the least squares estimate.

The least square estimate equate the gradient to zero to produce the solution

$$\hat{\theta} = \left(H^T H\right)^{-1} H^T y \tag{d.4}$$

This solution exists and is unique, provided that the inverse of $H^T H$ exists. If the columns of H are linear independent, then the inverse of $H^T H$ exists.

To solve Eq. (d.4), we can use QR-factoring method or Singular Value Decomposition method.

In this thesis, a curve fitting algorithm is used to extract the system frequency data, based on least square method, from generally distorted waveforms in power network. Assume a sinewave signal with a frequency of ω radians per second and a phase shift of ψ relative to some arbitrary time T_0.

$$x(t) = A\cos(\omega t - \psi) = A\cos\omega t\cos\psi + A\sin\omega t\sin\psi\ .$$

$\cos\omega t$ and $\sin\omega t$ are known if the fundamental frequency ω is known. However, the amplitude and phase of this frequency generally need to be found.

Suppose there are total *k* measurements, then

$$H = \begin{bmatrix} \cos\omega t_0 & \sin\omega t_0 \\ \cos\omega t_1 & \sin\omega t_1 \\ \vdots & \vdots \\ \cos\omega t_{k-1} & \sin\omega t_{k-1} \end{bmatrix}$$

$$\theta = \begin{bmatrix} A\cos\psi & A\sin\psi \end{bmatrix}^T$$

Substituting in Eq (d.4) yields

$$\begin{bmatrix} \theta_0 \\ \theta_1 \end{bmatrix} = \begin{bmatrix} \sum_{i=0}^{k-1}\cos^2\omega t_i & \sum_{i=0}^{k-1}\cos\omega t_i\sin\omega t_i \\ \sum_{i=0}^{k-1}\cos\omega t_i\sin\omega t_i & \sum_{i=0}^{k-1}\sin^2\omega t_i \end{bmatrix} \begin{bmatrix} \sum_{i=0}^{k-1} y(t_i)\cos\omega t_i \\ \sum_{i=0}^{k-1} y(t_i)\sin\omega t_i \end{bmatrix} \tag{d.5}$$

D.2 DIGITAL FOURIER ANALYSIS

Assume a periodic function with period 2π, the expansion of the 2π-period function into a series of trigonometric functions [102]:

$$f(t) = \frac{a_0}{2} + \sum_{n=1}^{\infty} \left(a_n \cos(\omega n t) + b_n \sin(\omega n t) \right) \tag{d.6}$$

with the Fourier coefficients

$$a_n = \frac{1}{\pi} \int_{-\pi}^{\pi} f(t) \cos(n\omega t) d\omega t \qquad n = 0,1,2,\cdots$$

$$b_n = \frac{1}{\pi} \int_{-\pi}^{\pi} f(t) \sin(n\omega t) d\omega t \qquad n = 1,2,\cdots$$

Eq. (d.6) can also be written in complex form:

$$f(t) = \sum_{n=-\infty}^{\infty} c_n e^{jn\omega t} \tag{d.7}$$

with coefficients

$$c_n = \frac{1}{2\pi} \int_{-\pi}^{\pi} f(t) e^{-jn\omega t} d\omega t$$

Relation between the coefficients a_n, b_n, and c_n:

$$\left.\begin{aligned} a_n &= c_n + c_{-n} \\ b_n &= j(c_n - c_{-n}) \end{aligned}\right\} n > 0 .$$

Above is the continuous version of Fourier transformation. Discrete Fourier transformation is used for functions whose values are given or can be scanned only in the interval [0, T] at discrete point.

Discrete form of Eq. (d.7) can be written as:

$$f(t_k) = \sum_{i=0}^{N-1} c_i e^{j2\pi i t_k / T} = \sum_{i=0}^{N-1} c_i e^{j2\pi i k / N} \tag{d.8}$$

with $t_k = k\Delta t$ and $T = N\Delta t$, where Δt is the grid interval.

And the coefficients obey the equation:

$$c_i = \frac{1}{N}\sum_{m=0}^{N-1} f(t_m) e^{-j2\pi i m/N} \quad .$$

Appendix E MODAL ANALYSIS – PRONY METHODS

Equivalencing techniques are widely used in power system simulation. They can significantly reduce computational resources while retain the system original dynamics. One of approaches to build equivalents for power networks is to analyze their responses to a certain excitement.

Generally the modeling of power network is dominated by a bunch of inductors and capacitors. Therefore, the responses from power networks are a combination of a number of exponentials. The analysis to the responses falls into the category of modal analysis.

In modal analysis, the data to be analyzed is assumed to consist of a sum of exponentials in additive white noise. When the exponentials have complex arguments, then the data contain complex modes, or damped sines and cosines.

Let's model the signal component of a received, or measured, data record as a finite sum of k damped cosines:

$$y_t = \sum_{i=0}^{k-1} A_i e^{\lambda_i t} \cos(\omega_i t + \phi_i), \qquad \mathrm{t} = 0,1,\cdots,\mathrm{N}\text{-}1 \tag{e.1}$$

The parameter A_{i-1} is the amplitude of *i*th cosine, $e^{\lambda_{i-1}}$ is its damping factor, ω_{i-1} is the speed, and ϕ_{i-1} is the phase.

The signal y_t can be represented as a finite sum of 2k complex modes,

$$y_t = \sum_{i=0}^{2k-1} R_i z_i^t \tag{e.2}$$

where any complex mode pair (R_i, z_i) is matched by a complex conjugate pair (R_i^*, z_i^*).

$$R_{2i} = R_{2i+1}^* = \frac{A_i}{2} e^{j\phi_i}, z_{2i} = z_{2i+1}^* = e^{(\lambda_i + j\omega_i)}$$

Eq. (e.2) is a modal representation for the signal $\{y_t\}$. The snapshot $y = [y_0 \quad y_1 \quad \cdots \quad y_{N-1}]^T$ has the corresponding modal decomposition,

$$y = \begin{bmatrix} y_0 \\ y_1 \\ \vdots \\ y_{N-1} \end{bmatrix} = VR$$

where V is a complex Vandermonde matrix of dimension Nxp ($p=2k$) and B is a $px1$ vector od mode weights:

$$V = \begin{bmatrix} 1 & 1 & \cdots & 1 \\ z_0 & z_1 & \cdots & z_{p-1} \\ \vdots & \vdots & & \vdots \\ z_0^{N-1} & z_1^{N-1} & \cdots & Z_{p-1}^{N-1} \end{bmatrix}, R = \begin{bmatrix} R_0 \\ R_1 \\ \vdots \\ R_{p-1} \end{bmatrix} \tag{e.3}$$

We call the ith column of V the ith mode. In general, complex conjugate modes are adjacent in V.

From the complex conjugate poles $(z_0, z_1, \cdots, z_{p-1})$, we may form the real polynomial $A(z)$:

$$A(z) = \prod_{i=0}^{p-1} \left(1 - z_i z^{-1}\right) = \sum a_i z^{-i};\ a_0 = 1 \tag{e.4}$$

and the corresponding "whitening" matrix A^T of dimension $(N-p)\times N$:

$$A^T = \begin{bmatrix} a_{p-1} & a_{p-2} & \cdots & a_0 & 1 & 0 & \cdots & 0 \\ 0 & a_{p-1} & & & \ddots & \ddots & \ddots & 0 \\ \vdots & \ddots & \ddots & & & a_0 & 1 & 0 \\ 0 & \cdots & 0 & a_p & \cdots & a_1 & a_0 & 1 \end{bmatrix}$$

The complex poles z_i are the zeros of the polynomial A^T. Therefore we have the property $A^T V = 0$ and $A^T y = 0$.

$$\begin{bmatrix} a_{p-1} & a_{p-2} & \cdots & a_0 & 1 & 0 & \cdots & 0 \\ 0 & a_{p-1} & & & \ddots & \ddots & \ddots & 0 \\ \vdots & \ddots & \ddots & & & a_0 & 1 & 0 \\ 0 & \cdots & 0 & a_p & \cdots & a_1 & a_0 & 1 \end{bmatrix} \begin{bmatrix} y_0 \\ y_1 \\ \vdots \\ y_{p-1} \\ \vdots \\ y_{N-1} \end{bmatrix} = \begin{bmatrix} 0 \\ \vdots \\ 0 \end{bmatrix} \tag{e.5}$$

In the absence of additive noise, the polynomial A^T is an annihilator of the time series $\{y_t\}$. The analysis equations of Eq. (e.5) may be written as linear

prediction equations by organizing the coefficients a_i into a vector and the data into a matrix.

$$\begin{bmatrix} y_0 & y_1 & \cdots & y_p \\ y_1 & y_2 & \cdots & y_{p-1} \\ \vdots & \vdots & & \vdots \\ y_{N-1-p} & & \cdots & y_{N-1} \end{bmatrix} \begin{bmatrix} a_{p-1} \\ \vdots \\ a_0 \\ 1 \end{bmatrix} = \begin{bmatrix} 0 \\ 0 \\ \vdots \\ 0 \end{bmatrix} \tag{e.6}$$

The column rank of Y is evidently p and not $p+1$, that is, the last column of Y lies in the range of the first p columns of Y, meaning N may be chosen to equal $2p+1$ and the resulting system of equations solved for $\{a_i\}$.

This is the original Prony method. The roots of the polynomial A^T determine the frequencies and associated damping factors of the poles z_i. A root-finding routine must be used to compute the roots of the polynomial A^T. The magnitude and phase of R_i parameters may then be computed by writing out the modal equation $y = VR$ and solving the following Vandermonde system of equations:

$$\begin{bmatrix} 1 & 1 & \cdots & 1 \\ z_0 & z_1 & \cdots & z_{p-1} \\ \vdots & \vdots & & \vdots \\ z_0^{N-1} & z_1^{N-1} & \cdots & Z_{p-1}^{N-1} \end{bmatrix} \begin{bmatrix} R_0 \\ R_1 \\ \vdots \\ R_{p-1} \end{bmatrix} = \begin{bmatrix} y_0 \\ y_1 \\ \vdots \\ y_{p-1} \end{bmatrix}.$$

This completes the identification of (R_i, z_i) in the complex exponential model, using $2p+1$ measurements.

The Prony procedure works perfectly well when no noise is present in the data, but when noise (or measurement imprecision) is introduced, then this method performs very poorly, largely due to the extreme sensitivity of root locations z_i to the coefficients of the polynomial A^T. It seems nature to use more measurements of $\{y_t\}$ to determine the polynomial coefficients. This is the foundation of the least squares Prony method. Except this, there are also some other versions of Prony method.